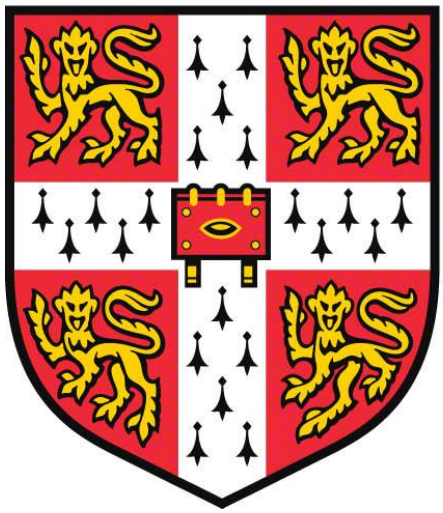

The development of functionalised stapled peptides as chemical tools to modulate biological processes in platelets and as novel antimicrobial therapeutics targeting *Pseudomonas aeruginosa*

Josephine Gaynord

Newnham College

University of Cambridge

July 2020

Supervised by Professor David R. Spring

This dissertation is submitted for the degree of Doctor of Philosophy

Abstract

Peptides are useful modulators of protein-protein interactions (PPIs) and cellular membranes, both of which are traditionally challenging to target using small molecules. Often therapeutic peptides suffer from issues including poor proteolytic stability. Two-component peptide stapling can improve stability and enable facile peptide functionalisation. This thesis describes the development of functionalised stapled peptides for two biological applications.

1. **The development of stapled peptides as chemical tools to investigate PPIs in human platelets**

Platelets are a vital, anuclear component of blood. The Bcl-2 family of proteins are known to be key mediators of apoptosis in nucleated cells, however the role of each Bcl-2 protein in platelet apoptosis and activation is unknown. Recently, stapled peptides were deemed useful chemical tools for studying PPIs in platelets. In this section, three polyarginine-functionalised stapled peptides were developed as Bcl-2 PPI inhibitors. These novel chemical tools are anticipated to provide valuable insight into the roles of Bcl-2 PPIs in platelet modulation, which could ultimately lead to new therapeutic targets.

2. **The development of cleavable stapled peptide-drug conjugates to target *Pseudomonas aeruginosa***

Antimicrobial resistance (AMR) is a major healthcare threat, and Gram-negative bacteria such as *Pseudomonas aeruginosa* pose a significant therapeutic challenge. Antimicrobial peptides disrupt bacterial membranes, however functionalised two-component stapled antimicrobial peptides (STAMPs) are underexplored. This section describes the development of a STAMP-drug conjugate, constructed by functionalisation of the STAMP staple with a small molecule antibiotic, attached *via* a β-lactamase-cleavable motif. The resulting conjugate combines two mechanisms of action, which is a validated strategy for overcoming AMR. To this end, two novel, unfunctionalised STAMPs were identified that exhibited good minimum inhibitory concentrations against *P. aeruginosa* (64 μg/mL) and selectivity over a Gram-positive strain, from a panel of seven novel STAMPs. Subsequently, a tractable synthesis of the proposed functionalised STAMP was investigated. It is hypothesised that the cleavable STAMP-drug conjugate will enable infection-controlled drug-release and dual-targeting of *P. aeruginosa*.

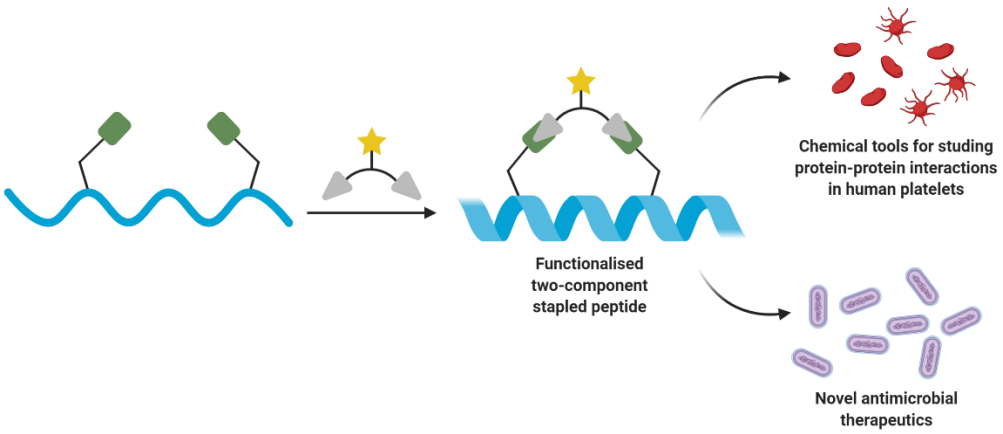

Figure 0 A summary of functionalised stapled peptides as both chemical tools to study protein-protein interactions in human platelets and as novel antimicrobial therapeutics.

Acknowledgments

First and foremost, I would like to thank Professor Spring for his support and encouragement over the past four years, and for giving me the opportunity to undertake research in such a wonderful group. I am grateful to AstraZeneca and the BBSRC for their financial support, and my industrial supervisor Dr. Jeremy Parker for his guidance and input.

I am extremely grateful to my collaborators, Dr. Martin Welch, Dr. Nicholas Pugh and Dr. Yaw Sing Tan, who have been so gracious with their time, lab space and expertise. A huge thank you to Tom O'Brien and Dr. Niaz Ahmed for patiently guiding me through the biology and for being so generous with your time.

I am indebted to those who gave up their time to proof-read my thesis, including Dr. Jessica Iegre, Dr. Elaine Fowler, Sam Rowe, Dr. Gabriele Fumagalli, Dr. David Twigg, Eleanor Atkinson, Dr. Hannah Stewart, Dr. Sarah Kidd and Dr. Bee Ha Gan. I'm sorry some of you had no way of avoiding it during lockdown. I owe a massive thank you to Elaine for answering my panicked questions and being so reassuring on so many occasions!

Thank you to Steve and Katrine for all of your support during my first few years, and a very special thank you to Jessy for being my bay-partner, mentor, the other half of team Jossy, and a great friend. I am also so grateful to Hannah Sore for your endless advice and encouragement, particularly with Pep2Smart.

A huge thanks to Springles past and present, for all the fun both in and out of the lab, particularly Hannah, Sarah and Súil. A very special thank you to Elaine and Jonny for all the friendship and camaraderie, and for making our trip to the ACS so incredible. Thank you to my Cambridge family from the past four years, including the Osberger-Nguyens, Spurious Discharge, the Love Island group chat, and finally Katherine, for jumping at every opportunity to go and have 'fun' on cold and wet mountains.

I would like to thank my ever-supportive family, particularly my parents for not rolling their eyes too much when I said I wanted to spend four more years at university. This thesis was written under strange circumstances and I will be forever thankful to Sam and Murphy who were stuck at home with me for the duration. Sam – thank you for coping whilst we shared a desk for many months, and for making every day a joy. Murphy – woof woof.

Abbreviations

˚C	degrees Celsius
µ	micro
δ	chemical shift
1NAl	1-naphthyl-L-alanine
7-ACA	7-aminocephalosporanic acid
7-ADCA	7-Aminodesacetoxycephalosporanic acid
Å	angstrom(s)
A1	Bcl-2 related protein A1
Ac	acetyl
ADME	adsorption, distribution, metabolism, excretion
ADP	adenosine diphosphate
AHL	acyl homoserine lactone
Ahx	6-amino hexanoic acid
AIDS	acquired immune deficiency syndrome
AMP	antimicrobial peptide
AMR	antimicrobial resistance
aq.	aqueous
Ar	aryl
ATCC	American Type Culture Collection
Bad	Bcl-2-associated death promoter
Bak	Bcl-2 associated k protein
Bax	Bcl-2 associated x protein
Bcl-2	B-cell lymphoma protein 2
Bcl-w	Bcl-2-like protein 2
Bcl-x_L	B-cell lymphoma extra-large protein
BH	Bcl-2 homology
BH3	Bcl-2 homology domain 3
Bid	BH3 interacting-domain death agonist
BL	β-lactamase(s)
Bmf	Bcl-2-modifying factor
Bn	Benzyl
Boc	*tert*-butoxycarbonyl
br.	broad
Bu	butyl
CAL-B	*Candida antarctica* lipase B
calcd.	calculated
cat.	catalytic
CD	circular dichroism
CF	cystic fibrosis
CFT	calcium-free Tyrode's
CK2	casein kinase II
CLIPS	chemical ligation of peptide onto scaffolds
conc.	concentration
COSY	correlation spectroscopy

CPP	cell penetrating peptides
CuAAC	copper-catalysed azido-alkyne cycloaddition
Cy	cyclohexyl
Da	Daltons
dba	dibenzylideneacetone
DCA	1,3-dichloroacetone
DCC	*N*,*N*'-dicyclohexylcarbodiimide
decomp.	decomposition
deg	degree(s)
DEL	DNA-encoded library
DEPT	distortionless enhancement by polarisation transfer
DIC	*N*,*N*'-diisopropylcarbodiimide
DIPEA	*N*,*N*-diisopropylethylamine
$DiSC_3(5)$	3,3′-dipropylthiadicarbocyanine iodide
DMF	*N*,*N*-dimethylformamide
DMSO	dimethylsulfoxide
DMT-MM	4-(4,6-dimethoxy-1,3,5-triazin-2-yl)-4-methylmorpholinium chloride
DP	desired product
DPC	dodecylphosphocholine
dppf	1,1′-bis(diphenylphosphino)ferrocene
DRAMP	data repository of antimicrobial peptides
DVH	divinylheterocycle
DVP	divinylpyrimidine
DVT	divinyltriazine
EDC	*N*-(3-dimethylaminopropyl)-*N*'-ethylcarbodiimide hydrochloride
EDT	1,2-ethanedithiol
EDTA	ethylenediaminetetraacetic acid
eq.	equivalents
ESI	electrospray ionisation
Et	ethyl
EUCAST	European Committee on Antimicrobial Susceptibility Testing
FCC	flash column chromatography
FDA	United States Food and Drug Administration
FITC	fluorescein 5-isothiocyanate
Fmoc	9-fluorenylmethoxycarbonyl
FSC	forward scatter
g	gram(s) or gravity
GEL	genetically-encoded library
h	hour(s)
hArg	homoarginine
HATU	1-[bis(dimethylamino)methylene]-1*H*-1,2,3-triazolo[4,5-b]pyridinium 3-oxid hexafluorophosphate
HDM2	human homolog of MDM2
HEPES	4-(2-hydroxyethyl)-1-piperazineethanesulfonic acid
HFIP	hexafluoro2-propanol
HMBC	heteronuclear multiple bond correlation

HMQC	heteronuclear multiple quantum correlation
HOAt	1-hydroxy-7-azabenzotriazole
HPLC	high performance liquid chromatography
HRMS	high resolution mass spectrometry
HSQC	heteronuclear single quantum correlation
HyP	4-hydroxyproline
IACG	Interagency Coordination Group
IC_{50}	concentration required to reduce response by a half
IR	infrared
J	coupling constant
k	kilo
K_d	dissociation constant
K_i	ionisation constant
L	litre(s)
LB	Lysogeny broth
LCMS	liquid chromatography-mass spectrometry
Lit.	literature
LRMS	low resolution mass spectrometry
m	milli / metre(s)
M	mole(s) / mega
mp	melting point
m/z	mass-to-charge ratio
MBHA	4-methylbenzhydryl amine
MCl-1	induced myeloid leukaemia cell differentiation protein
MDM2	mouse double minute 2
MDR	multi-drug resistance / multi-drug resistant
Me	methyl
MeCN	acetonitrile
MES	4-morpholineethanesulfonic acid
MH-B	cation-adjusted Mueller-Hinton broth
MHz	megahertz
MIC	minimum inhibitory concentration
min	minute(s)
MLC	minimum lethal concentration
MRSA	methicillin-resistant *Staphylococcus aureus*
n	nano
N	Normal
ND	no data / not determined
NBS	*N*-bromosuccinimide
NCTC	National Collection of Type Cultures
NMR	nuclear magnetic resonance
Noxa	phorbol-12-myristate-13-acetate-induced protein 1
NP	natural product
OD	optical density
Orn(N_3)	L-δ-azido ornithine
Oxyma Pure	ethyl cyano(hydroxyimino)acetate

p53	phosphoprotein 53
PDB	protein data bank
PDC	peptide-drug conjugate
PE	petroleum ether
PEG	polyethylene glycol
Ph	phenyl
Pi	inorganic phosphate
PPI	protein-protein interaction
ppm	parts per million
PS	phosphatidylserine
Puma	p53 upregulated modulator of apoptosis
QS	quorum sensing
QSI	quorum sensing inhibitor
R	variable chemical group
RCM	ring-closing metathesis
R_f	retention factor
RNA	ribonucleic acid
rpm	revolutions per minute
rt	room temperature
RTHS	reverse two-hybrid system
s / *sec*	secondary
SAHB	stabilised α-helix of Bcl-2 domain
sat.	saturated
SDS	sodium dodecyl sulfate
SICLOPPS	split-intein circular ligation of peptides
S_N2	bimolecular nucleophilic substitution
S_NAr	nucleophilic aromatic substitution
SPAAC	strain promoted azide-alkyne cycloaddition
SPPS	solid phase peptide synthesis
STAMP	stapled antimicrobial peptide
t / *tert*	tertiary
T3P	propylphosphonic anhydride
TAMRA	carboxytetramethylrhodamine
TBAOH	tetrabutylammonium hydroxide
Bid	BH3 interacting-domain death agonist
TFA	trifluoroacetic acid
TFE	2,2,2-trifluoroethanol
THF	tetrahydrofuran
THPTA	tris(3-hydroxypropyltriazolylmethyl)amine
TIPS	triisopropylsilane
TMS	tetramethyl silyl ether
TMSI	trimethylsilyl iodide
TxA2	thromboxane A2
UV	ultraviolet
v_{max}	absorption maximum
VWF	Von Willebrand factor

WHO	World Health Organisation

Table of contents

Chapter 1

Introduction

1. Chapter 1 - Introduction

1.1 Peptides as drugs and tool compounds: pros and cons

Historically, drug discovery has focused on small molecule therapies, which typically bind to well-defined pockets on proteins. At the other end of the scale with respect to size, biologics (e.g. monoclonal antibodies) are primarily used to target protein-protein interactions (PPIs), which are usually shallow and cover a comparatively large surface area, however they lack cellular penetration.[1] Peptides occupy the space between these two extremes in terms of their size and properties as biologically active chemicals (Table 1).[2] Peptides can access a range of different biological targets, including PPIs, and display distinct pharmacologic profiles.[3] A comparison of these three classes of therapeutics is drawn in Table 1.

Table 1 A comparison of small molecules, peptides and biologics looking at typical characteristics of each class of drugs. Adapted from Passioura.[4]

	Small molecules	**Peptides**	**Biologics**
Example	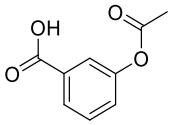 Aspirin	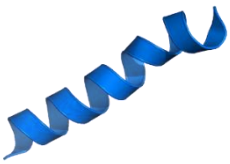 Esculentin-1a (PDB 5XDJ)	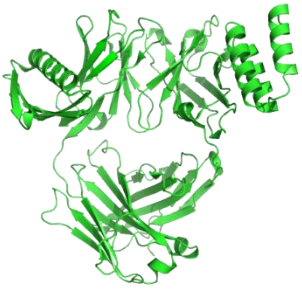 Trastuzumab (PDB 4HJG)
Size (Da)	<500	500-5,000	>5,000
Targets	Small, well-defined binding pockets	Cannot target small, well-defined binding pockets	Extracellular proteins
Plasma half life	Hours	Minutes-hours	Weeks
Membrane permeable?	Yes	Sometimes	No
Orally bioavailable?	Usually	Sometimes	No
Specificity for target	Moderate	High	High

Insulin became the first peptide drug to enter the market in 1923 for the treatment of diabetes; today there are over 150 peptide-based drugs in clinical trials, with around 60 on the market.[5] The first peptide drugs targeted extracellular hormone receptors, and it is still the case that most peptides in the clinic have extracellular targets, including G-protein coupled receptors, immunoglobulin family receptors and ion channels.[2] Today, the variety of targets accessed by peptides has increased, with intracellular targets no longer off limits.[6,7]

Aside from their uses as disease-modifying therapeutics, peptides can also be used as chemical tools (or 'probes'). A chemical tool is any compound with high affinity and specificity for its target that can be used to study a biological system; it may not have the appropriate physicochemical properties or pharmacokinetics to be developed into a drug. As chemical tools, peptides enable biological investigations of targets that were previously inaccessible with small molecule probes.[8]

Due to their unique size and composition, peptides have a number of advantages and disadvantages which are summarised in Table 2.

Table 2 A summary of key advantages and disadvantages of peptides as drugs.

Advantages of peptides	Disadvantages of peptides
High potency and selectivity	Poor proteolytic stability
Applicable to a broad range of targets	Short half-life and fast elimination
Easy access to chemically and biologically diverse therapeutics	Low membrane permeability
	Usually not orally bioavailable
Good safety and efficacy	Rapid renal clearance

With respect to their disadvantages, peptides suffer from poor absorption, distribution, metabolism and excretion (ADME) properties,[5] and they often have short half-lives (e.g. minutes) due to rapid renal excretion and proteolytic degradation in plasma.[9] Additionally, peptides are much less likely to be cell permeable than small molecules due to their comparatively high molecular weight, numbers of hydrogen bond donors and acceptors and high polar surface area.[10] Most peptides have extremely low bioavailability (<1%) meaning that very few peptide drugs can be taken orally, the more favourable route due to higher patient compliance.[5] Indeed, analysis of the marketed peptide drugs (Table 4, Section 1.4) shows that only one linear peptide (semaglutide) and two cyclic peptides (cyclosporin A and linaclotide) can be taken orally.[11,12]

Despite these potential disadvantages, peptides offer many advantages over both biologics and small molecules. Peptides can give comparable affinity and target selectivity as biologics, such as antibodies, however bulk peptide synthesis can be much cheaper.[13] Additionally, peptides can access intracellular targets and have vastly improved tissue penetration over biologics.[14] Compared to small molecule drugs, peptides can have much stronger interactions with their intended targets and higher specificity as they are comprised of endogenous amino acids capable of making high numbers of interactions with target proteins. Finally, peptides often display low toxicity and immunogenicity and present a lower risk of drug-drug interactions than small molecule drugs.[3,10]

1.2 Overcoming the problems with peptides

Synthetic modifications can be made to peptides to improve their properties and overcome the disadvantages discussed in the previous section. The result of modifying a peptide is a peptidomimetic: a molecule which mimics the binding properties of the parent peptide. Peptidomimetics can range from peptides with minimal structural alterations to structurally unrelated small molecules which mimic the mechanism of action of the parent peptide. A modern classification of peptidomimetics is proposed by Grossmann and co-workers:[15]

- Class A – peptides where a few amino acids may have been introduced and minor modifications made to the backbone, but are mostly unchanged overall.
- Class B – peptides which have undergone significant backbone modifications, multiple amino acid substitutions and/or the incorporation of small molecule fragments (includes peptoids).
- Class C – non-peptidic small molecules where substituents are presented in a similar fashion to the key residues of the parent peptide.
- Class D – small molecules which do not relate to the parent peptide structure, but which mimic the mode of action of the peptide.

Examples of the types of modifications which can be made to peptides are shown in Figure 1. To reduce proteolytic degradation L-amino acids (A, Figure 1) can be replaced with D-amino acids (B, Figure 1), *N*-methylation and α-methylation performed (C, Figure 1) or β-amino acids or peptoids (D and E respectively, Figure 1) can be introduced into the peptide.[16] To avoid metabolic instability, specific amino acids which have been identified as metabolically liable can be replaced with unnatural analogues.[5]

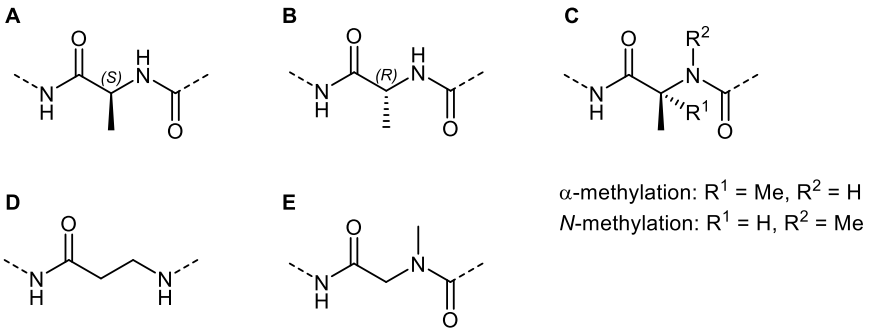

Figure 1 Selected strategies for improving the proteolytic stability of peptides. A: A standard L-amino acid, B: A D-amino acid, C: α-methylation and N-methylation, D: Use of β-amino acids, E: An alanine peptoid.

Macrocyclisation is another strategy which has the potential to improve multiple properties of therapeutic peptides. Macrocyclisation can occur either head-tail, side chain-head, side chain-tail or side chain-side chain (Figure 2): all of these different connections are represented in natural products and marketed cyclic peptide drugs.[17]

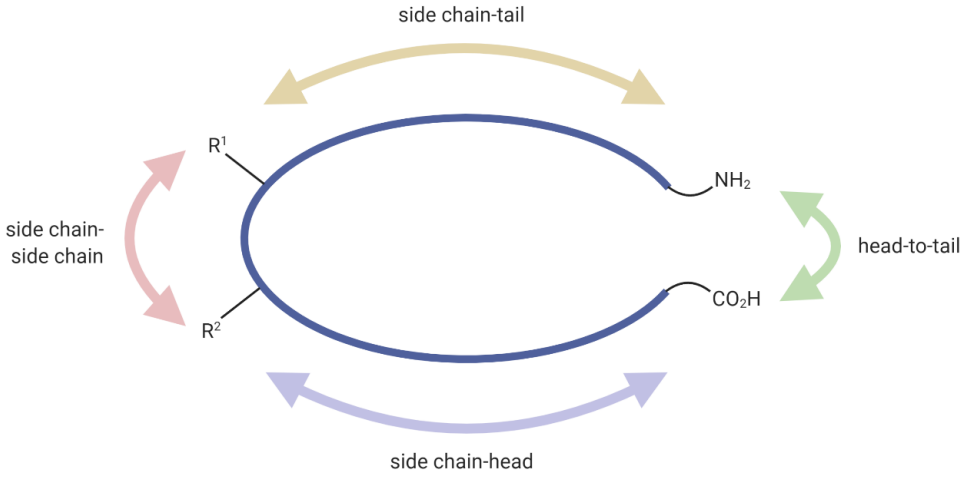

Figure 2 A cartoon depicting the possible macrocyclisation positions on a linear peptide. Adapted from White and Yudin.[18]

Peptide cyclisation can be beneficial for:

1. Constraining the peptide in a biologically relevant conformation such as an α-helix or β-turn to reduce the entropic penalty upon binding to the target.[18–20]
2. Improving the proteolytic stability.[21]
3. Improving the cellular permeability.[22]
4. Introducing further functionality (e.g. a fluorescent tag for biochemical assays).[23–25]
5. Modulating the physicochemical properties of the peptide.[18]

The work in this thesis is concerned with side chain-side chain macrocyclisation, often called ‘stapling’, as it will be referred to from herein. The following section discusses different approaches to peptide stapling.

1.2.1 Stapled peptides

Peptide stapling can be performed in either a one-component or two-component manner. One-component stapling involves the intramolecular reaction of two amino acid side chains (A, Figure 3), whereas two-component stapling involves the reaction of an external linker with two amino acid side chains (B, Figure 3).

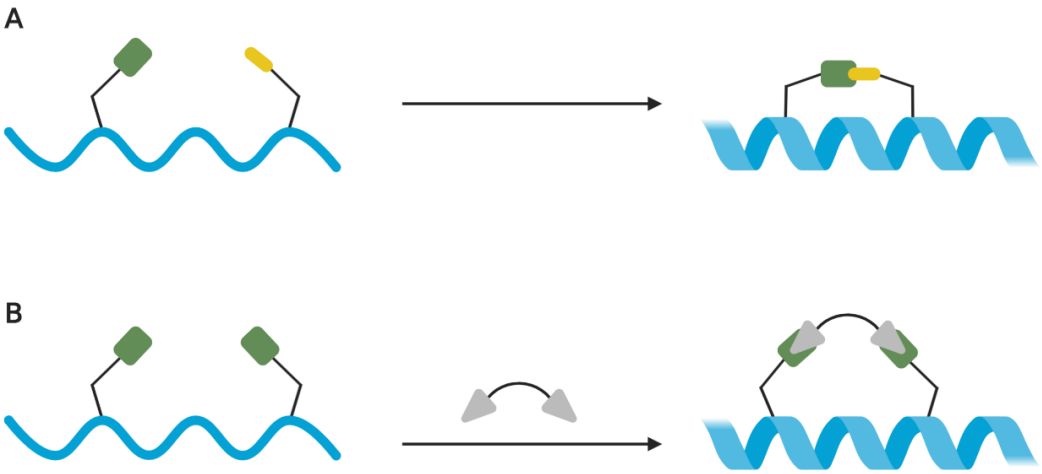

Figure 3 A schematic overview of peptide stapling. A) One-component peptide stapling, and B) two-component peptide stapling. The peptide is shown as a blue line or helix, amino acid side chains as green rectangles or yellow ovals and the reactive handles on the linker as grey triangles.

Often one of the aims of peptide stapling is to fix the peptide in a particular conformation to reduce the entropic penalty associated with re-organisation prior to target-binding.[15] In particular, peptides are commonly stapled to induce an α-helical conformation as this structural motif is of high biological relevance: around 30-40% of the structural features in proteins are α-helices.[26] Furthermore, PPIs are a common target for peptide therapeutics and chemical tools and it has been estimated that α-helices contribute to binding in over 60% of PPIs.[27] One turn of an α-helix spans 3.6 residues and helices are naturally stabilised by intramolecular hydrogen bonding between the carbonyl and peptide backbone NH at positions *i,i*+4.[15] If an α-helical peptide is desired, stapling is often performed at *i,i*+4, 7 or 11 positions (Figure 4). However the advantages of peptide stapling go beyond conferring conformational rigidity and some of the examples discussed in the following sections involve peptide stapling at alternative positions to those which promote α-helicity. In these cases, stapling was performed either to achieve different biologically relevant conformations, improve proteolytic stability or to introduce functionality to the peptide sequence.

Figure 4 A cartoon of an α-helix showing the optimal staple positions for the stabilisation of the secondary structure. Residues at i, i+4, i+7 and i+11 positions span one, two or three turns of the helix, respectively.

1.2.1.1 An overview of one-component peptide stapling

The earliest reported approach to peptide stapling involved one-component lactamisation between acid- and amine-bearing canonical amino acid side chains.[28] Another of the first methods to be reported was the formation of disulfide bonds, however, due to the chemical

instability of the resulting linkage this approach has not been widely adopted.[29] In recent years the field has advanced significantly, and now unnatural amino acids are frequently employed in stapling strategies. The current 'gold standard' of one-component peptide stapling is hydrocarbon stapling, wherein unnatural alkenyl amino acids are introduced into the peptide sequence, which is subsequently cyclised by ring-closing metathesis (RCM). This method yields an all-hydrocarbon stapled peptide and was first reported by Blackwell and Grubbs,[30] and later developed by Verdine (Scheme 1).[31] RCM stapling is popular due to its synthetic simplicity; however, the alkene-containing unnatural amino acids are expensive or can require long synthetic routes.

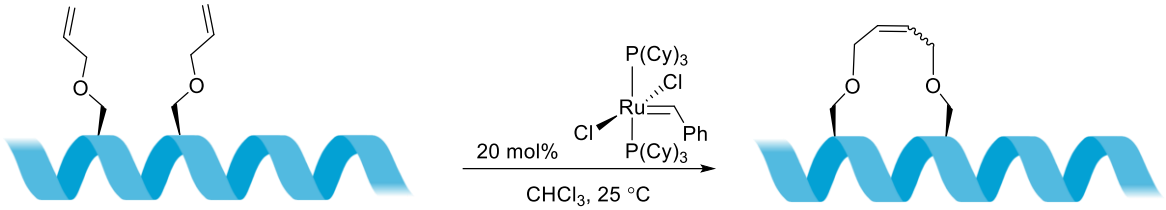

Scheme 1 The initial peptide macrocyclisation via RCM reported by Grubbs and Blackwell.[30]

Other one-component stapling methodologies which make use of unnatural amino acids include copper-catalysed azide-alkyne cycloadditions (CuAAC),[32] UV-promoted cycloadditions,[33] thiol-ene reactions,[34] oxime formation,[35] thioether formation,[36] and CH activation.[37,38]

One major downside to one-component peptide stapling is that it does not usually append any functionality onto the peptide. A straightforward site of functionalisation is the *N*-terminus of the peptide, or a reactive amino acid side chain residue (e.g. the lysine ε-amino group).[39] Alternatively, the staple linker can be functionalised, which can occur *via* two different methods (Figure 5). Modification of the linker can take place before macrocyclisation, however every different analogue would require re-synthesis of the unnatural amino acids and peptide chain. Alternatively, once stapled the linker can be modified, although this method of functionalisation has seldom been reported in the literature.[40] The dual functionalisation of one-component stapled peptides poses a significant synthetic challenge and would require a combination of different approaches to be achieved.

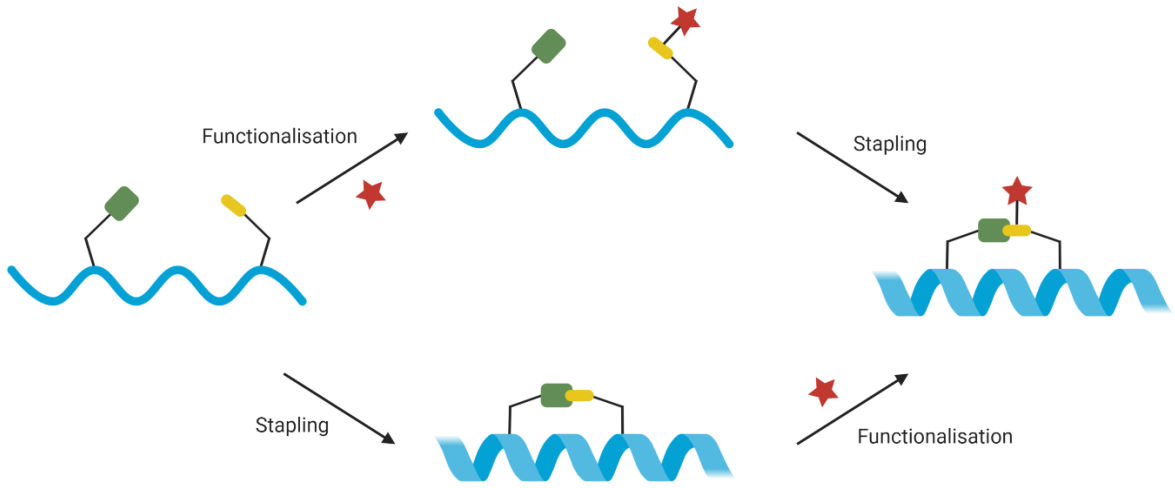

Figure 5 A cartoon depicting the functionalisation of a one-component stapled peptide via appendage of the functionality onto the staple either pre or post-macrocyclisation. The peptide is shown as a blue line or helix, amino acid side chains as green rectangles or yellow ovals and the functionality as red stars.

1.2.1.2 Two-component peptide stapling

Two-component peptide stapling involves a bimolecular reaction between a linker and two amino acid side chain residues. The major advantage of two-component peptide stapling is that the linker and peptide can be varied independently of each other and brought together in a combinatorial manner. One disadvantage is the possibility of forming double-addition products instead of the desired macrocyclic peptides (Figure 6).[41] To combat this, two-component stapling reactions are typically performed at low concentrations with near-equivalent amounts of peptide and linker.

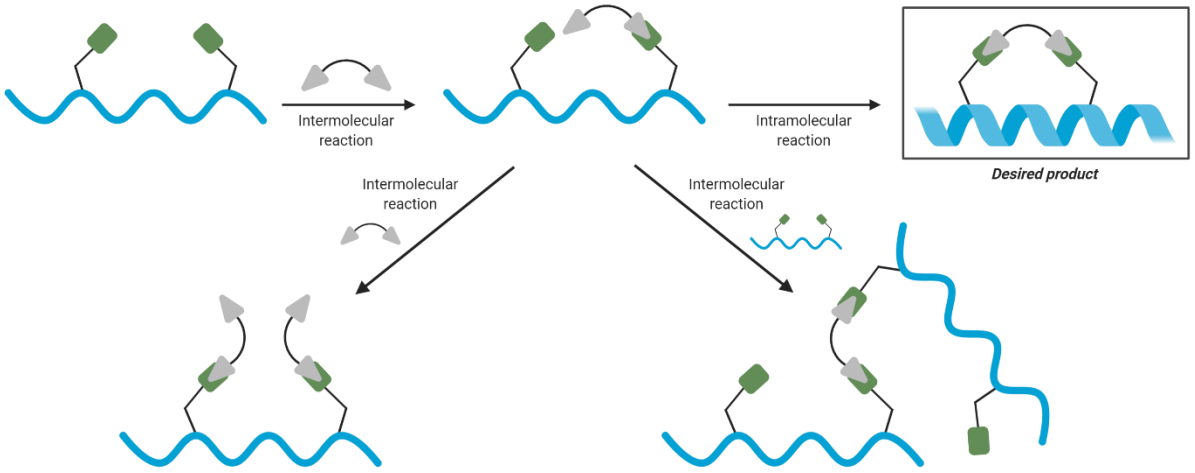

Figure 6 A cartoon depicting the formation of possible side-products during two-component peptide stapling. The peptide is shown as a blue line or helix, amino acid side chains as green rectangles and the linker reactive handles as grey triangles.

Two-component stapling can be performed using natural and unnatural amino acids, and the linkers can vary in size from a simple methylene unit to much larger linkers.[42]

1.2.1.2.1 Two-component peptide stapling using unnatural amino acids

The use of unnatural amino acids in two-component stapling provides excellent chemoselectivity, which is important given the number of potentially competing reactive groups in a peptide. However, unnatural amino acids must be synthesised or purchased, often at a high cost. The most common method of two-component peptide stapling using unnatural amino acids is double CuAAC stapling. This involves the incorporation of two azide-containing amino acids into the peptide sequence and stapling with a bis-alkynyl linker. This approach was initially reported by Bong and co-workers,[43] and developed further by the Spring group,[44] Pedersen and co-workers,[45] and Thurber and co-workers.[46] The conditions developed by the Spring group for two-component CuAAC stapling are shown in Scheme 2.[44]

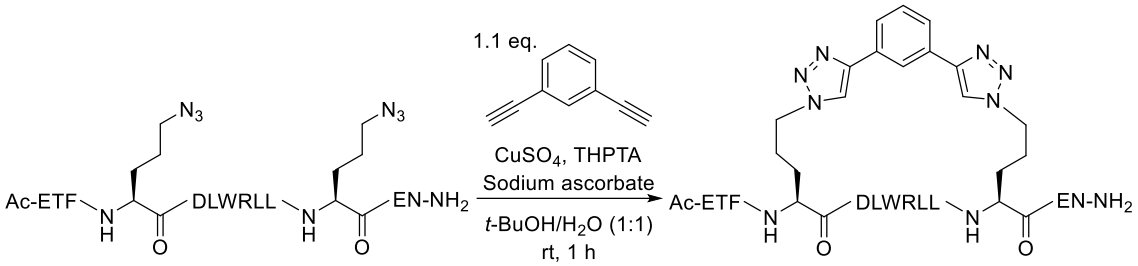

Scheme 2 The CuAAC stapling of a peptide designed to disrupt the p53/MDM2 PPI under conditions reported by Lau et al.[44]

A complementary approach was also developed by the Spring group using a strain-promoted azide-alkyne cycloaddition (SPAAC), which removes the need for the potentially cytotoxic copper catalyst required for CuAAC, thus allowing *in situ* peptide stapling (Scheme 3).[47]

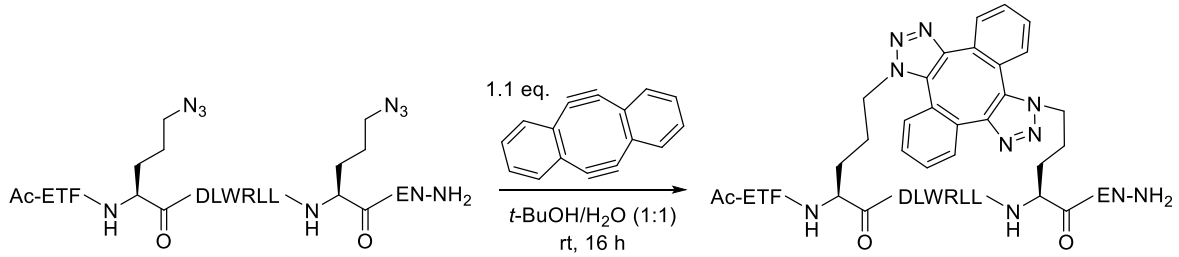

Scheme 3 The SPAAC stapling of a peptide a peptide designed to disrupt the p53/MDM2 PPI under conditions reported by Lau et al.[47]

1.2.1.2.2 Two-component peptide stapling using cysteine

Using natural amino acids for peptide stapling provides the benefits that they are widely available and cheap, however, they are more likely to result in issues of chemoselectivity. To mitigate this problem, numerous methods based upon the reactivity of the thiol group in cysteine have been developed. Cysteine has a relatively low natural abundance in proteins and peptides and, under the correct reaction conditions, can display orthogonal reactivity to the other functionalities commonly present in peptides, thus making it an ideal candidate for peptide stapling methodologies.[48]

The most prolific two-component cysteine stapling reaction is alkylation, which has been reported by several groups. The use of benzyl and alkyl halides was developed by Timmerman and co-workers, and named chemical linkage of peptides onto scaffolds (CLIPS, A, Figure 7).[49] The CLIPS technology can give mono-, bicyclic and functionalised peptides;[50,51] it can also be combined with orthogonal ring-forming reactions (such as CuAAC) to give complex tri- and tetra-cyclic peptide scaffolds.[52,53] Additionally, the CLIPS methodology has been applied to the generation of cyclic peptide libraries *via* phage display by Winter and co-workers.[54] Woolley and co-workers used cysteine alkylation to perform a peptide stapling screen, investigating the effect of the linker length and rigidity on the helical content of the resulting cyclic peptides.[55] The same group used this stapling reaction to introduce diazobenzene linkers, allowing photocontrol of the helical content of the stapled peptides (B, Figure 7).[56,57]

The simplest staple scaffold for cysteine alkylation was developed by Kourra and co-workers, in which diiodomethane is used to introduce a methylene unit (C, Figure 7). This has been used to mimic native disulfide bonds, eliminating the potential for disulfide reduction which can result in a loss of activity.[58] Dawson and co-workers published the stapling of peptides by alkylation with 1,3-dichloroacetone (DCA),[59] and illustrated that the resulting macrocyclic peptides could be functionalised *via* oxime formation (D, Figure 7). Finally, Bernardes and co-workers reported the grafting of peptides using a dibromo isobutylene linker (E, Figure 7).[60]

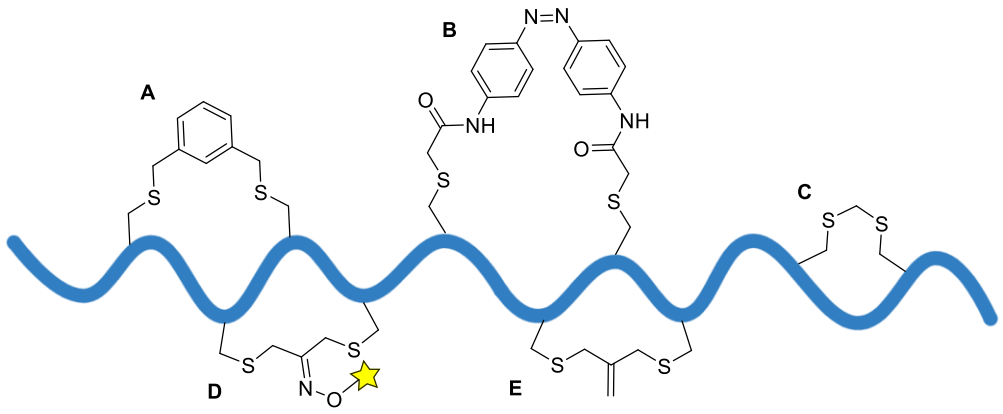

Figure 7 A cartoon depicting two-component stapling methodologies which use an S_N2 reaction to bridge between two cysteine residues with an alkyl halide linker. A) alkylation with various alkyl and aryl halides,[49] B) incorporation of a photo-switchable linker via alkylation,[57,56] C) formation of a methylene bridge with diiodomethane,[58] D) DCA stapling and functionalisation via oxime formation,[59] and E) peptide grafting with an isobutylene linker.[60] The peptide is represented by a blue line, and functionality as a yellow star.

There are several approaches to peptide stapling based around S_NAr reactions with suitable aromatic linkers (Figure 8). Pentelute and co-workers published two-component peptide stapling between Cys residues with perfluoroaryl linkers (A, Figure 8).[61] The lipophilic nature of these perfluoroaryl linkers was used to improve the blood-brain-barrier penetration of a Bim BH3-only peptide which, once stapled, showed enhanced *in vivo* brain penetration relative to the linear peptide.[62] Similarly Derda and co-workers published a similar macrocyclisation,

instead using a decafluoro-diphenylsulfone linker (B, Figure 8).[63] Finally, Smith and co-workers published a stapling approach using a dichloro-tetrazine linker (C, Figure 8). The resulting stapled peptide could be functionalised *via* an inverse electron-demand Diels-Alder reaction, and the staple could be completely removed in a two-step process involving irradiation with UV and treatment with cysteine, returning the linear peptide.[64]

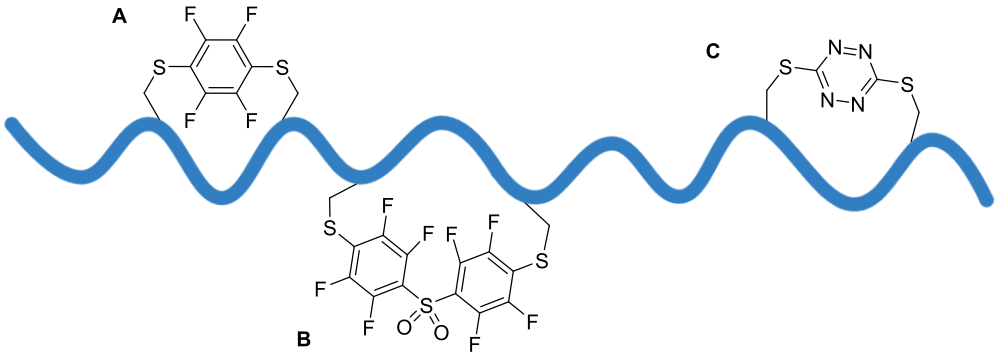

Figure 8 A cartoon depicting two-component Cys peptide stapling methodologies which use S_NAr chemistry. A) Stapling with perfluoroaryl linkers,[61,62] B) Stapling with a decafluoro-diphenylsulfone linker,[63] and C) Stapling with a tetrazine linker.[64] The peptide is represented by a blue line.

Thiol-ene reactions have been incorporated into peptide stapling approaches: Chou *et al*. published the reaction between a peptide bearing two Cys residues and a bis-alkenyl linker in the presence of a radical initiator and UV irradiation (A, Figure 9).[34] There are also multiple methods using conjugate addition, and the groups of Keillor and Wilson have published similar approaches using maleimide linkers. Keillor and co-workers performed peptide macrocyclisation with a bis-maleimide linker, onto which functionality could be appended (B, Figure 9).[65] Wilson and co-workers used a single dibromomaleimide to bridge between Cys residues, and functionality (e.g. a FITC tag or a PEG chain) was added *via* the nitrogen (C, Figure 9).[66] This stapling procedure is also reversible, as the addition of excess thiol, such as glutathione returns the linear peptide.

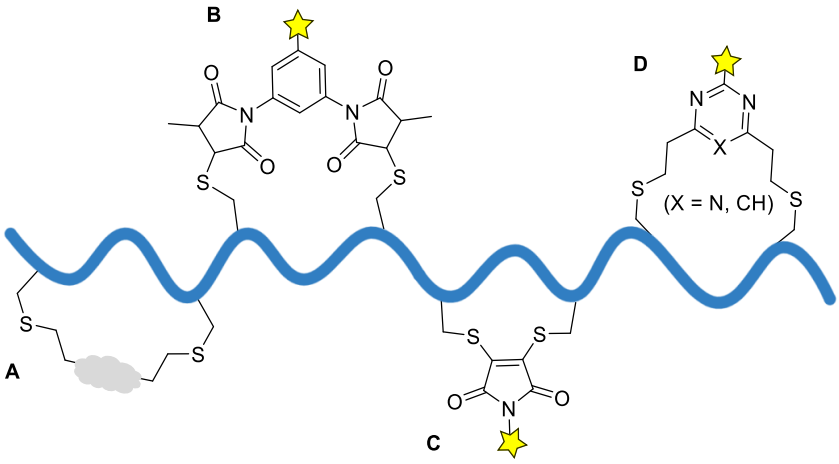

Figure 9 A cartoon depicting peptide stapling methodologies involving the conjugate addition, or thiol-ene reactions of Cys residues. A) The thiol-ene reaction with bis-alkenyl linkers,[34] B) Stapling via conjugate addition with a bis-maleimide linker,[65] C) Stapling via a double conjugate addition into a dibromomaleimide,[66] and D) Cyclisation via the conjugate addition of Cys residues with divinylheterocycles.[67] The peptide is represented by a blue line, variable groups as a grey shape, and functionality as a yellow star.

The reaction of Cys residues and divinyl heterocycles (DVHs) has been applied to the macrocyclisation of unprotected peptides under mild conditions (D, Figure 9).[67,68] A peptide designed to inhibit the p53/MDM2 PPI was stapled with a divinyl triazine (DVT) linker between *i,i*+7 positions (A, Scheme 4), and the cyclic peptide showed improved serum stability and increased α-helicity compared to a linear analogue. In addition to this, fluorescence polarisation showed that the Cys-DVT stapling gave K_i = 13 ± 0.7 nM, around a 60-fold increase in binding affinity compared to literature values for the wild-type p53 peptide (K_i = 821 ± 56 nM).[23] The same peptide was stapled with a FITC-functionalised divinylpyrimidine (DVP) linker, and a polyarginine CPP was appended to the macrocyclic peptide *via* CuAAC (B, Scheme 4).[69] Confocal microscopy of the resulting stapled peptide, Pep-FITC-RRR, confirmed uptake by U2OS cells, whereas an analogue lacking the polyarginine CPP was not cell permeable.

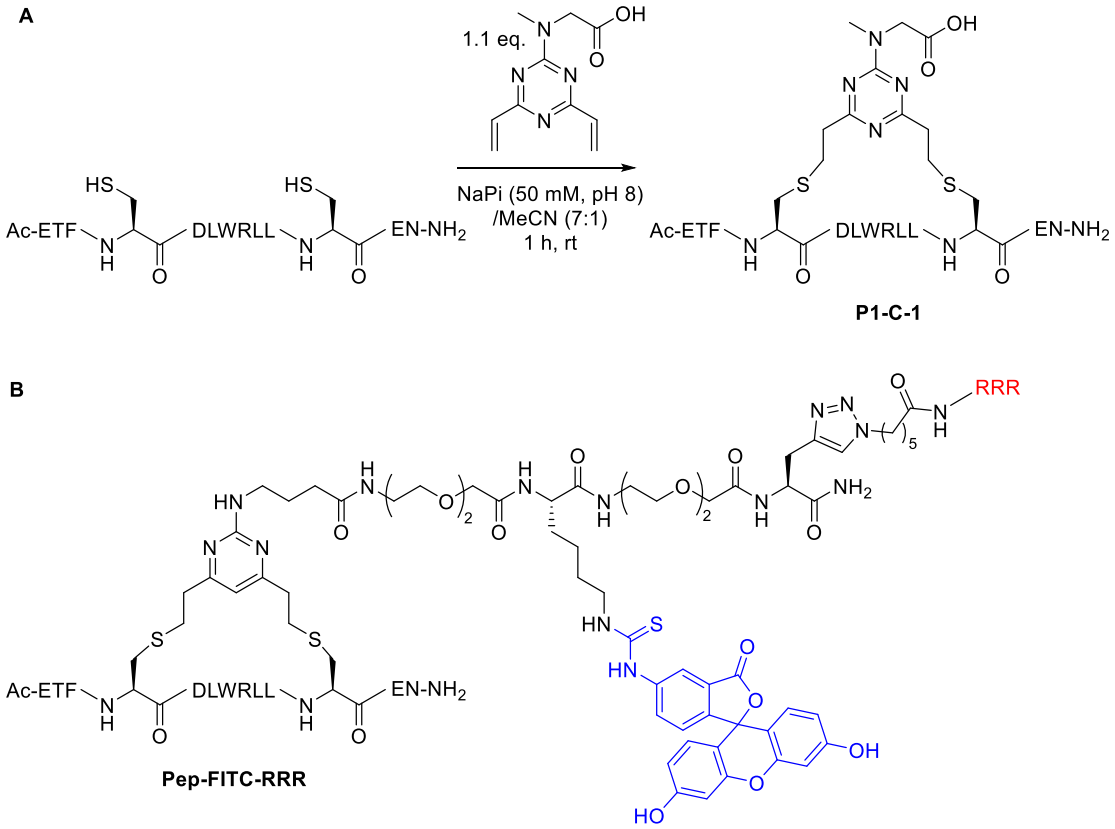

Scheme 4 The Cys-DVH stapling of a p53/MDM2 peptide. A) The literature stapling conditions to give an unfunctionalised DVT stapled peptide reported by Robertson et al.[67]and B) The structure of a dual-functionalised DVP stapled peptide reported by Walsh et al.[69] The CPP is highlighted in red and FITC in blue.

Finally, peptide macrocyclisation strategies have been reported which use palladium-mediated arylation of cysteine. The groups of Pentelute and Buchwald published a two-component cysteine arylation using bis-palladium(II) aryl complexes (Figure 10).[70–72]

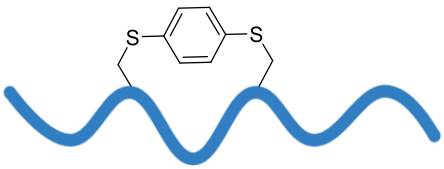

Figure 10 A cartoon depicting peptide macrocyclisation via the palladium-mediated arylation of Cys residues.[70–72] *The peptide is represented by a blue line.*

1.2.1.2.3 Two-component peptide stapling using lysine

After cysteine, lysine is the next most common amino acid residue for use in peptide stapling, due to the high nucleophilicity of the ε-amino group. One of the earliest two-component stapling methodologies was published by Phelan and co-workers in 1997.[28] They prepared macrocyclic peptides *via* a double lactamisation with two glutamic acid residues and a bis-amino linker, however, this required an orthogonal protection strategy and often lead to the formation of significant side-products (A, Figure 11). This methodology was employed by Fujimoto *et al*. to investigate the effect of different staple lengths and rigidities on the helicity of the resulting macrocyclic peptides (B, Figure 11).[73] There are several two-component stapling technologies which use a combination of different strategies. A recent example was published by the groups of Pentelute and Buchwald, wherein an initial palladium-mediated Cys arylation introduces a phenyl carbamate, which then reacts with a lysine residue to give the cross-linked peptide (C, Figure 11).[74]

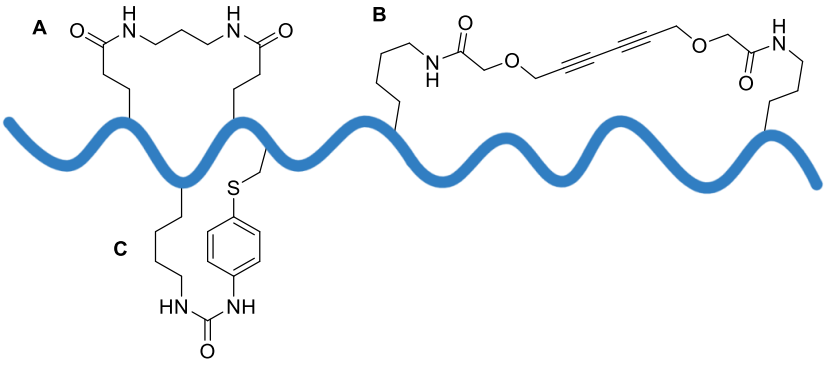

Figure 11 A cartoon depicting the peptide stapling methodologies which incorporate lysine residues. A) Peptide stapling via lactamisation between Glu residues with a bis-amino linker,[28] *B) stapling between Lys residues with a bis-carboxylic acid linker,*[73] *C) peptide stapling via Cys arylation and subsequent cyclic urea formation.*[74] *The peptide is represented by a blue line.*

1.2.1.2.4 Two-component peptide stapling using other amino acids

Tryptophan is the only other canonical amino acid for which there is a published two-component stapling methodology. Johannes and co-workers reported a condensation reaction between two Trp residues and an aryl aldehyde yielding a macrocyclic peptide (Figure 12).[75]

This method has the potential to allow functionalisation of the cyclic peptide, by modification of the aryl bromide.

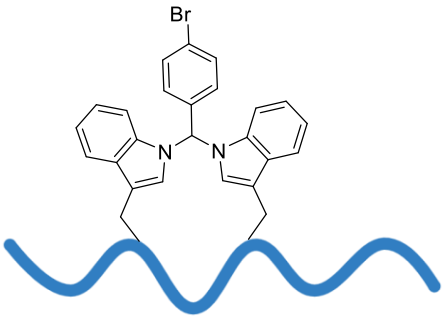

Figure 12 A cartoon depicting the condensation reaction between two Trp residues and an aryl aldehyde.[75]

1.2.1.3 Functionalised two-component stapled peptides

Two-component peptide stapling allows the facile appendage of tags (e.g. fluorescent dyes) to the staple itself. The advantages of this approach are two-fold: placing the functionality on the staple (rather than the *N*- or *C*-terminus of peptide) distances this added group from the interacting region of the peptide, thus making it less likely to negatively impact binding. Additionally, from one peptide sequence, different analogues can be rapidly produced by performing parallel stapling reactions with different linkers (Figure 13).

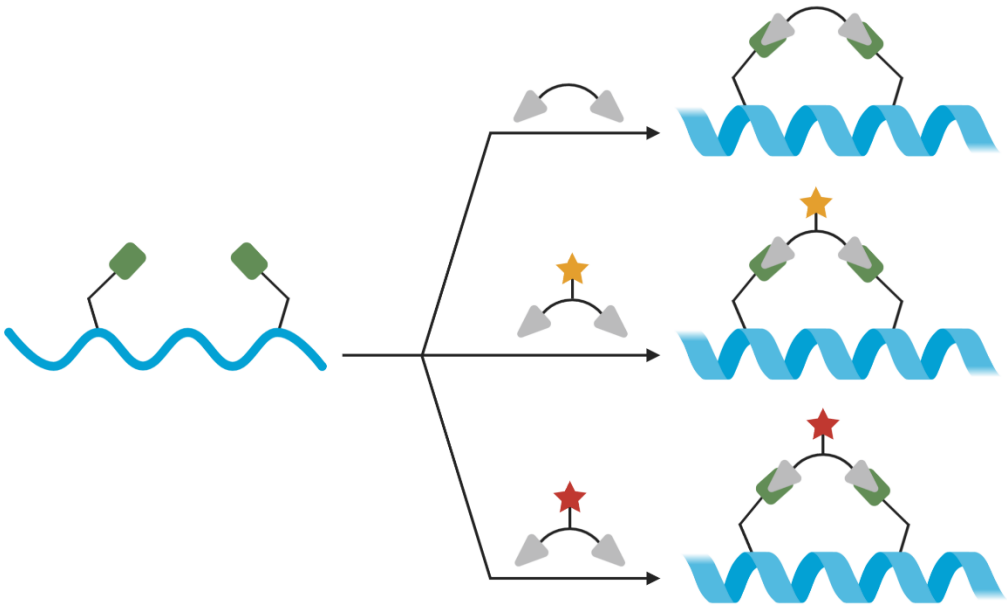

Figure 13 A cartoon showing the ease of functionalisation for two-component stapled peptides: from one linear peptide sequence a library of stapled analogues can be rapidly constructed using different linkers. The peptide is shown as a blue line or helix, amino acid side chains as green rectangles and the reactive handles on the linker as grey triangles. Functionality on the linker is shown as either yellow or red stars.

The ability to easily add functionality to peptides is particularly relevant in the development of biologically active peptides, which frequently require modification if they are to be studied *via*

biochemical assays: for example the attachment of fluorescent tags onto peptides is often required to track their cellular localisation. The ease with which this can be performed was demonstrated by Lau *et al.*, who appended a TAMRA dye onto a p53 peptide *via* two-component CuAAC stapling (A, Figure 14).[23] In the literature there are many other examples of fluorescently-labelled stapled peptides where the dye has been appended *via* stapling.[59,76]

Whilst there are some examples in the literature of stapled peptides exhibiting cell penetration, it is not the case that stapling a peptide will always confer cellular penetration.[18] Therefore, a growing area of research includes the appendage of cell penetrating peptides (CPPs) to biologically-active peptides to improve their cellular penetration.[23,77,78] An illustrative example from Dawson and co-workers consists of a polyarginine CPP appended to a model peptide using Cys-DCA stapling (B, Figure 14).[59] Iegre *et al.* achieved dual functionalisation of a two-component CuAAC stapled peptide targeting the protein kinase CK2. Both a polyarginine CPP and FITC label were introduced on the staple linker (C, Figure 14), resulting in a cell-permeable stapled peptide which was significantly more stable in serum than a linear analogue.[25] This example illustrates the utility of two-component peptide stapling for developing useful chemical tools and therapeutics.

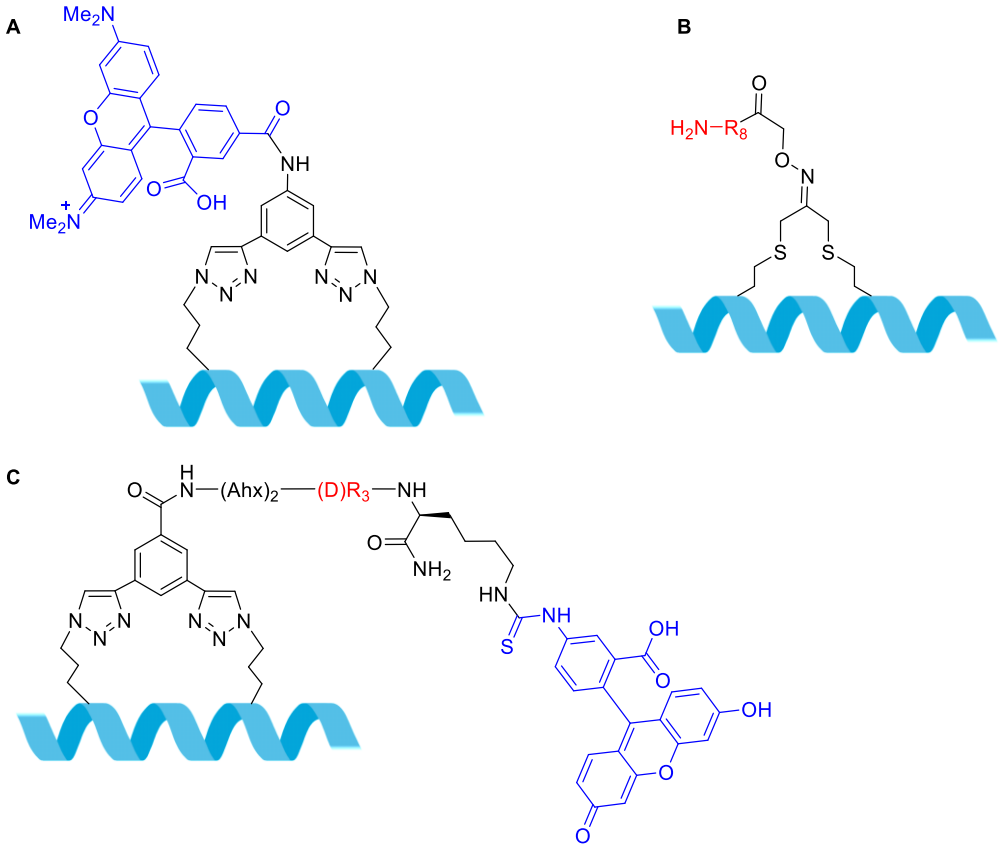

Figure 14 Selected examples of functionalised two-component stapled peptides. A: The fluorescent tag TAMRA (blue) introduced via CuAAC stapling.[23] B: Polyarginine CPP (red) introduced via DCA stapling.[59] C: Dual-functionalisation wherein both a polyarginine CPP (red) and fluorescent tag FITC (blue) are introduced via CuAAC stapling.[25] Peptide is shown as a blue helix.

The appendage of affinity tags to biologically active molecules allows the study of their interactions, as well as their isolation from complex mixtures. Dawson *et al*. introduced biotin, a streptavidin-affinity tag, to a model peptide using DCA stapling and oxime functionalisation (A, Figure 15).[59] Photoaffinity tags (e.g. the benzophenone moiety) form covalent bonds with biomolecules upon exposure to UV light, and have previously been incorporated into stapled peptides by the introduction of a benzophenone-containing unnatural amino acid.[79] However, this approach has several disadvantages: the reactive moiety could negatively affect the peptide binding and investigating different photoaffinity motifs would require the synthesis of multiple different unnatural amino acids and peptides. Introducing the photoaffinity motif *via* peptide stapling circumvents these issues, and was demonstrated by Wu *et al*., who synthesised a p53 CuAAC-stapled peptide bearing a benzophenone photoaffinity motif on the peptide staple (B, Figure 15).[24]

In the same way, the introduction of an electrophilic motif to a stapled peptide to give a covalent inhibitor can be achieved through the introduction of an unnatural amino acid bearing the reactive moiety.[80] However, for the same reasons as discussed above, it is beneficial to introduce the functionality away from the peptide sequence. Charoenpattarapreeda *et al.* demonstrated this, introducing an electrophilic moiety to a p53 peptide *via* two-component CuAAC stapling (C, Figure 15).[81]

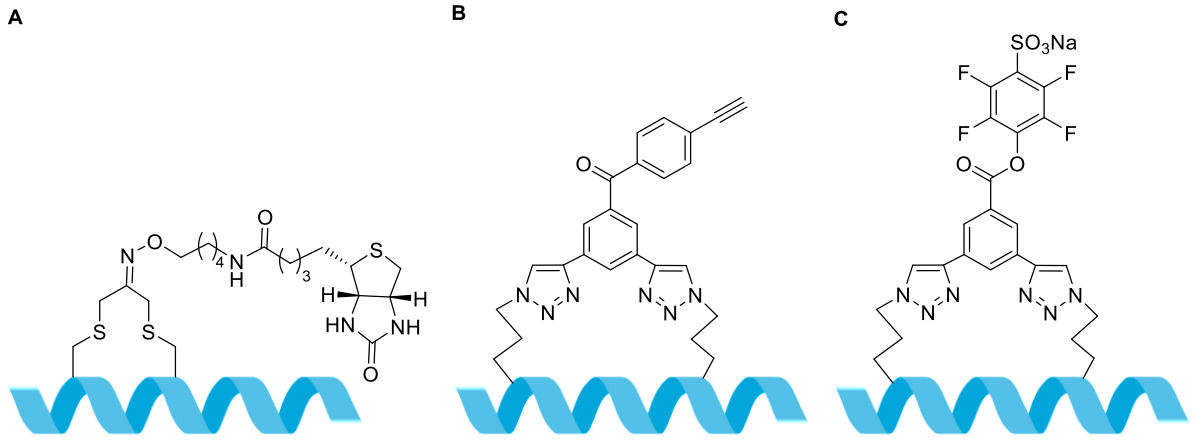

Figure 15 Examples of functionality that can be added via the staple; A) an affinity probe, biotin, introduced via DCA stapling,[59] B) a benzophenone photoaffinity probe introduced via CuAAC,[24] and C) an electrophilic motif introduced via CuAAC.[81] Peptide is shown as a blue helix.

1.3 Sources of biologically active cyclic peptides

Biologically active peptides can be sourced from nature, biological and chemical library construction, and structure-based design. Each of these approaches will be discussed in this section, highlighting notable peptides which have been discovered using each method.

1.3.1 Cyclic peptides from natural sources

Nature provides a vast repertoire of biologically active peptides with different structures and functions. For example, mammals produce peptide hormones such as insulin and somatostatin,[2] and many organisms, including insects and bacteria, produce peptides with antimicrobial activity.[82] These natural peptides have served as the inspiration for many marketed peptide therapeutics, including oxytocin, a natural-hormone used to induce labour,[83] and the antimicrobial colistin (Figure 16). Both of these drugs have been designated essential medicines by the World Health Organisation (WHO).[84]

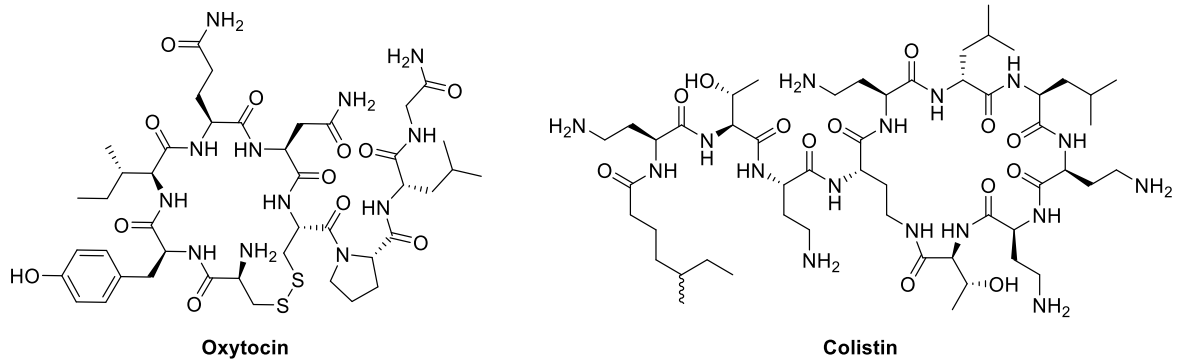

Figure 16 The structure of oxytocin, a drug derived from a natural peptide hormone, and colistin, a marketed antimicrobial peptide which is a natural product first isolated from bacteria.

1.3.2 Cyclic peptides from library screening

An important approach to identifying target-binding peptides is the screening of chemical libraries. In particular, genetically-encoded libraries (GELs) represent an extremely powerful method for peptide discovery as vast libraries of high diversity can be rapidly generated and screened.[85] There are several approaches to the construction of GELs:

- DNA-encoded libraries (DELs)
- mRNA display
- Phage display
- Split-intein circular ligation of peptides and proteins (SICLOPPS)

Synthetic DELs can be prepared in a combinatorial manner, wherein each peptide is covalently attached to a DNA ‘barcode’ containing genetic information relevant to the amino acid sequence.[86] Whilst these libraries are relatively cheap and easy to prepare, the possible synthetic transformations are limited to those which are compatible with DNA.[87]

DELs, phage display and mRNA display libraries share similar screening procedures: once synthesised, the peptides remain covalently attached to their coding entity and are screened

against an immobilised protein target to identify active binders. The peptide sequence and structure can be determined by sequencing the attached genetic information. These methods all, therefore, share the potential disadvantage that the affinity of the peptide may be negatively affected by the presence of the large encoding moiety.

mRNA display involves *in vitro* translation and transcription, thus avoiding the dependency of peptide synthesis on *E. coli* transformation (Figure 17). The Suga group developed *de novo* ribozymes, named the 'Flexizyme' technology, which enable the incorporation of unnatural amino acids into a growing peptide chain.[88] The result of mRNA display is a library of peptides linked to their encoding mRNA strand *via* a puromycin linker. Cyclisation can occur by the incorporation of an *N*-chloroacetyl group and subsequent reaction with a cysteine residue in the peptide to form a thioether linkage (Figure 17),[89] although several other cyclisation techniques have also been reported.[90]

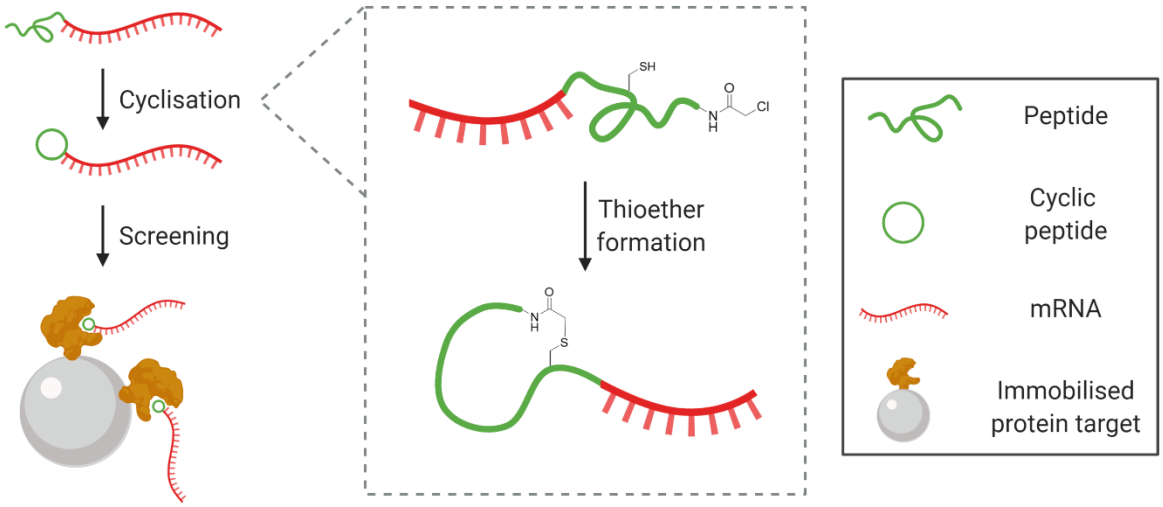

Figure 17 A cartoon depicting mRNA display for the screening of cyclic peptides. The linear peptide is attached to an encoding mRNA strand and then cyclised in situ, often via thioether formation (inset). The cyclic peptide is then screened against an immobilised protein target.

During phage display library construction, bacteriophages are engineered to produce and 'display' peptides on their surface (Figure 18). Among many different cyclisation methods,[90] the most common and straightforward include disulfide formation,[91] or cysteine alkylation using the proprietary CLIPS technology which was developed by Timmerman and applied to phage display by Heinis and Winter (Figure 18).[49,54]

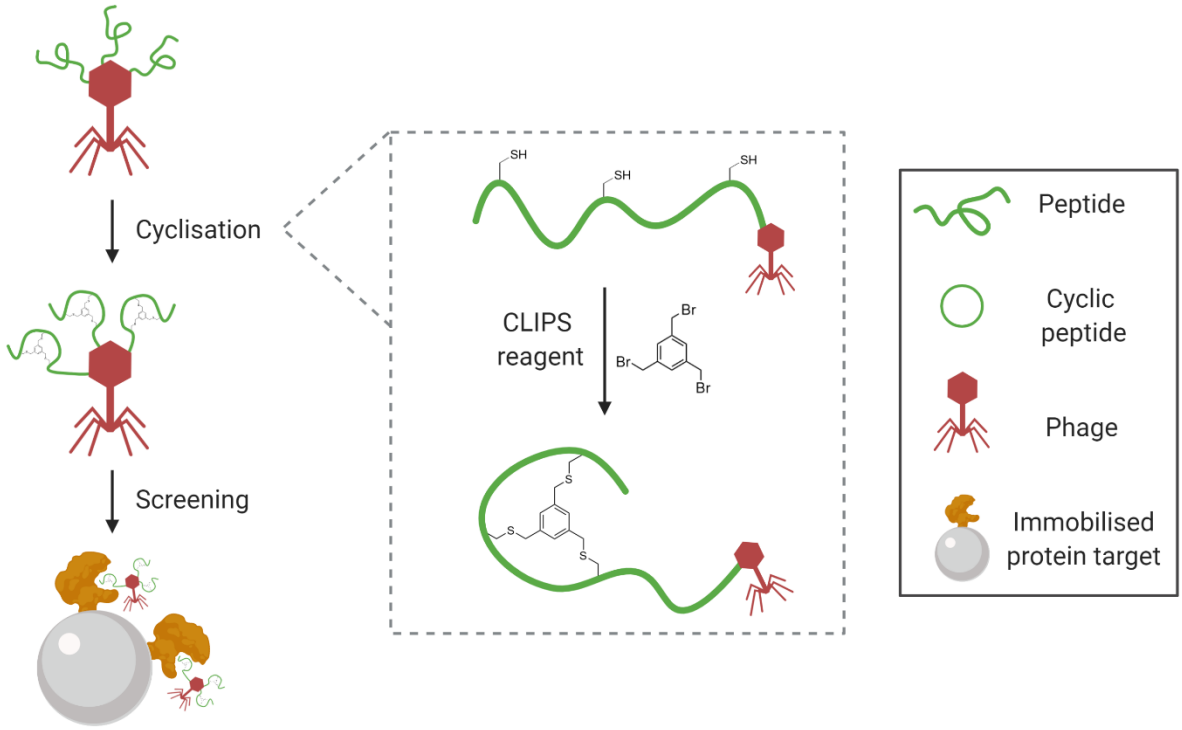

Figure 18 A cartoon depicting peptide screening via phage display, wherein bacteriophages are engineered to display a peptide on their surface. Peptide macrocyclisation can occur via alkylation of cysteine residues with CLIPS reagents (inset), and screening is performed using immobilised protein targets.

Tavassoli and co-workers have developed an alternative approach, SICLOPPS, wherein protein splicing is manipulated for cyclic peptide production.[92] Plasmids are engineered which code for the desired peptide sequence, flanked by two self-excising intein domains (the 'split intein'). After translation, the desired peptide is spliced and cyclised head-to-tail; a process which can be performed in yeast, bacterial and human cells (Figure 19).[93] To identify active PPI inhibitors, SICLOPPS is frequently combined with a Reverse Two-Hybrid System (RTHS) in genetically-engineered *E. coli*. The bacteria are dependent on the disruption of the target PPI for survival, so when effective cyclic peptide inhibitors are produced *via* SICLOPPS, the PPI is disrupted or inhibited, allowing the RTHS bacteria to survive and grow.[94] The SICLOPPS/RTHS approach allows the identification of cyclic peptides by the desired phenotype, rather than affinity data.[85]

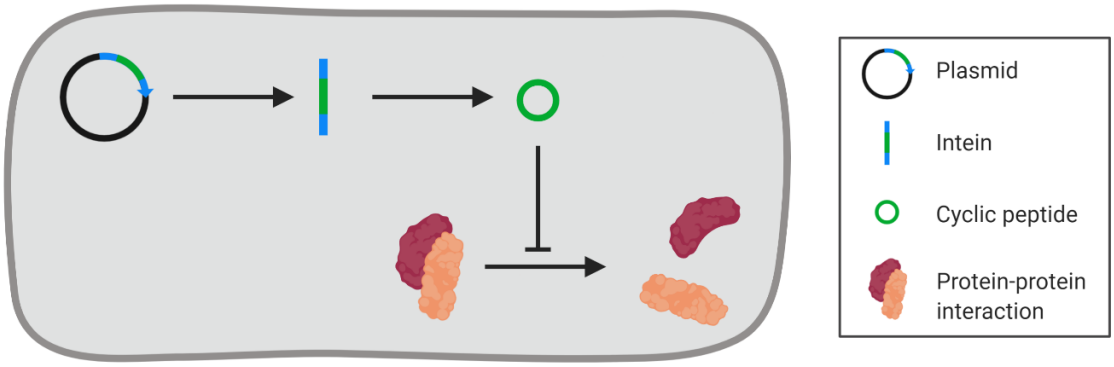

Figure 19 A schematic overview of SICLOPPS approach to cyclic peptide production and screening. A library of SICLOPPS plasmids are produced, which code for the peptide of interest. Splicing of the desired sequence from the split-intein gives cyclic peptides. Combining SICLOPPS with a RTHS allows the identification of PPI inhibitors in an intracellular environment based on functional data.

The methods of discovering biologically active cyclic peptides discussed in this section are extremely powerful; each method has distinct advantages and disadvantages, which are summarised in Table 3.

Table 3 An overview of some library-based approaches of discovering therapeutic cyclic peptides. Adapted from Sohrabi et al.[85] and Taylor et al.[95]

Method	***Library size/diversity†***	***Advantages***	***Limitations***
SICLOPPS	10^6-10^9	Functional assay data	Library size dependent on transformation of host Limited to natural amino acids Generally lower affinity
Phage display	10^8-10^{10}	Practically simple; commercial kits available High-affinity (nM) peptides can be identified	Diversity limited by transformation efficiency of the host Screening with peptide linked to bacteriophage; can affect binding affinity
mRNA display	10^{12}	*In vitro*; no limitation on library size due to transformation efficiency Multiple unnatural amino acids can be incorporated	Screening with peptide linked to large mRNA strand; can affect binding affinity

†SICLOPPS: Lower estimate (for hexamers) from Valeur *et al.*,[94] upper estimate from Sohrabi *et al.*,[85] Phage display: lower estimate from Sohrabi *et al.*,[85] upper estimate from Passioura and Suga.[89]

In the last two decades, several drug-discovery companies have been founded based on these technologies.[41] One example is Bicycle Therapeutics, who employ phage display and the CLIPS cyclisation technology to discover therapeutic macrocyclic peptides, bicyclic peptides and peptide-drug conjugates (PDCs).[96] Similarly, PeptiDream was founded by Hiroaki Suga to develop cyclic peptides using mRNA display techniques and the previously described

Flexizyme technology. Most recently, Curve Therapeutics was founded by Ali Tavassoli to develop cyclic peptide PPI inhibitors using SICLOPPS technique.[85] There are five peptides in the clinic which were first synthesised and identified using display techniques,[97] as well as three PDCs which will be discussed in Chapter 3.

1.3.3 Cyclic peptides from structure-based design

If significant structural information about the target is available (e.g. X-ray crystallography data) then peptides can be rationally designed with the assistance of *in silico* experiments. This approach is often adopted for the design of peptides to inhibit well-characterised PPIs, as the starting peptide sequence can often be derived from the protein-binding epitopes.[15] Computational experiments such as alanine scanning can determine key interactions and, along with molecular dynamics, this can guide the design of peptidomimetics.[98] A key example of a peptide developed by structure-based design is ALRN-6924, an RCM stapled peptide PPI inhibitor targeting the HDM2/p53 PPI. ALRN-6924 is currently in Phase I/II clinical trials for patients with solid tumours or lymphoma (due for completion in 2020)[99] and represents one of the very first stapled peptides to enter clinical trials.[94]

1.4 Cyclic peptides on the market

The presence of multiple cyclic peptides on the market demonstrates the success of macrocyclisation as a strategy for realising their therapeutic potential. Cyclic peptides account for 14 of the 60 marketed peptide drugs (Table 4), all of which are either natural products, or analogues of natural products.

Table 4 An overview of selected marketed cyclic peptide drugs and their key features. Information from Choi and Joo,[100] Lau and Dunn,[2] and Baeriswyl and Heinis.[101] NP = natural product, source given in brackets. IBS = irritable bowel syndrome. Some endogenous peptide hormones such as vasopressin and oxytocin have been excluded.

	Peptide	Use	Type of macrocycle	First clinical use	Source	Administration route
1	Bacitracin	Antibiotic	*C*-terminus to side chain	1948	NP (Bacteria)	Topical
2	Vancomycin	Antibiotic	Polycyclic	1954	NP (Soil bacteria)	Injection
3	Colistin	Antibiotic	*C*-terminus to side chain	1959	NP (Bacteria)	Topical, injection
4	Dactinomycin	Anticancer	Bicyclic	1964	NP (Soil bacteria)	Injection
5	Cyclosporine A	Immuno-suppressant	Head-to-tail	1983	NP (Fungus)	Topical injection, oral
6	Octreotide	Anticancer	Disulfide	1988	Synthetic (NP analogue)	Injection
7	Eptifibatide	Antiplatelet	Disulfide	1998	Synthetic (NP analogue)	Injection
8	Caspofungin	Antifungal	Head-to-tail	2001	Synthetic (NP analogue)	Injection
9	Ziconotide	Analgesic	Polycyclic	2004	Synthetic (NP analogue)	Intrathecal injection
10	Anidulafungin	Antifungal	Head-to-tail	2006	Synthetic (NP analogue)	Injection
11	Lanreotide	Anticancer	Disulfide	2007	Synthetic (NP analogue)	Injection
12	Romidepsin	Anticancer	Polycyclic	2009	NP (Soil bacteria)	Intravenous
13	Linaclotide	IBS, chronic idiopathic constipation	Multiple disulfide bonds	2012	Synthetic (NP analogue)	Oral
14	Bremelanotide	Treatment of low sexual desire	Lactam (side chain-side chain)	2019	Synthetic (NP analogue)	Injection

Focusing on stapled peptides, bremelanotide is a cyclic analogue of α-melanocyte-stimulating hormone and is currently the only marketed stapled peptide, prescribed for the treatment of low sexual desire.[102] Bremelanotide contains a one-component lactam bridge between a lysine and aspartic acid (Figure 20).[103]

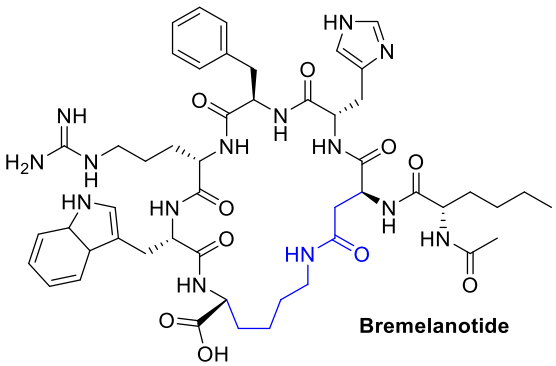

Figure 20 The structure of marketed peptide Bremelanotide, featuring a lactam bridge between a lysine and aspartic acid residue, highlighted in blue.

There are two RCM stapled peptides that have entered clinical trials, both developed by Aileron Therapeutics. ALRN-5281 is an agonist of growth hormone-releasing factor, developed to treat adult endocrine disorders. It was the first stapled peptide to be tested in the clinic, and a Phase I safety trial was completed in 2013, although no further clinical trials have been reported since.[104] ALRN-6924, an HDM2/p53 PPI inhibitor was discussed previously (Section 1.3.3). These are both the first stapled peptides and the first peptides produced *via* structure-guided design to enter clinical trials.

There are currently three chemotherapeutic peptide-drug conjugates in clinical trials, all of which contain bicyclic stapled peptides. These PDCs were developed by Bicycle Therapeutics and, for each, the peptide was identified by phage display and cyclised with CLIPS reagents.[105] A cytotoxin has been attached to each peptide *via* a cleavable linker; these PDCs will be discussed in more detail in Chapter 3.

It is clear from the presence of over 60 marketed peptides that they have an important role in the therapeutic landscape, providing a wider repertoire of accessible targets and therefore allowing the treatment of a wider range of diseases. Stapling is an enabling technology for therapeutic peptides, addressing their short-comings and providing an opportunity to modulate their properties. As it has been outlined in this introduction, the functionalisation of two-component stapled peptides provides a straightforward method of attaching moieties that can greatly improve their therapeutic potential.

Chapter 2

The development of stapled peptides as chemical tools to investigate protein-protein interactions in human platelets

2. Chapter 2 - The development of stapled peptides as chemical tools to investigate protein-protein interactions in human platelets

2.1 Introduction

2.1.1 Protein-protein interactions as drug targets

Biological systems in the body are governed by a complex network of protein-protein interactions (PPIs), known collectively as the interactome.[3] PPIs can be very important in disease states, thus providing a wealth of possibilities for the research of these diseases and the development of therapeutics. They can be divided into different structural classes, which include the interactions between two globular proteins or between a globular protein and a peptide (A and B respectively, Figure 21).

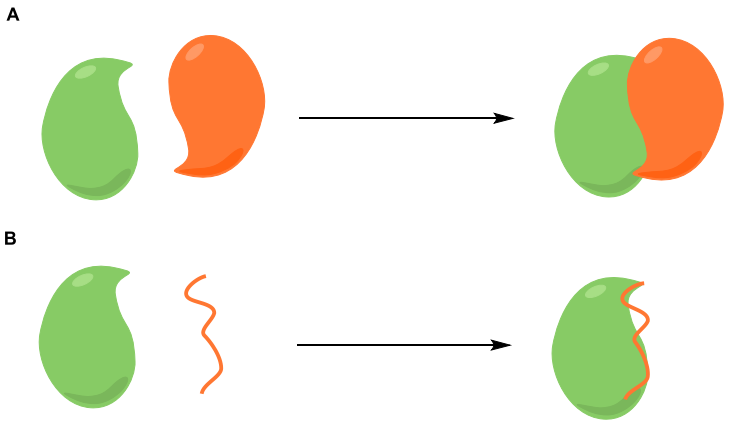

Figure 21 A schematic diagram of two classes of PPIs: A) the interaction between two globular proteins (green and orange) and B) the interaction between a globular protein (green) and a peptide (orange).

Compared to a deep, well-defined binding pocket, PPIs have vastly different compositions and topographies. They are typically large and shallow (surface area ~1,000-6,000 Å^2), and binding usually depends on key interactions, named 'hot spots', which can be spread out over a large area.[3] Historically, PPIs have been considered 'undruggable', meaning that for decades pharmaceutical research largely ignored a vast number of possible targets. Biologics, in particular antibodies, were amongst the first PPI inhibitors to be developed, although they are limited to extracellular PPIs.[106,107] Improvements in structural biology and *in silico* methods have allowed the structure-based design of small-molecule PPI inhibitors, examples of which will be discussed in Section 2.1.2.1.[108]

Peptides offer several advantages as PPI inhibitors; they are larger than small molecules and so can more easily span the interaction surface.[109] Unlike biologics, they are capable of cell penetration and therefore can be considered for intracellular PPIs.[110] Lastly, in some situations, peptide PPI inhibitors can be easily designed by mimicking one of the endogenous PPI binding partners. In particular, research has focused on the development of α-helical

peptides, as this is a key structural motif found in PPIs,[111] for example in the Bcl-2 family of proteins.

2.1.2 The Bcl-2 protein family

Apoptosis, or programmed cell death, is vital in many biological processes, such as the maintenance of certain cell populations or as a defence mechanism after cells are damaged by disease.[112] Inappropriate apoptosis events are central to many diseases, for example neurodegenerative diseases and cancer. In nucleated mammalian cells, there are two distinct pathways to apoptosis, the extrinsic and intrinsic, which eventually converge.[112] Initiation of the extrinsic pathway involves the binding of ligands at cell-surface 'death receptors', whilst the intrinsic pathway depends on intracellular signalling due to cellular stresses such as DNA damage or oncogene activation.

The Bcl-2 protein family are vital apoptosis-regulating proteins of the intrinsic pathway in nucleated mammalian cells.[113] The Bcl-2 family includes pro-survival proteins Bcl-2, Bcl-x_L, Bcl-w, Mcl-1 and A1. It also includes pro-apoptotic proteins Bax and Bak, and the BH3-only proteins Bad, Bmf, Bim, Bid, Puma and Noxa. The BH3-only proteins are so named because they only share the Bcl-2 homology (BH) domain 3, whereas Bcl-2, Bcl-x_L, Bcl-w, Mcl-1 and A1 have multiple BH domains in common.[114] The BH3 domain is an amphipathic α-helix approximately 26 amino acids long, and it is through this motif that the BH3-only proteins bind to other members of the Bcl-2 protein family (an example is shown in Figure 22 of Bcl-x_L in complex with Bim).[113]

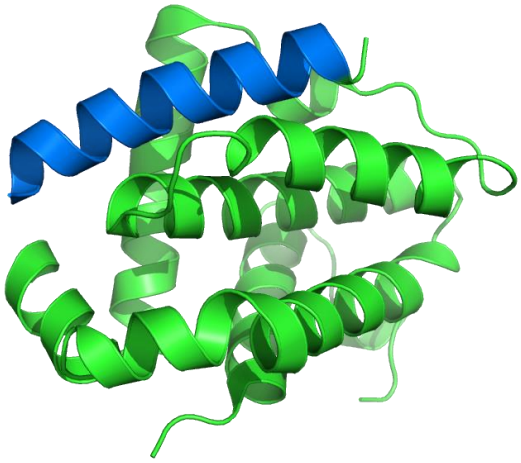

Figure 22 An X-ray crystal structure of Bcl-x_L in complex with Bim (residues 141-166). The α-helix of Bim is shown as a blue ribbon and Bcl-x_L in green. PDB: 4QVF.[115]

Under normal conditions, the pro-survival proteins sufficiently sequester Bak and Bax, promoting survival. When a cell is exposed to stress, the pro-apoptotic BH3-only proteins are induced; they can bind to and neutralise the pro-survival proteins or bind directly to pro-apoptotic Bax and Bak,[116] resulting in apoptosis *via* mitochondrial permeabilisation and subsequent cytochrome c release.[117] Each BH3-only protein has a different affinity for the pro-survival proteins, which is indicated in Figure 23. The exact nature of Bak and Bax activation by the BH3-only proteins is debated:[113] it has been proposed that some of the BH3-only proteins (Bim, Bid and Puma) are so-called 'activators' and bind directly to Bak and Bax, leading to apoptosis.[118] The other BH3-only proteins are 'sensitisers' which bind to complexes of pro-survival Bcl-2 proteins and cause the release of 'activator' BH3-only proteins, which are then free to bind to Bax and Bak.

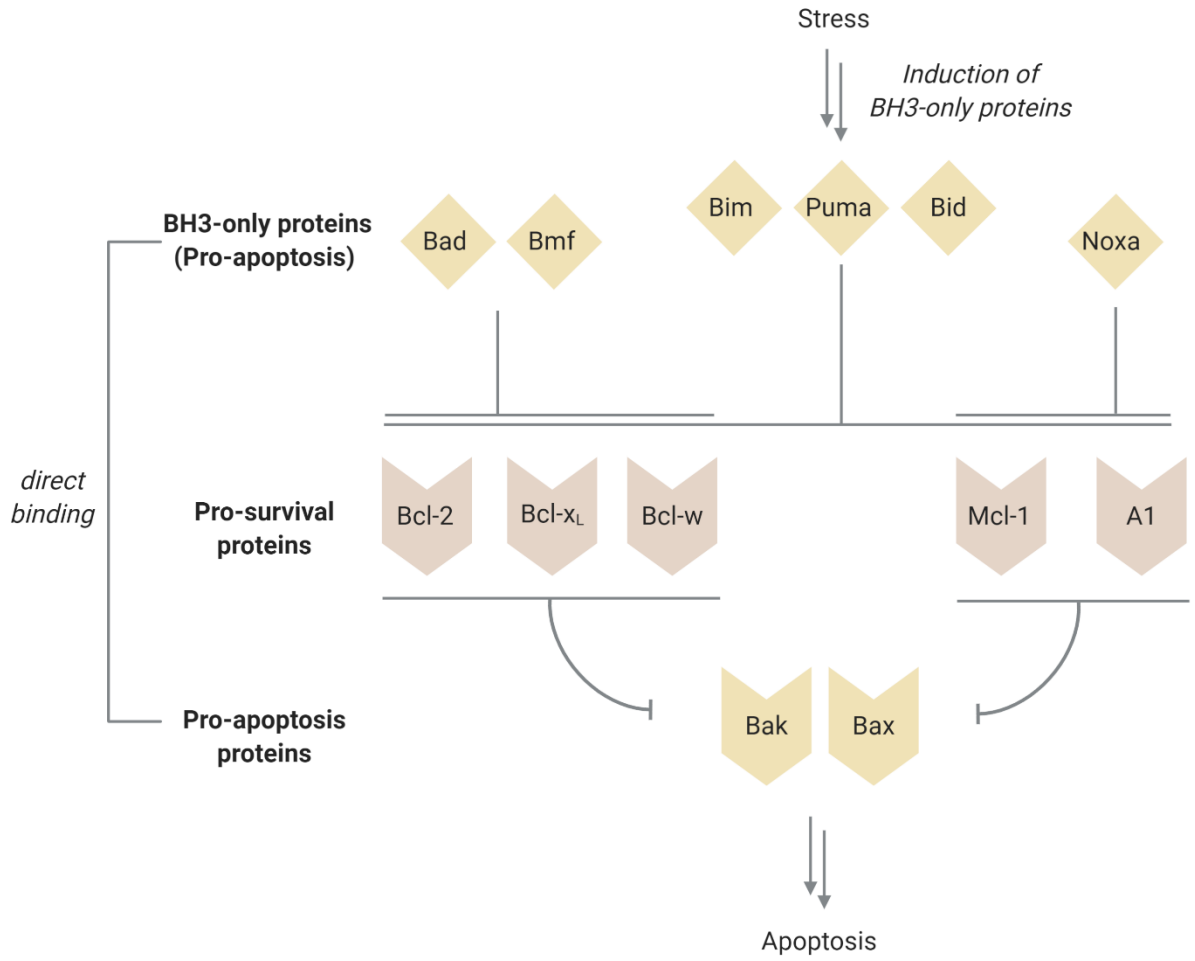

Figure 23 An overview of the Bcl-2 proteins and their role in the intrinsic pathway of apoptosis. The lines represent the specificities of the BH3-only proteins for the pro-survival proteins. Adapted from Happo et al.[113]

Abnormal expression of Bcl-2 proteins is found in many different cancers, and as the PPIs between the BH3-only and Bcl-2 proteins (referred to as 'BH3 PPIs' from herein) play a key role in modulating apoptosis, they have been identified as key targets for anti-cancer agents.[119,120]

2.1.2.1 Small molecule BH3 PPI inhibitors

Before significant structural information was obtained for the Bcl-2 proteins, biologics were considered as PPI inhibitors. Although antibodies lend themselves to successful inhibition of PPIs, the BH3 proteins are intracellular, and therefore cannot be accessed by these large biomolecules.[120] An alternative approach was trialled, employing oligonucleotides to target Bcl-2 mRNA.[121] Three such compounds entered clinical trials, one reaching phase III, however, it was not progressed further due to a lack of demonstrated therapeutic benefit.[122]

Many small-molecule inhibitors of the BH3 PPIs have been developed,[123] and those developed by Abbott Laboratories (now AbbVie) are amongst the first and most important to the field.[122] Research into small-molecule BH3 PPI inhibitors was initiated when the first X-ray crystal structures of Bcl-x_L and Bcl-2 complexes were published, providing structural data on the nature of the PPI binding interfaces.[124,125] A hydrophobic crevice was identified on the surface of Bcl-x_L and Bcl-2 (A, Figure 24), where the α-helical BH3 domain of BH3-only proteins and peptides bind (B, Figure 24).

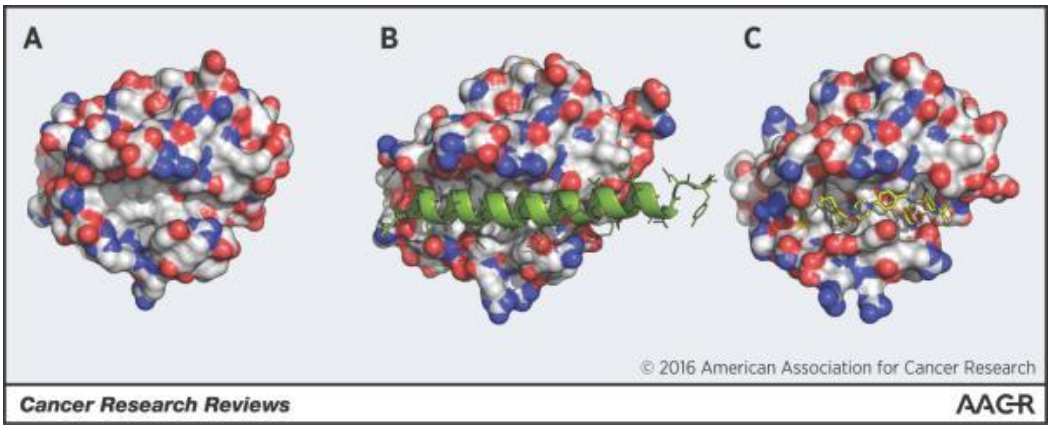

Figure 24 X-ray crystal structures of Bcl-2 proteins. A) The 3D structure of Bcl-x_L, showing the hydrophobic crevice on the front face which forms the PPI interface (PDB: 1MAZ). B) The structure of Bcl-x_L bound to a Bim peptide (green, PDB: 1PQ1). C) The structure of Bcl-2 bound to an analogue of ABT263 (PDB: 4MAN). The proteins are shown as a solvent-accessible surface with the following atom labelling: carbon, white; nitrogen, blue; oxygen, red; sulfur, yellow. Reprinted from Croce and Reed, copyright 2016, with permission from AACR.

A key challenge of developing small-molecule BH3 PPI inhibitors with 'drug-like' properties was the large size of the PPI interface. A novel chemical fragment screening approach using solution NMR was employed to determine fragment binding to Bcl-2 proteins,[126] and this discovery campaign lead to the identification of ABT737, a potent antagonist of Bcl-2, Bcl-w and Bcl-x_L, which represents the first example of a BH3 protein-mimicking drug.[120,127] X-ray crystal structures confirmed that ABT737 bound in the same hydrophobic crevice on Bcl-2 as the native Bim peptide (C, Figure 24).

Despite causing complete regression of tumours in animal models, ABT737 was not orally bioavailable, so ABT263 (Navitoclax) was developed as an orally-bioavailable analogue and

was progressed to phase I clinical trials; however, a mechanism-based side-effect of thrombocytopaenia was observed.[128,129] As both ABT737 and ABT263 were non-selective Bcl-2 inhibitors, ABT199 (Venetoclax) was developed by structure-based design as a selective Bcl-2 inhibitor to avoid this adverse side-effect and improve the oral availability. Venetoclax was approved by the US Food and Drug Administration (FDA) in 2016 for the treatment of chronic lymphocytic leukaemia and small lymphocytic lymphoma (Table 5).[130,131]

Table 5 The structures of ABT737, ABT263 and ABT199 and their affinity for selected Bcl-2 proteins. Adapted from Vogler et al.[120] and Souers et al.[130] ND = no data.

Compound	Structure	K_i (nM)				
		Bcl-2	Bcl-x_L	Mcl-1	Bcl-w	Bcl2-A1
ABT737	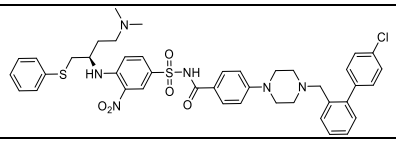	120	64	<20,000	24	<20,000
ABT263	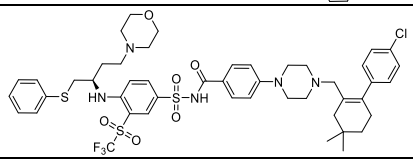	<1	<0.5	550	<1	354
ABT199	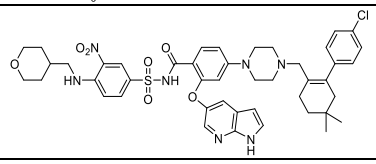	< 0.01	48	ND	245	ND

2.1.2.2 Stapled peptide BH3 PPI inhibitors

As previously discussed, peptides can be better suited to targeting PPIs and have been employed as successful PPI inhibitors against Bcl-2 protein family members.[18] An overview of stapled peptides of particular relevance to this thesis is given in Table 6. These peptides are predominantly based on RCM stapling, with one example of two-component stapling reported: a Bim BH3-only peptide which was stapled using the perfluoroaryl macrocyclisation approach published by Pentelute and co-workers.[62,132]

*Table 6 The sequences of selected stapled peptide PPI inhibitors of BH3-only proteins and comments on their biological activity and uses. Adapted from Walensky and Bird.[25] * denotes a two-component stapled peptide. All other peptides are RCM stapled. Residues used for stapling shown in bold, X = non-canonical alkene-bearing amino acid, N_L = norleucine.*

Protein	Sequence	Comments on biological activity	Ref.
Noxa	QPSPAEAPAELEVECATQLR**X**FGD**X**LNFRQ	Employed as a chemical tool to study conformation changes of Bak upon activation.	133
	LEVESATQLR**X**FGD**X**LNFRQKL	High-affinity Mcl-1 ligand (K_d 22 ± 12 nM).	134
Bim	IWIAQELR**X**IGD**X**FNAYYARR	High-affinity Mcl-1 ligand (K_d 17 ± 8 nM).	135,134,136
	IWIAQELR**C**IGD**C**FNAYYARR*	Perfluoroaryl analogues displayed improved brain penetration compared to alkyl analogue *in vivo*.	62,132
	EIWIAQELR**X**IGD**X**FNAYYA	Selective chemical tool used to elucidate a novel binding site on Bax for direct activation.	137
Puma	EQWAREIGAQLR**X**N_LAD**X**LNAQYE	High-affinity Bcl-x_L ligand (K_d 12 ± 1.2 nM). Induces apoptosis in neuroblastoma.	138
	QWAREIGAQLR**X**GAD**X**LNAQY	High-affinity Mcl-1 ligand (K_d 14 ± 5 nM).	134
Bid	DIIRNIARHLA**X**VGD**X**N_LDRSI	High-affinity Bax and Bcl-2 ligand (EC_{50} 885 and 230 nM respectively).	139
	FITC-EIIHNIARHLA**X**IGD**X**N_LDHNIQ	High-affinity Bak-binder (K_d 95 ± 15 nM). Chemical tool used to reveal that Bak and Bax are activated by direct BH3 interaction at different binding sites.	140
	EDIIRNIARHLA**X**VGD**X**N_LDRSI	Selective chemical tool used to study conformation changes of Bak upon activation.	133
	DIIRNIARHLA**X**VGD**X**N_LDRSIRR	High-affinity Mcl-1 ligand (K_d 50 ± 8 nM).	134
	EDIIRNIARHLA**X**VGD**X**NLDRSIW	Inhibited the growth of human leukaemia xenografts *in vivo*.	141

Whilst none of these peptides have yet entered the clinic, some have served as invaluable chemical tools for the discovery of selective small-molecule Bcl-2 inhibitors.[142] Walensky and co-workers found that a stapled peptide based on the sequence of the Mcl-1 BH3 α-helix bound with high affinity to the Mcl-1 protein (A, Figure 25). Using this, the group developed a screening platform for the identification of small-molecule Mcl-1 antagonists.[143] Through this platform they identified and validified MIM1, a potent and selective small-molecule Mcl-1 antagonist which was able to prevent Mcl-1-mediated suppression of the pro-apoptotic Bax protein (B, Figure 25). In an Mcl-1-dependent leukaemia cell line, MIM1 caused caspase activation and cell death.

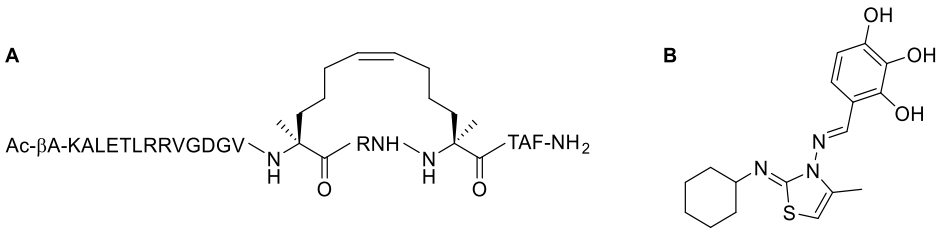

Figure 25 A) The structure of the Mcl-1 RCM stapled peptide, developed by Walensky and co-workers and used to identify Mcl-1 antagonists.[143] B) The structure of MIM1, a selective Mcl-1 antagonist identified using the stapled peptide screening platform. βA = β-alanine.

2.1.3 Platelets and haemostasis

When vascular injury occurs, a complex signalling pathway is initiated which ultimately results in the formation of a blood clot (or thrombus). This process is called haemostasis and it is dependent on the activity of sub-endothelial proteins such as collagen and von Willebrand factor (VWF), as well as platelets, small blood cells which play a critical role in several stages of haemostasis.[144] Platelets circulate in a resting state (A, Figure 26) and to enact their primary role of thrombus formation in response to blood vessel damage they must become activated (B, Figure 26).[145] Activation describes a series of phenotypic and morphological changes which occur in resting platelets upon exposure to certain stimuli. Platelet activation is known as primary haemostasis and it occurs simultaneously with coagulation events (known as secondary haemostasis); together the two systems form a thrombus (a blood clot).[146]

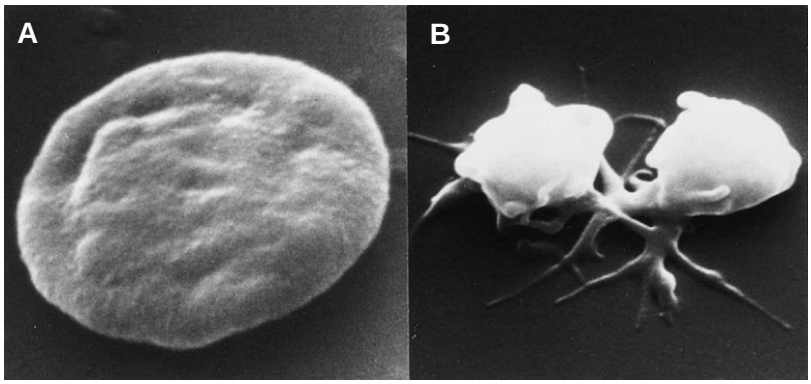

Figure 26 Scanning electron micrographs of (A) a resting platelet and (B) activated platelets. Reprinted from The Lancet, Vol. 355, J. George, Platelets, 1531-1539, © 2020 with permission from Elsevier.

Platelets aggregate at the site of blood vessel damage, where pro-thrombotic species (such as VWF, collagen and fibrinogen) have become exposed in the vascular wall and provide an adhesive surface through interactions with specific integrins expressed on the platelet membrane, namely GPIIb/IIIa, GPIb and GPVI (A, Figure 27).[144] Platelets are subsequently activated, which leads to the formation of a thrombotic plug (B, Figure 27). The formation of the thrombotic plug occurs in several stages; the first stage is primary reversible adhesion wherein the platelets aggregate with each other and to the vascular wall. Following this, the initial plug grows and is stabilised. Blood vessel damage also initiates the coagulation cascade, causing coagulation events (secondary haemostasis). This results in the conversion of prothrombin to active thrombin, itself converting soluble fibrinogen into fibrin. Fibrin forms a fibrous mesh which is a vital component of thrombus formation (C, Figure 27).

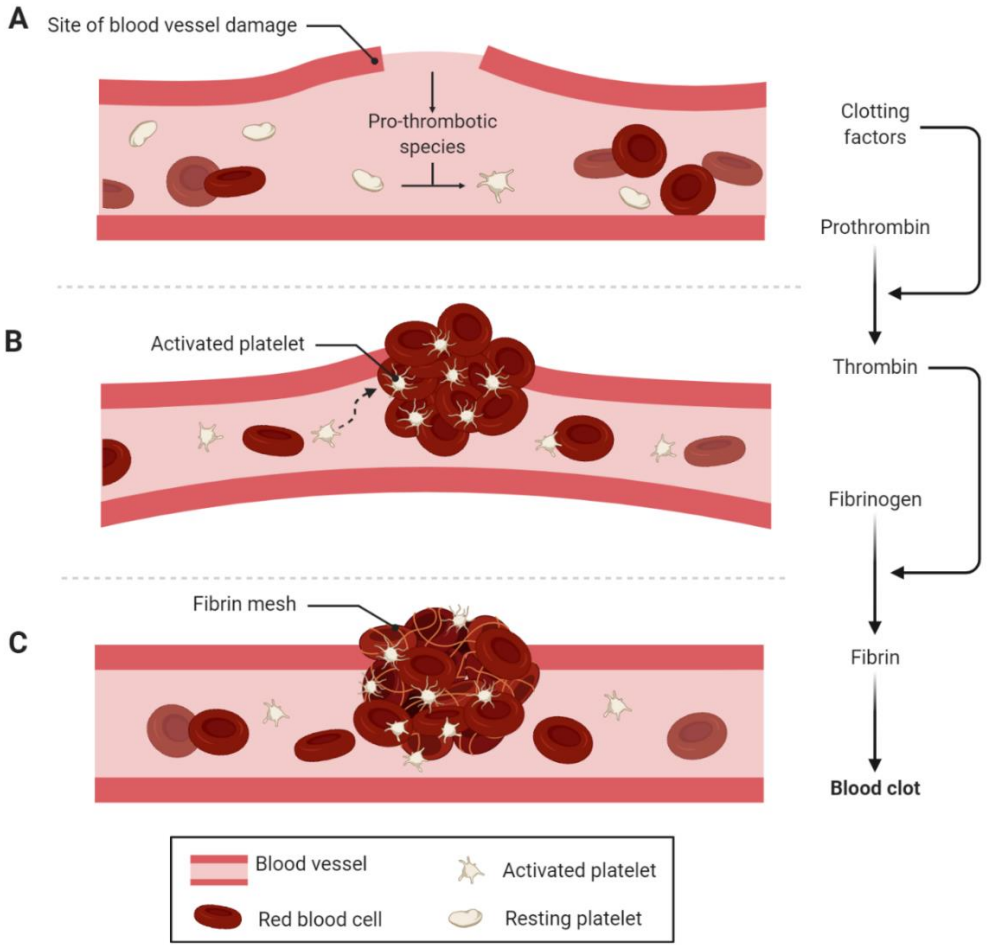

Figure 27 A cartoon depicting thrombus formation. A: Blood vessel damage exposes pro-thrombotic species (e.g. VWF, collagen, fibrinogen) which bind to resting platelets via specific cell-surface receptors and cause platelet activation. B: Platelet activation and adhesion occur, forming a thrombus. C: The coagulation cascade results in the formation of insoluble fibrin, which stabilises the thrombus.

Platelet formation occurs when megakaryocytes in the bone marrow undergo nuclear duplication and fragmentation; as fragments of cells, platelets are small and anuclear, a factor which has major implications when studying their intracellular pathways.[147] Platelets circulate for 10 days on average, and about a third of platelet sequestration occurs in the spleen.

2.1.4 Platelet activation

There are a wide range of signalling molecules (platelet agonists) which cause platelet activation, including thromboxane A2 (TxA2), ADP and thrombin, which all bind to G-protein coupled receptors on the platelet surface (Figure 28).[148] Additionally, collagen, thrombin and VWF are released from activated platelets and cause activation of resting platelets in a positive feedback cycle.[149]

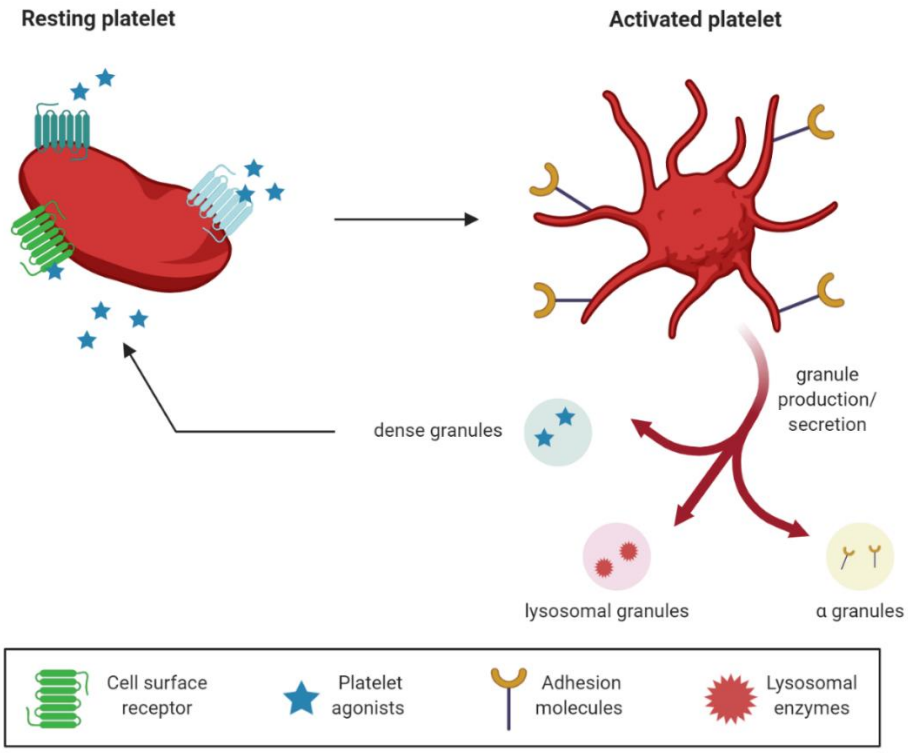

Figure 28 A cartoon depicting platelet activation. The binding of platelet agonists (e.g. VWF, collagen, thrombin) to receptors on the surface of the platelet induce activation, causing morphological changes, the presentation of adhesion molecules and granule release. Adapted from J. Ware,[150] Gay and Felding-Habermann,[149] and Nieswandt, Pleines and Bender.[148]

The observed morphological change is believed to be due to the binding of thrombin to G-protein coupled protease-activated receptors on the surface of the platelet. This causes a reduction in the intracellular cyclic AMP concentration and an increase in calcium, thus allowing the reorganisation of the platelet cytoskeleton and associated morphological changes.[149] The composition of the platelet cell surface is also changed upon platelet activation. For example, P-selectin (CD62), a transmembrane protein stored in the α-granules of resting platelets, is translocated to the extracellular surface.[151] Similarly, integrins such as GPIIb/IIIa which are also stored in α granules are released upon activation, increasing the cell-surface expression of this adhesion receptor.[152] Phosphatidylserine (PS), a phospholipid typically located on the inner leaflet of the platelet membrane bilayer, is also redistributed to the cell surface.[153]

Activation also involves the release of granules from platelets; the species released in the granules have specific roles in platelet activation.[151] There are three types of storage granules in platelets; dense, α and lysosomal and their contents also fit into three functional classes. Dense granules contain platelet agonists (e.g. ADP, calcium and TxA2), α granules contain adhesion molecules (e.g. P-selectin, fibrinogen and VWF) and lysosomal granules contain lysosomal enzymes (e.g. cathepsin).

The mechanisms involved in platelet granule secretion are not fully understood; however, it is widely believed that platelet shape change is a major effector. Many of the morphological and biochemical changes that happen during platelet activation are also observed during apoptosis of nucleated cells.[153] These changes include PS exposure, cell shrinkage, and membrane blebbing.[153,154] It has also been suggested that caspase activation, which plays a major role in apoptosis, may be involved in platelet activation.[155]

2.1.5 The roles of platelets in disease states

In addition to platelet activation as a result of wound formation, it can also occur as part of a wider systemic inflammatory response, with stimuli including cytokines, infective agents and shear stress.[156] Predictably, severe platelet abnormalities such as thrombocytopenia (low platelet count) can result in various bleeding disorders.[147] There are numerous anti-platelet therapeutics on the market, the most well-known of which is Aspirin.[157] Aspirin is a widely used anti-inflammatory drug which prevents the biosynthesis of platelet agonist TxA2 through irreversible covalent inhibition of cyclo-oxygenase-1. As TxA2 is typically stored in α granules and released upon platelet activation, this ultimately decreases the amount of platelet activation, thus reducing inflammatory responses.[152]

There are definite links between the functions of platelets and cancer metastasis, however, the exact nature of these are yet to be determined. In general, platelets can affect the development of a tumour in three ways; by complementing tumour adhesion, through shielding tumour cells from the immune system and by assisting in the selection of metastatic tumour cell phenotypes.[149] It has therefore been noted that anti-platelet therapies which target the specific tumour-platelet interactions that enable the above-mentioned events would complement current anticancer therapies.[149] Furthermore, the presence of platelet-leucocyte aggregates has been observed in various disease states, making them an interesting and underexplored target.[149,158]

2.1.6 Bcl-2 proteins in platelets

Certain members of the Bcl-2 proteins are known to be present in platelets; mRNA sequences encoding BH3-only proteins Bim, Bad, Bid, Bmf and Puma are known to be expressed in mouse platelets, along with Bax, Bak, Mcl-1, Bcl-2 and Bcl-x_L.[159] Additionally, protein expression in human platelets has been confirmed for Bax, Bak, Bcl-2 and Bcl-x_L.[160] It was found through studies of knockout mice that pro-survival Bcl-x_L is vital for platelet survival: in

mice with a deletion of Bcl-x_L the megakaryocytes platelet lifespan is reduced from 5 days to 5 hours, resulting in thrombocytopenia which can be reversed through further deletion of pro-apoptotic Bax and Bak.[161] Conversely, it was shown that removing both the Mcl-1 and Bcl-2 proteins in knockout mice did not adversely affect the production or survival of platelets.[117]

Whilst small-molecule PPI inhibitor ABT737 caused complete regression of tumours in animal models, an associated thrombocytopenia was observed. The effects of ABT737 on platelets were examined, and it was found that the drug caused concentration-dependent PS exposure and induced higher levels of cytochrome c and caspase-3 activity, all of which are associated with activation of the intrinsic apoptotic pathway.[160] Conversely, ABT737 had a modest effect on platelet activation-associated events, as measured by granule release and the increase in expression of the integrin GPIIb/IIIa on the platelet surface. The authors concluded that ABT737 causes rapid platelet apoptosis without activation.[160] The same biological profile was true for ABT263, a related compound which also inhibits Bcl-2, Bcl-x_L and Bcl-w.[162,163] However, ABT199, a selective Bcl-2 inhibitor, was found to cause tumour regression without thrombocytopenia.[130,164] The different biological responses these small molecules provoke indicate that the BH3-only proteins have distinct and important roles in human platelets, which require further elucidation.

2.1.6.1 Issues with studying PPIs in human platelets

To fully understand the relationship between BH3-only protein-mediated apoptosis and activation in platelets it is necessary to elucidate the PPIs of the Bcl-2 protein family. However, the common methods for the study of PPIs include the use of transgenic animals, recombinant methods and small molecule inhibitors, all of which face significant issues when studying platelets.

The use of transgenic animals is often costly and time-consuming, and there are key differences between species. For example, mice have smaller platelets and more platelet-rich plasma than humans.[150] The study of BH3-only proteins in platelets is not possible using standard recombinant methods, as platelets are anuclear.[165] Finally, the design of small molecule inhibitors for targeting large, shallow PPI sites is often challenging.[13] Although there are numerous examples of successful PPI inhibitors, including ABT737, -263 and -199, this approach is not general, and each individual inhibitor often requires significant development. Additionally, highly selective chemical tools are necessary to unambiguously probe the roles of each BH3 protein.

Stapled peptides present themselves as convenient chemical tools to study the BH3 PPIs in human platelets for several reasons. Firstly, significant structural information is available for

the BH3-only proteins, and the native sequences of the BH3 binding domains can provide the basis for peptide design. The stapled peptides listed in Table 6 (Section 2.1.2.2) provide numerous examples of this approach, and peptides developed in this way have the potential to be highly selective for their individual targets.[13] Two-component peptide stapling allows the facile introduction of functionality; for example, cell-penetrating peptides (CPPs) to endow cellular permeability onto the peptides, and fluorescent tags to enable visualisation assays. Peptide stapling can also lock the peptide in a biologically relevant conformation, and significantly improve the proteolytic stability. It was for these reasons that stapled peptides were developed as novel chemical tools to study the BH3 PPIs in human platelets.[77]

2.1.7 Previous work on stapled peptides in human platelets

Previous work in the Spring group investigated whether stapled peptides could enter human platelets, and whether a stapled peptide based on the sequence of the Bim BH3 domain could elicit a biological response in human platelets. This work is published in Iegre *et al.*,[77] and is reported in the thesis of Dr. Jessica Iegre.[166] Unless otherwise stated all of the experiments reported in this section were performed by Dr. Jessica Iegre.

To assess whether stapled peptides could enter human platelets, a model peptide was stapled with a variety of functionalised linkers using CuAAC stapling.[a] The platelet-penetration of these peptides was investigated by confocal microscopy and flow cytometry. A model peptide functionalised with a polyarginine CPP showed high levels of platelet uptake, localisation in the platelet cytosol and did not cause platelet activation. The individual roles of the BH3-only proteins in platelet apoptosis and activation are unknown, therefore, to investigate a biologically-relevant peptide sequence a stapled peptide based on the BH3 binding domain of Bim was synthesised and functionalised with a polyarginine R_3 CPP (**P19**, Figure 29). **P19** was shown to be platelet permeable and to localise in the platelet cytosol using flow cytometry and confocal microscopy. The binding of **P19** to Bcl-x_L was assessed using a surface plasmon resonance assay, and it displayed comparable binding to the wild-type peptide **P17** (**P19** K_{Dapp} = 26 nM, **P17** 7.3 nM), and greater binding than a literature *i,i*+4 Bim RCM stapled peptide,[139] (**Bim-SAHBa** K_{Dapp} > 33 nM, B, Figure 29).

[a] The peptides were synthesised by Dr. Yuteng Wu. Model peptide based on p53 sequence = TAMRA-Ahx-ETFXDLWRLLXEN-NH_2 where X= azido ornithine and Ahx = 6-aminohexanoic acid.

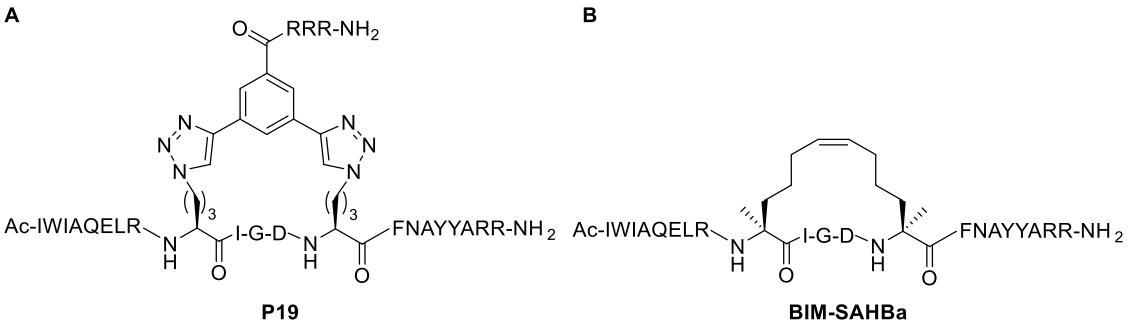

*Figure 29 The structures of stapled Bim peptides. A) The CuAAC stapled Bim peptide **P19** reported by Iegre et al.[77] and B) the Bim SAHBa peptide reported by Walensky and co-workers.*[139]

The effect of Bim peptide **P19** on platelet apoptosis and action was measured and compared to ABT737, which does not activate platelets, but does causes PS exposure, a marker of apoptosis.[160] PS exposure was assessed by measuring platelet-annexin V binding: **P19** caused 78 ± 1.3% annexin V binding after 3 hours, which is comparable to ABT737, and more potent than the literature Bim SAHBa peptide. **P19** caused integrin GPIIb/IIIa activation (24.1 ± 2.4% positive platelets, measured by PAC-1 binding) and CD62P (53.7 ± 2.5%) and CD63 (72.9 ± 5.3%) expression, which indicate α- and dense granule release, respectively. Conversely, treatment with ABT737 gave a negligible response for these activation markers, which is concurrent with literature reports.[160]

This work revealed that functionalised stapled peptides can be platelet permeable and exert a biological effect. Mechanistic differences were revealed between the Bim stapled peptide **P19** and ABT737, which is referred to as a 'Bad mimetic' as it has comparable selectivity to Bad, binding to pro-survival proteins Bcl-2, Bcl-x_L and Bcl-w. Whilst both treatments caused similar levels of PS exposure, only **P19** caused platelet activation, indicating that the Bim and Bad BH3-only proteins could have different roles in human platelets.

2.2 Project aims and outline

Following on from this promising work, it was proposed to synthesise stapled peptides corresponding to the remaining BH3-only proteins, incorporating a polyarginine CPP on the staple. The effect of these stapled peptides on events related to apoptosis and activation in human platelets would be investigated using flow cytometry. It was envisaged that these platelet-permeable chemical tools would enable more information to be gathered regarding the roles of the individual BH3-only family proteins, and that the information gained could provide the basis for the development of future therapeutics. The BH3-only family members are Bim, Bad, Bik, Bmf, Puma and Noxa - peptides corresponding to Bim, Bad and Bik were synthesised by Dr. Jessica Iegre,[166] and the work reported in this thesis relates to the synthesis and preliminary biological testing of Bmf, Puma and Noxa stapled peptides.

Initially, two-component CuAAC stapling at *i,i*+11 positions was employed for the Bmf, Puma and Noxa peptides (A, Figure 30), as it was believed that by spanning multiple turns of the helix, greater proteolytic stability might be imparted. However, it was found that these peptides could not be easily functionalised and therefore, the series was retired. A second series of peptides were synthesised with stapling at *i,i*+7 positions, using a linker which allowed facile functionalisation of the peptides (B, Figure 30).

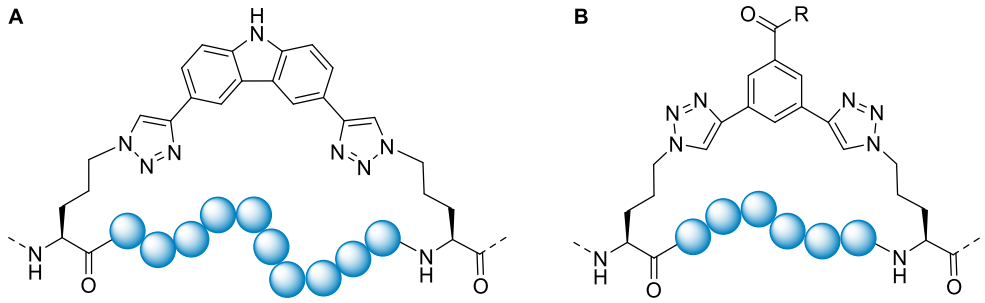

Figure 30 The general structures of the two series of CuAAC stapled peptides developed in this project. A) i,i+11 peptides and B) i,i+7 peptides. Amino acids are represented by blue spheres. R = either OH or Ahx$_2$-(D)Arg$_3$.

Overall, 12 peptides were synthesised, including three polyarginine functionalised stapled peptides based on the sequences of the Bmf, Puma and Noxa BH3-only proteins. For both series of unfunctionalised stapled peptides, the peptide secondary structures were analysed by circular dichroism spectroscopy (Figure 31). For the three functionalised stapled peptides, preliminary investigations into their effect on events associated with platelet apoptosis and activation were performed.

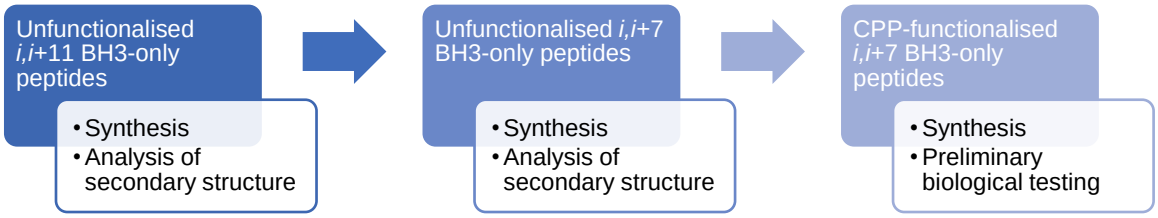

Figure 31 A schematic overview of the work-flow described in this chapter.

2.3 Results and discussion

2.3.1 Development of *i,i*+11 BH3-only stapled peptides

2.3.1.1 Stapled peptide design

For the Bmf, Noxa and Puma peptides, stapling positions beyond *i,i*+4 were considered; it was decided that *i,i*+11 stapling positions may improve the proteolytic stability of the peptides, as the staple would span more turns of the α-helix (3 helical turns for *i,i*+11, 1 for *i,i*+4). The literature indicated that a bis-alkynyl carbazole linker would be suitable for *i,i*+11 stapling, as a model peptide synthesised by Dr. Yu Heng Lau with azido ornithine at *i,i*+11 positions exhibited 87% α-helicity when stapled with a carbazole staple (Figure 32).[167]

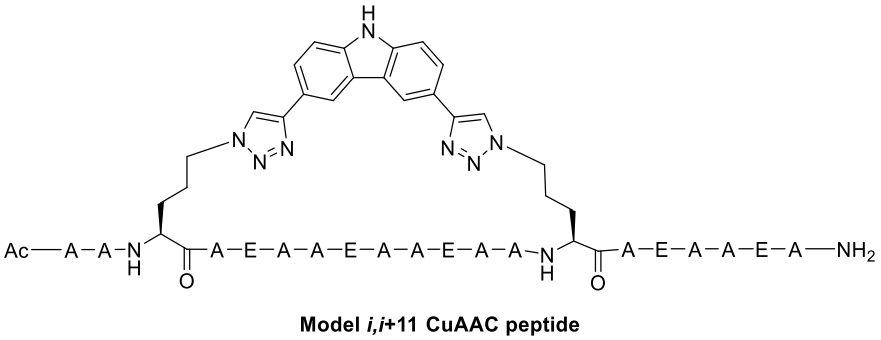

Figure 32 The model peptide synthesised by Dr. Yu Heng Lau, with stapling between azido ornithine residues at i,i+11 positions with a bis-alkynyl carbazole linker.[167]

The optimal positions within the native peptide sequences to place the azido ornithine residues were determined computationally.[b] For the Bcl-2 proteins there is comprehensive structural data allowing the rational design of stapled peptides. The stapled peptide sequences were derived from X-ray crystal structures of BH3-only protein complexes,[c] the analysis of which indicated suitable *i,i*+11 stapling positions where the staple was solvent-exposed and no clashes were predicted between the staple and intervening residues. The proposed peptide sequences for the *i,i*+11 stapled Bmf, Puma and Noxa peptides are shown in Table 7.

*Table 7 The sequences of the wild-type BH3 peptides **P1**-**P3**, and the i,i+11 BH3 peptides **P4**-**P6**. X = position of azido ornithine in the linear peptides. All peptides have a C-terminal amide.*

Peptide	Peptide	Sequence
Bmf wild-type	**P1**	Ac-IARKLQCIADQFHRL
Puma wild-type	**P2**	Ac-IGAQLRRMADDLNAQY
Noxa wild-type	**P3**	Ac-CATQLRRFGDKLNFR
Bmf *i,i*+11	**P4**	Ac-IA**X**KLQCIADQFH**X**L
Puma *i,i*+11	**P5**	Ac-IG**X**QLRRMADDLN**X**QY
Noxa *i,i*+11	**P6**	Ac-CA**X**QLRRFGDKLN**X**R

[b] Computational modelling performed by Dr Yaw Sing Tan (A*STAR Institute, Singapore).

[c] PDB codes of the X-ray crystal structures of protein complexes are Bmf: 5TZQ, Puma: 5UUL and Noxa: 3MQP.

2.3.1.2 Peptide synthesis

To synthesise the peptides listed in Table 7, Fmoc-protected azido ornithine **3** was required, and could be easily accessed from commercially available N_α-Fmoc-N_δ-Boc-L-ornithine, *via* deprotection and diazo transfer. The required diazo transfer reagent **1** was synthesised from sulfuryl chloride following the literature procedure (Scheme 5) in a moderate yield, with no purification required.[168] Azido ornithine **3** was prepared according to the literature route;[169] Boc deprotection of the commercially available starting material yielded the hydrochloride salt **2**, and subsequent treatment of **2** with diazo transfer reagent **1** under the literature conditions gave **3** in a good yield (Scheme 5).[169] Azido-ornithine **3** was used in subsequent solid-phase peptide synthesis (SPPS) without further purification.

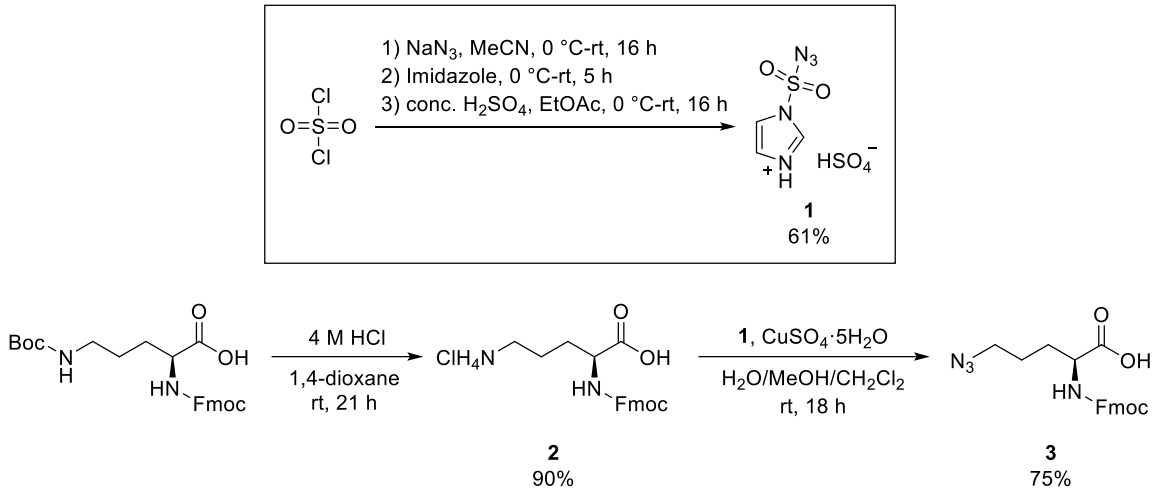

*Scheme 5 The one-pot synthesis of diazo transfer reagent **1**, and the synthetic route towards azido ornithine **3** via Boc deprotection of the commercially available starting material and subsequent diazo transfer.*

The wild-type (**P1**-**P3**) and linear azido (**P4**-**P6**) peptides were synthesised using automated microwave-assisted Fmoc-SPPS (Table 8). Low-loading Rink amide resin was used to prevent aggregation during peptide synthesis and give a *C*-terminal amide upon cleavage from the resin.[d] It was found that for the Noxa peptide **P6** the *N*-terminal cysteine residue required manual coupling, as all attempts at synthesis of the full sequence on the automated peptide synthesiser were unsuccessful. The peptides were all capped at the *N*-terminus with an acetyl group, cleaved from the resin in a TFA cocktail containing 1,2-ethanedithiol (EDT)[e] to avoid potential side-reactions of methionine and cysteine residues,[170] and purified by preparative HPLC prior to stapling.

[d] A *C*-terminal amide is preferred over a carboxylic acid as it does not reduce the net positive charge of the peptide, a significant factor for cell permeability.[98] Additionally, an amide moiety would be present at this position in the full protein sequences; this is also the reason for *N*-terminal acetyl capping.
[e] Cleavage solution: TFA/TIPS/H_2O/EDT (94:1:2.5:2.5).

*Table 8 The sequences of the i,i+11 linear azido peptides **P4-P6**, wild-type peptides **P1-P3**, and their method of synthesis. All peptides have a C-terminal amide, X = azido ornithine.*

BH3 Protein	Peptide	Sequence	Synthesis
Bmf	**P1**	Ac-IARKLQCIADQFHRL	All amide couplings and *N*-terminal capping automated
	P4	Ac-IA**X**KLQCIADQFH**X**L	
Puma	**P2**	Ac-IGAQLRRMADDLNAQY	
	P5	Ac-IG**X**QLRRMADDLN**X**QY	
Noxa	**P3**	Ac-CATQLRRFGDKLNFR	
	P6	Ac-CA**X**QLRRFGDKLN**X**R	*N*-terminal cysteine residue coupling, and acetyl capping performed manually

2.3.1.3 Synthesis of carbazole linkers **6** and **7**

The carbazole linker **6** required for the *i,i*+11 stapling was synthesised according to the literature route (Scheme 6).[167] Commercially available carbazole was brominated with *N*-bromosuccinimide (NBS) to give **4** in a moderate yield, followed by a double-Sonogashira cross-coupling reaction to install the protected alkyne moieties, which proceeded in a good yield to give **5**. The protected bis-alkynyl carbazole **5** could then be deprotected upon treatment with potassium carbonate to give the unfunctionalised linker **6** in a high yield after chromatographic purification. Alternatively, from intermediate **5**, linker **7** could be synthesised *via* a one-pot alkyne deprotection and *N*-alkylation with 6-bromohexanoic acid under ultrasonic irradiation (Scheme 6). The carboxylic acid moiety in **7** provides a reactive handle for the attachment of the cell penetrating peptide.

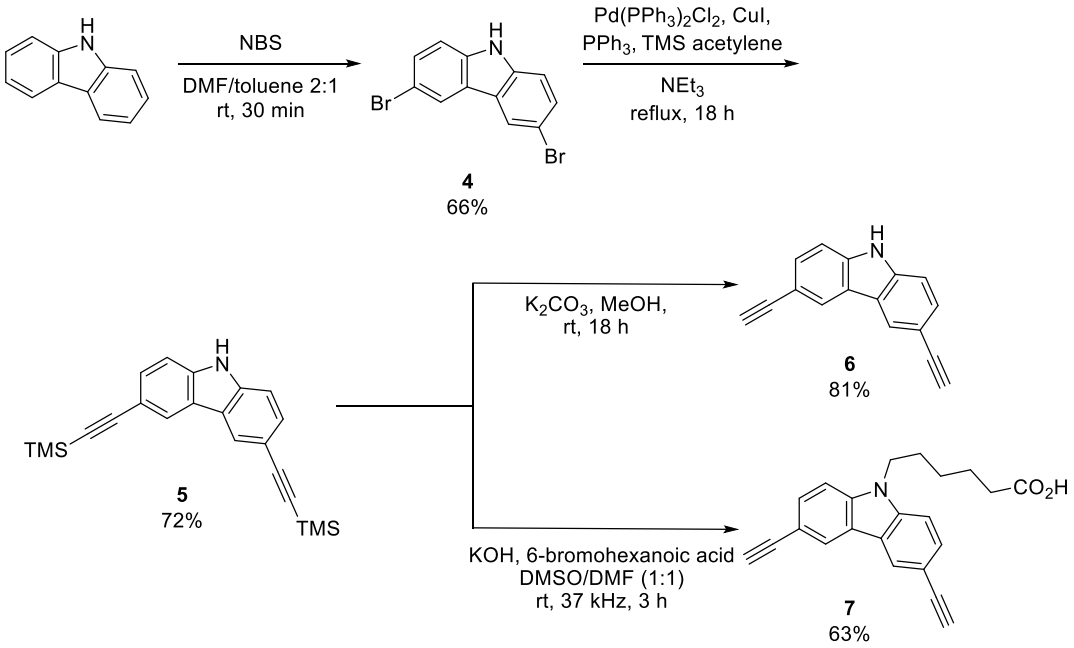

*Scheme 6 The synthesis of staple linkers **6** and **7** from commercially available carbazole.*

Previous studies indicated that the peptides would require functionalisation with a polyarginine CPP to promote platelet uptake (A, Figure 33).[77] Therefore, a functionalised staple linker would be required bearing an R_3 motif. It was decided for this series that two 6-aminohexanoic acid spacers would be introduced to increase the distance between the large staple and the binding residues of the peptide (B, Figure 33). It was also decided to use D- rather than L-arginine in the CPP, as the use of D-amino acids in CPPs can improve their proteolytic stability without negatively affecting their ability to translocate the cellular membranes.[171]

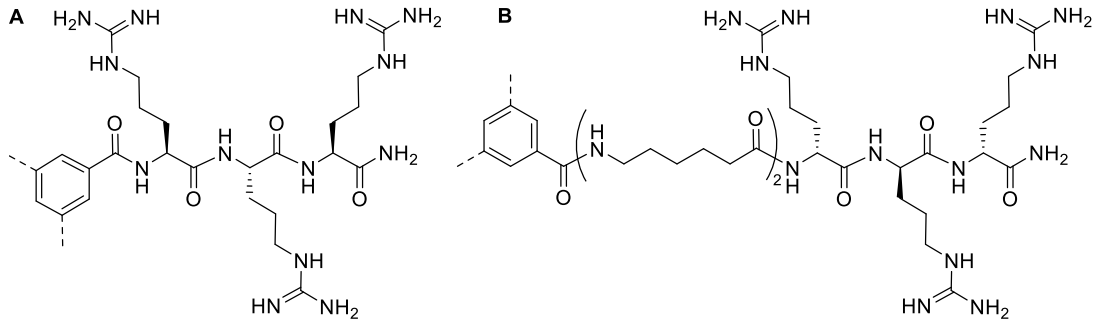

Figure 33 A) The structure of the poly-L-arginine CPP used for the literature Bim stapled peptide,[77] and B) the structure of the poly-D-arginine CPP proposed for these peptides, incorporating two 6-aminohexanoic acid spacers between the benzene linker and the polyarginine peptide.

It was proposed that the synthesis of the CPP-functionalised linker could be achieved by SPPS of the CPP **P7**, then performing an amide coupling with the deprotected *N*-terminus of the resin-bound **P7** and linker **7** (Scheme 7). The resulting functionalised alkyne staple could be cleaved from the resin under standard cleavage conditions[f] and purified by preparatory HPLC to give the functionalised linker, **8**. This linker could then be used in peptide stapling reactions with the linear azido peptides **P4**-**P6**.

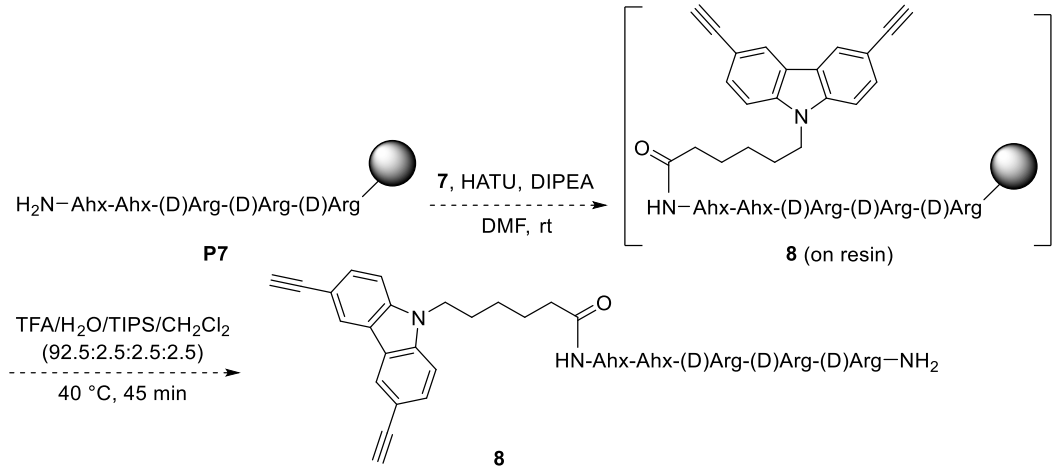

*Scheme 7 The proposed synthesis of **8**, the polyarginine functionalised carbazole linker. The polyarginine CPP **P7** would be synthesised by SPPS, and the N-terminus of the peptide capped with linker **7**. The linker-peptide conjugate could then be cleaved from the resin to give **8**.*

[f] TFA/H_2O/TIPS/CH_2Cl_2 (95:2.5:2.5:2.5).

P7 was synthesised by automated SPPS as previously described, and the coupling of **P7** and **7** proceeded smoothly. It was found, however, that the carbazole moiety was not compatible with the resin cleavage conditions, and upon addition of the cleavage cocktail to resin-bound **8** the reaction mixture turned black and no desired product could be detected by LCMS. This was also observed under alternative cleavage conditions consisting of 0.1 N HCl in hexafluoroisopropanol (HFIP), and treating carbazole linker **7** with either TFA or HCl resulted in a black mixture, which, when analysed by ^{1}H NMR showed no peaks correlating to the carbazole.[g] Consequently, a different stapling architecture was required for the synthesis of stapled polyarginine functionalised peptides, as a solution-phase synthesis of the proposed **8** would be time consuming. It was decided that the unfunctionalised stapled peptides would be synthesised using **P4**-**P6** and linker **6**, and the α-helicity of these peptides would be analysed by circular dichroism (CD) spectroscopy. This data would guide the decision of whether to develop a functionalisable *i,i*+11 linker, or whether to focus on alternative staple lengths.

2.3.1.4 Stapling with unfunctionalised linker **6**

The linear azido *i,i*+11 peptides **P4**-**P6** were cyclised with linker **6** using standard two-component CuAAC stapling conditions, as reported in the literature (Table 9).[44]

*Table 9 The sequences of azido peptides **P4**-**P5**, and the conversion of the CuAAC stapling reactions of these peptides and linker **6** under the conditions shown. X = azido ornithine. Amino acids are shown as blue spheres. % Conversion determined by LCMS analysis of the reaction mixtures after 18 h.*

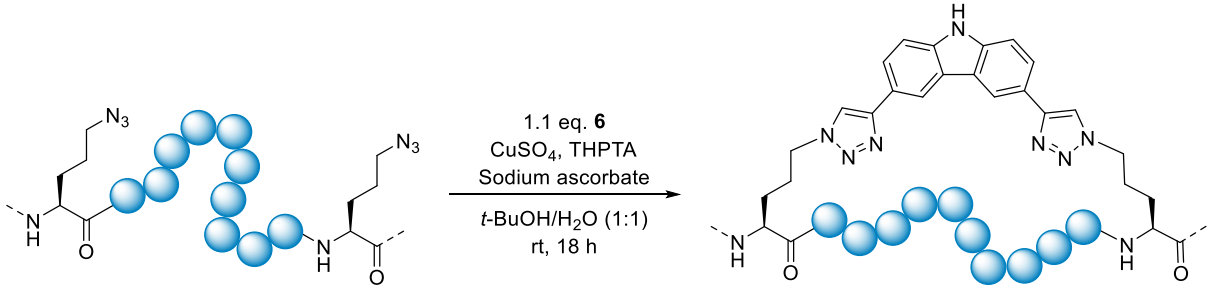

Linear peptide	Sequence	Stapled peptide	Conversion (%)
P4	Ac-IA**X**KLQCIADQFH**X**L	**P4-6**	>99
P5	Ac-IG**X**QLRRMADDLN**X**QY	**P5-6**	88
P6	Ac-CA**X**QLRRFGDKLN**X**R	**P6-6**	>99

During the preparatory HPLC purification of the Noxa stapled peptide **P6-6**, it was observed that the peak corresponding to the desired stapled peptide on the HPLC chromatograph was extremely broad. A similarly broad peak was observed in the analytical HPLC trace of the purified peptide (Appendix 6.2); it is possible that the cause of this broad peak is complexation of the peptide and copper catalyst.[44] As a purity could not be determined for peptide **P6-6** it

[g] Reactions and analysis performed by Dr. Jessica Iegre, University of Cambridge.[166]

could not be used in further peptide characterisation or biological assays with confidence, and was excluded from subsequent analysis.

2.3.2 Circular dichroism spectroscopy for studying peptide secondary structures

Circular dichroism (CD) is a spectrographic technique which allows the study of protein and peptide secondary structures in solution.[172] In CD spectroscopy, the differential absorption of circularly-polarised light is measured, and common structural features such as α-helices and β-sheets can be identified by differences in these absorptions in the far-UV;[173] for example, α-helices have a characteristic minimum at 222 nm (Figure 34).[172] Although CD spectroscopy is not definitive for the study of peptide secondary structures, it is practically straightforward and gives a good estimation.

In the native BH3-only proteins, the BH3 domain has an α-helical structure.[113] However, taken out of the stabilising environment of the protein tertiary structure, linear peptides often display random coil structures in solution. It was anticipated that stapling linear BH3 sequences will result in macrocyclic peptides which display a comparable or higher α-helicity than the wild-type sequences. This has been illustrated in the literature for BH3-only stapled peptides (Figure 34),[18] although it has also been reported that an increase in binding affinity is not necessarily related to an increase in α-helicity.[174]

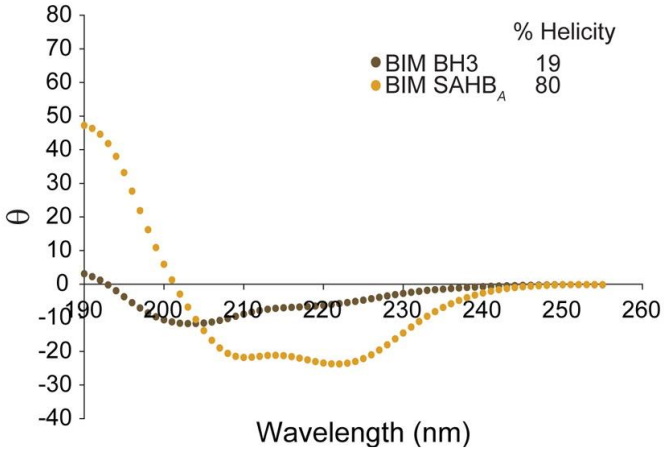

Figure 34 The CD spectra for the wild-type Bim peptide (Bim BH3, brown) displaying a random coil structure, and the Bim SAHBa peptide (yellow) displaying an α-helical structure. Figure from Walensky et al.[18] *(https://pubs.acs.org/doi/10.1021/jm4011675).*[h]

[h] Further permissions related to the material excerpted should be directed to the ACS.

2.3.2.1 Analysis of *i,i*+11 BH3-only stapled peptides by CD spectroscopy

The secondary structures of the *i,i*+11 BH3 stapled peptides were analysed by CD spectroscopy and compared to the linear sequences. Pure samples of the Bmf and Puma peptides were measured in MeCN/H_2O (1:1) at 100 µM. The measured ellipticity (millidegrees) was normalised against the measured ellipticity at 207 nm and plotted, and the percentage of α-helical content was calculated for each peptide.[175,176] For the Bmf series, the stapled peptide **P4-6** displayed a significantly lower α-helical content (8%) than the wild-type peptide **P1** (32%, A, Figure 35). A decrease in helical content upon stapling was also observed for the Puma peptides: the wild-type peptide **P2** displayed a higher α-helical content than the stapled peptide **P5-6** (34% vs. 24% respectively, B, Figure 35). This shows that the *i,i*+11 stapling actively disrupted the adoption of an α-helical secondary structure for these sequences.[i]

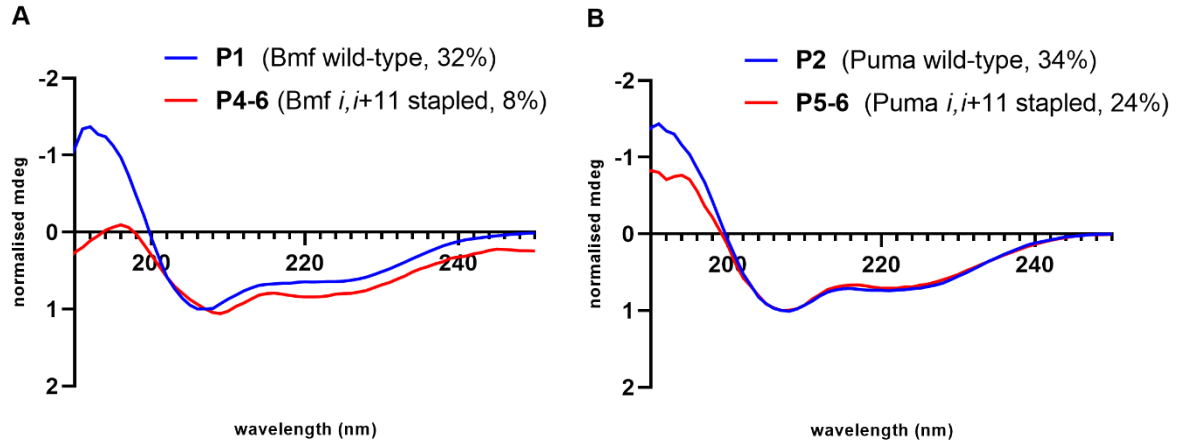

*Figure 35 CD spectra for (A) Bmf peptides **P1** and **P4-6**, and (B) Puma peptides **P2** and **P5-6**. All ellipticities (mdeg) have been normalised to the ellipticity at 207 nm. The % α-helicity is given in brackets after the peptide number in the legend.*

The CD data, along with the challenges faced during the attempted functionalisation of carbazole linker **7**, lead to the termination of the *i,i*+11 series of BH3-only stapled peptides. Instead, *i,i*+7 stapling was investigated, as this would still span multiple turns of an α-helix (two turns compared to one turn for *i,i*+4 stapling), and therefore, may improve the proteolytic stability of the peptides, however it does not require the problematic carbazole linker.

2.3.3 Development of *i,i*+7 BH3-only stapled peptides

2.3.3.1 Stapled peptide design

Based on literature reports, whilst the optimal linker for inducing α-helicity with *i,i*+11 stapling is the carbazole scaffold (A, Figure 36), the optimal linker for *i,i*+7 two-component CuAAC is

[i] Low α-helicities were also observed for *i,i*+11 CuAAC stapled Bad, Bid and Bim peptides, which were synthesised and analysed using CD spectroscopy by Dr. Jessica Iegre.[166]

based on a 3,5-diethynylbenzoic acid scaffold (B, Figure 36).[167,23] The same benzene scaffold was used for the literature *i,i*+4 stapled Bim peptides.[77,166] Unlike the carbazole linker **E**, the 3,5-diethynylbenzoic acid staple is compatible with TFA-mediated resin cleavage and can therefore be functionalised *via* a similar route as was proposed in Scheme 7.

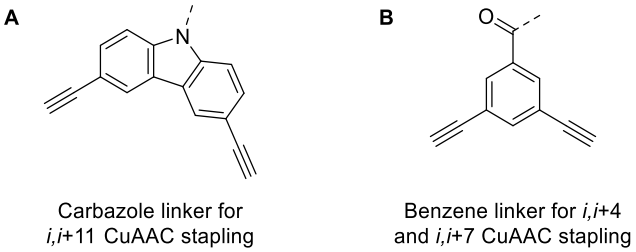

Figure 36 The structures of the optimal stapling linkers for different CuAAC stapling positions. The carbazole linker (A) is optimal for i,i+11 stapling and the benzene linker (B) is i,i+4 and i,i+7 stapling.[167]

The *i,i*+7 series of azido peptides were designed computationally following the same principles as was described for the *i,i*+11 peptides (Section 2.3.1.1).[j]

2.3.3.2 Peptide synthesis

Azido ornithine **3** was prepared as described previously (Section 2.3.1.2), and the linear azido peptides were synthesised *via* automated Fmoc-SPPS.

*Table 10 The sequences of the azido i,i+7 peptides **P8**-**P10**. All peptides have a C-terminal amide. X = azido ornithine.*

BH3-only protein	Peptide	Sequence
Bmf	**P8**	Ac-IARKLQ**X**IADQFH**X**L
Puma	**P9**	Ac-IGA**X**LRRMAD**X**LNAQY
Noxa	**P10**	Ac-CATQLR**X**FGDKLN**X**R

2.3.3.3 Synthesis of benzene linker **10**

Benzene linker **10** was prepared according to the literature synthesis (Scheme 8).[23] From commercially available methyl 3,5-dibromobenzoate, a double-Sonogashira cross-coupling reaction introduced the protected alkyne moieties to give **9** in an excellent yield after chromatographic purification. The final step, a base-mediated one-pot deprotection and ester hydrolysis gave the desired linker **10** in a good yield after recrystallisation.

[j] Computational modelling and peptide design performed by Dr Yaw Sing Tan (A*STAR Institute, Singapore).

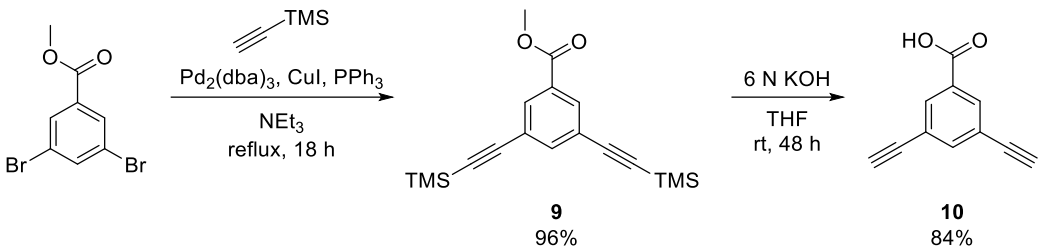

*Scheme 8 The synthesis of **10** from commercially available methyl 3,5-dibromobenzoate.*

2.3.3.4 Stapling with unfunctionalised linker **10**

Two-component CuAAC stapling reactions were performed with the *i,i*+7 azido peptides **P8**-**P10** and the unfunctionalised linker **10** under the literature conditions.[77] The stapling proceeded smoothly for the Bmf and Puma peptides **P8** and **P9**, to give the unfunctionalised *i,i*+7 stapled peptides **P8-10** and **P9-10** respectively (Table 11).

*Table 11 The sequences of azido peptides **P8**-**P10** and their conversions in peptide stapling reactions under the conditions shown. X = azido ornithine. Amino acids are shown as blue spheres. % Conversion determined by LCMS analysis.*

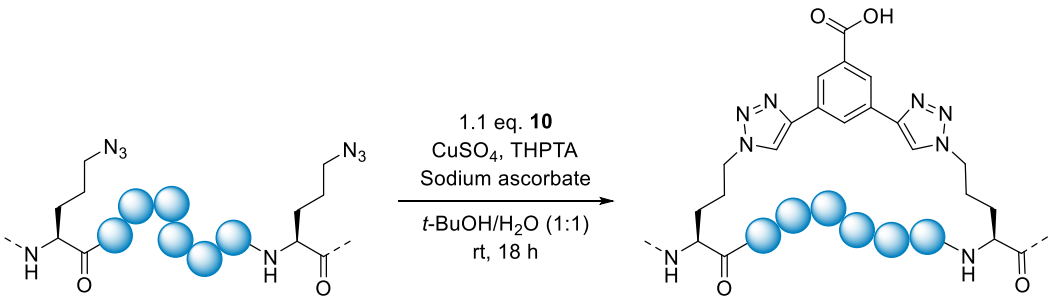

Linear peptide	Sequence	Stapled peptide	Conversion (%)
P8	Ac-IARKLQ**X**IADQFH**X**L	**P8-10**	>99
P9	Ac-IGA**X**LRRMAD**X**LNAQY	**P9-10**	88
P10	Ac-CATQLR**X**FGDKLN**X**R	**P10-10**	-

However the stapling reaction of the Noxa peptide **P10** gave a complex mixture, and analysis of the reaction mixture by analytical HPLC showed a broad peak in the region around 6.8 minutes (A, Figure 37). This phenomenon was also observed during the purification of *i,i*+11 Noxa stapled peptide **P6-6**, and one possible explanation was the coordination of the peptide sequence to the copper species present in the stapling reaction mixture.[44] This was somewhat confirmed when copper-chelator EDTA was added to the **P10-10** stapling reaction mixture; subsequent HPLC analysis showed that broad peak disappeared (B, Figure 37). This suggests that stapled peptide **P10-10**, unlike the other peptides investigated, was able to coordinate to the copper.

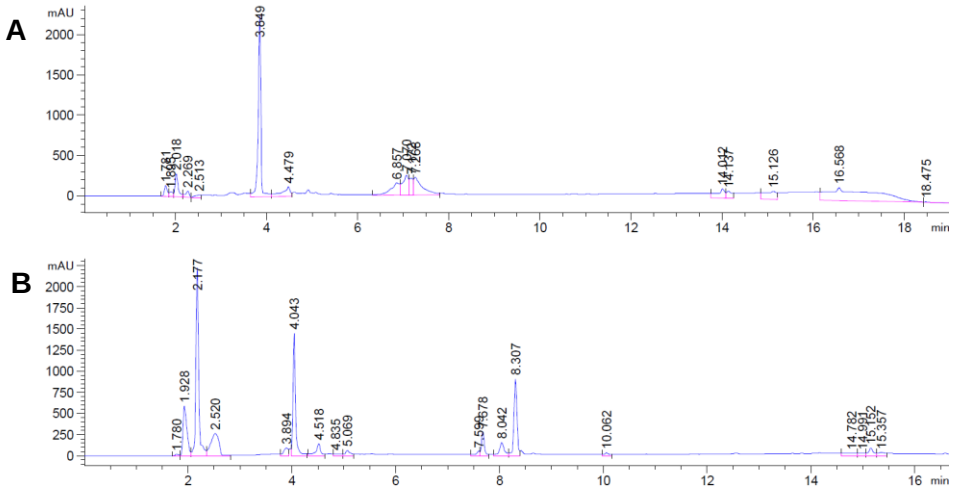

*Figure 37 The analytical HPLC traces of the **P10-10** stapling reaction mixture, in the absence (A) and presence (B) of copper-chelator EDTA. The disappearance of the broad peak at ~7 minutes after addition of EDTA suggests that the peptide is chelating to copper species present in the reaction mixture.*

It was suspected that the *N*-terminal cysteine residue of the Noxa peptide **P10** was causing a significant contribution to the coordination of the peptide to copper. The same cysteine residue was believed to be the reason for issues experienced during the SPPS of this peptide, as it was not amenable to microwave-assisted coupling on the automated peptide synthesiser and required manual coupling. Therefore, a mutant peptide **P11** was designed, replacing the *N*-terminal cysteine residue with isoleucine (**P11** sequence: Ac-IATQLRXFGDKLNXR, where X = azido ornithine). This mutation was suggested as isoleucine is present instead of cysteine at the same position in other BH3-only peptides.[134,135] The mutated peptide was modelled and compared to the X-ray crystal structure of the original Bim peptide in complex with a Bcl-2 protein, which suggested that the isoleucine would fit well in the binding pocket.[k]

CuAAC stapling was performed with **P11** and linker **10** and gave a significantly improved reaction profile, yielding the desired stapled peptide after preparatory HPLC purification (Scheme 9). Analysis of the reaction mixture by analytical HPLC did not indicate any complexing of the peptide to the copper catalyst species.

[k] Computational modelling performed by Dr. Yaw Sing Tan, A*STAR Institute, Singapore. PDB: 3MQP.

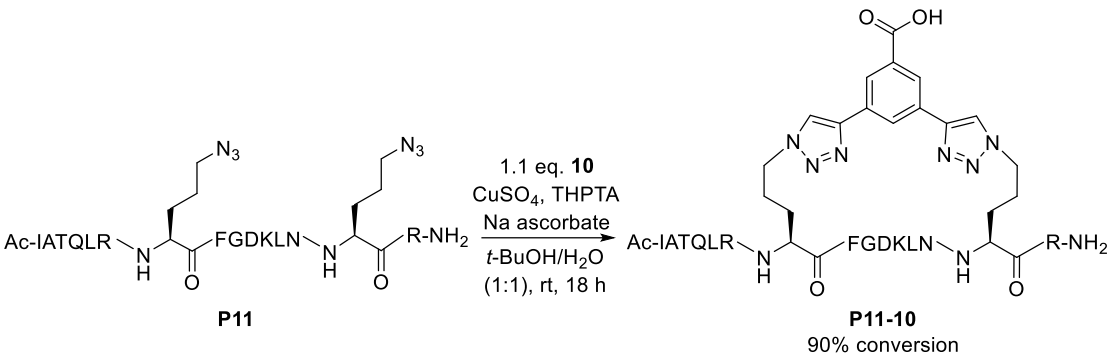

*Scheme 9 The synthesis of **P11-10** by CuAAC stapling with linear peptide **P11** and linker **10** under the literature conditions.*[44]

2.3.3.5 Synthesis of polyarginine-functionalised linker **11**

The polyarginine CPP **P7** was synthesised by standard SPPS (Scheme 10). The *N*-terminal amine of the peptide chain was coupled to **10** then cleaved from the resin under standard cleavage conditions and purified by preparative HPLC to give the functionalised linker **11**.

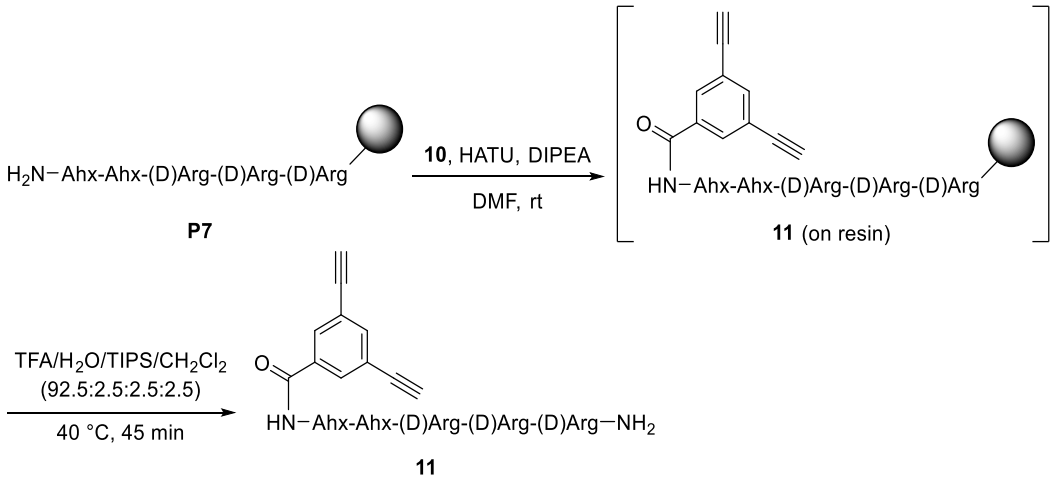

*Scheme 10 The synthesis of functionalised linker **11**. CPP **P7** was synthesised via standard SPPS and capped with linker **10**. The peptide was cleaved from the resin and purified by HPLC to yield **11**.*

2.3.3.6 Stapling with functionalised linker **11**

CuAAC stapling was performed with linear peptides **P8**, **P9** and **P11** and functionalised linker **11** under the literature conditions.[44] For each reaction, the reaction time was extended until complete conversion to the desired stapled peptide was achieved, with analysis of the reaction mixtures performed by analytical HPLC and LCMS (Table 12). These stapling reactions proceeded to completion within 3 hours, and **P8-11**, **P9-11** and **P11-11** were obtained after preparatory HPLC purification.

*Table 12 The sequences of azido peptides **P8**, **P9** and **P11** and the reaction times required for complete conversion to DP in peptide stapling reactions with **11** under the conditions shown. X = azido ornithine. Amino acids are shown as blue spheres. % Conversion determined by LCMS analysis.*

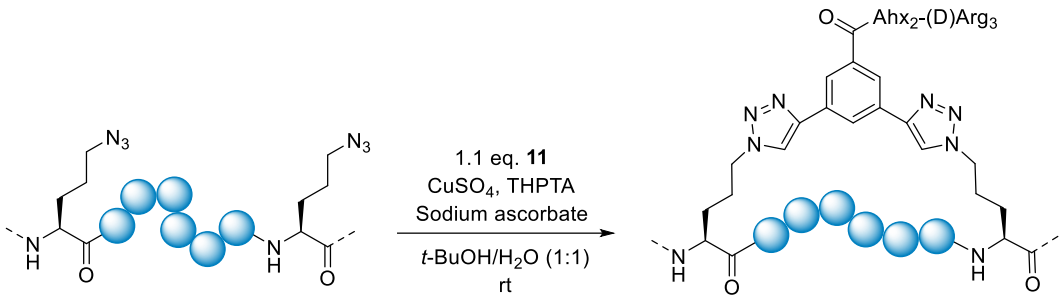

Linear peptide	Sequence	Stapled peptide	Reaction time (h)	Conversion (%)
P8	Ac-IARKLQ**X**IADQFH**X**L	**P8-11**	1	>99
P9	Ac-IGA**X**LRRMAD**X**LNAQY	**P9-11**	1	>99
P11	Ac-IATQLR**X**FGDKLN**X**R	**P11-11**	3	>99

2.3.4 Analysis of *i,i*+7 BH3-only stapled peptides by CD spectroscopy

CD spectroscopy of the peptides was performed as previously described for the *i,i*+11 peptides (Section 2.3.2). The wild-type peptides **P1**-**P3** were compared to their unfunctionalised stapled analogues (**P8-10**, **P9-10** and **P11-10**), to avoid any interference from the polyarginine CPP. From the CD data it is apparent that the *i,i*+7 stapling is successful in inducing helicity, as for all of the peptides the stapled analogues displayed higher percentage helicities than the wild-type peptides. For the Bmf peptides (A, Figure 38), the stapled peptide **P8-10** displayed a higher helicity (40%) than the wild-type peptide **P1** (32%). For the Puma peptides (B, Figure 38), the stapled peptide **P9-10** displayed the highest percentage α-helicity of all the peptides analysed (44%), an improvement over the wild-type peptide **P2** (34%). The greatest improvement in helicity upon stapling was observed for the Noxa peptides (33% for **P11-10** vs. 21% for **P3**, C, Figure 38). It is hoped that this increase in helicity upon stapling will translate into a reduced entropic penalty upon binding of the BH3-only peptides to pro-survival Bcl-2 proteins compared to the linear sequences, although this requires experimental confirmation. Furthermore, the presence of the staple should lead to an increase in proteolytic stability.

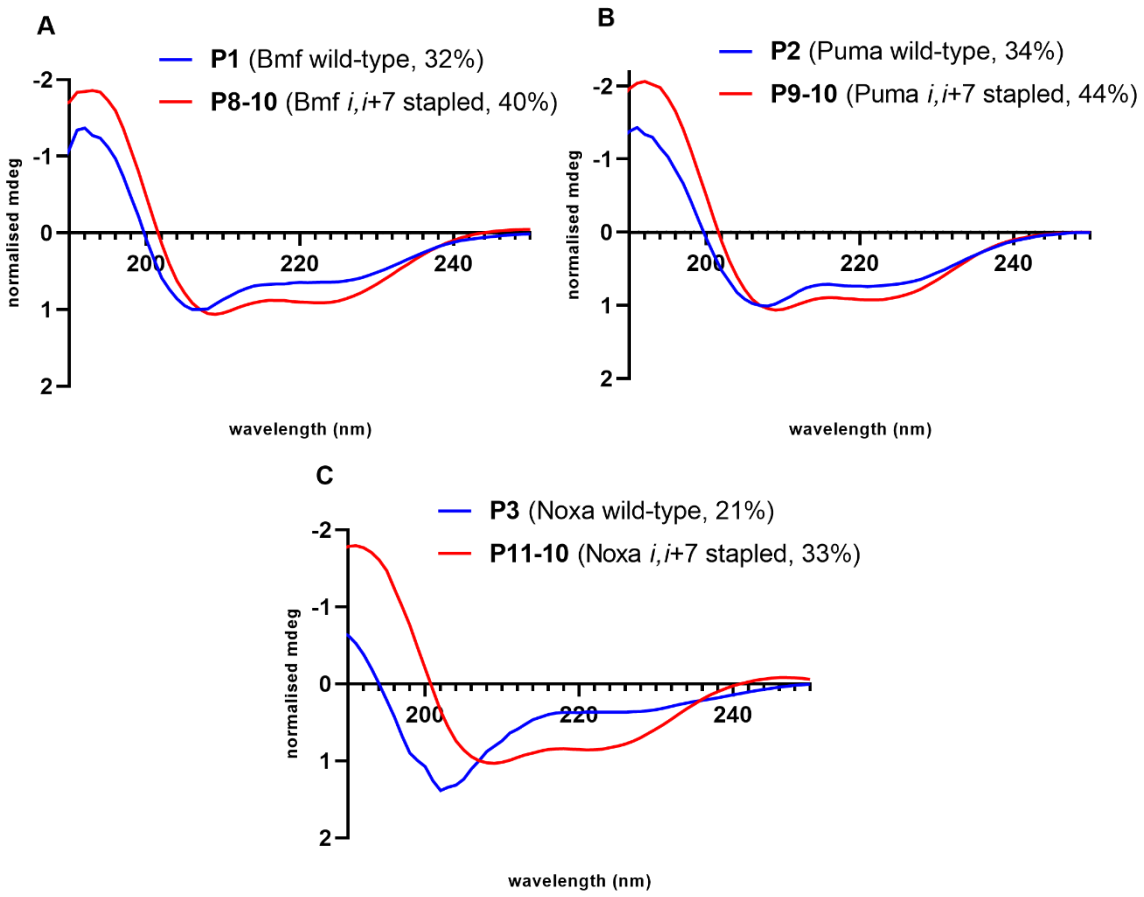

*Figure 38 CD spectra and % α-helicities for selected i,i+7 peptides: A) Bmf peptide **P8-10**, B) Puma peptide **P9-10** and C) Noxa peptide **P11-10** with the wild-type peptides **P1**-**P3** for comparison. All ellipticities have been normalised to a single wavelength (207 nm) and % α-helicity is given in brackets after the peptide number in the legend.*

2.3.5 Preliminary biological evaluation of *i,i*+7 BH3-only stapled peptides

The bioactivity of the functionalised BH3-only peptides **P8-11**, **P9-11** and **P11-11** were assessed in human platelets alongside ABT737,[160] initially looking at events associated with platelet apoptosis and activation.

PS exposure, which is indicative of platelet apoptosis,[177] and activation,[178] can be quantified in human platelets by measuring the specific binding of a fluorescently-labelled recombinant protein, annexin V, to PS. The percentage of positive platelets corresponds to annexin V-binding and consequently to PS exposure.[112] In a preliminary assay, human platelets were incubated with **P8-11**, **P9-11** and **P11-11**, and the binding to annexin V was measured over 3 hours (A, Figure 39). Whilst the control compounds (DMSO and ABT737) displayed the anticipated biological response,[160] only the result for **P8-11** after 3 hours (21.9% annexin V binding) was significantly different to the vehicle, DMSO. The other time points for **P8-11**, and the data for **P9-11** and **P11-11** do not show any significant difference from DMSO, indicating that these peptides do not cause PS exposure in human platelets.

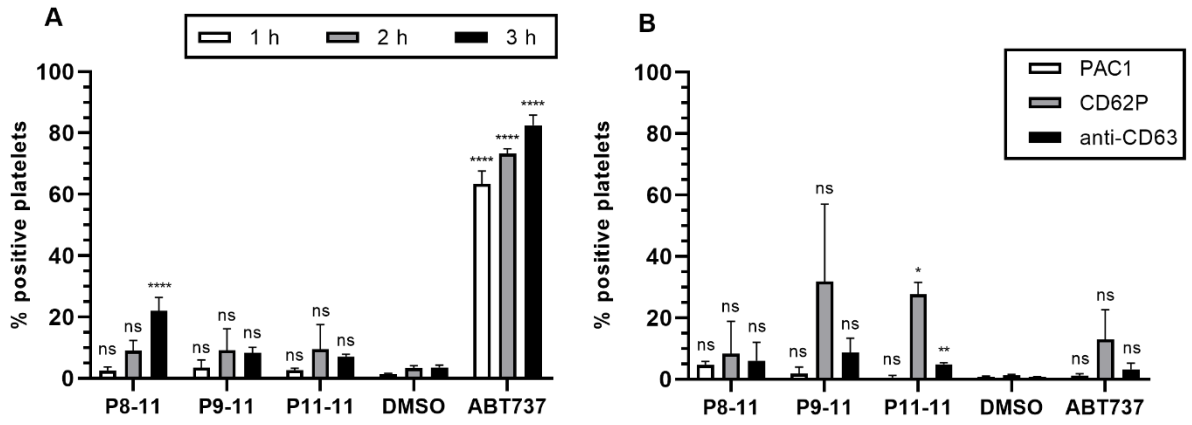

*Figure 39 The preliminary data for platelet PS exposure and activation marker binding after treatment with **P8-11**, **P9-11** and **P11-11**. A) The percentage positive platelets after incubation with peptides (10 μM), after 1, 2 and 3 h. B) The percentage positive platelets for PAC1 (white bar), CD62P (grey bar) and anti-CD63 (black bar) binding after incubation with peptides (10 μM) for 1 h. Each data point was replicated at least twice on two separate days. DMSO (1%) and ABT737 (10 μM) were included as controls. Data represent the mean ± standard deviation. Statistical significance compared to DMSO: **** P < 0.0001, ** P between 0.005 and 0.01, * P between 0.01 and 0.05, ns = non-significant.*

Events associated with platelet activation, such as increased expression of integrins and the secretion of both α- and dense granules, can be measured by flow cytometry with fluorogenic antibodies that bind specifically to certain receptors.[152] Standard platelet activation markers include:

- PAC-1, an antibody that specifically binds to the active form of integrin GPIIb/IIIa.
- CD62P that binds to P-selectin, an α-granule membrane protein.[179]
- An anti-CD63 antibody that specifically binds to CD63, a marker found in dense granules that becomes externalised on the platelet surface during activation.[160,151]

In a preliminary assay, washed platelet suspensions were incubated with **P8-11**, **P9-11** and **P11-11** for 1 hour and the percentage of platelets that bound to each of these antibodies was measured by flow cytometry (B, Figure 39). Treatment with ABT737 resulted in very low levels of activation marker binding, which is in-keeping with literature reports.[160] Only the results for CD62P and anti-CD63 binding after treatment with **P11-11** were significant (28 and 4.8% respectively), meaning that this peptide caused α- and dense granule release, events associated with platelet activation. For the other combinations of peptide treatment and activation marker, non-significant binding was observed, although, there is a large error associated with several of these results, therefore it is imperative that the data are replicated.

These combined results from the preliminary assays were somewhat unexpected. Bmf and Bad have the same specificities for Bcl-2 proteins in nucleated cells, therefore Bmf peptide **P8-11** could be expected to display a similar level of PS exposure as 'Bad-mimetic' ABT737 (ABT737 gives >80% annexin V-binding after 3 hours). Similarly, in nucleated cells Puma and Bim have the same specificity for the pro-survival proteins,[113] and an analogous *i,i*+7

polyarginine-functionalised Bim peptide displayed >60% annexin-V binding after 3 hours and >30% positive platelets for all three activation markers after 1 hour,[I] whereas treatment with Puma peptide **P9-11** was no different to the vehicle for both annexin V and activation marker binding. Finally, to date there are no literature reports of Noxa expression in human platelets, however peptide **P11-11**, gave significant levels of CD62P and anti-CD63 binding.

These assays will be repeated to improve the reliability of the data and allow confident conclusions to be drawn as to the effect of peptide treatment on annexin V and activation marker binding. If the observations discussed above are found to be valid, then further biological investigations are required to confirm that the observed phenotypic changes are a result of the peptides disrupting BH3 PPIs.

[I] Dr. Jessica Iegre, University of Cambridge, unpublished work.

2.4 Conclusions

The aim of this project was to develop chemical tools with which the roles of the BH3-only proteins in human platelets could be further elucidated. To this end, nine novel CuAAC stapled peptides were synthesised, based on the sequences of the α-helical BH3 domains of the Bmf, Puma and Noxa BH3-only proteins (Figure 40). Two different positions for CuAAC stapling, *i,i*+7 and 11, were investigated for synthetic tractability and the ability to induce α-helicity in the resulting stapled peptides. CD spectroscopy confirmed that the *i,i*+7 stapling architecture was successful in inducing α-helicity in the peptides, and this stapling methodology was used to rapidly synthesise polyarginine-functionalised stapled peptides **P8-11**, **P9-11** and **P11-11**.

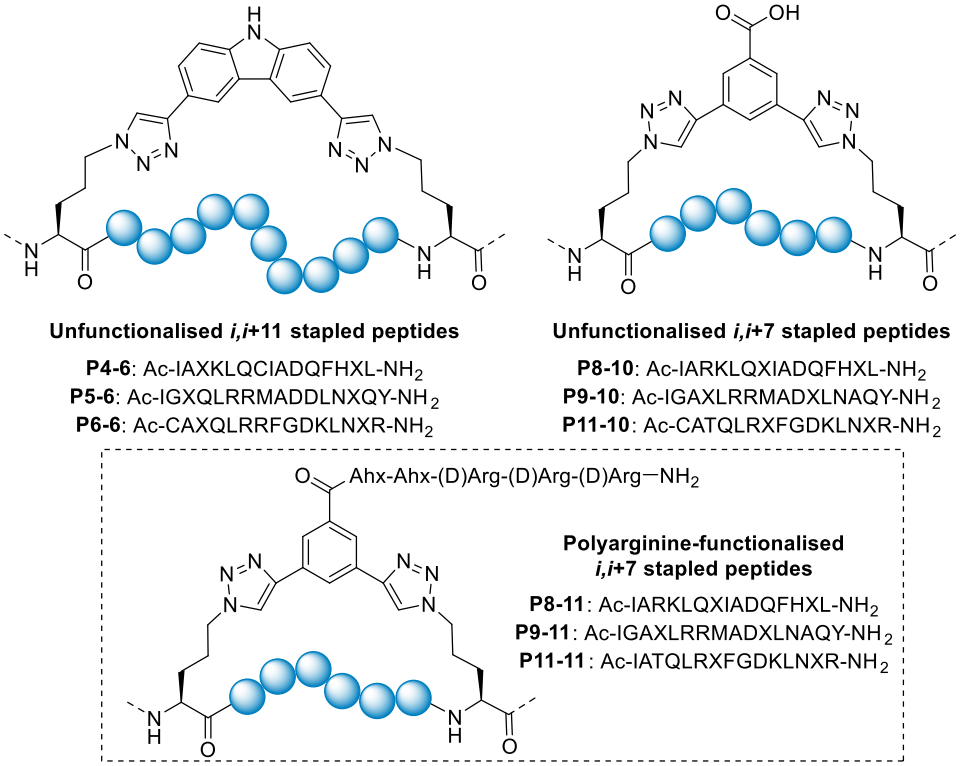

Figure 40 The BH3-only stapled peptides synthesised in this project. All peptides are C-terminal amides. X = Orn(N_3), Ahx = 6-aminohexanoic acid. Amino acids are represented by blue spheres.

In preliminary assays measuring the effect of the peptides on platelet activation and apoptosis, Bmf peptide **P8-11** caused a low level of PS exposure, and Noxa peptide **P11-11** induced dense- and α granule release. No significant activity was observed for the remaining peptides, indicating a heterogeneous phenotypic response to the different BH3-only stapled peptides. Further investigations are ongoing to confirm these preliminary results and to validate the mode of action of the peptides. It is anticipated that these chemical tools will enable further information to be gathered regarding the individual roles of the Bmf, Puma and Noxa BH3-only proteins in human platelets, and consequently may provide the basis for the development of novel therapeutics.

2.5 Future work

First, the data regarding the effect of **P8-11**, **P9-11** and **P11-11** on PS exposure and activation marker-binding in platelets will be replicated. The binding of the peptides to different pro-survival proteins (e.g. Bcl-x_L for Bmf and Puma peptides **P8-11** and **P9-11**, and Mcl-1 for the Noxa peptide **P11-11**) can be measured by surface plasmon resonance.[77] X-ray crystallography will be used to confirm that the stapled peptides are binding at the PPI interface of the pro-survival proteins for peptides with high binding affinities.[m] Additionally, the platelet uptake of fluorescently-labelled peptides will be measured, and the cellular localisation confirmed with confocal microscopy.[77] If it is identified that the peptides do not bind to any of the pro-survival proteins, or are unable to enter human platelets then alterations to the peptide sequences, staple architectures or CPP will be investigated.

To further probe the role of the Bcl-2 protein family in apoptosis of human platelets, assays measuring events that are closely related to mitochondrial apoptosis will be performed, and compared to ABT737, which has already been widely studied in the literature. Examples of assays that can be performed include measuring cytochrome c release,[160] caspase activity,[180,153] and mitochondrial membrane depermeabilisation.[156] To confirm whether the *i,i*+7 stapling does improve the proteolytic stability of the stapled peptides, the serum stability will be measured and compared to the wild-type sequences.[77]

Finally, the development of the selective Bcl-2 inhibitor ABT199 illustrates that selective Bcl-2 inhibitors that do not cause platelet apoptosis have potential as anti-cancer agents. Therefore, any stapled peptide which binds with high affinity to a pro-survival protein but has no effect on platelet apoptosis will be investigated as a new-modality anti-cancer therapeutic. Furthermore, to target the peptide to a specific cell-type, a homing peptide could be appended in place of, or in addition to the cell-penetrating tag on the staple.

[m] This will be done in collaboration with AstraZeneca, Cambridge.

Chapter 3

The development of cleavable stapled peptide-drug conjugates to target *Pseudomonas aeruginosa*

3. Chapter 3 - The development of cleavable stapled peptide-drug conjugates to target *Pseudomonas aeruginosa*

3.1 Introduction

3.1.1 Antimicrobial resistance

Antimicrobial resistance (AMR) describes the way in which bacteria (and other pathogens) modify their phenotype in order to evade the activity of antimicrobial drugs. As early as 1945, Sir Alexander Fleming warned in his Nobel Prize lecture: "*It is not difficult to make microbes resistant to penicillin in the laboratory by exposing them to concentrations not sufficient to kill them, and the same thing has occasionally happened in the body*."[181] As highlighted by Fleming, a pressing factor in AMR development is the over- and misuse of antimicrobials, which select for advantageous mutations. AMR can be passed from one resistant organism to another, leading to resistant populations of infecting pathogens.

Today, AMR is a very real and alarming threat to global health, garnering significant attention from global organisations. In 2016 the UK government, in collaboration with the Wellcome Trust, commissioned a report on AMR. The report estimated that by 2050 the number of global AMR-related deaths could be as high as 10 million per year, significantly outnumbering the predicted deaths due to cancer.[182] In 2019, the Interagency Coordination Group (IACG) on AMR produced a report for the Secretary-General of the United Nations.[183] The IACG stated that if effective action is not taken now, the economic cost of AMR could be comparable to that of the 2008 global financial crisis.

Preventing the progression of AMR requires a multi-faceted approach. The Pew Charitable Trusts put together a working group of leading scientists and experts to produce a 'Scientific Roadmap for Antibiotic Discovery'.[184] Recommendations include increasing public awareness, using existing drugs sparingly and enriching the current antibiotic discovery pipeline. However, the rapid onset of AMR makes the development of new antimicrobials challenging. It is not surprising therefore that the pharmaceutical industry is divesting from antimicrobials in favour of therapeutic areas with more commercial return, for example oncology.[185] Current antibiotic pipelines are heavily focused on prophylactics, leaving a need for antibiotics to treat infections.[186] The Pew Charitable Trusts report specifically points towards the need for non-traditional and multi-targeted therapies. This is echoed by the key messages and recommendations of the IACG 2019 report, which include the need for the development of *"…new antimicrobials (particularly antibiotics) [and] novel compounds…"*[183]

3.1.2 *Pseudomonas aeruginosa*

Pseudomonas aeruginosa is an opportunistic pathogen that presents a major threat to immunocompromised individuals such as patients with AIDS, cystic fibrosis (CF), burns victims and new-born babies.[187] It is also responsible for around 10% of nosocomial bacterial infections.[188] As an ESKAPE pathogen,[n] *P. aeruginosa* demonstrates high levels of resistance to standard antibiotics and, consequently, the World Health Organisation (WHO) have identified the development of novel antibiotics to treat this pathogen as a critical priority.[189]

Current treatment for *P. aeruginosa* infections are antibiotics including aminoglycosides (e.g. tobramycin), fluoroquinolones (e.g. ciprofloxacin), polymyxins (e.g. colistin), cephalosporins (e.g. ceftazidime), carbapenems (e.g. meropenem) and penicillin/β-lactamase inhibitor combinations (e.g. piperacillin-tazobactam).[190] The extensive use of these drugs exposes the bacteria to intense selection pressures, resulting in the rapid emergence of multi-drug resistance (MDR). As the prevalence of MDR *P. aeruginosa* infections increases, determining the appropriate medication requires the analysis of patient isolates for drug susceptibility, which increases the treatment time and cost.[191]

Developing effective treatments for *P. aeruginosa* infections is extremely challenging due to the intrinsic resistance mechanisms displayed by this pathogen; the formation of biofilms and the nature of the Gram-negative bacterial envelope are two contributing features.

3.1.2.1 Biofilms

A biofilm consists of bacteria embedded in an extracellular matrix composed of lipids, DNA, polysaccharides, and proteins. Biofilm composition has a large impact on cell-to-cell interactions and the overall bacterial virulence.[191] Biofilms are intrinsically resistant to antibiotics and host clearance mechanisms, such as phagocytes.[192] It is therefore beneficial for bacteria to form biofilms as they protect the bacteria from antibiotics, bacteriophages and other competing organisms. *P. aeruginosa* readily forms biofilms on the surface of medical implants, often necessitating intensive courses of antibiotics and additional surgeries.[193] Additionally, chronic *P. aeruginosa* infections are common in CF patients, as the mucus plugs formed in the lungs provide an ideal environment for colonisation and biofilm formation.[194] Such infections represent a major cause of mortality in the CF patient population.[188,195]

[n] ESKAPE = *Enterococcus faecium*, *Staphylococcus aureus*, *Klebsiella pneumoniae*, *Acinetobacter baumannii*, *Pseudomonas aeruginosa*, and *Enterobacter* spp. Together these pathogens are the leading cause of nosocomial infections globally.[347]

One cause of the AMR displayed by bacterial biofilms is the delayed penetration of drugs through the biofilm matrix. However, it has been suggested that, for *P. aeruginosa* infections, this is not the primary protective mechanism.[196] Instead, it has been shown that a more probable explanation is that bacteria in biofilms have reduced rates of metabolism and growth. As most antibiotics are more effective against rapidly-growing cells, bacteria living within biofilms are less susceptible.[192] A final, more putative mechanism involves the growth of 'persister' cells within the biofilm.[197] This theory states that some cells within the biofilm develop a specific MDR phenotype. Treatment with antibiotics kills most of the non-persister cells in the biofilm, leaving a population of MDR, persister bacteria.[198]

3.1.2.2 Gram-negative bacterial membranes

Unlike mammalian cells, most bacteria have an outer layer that determines the shape of the cell and protects the cellular contents from damage.[199] This is the bacterial cell wall, which is comprised of peptidoglycan, a mesh-like structure made up of polysaccharide strands crosslinked with short peptides.[200] Bacteria are characterised according to the composition of their cell wall using the Gram staining test. Gram-positive bacteria are named as such because they have a thick cell wall which absorbs and retains a crystal violet dye. Conversely, Gram-negative bacteria have a thin cell wall protected by an outer membrane, therefore, they only absorb a small amount of dye and are decolourised after washing.[187]

The Gram-negative cell envelope consists of the outer membrane, a periplasmic space containing a thin peptidoglycan cell wall and the inner membrane (Figure 41).[201] Gram-positive bacteria, by comparison, have just an inner membrane, but a much more extensive peptidoglycan layer, hence why they retain the crystal violet dye during the Gram staining test. The outer membrane in Gram-negative bacteria has a distinct composition compared to the inner membrane; it is asymmetric, with the inner leaflet comprised of phospholipids and the outer leaflet made up of lipopolysaccharide, a glycolipid containing lipid A which is unique to Gram-negative bacteria (Figure 41). The outward-facing phosphate groups of the lipopolysacharide give the outer membrane a negatively charged exterior.[201] The outer membrane contains surface proteins involved in a variety of roles such as transport; multi-component proteins such as porins span the outer membrane allowing the passage of specific ions and molecules (Figure 41).[201]

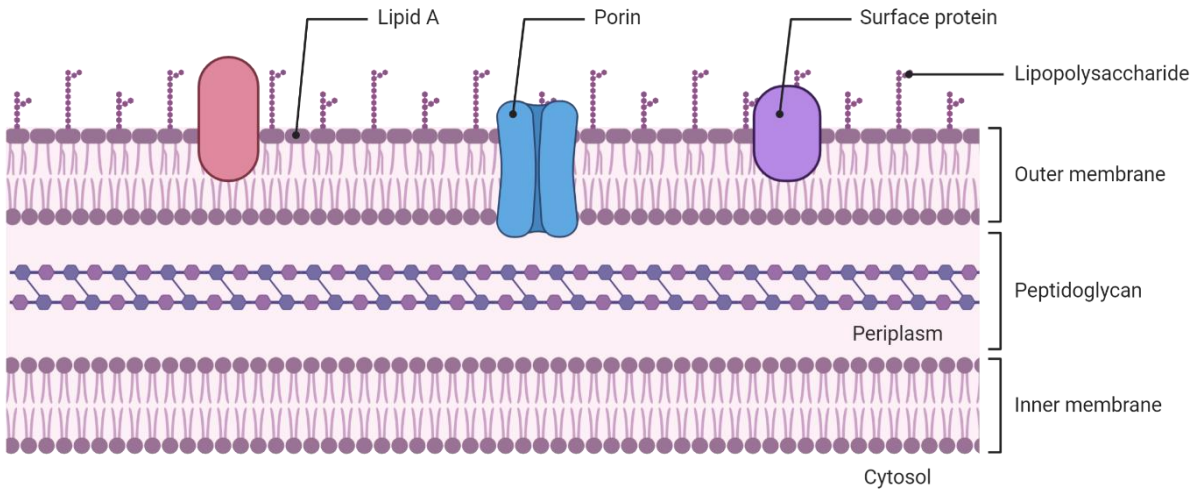

Figure 41 A simplified diagram showing the Gram-negative bacterial envelope, consisting of the outer membrane, a thin peptidoglycan layer and the inner membrane. The outer membrane contains lipopolysaccharide, lipid A, porins and surface proteins.

The integrity of the cell envelope is vital for bacterial survival; the cell wall provides structural rigidity to the bacteria and prevents it from swelling. The outer membrane is also necessary as a selective barrier, allowing the transport of essential nutrients and the exclusion of potentially toxic chemicals; it is generally permeable to small ions and small hydrophilic molecules and impermeable to larger hydrophobic and amphipathic molecules. The unique properties of the bacterial outer membrane allow the selective targeting of Gram-negative bacteria over Gram-positive bacteria and mammalian cells.[202]

The outer membrane of *P. aeruginosa* exhibits a particularly low permeability to drugs. Furthermore, it contains a battery of efflux pumps with wide substrate scopes that are capable of removing xenobiotic drugs that do manage to bypass this membrane and gain entry to the cell.[203] Consequently, common antibiotics such as penicillins, cephalosporins, tetracyclines, quinolones and chloramphenicol are often ineffective against this species.[187]

3.1.3 Antibiotics

Antibiotics are chemicals that either kill or prevent the growth of microbes. The word antibiotic can be literally translated to ‘anti-life’, however the term is generally used today to mean either antibacterial or antifungal agents.[204] The broader term antimicrobials extends this definition to include antiviral and antiparasitic agents; this report focusses on the bacterium *P. aeruginosa* and so the two terms will be used interchangeably.

Humankind has been benefitting from the use of antimicrobial agents for thousands of years: there are documented examples of mouldy bread, honey and herbs being used to treat infections in ancient Egypt, China and Rome.[187] In the early 20th century, Paul Ehrlich noticed

whilst developing dyes for bacterial stains that some compounds had an antibacterial effect. This led to his laboratory searching for the 'magic bullet' – a drug which would have the desired therapeutic effect without affecting human cells. Their screening efforts resulted in arsphenamine, the first synthetic antimicrobial agent that was used to treat syphilis.[205] The next era of antimicrobial discovery involves the well-known story of penicillin G discovery by Sir Alexander Fleming. The translation of his original observation into a clinically relevant medicine undoubtedly saved many lives and sparked a campaign of antimicrobial discovery and development that resulted in many of the key drugs still in use today.[206] In 2019, WHO published the 21st Essential Medicines List, which documents the drugs that are necessary to meet the needs of a healthcare system, and includes over 40 antimicrobials.[84] Antimicrobial agents can be fully synthetic, semi-synthetic, natural products or novel modalities; some of the major classes of antibiotics are listed in Table 13.

Table 13 An overview of the major classes of antibiotics, with key examples, sources and targets. Adapted from Brown and Wright.[207]

Class	Example	Target	Source
Sulfonamides	Sulfanilamide	Folate synthesis	Synthetic
Fluoroquinolones	Ciprofloxacin	DNA topoisomerases	Synthetic
β-Lactams	Ceftazidime	Cell wall synthesis	Natural product
Oxazolidinones	Linezolid	Protein synthesis	Synthetic
Aminoglycosides	Neomycin	Protein synthesis	Natural product
Glycopeptides	Vancomycin	Cell wall synthesis	Natural product
Polymyxins	Polymyxin B	Bacterial cell membrane	Natural product
Cyclic lipopeptides	Daptomycin	Bacterial cell membrane	Natural product
Tetracyclines	Tetracycline	Protein synthesis	Natural product

These classes of antibiotics have been reviewed extensively elsewhere, but particular attention will be afforded here to the fluoroquinolones and β-lactams as they are of particular relevance to this chapter.[187,204,208]

3.1.3.1 Quinolones and fluoroquinolones

The quinolones are a class of broad spectrum, fully synthetic antibiotics which are amongst the most prescribed antibiotics globally.[209] They act by inhibiting two DNA topoisomerases, DNA gyrase and topoisomerase IV. DNA gyrase is responsible for actively introducing negative supercoils into DNA and DNA topoisomerase IV relaxes positive supercoils; both are essential for bacterial survival.[204] The first generation of quinolones were introduced in 1962, and two decades later a second generation, the fluoroquinolones, were developed with improved pharmacokinetic and pharmacodynamic properties.[187] Ciprofloxacin, levofloxacin and moxifloxacin are fluoroquinolone antibiotics included in the WHO Essential Medicines List (Figure 42).[84]

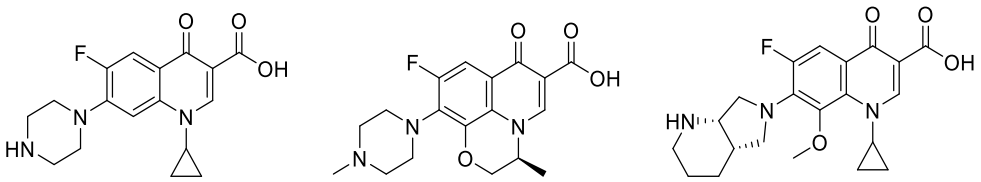

Figure 42 The structures of fluoroquinolone antibiotics ciprofloxacin, levofloxacin, and moxifloxacin.

Resistance to fluoroquinolones is increasing, in part due to their widespread usage.[210] Bacteria are capable of modifying drug targets so that the drug becomes ineffective and the target is functional.[204] In *P. aeruginosa*, DNA gyrase mutations are often the first step in the development of resistance.[211] Other mechanisms involve the over-expression of efflux pumps, which reduces the intracellular concentration of the drug: a lowered concentration at the target not only reduces the antibacterial effect but also can favour mutations in the target leading to resistance.[212,213] As many efflux pumps have a broad substrate scope, their over-expression can increase resistance not just against the treating antibiotic, but other classes as well.

3.1.3.2 β-Lactams

The β-lactams are a class of antibiotics which contain a β-lactam ring motif and include penicillins, cephalosporins, monobactams and carbapenems. They represent the most commonly consumed antibiotics globally.[214] Penicillin G and cephalosporin C represent the first molecules in each of these classes of β-lactams (Figure 43).[187]

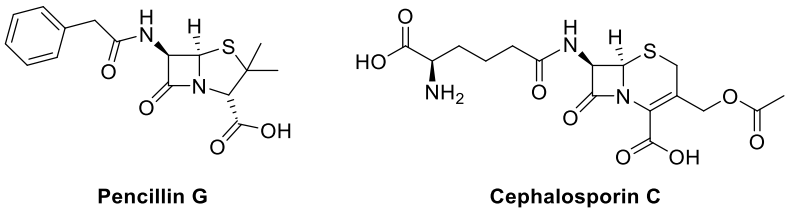

Figure 43 The structure of β-lactam antibiotics penicillin G and cephalosporin C.

β-Lactam antibiotics target the transpeptidase enzymes which contain a catalytic serine residue and facilitate cross-linking within the peptidoglycan portion of the bacterial cell wall. The integrity of the cell wall is vital for survival; inhibiting the cross-linking reactions within the peptidoglycan weakens the cell wall and causes bacteria to rupture. In the transpeptidase mechanism, a (D)Ala-(D)Ala moiety at the end of one peptide chain binds to the enzyme, and a catalytic serine residue facilitates the formation of an amide bond between this peptide chain and another (Figure 44).[187]

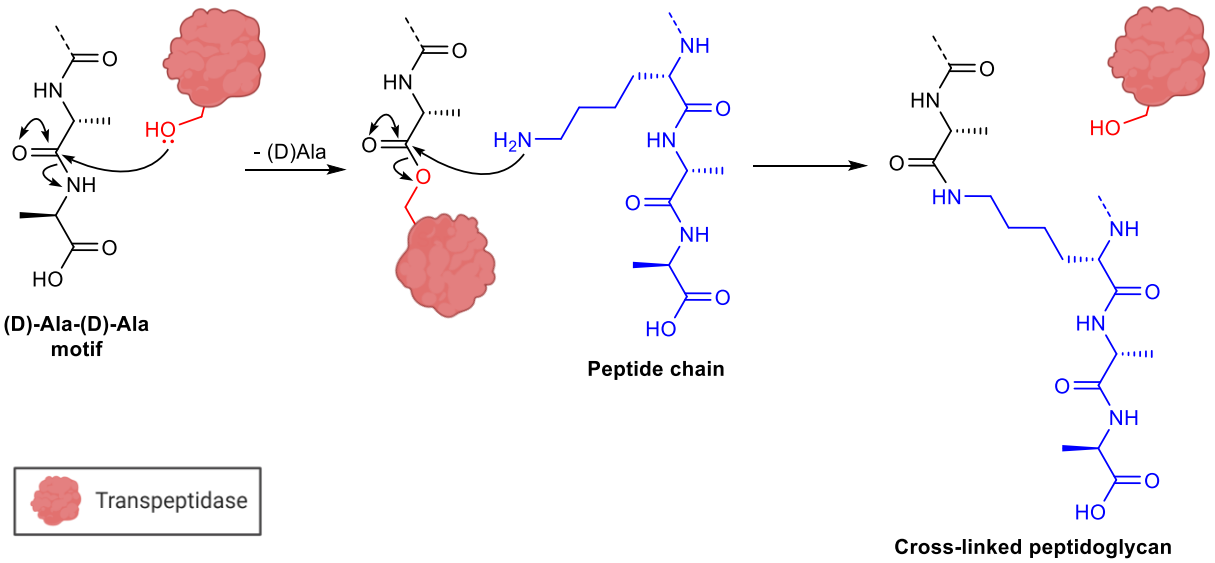

Figure 44 A simplified mechanism of transpeptidase-catalysed peptidoglycan cross-linking. The catalytic serine residue of the transpeptidase enzyme is highlighted in red, the (D)Ala-(D)Ala moiety is shown in black, and the cross-linking peptide chain is highlighted in blue.

It is thought that penicillin works by binding to the transpeptidase enzyme as it has a similar structure to the terminal (D)Ala-(D)Ala dipeptide (A, Figure 45).[187] The normal transpeptidase mechanism is initiated with penicillin as the substrate, however due to the structure of the β-lactam, a covalent intermediate is formed which blocks the active site (B, Figure 45).

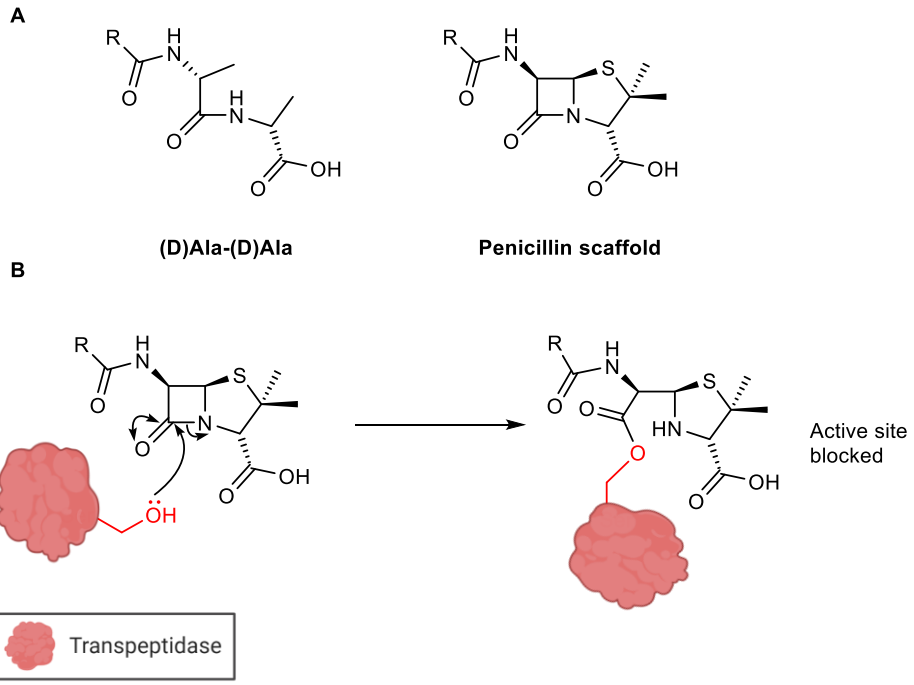

Figure 45 A) A comparison of the structure of the (D)Ala-(D)Ala dipeptide and a general penicillin scaffold, B) the mechanism by which a β-lactam antibiotic blocks the active site of transpeptidase enzymes. R = variable group.

Since the mass production of penicillin G was enabled by the combined research efforts of Fleming, Corey and Chain, this class of antibiotics has benefitted millions of patients.[206] The

second class of β-lactam antibiotics to be discovered were the cephalosporins, which are structurally related to penicillins but display higher resistance to acid degradation and β-lactamase (BL) activity (two major drawbacks with the earlier penicillin drugs).[187]

Bacterial resistance towards β-lactam antibiotics is well understood, and is mainly due to the production of BL enzymes.[215] BLs are structurally similar to transpeptidases and can sequester β-lactam antibiotics by hydrolysing the 4-membered ring, rendering the drug inactive. For most BL enzymes, this problem can be overcome through the co-administration of BL inhibitors, for example clavulanic acid.[187] Additional resistance mechanisms are similar to those discussed for the fluoroquinolones; porins and efflux pumps also play a major role in β-lactam resistance, particularly in *P. aeruginosa,* by maintaining a low intracellular concentration of the drug.[204] The final key mechanism by which resistance emerges is the mutation of the drug target, in this case certain transpeptidases.[187]

3.1.3.3 Problems with current antibiotics

Many antibiotics suffer from low bioavailability, requiring high and regular dosing to maintain a sufficient concentration of the drug at the site of infection.[216] This can lead to several problems, one of the most threatening of which is the development of resistance mechanisms. However, another major issue is the systemic toxicity that is inherent for some classes of antibiotics. Key examples include the polymyxin family of antibiotics, which are last-resort drugs for *P. aeruginosa* infections however their clinical use has been limited for years due to associated nephro- and neuro-toxicity.[217] Additionally, the FDA recently updated the guidance for ciprofloxacin to include warnings about adverse effects associated with low blood sugar and mental health.[218] Whilst broad-spectrum antibiotics are valuable as they allow treatment without the need for time-consuming and costly diagnosis, their use can result in significant side-effects.[219] Conversely, narrow-spectrum antibiotics (or 'precision antibiotics') allow the selective targeting of certain strains whilst sparing other bacterial communities in the body, but precise and reliable diagnostic tests are required to determine a suitable drug.[220] Many antibacterial targets are conserved amongst different species, so antibiotic treatments frequently risk harming non-infecting, non-pathogenic bacteria, which can result in gastro-intestinal side effects.[216] Whilst trivial for most, this can be dangerous for patients with additional health conditions.

Within the current arsenal of antibiotics, there is a chronic lack of new chemical structures and bacterial targets. Current treatments are heavily reliant on a few structural classes of drugs and a small reserve of targets. WHO surveillance of AMR has highlighted that pathogenic bacteria are showing increasing levels of resistance towards last-resort antibiotics such as

carbapenems, and, since 2000, only six new classes of antibiotics have been brought to market.[221] Promisingly, several of these drugs have novel mechanisms of action, however, they only target Gram-positive bacteria,[222] and four out of the six ESKAPE pathogens are Gram-negative, leaving a niche that remains to be filled.[223] More efforts are required to develop effective drugs capable of overcoming the challenges posed by Gram-negative bacteria, such as the low permeability of the outer membrane and formation of drug-resistance biofilms.[216]

The current lack of new antibiotics is the result of a more general issue, the poor rate of antibiotic discovery. After the initial rush of the so-called 'Golden-era' of antibiotic discovery, very few new classes of antibiotics were brought to market between the 1960s and 2000s.[224] During this time, new drugs were typically structurally-similar members of existing classes, which do little to solve the emerging resistance crisis.[225] It is clear that there are too few antibacterial agents in development to address the challenge of MDR.[226]

Various organisations and government entities are united in calling for more investment in antibiotic discovery. Aside from traditional small molecule drugs, recommendations have been made for the investigation of non-traditional and alternative therapies, focussing on different bacterial targets and more unusual molecular architectures. The 2015 WHO Global Action Plan on AMR calls for investment in the development of new medicines,[226] which is echoed by The Pew Charitable Trusts' Scientific Roadmap for Antibiotic Discovery, which identifies the need for research into '*non-traditional therapeutic approaches*' including '*non-small molecule approaches*'.[184] The UK Government Review on AMR goes one step further, specifically naming antimicrobial peptides (AMPs), phage therapy and antibodies as promising alternative therapies requiring investment and research.[185]

3.1.4 Alternative antimicrobial strategies

AMR has forced researchers to consider novel approaches to combat bacterial infections. These approaches can be broadly split into two categories: the re-purposing of existing antimicrobials and the development of novel therapeutic agents. Existing drugs can be repurposed as prodrugs and hybrid antimicrobials. Novel therapies include new targets such as quorum sensing inhibitors, efflux pump inhibitors and membrane-disrupting peptides.[208,227] Key examples which are of relevance to this thesis will be discussed in this section.

3.1.4.1 Prodrugs

A prodrug is an inactive chemical which is converted into an active drug once inside the body, either *via* a chemical or enzymatic transformation.[228] Prodrugs can have improved aqueous solubility and reduced side effects compared to the active drug and therefore represent an attractive method for re-purposing existing antibiotics.[229] In particular, producing a prodrug that has masked polarity and charged functional groups can improve bacterial cellular penetration.

Fluoroquinolone ciprofloxacin suffers from poor aqueous solubility and low intestinal permeability. As a result, ciprofloxacin prodrugs have been investigated *via* modifications of the carboxylic acid moiety, for example a triethylene glycol-ciprofloxacin prodrug (Figure 46), which showed a 400-fold improvement in aqueous solubility and a comparable minimum inhibitory concentration (MIC) to ciprofloxacin in the presence of esterase enzymes.[230]

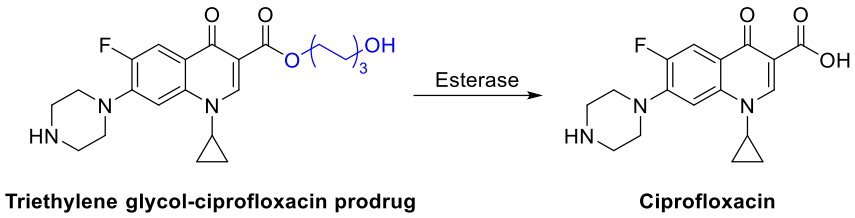

Figure 46 The structure of a ciprofloxacin-PEG prodrug, with the PEG ester group highlighted in blue.[230] Esterases catalyse the release of free ciprofloxacin.

Whilst the previous example used human esterases to release the active therapeutic, a more refined approach is to use bacterial enzymes so that the active drug is only revealed in the presence of bacteria. To this end, cephalosporin moieties have been used as release mechanisms. In this instance the β-lactam ring of the cephalosporin is selectively cleaved by BLs and the intermediate 6-membered ring can undergo a 1,4-elimination, resulting in the release of the cargo at the 3'-methylene position (Scheme 11). The cephalosporin ring system is favoured over other β-lactam scaffolds as it has obvious handles for synthetic derivatisation and it exhibits superior stability compared to penicillin scaffolds.[187]

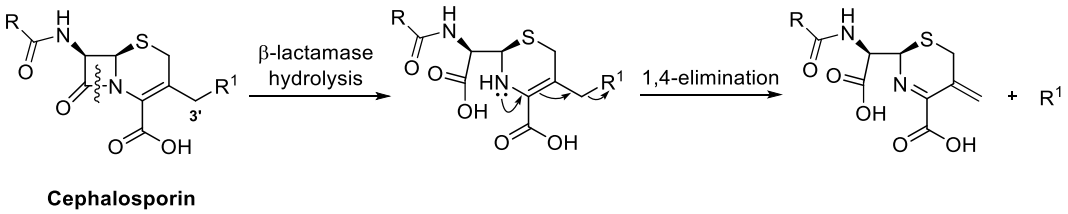

Scheme 11 The BL hydrolysis of the β-lactam ring in a cephalosporin. This is followed by 1,4-elimination and subsequent release of a leaving group, R^1. R is a variable group on the cephalosporin.

The cephalosporin group was first used as a prodrug moiety in antibody-directed enzyme therapy for cancer treatment in the 1990s.[231] In this therapy, treatment with a prodrug of the desired cytotoxin is followed by an antibody targeting a specific tumour cell type, with BL

enzymes covalently attached to it. Consequently, the cytotoxin prodrug is only converted to the active drug at the desired site of action. For this approach, an enzyme was required which had satisfied the following criteria: to be highly substrate specific, to have the ability to catalyse a scission reaction, and to be highly orthogonal to enzyme activity in the body so that the drug would not be released elsewhere. These requirements are satisfied in the cephalosporin group. The BL-mediated release of many drugs was investigated including for taxol and doxorubicin.[232–234]

More recently a cephalosporin prodrug of ciprofloxacin was reported, masking the carboxylic acid that is necessary for antibiotic activity, but contributed to the poor solubility and permeability of this drug (A, Figure 47).[235] In the presence of BL-producing bacterial strains the prodrug had a two-fold lower MIC value than ciprofloxacin, whereas in BL-negative strains the prodrug was 10-fold less active.

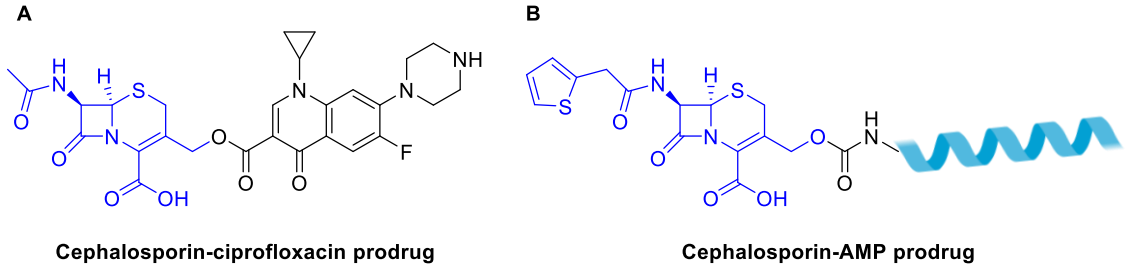

Figure 47 The structure of two prodrugs featuring a cephalosporin release mechanism. A) A cephalosporin-ciprofloxacin prodrug,[235] and B) A cephalosporin-peptide prodrug developed by Desgranges et al.[236]

Desgranges *et al.* applied a similar prodrug strategy to a peptide with antimicrobial activity, which exhibited an intimate relationship between its overall positive charge and antimicrobial activity (B, Figure 47).[236] Modifying the *N*-terminus of the peptide with a cephalosporin moiety would reduce this overall charge and the authors hypothesised that the resulting prodrug would have a lower activity. The cephalosporin group ensures that the 'free' peptide is only released in the presence of BL producing bacteria, allowing selective release. When tested against BL-positive strains of *Escherichia coli* and *Staphylococcus aureus* the prodrug was not as active as the parent peptide, however the prodrug was about two-fold more active in BL-positive *E. coli* than a BL-negative strain. The authors hypothesised that this approach may be more effective with a shorter peptide with a lower overall positive charge, as there would be a greater differential between the prodrug and parent peptide.

3.1.4.2 Drug-drug conjugates

Combination treatments are frequently used in the clinic, the most common being the co-administration of a β-lactam antibiotic with a BL inhibitor. Amoxicillin/clavulanic acid is one such combination which features on the WHO List of Essential Medicines.[84]

Certain drug combinations are considered to be synergistic if their overall inhibitory effects are greater than the sum of their individual inhibitory effects, which allows lower doses of each component, thus reducing side-effects and off-target toxicity.[237] The probability of a bacterium developing resistance towards two drugs at the same time is low, therefore combination therapies can slow down the rate at which resistance emerges.[238] However, synergistic effects observed *in vitro* often do not translate *in vivo*, particularly for Gram-negative bacteria.[239] A possible cause for this is the different pharmacokinetic properties of the individual drugs, however, covalently linking the drugs can solve this problem by forcing them to adopt the same pharmacokinetic profile.[238] Additionally, the properties of one of the drugs can improve those of the other, for example by increasing its cellular penetration and reducing efflux.[240] There is precedent for the production of conjugated, hybrid antimicrobial agents in nature, an example being the thiomarinols.[241]

Antibiotic conjugates where both parts exert an antimicrobial function of their own are sometimes referred to as 'hybrid' drugs.[238] The construction of these hybrids is one of the strategies deployed to expand the use of fluoroquinolone antibiotics in the face of widespread AMR. Conjugates of ciprofloxacin account for a large proportion of the literature on hybrid antibiotics for several reasons.[242] Firstly, fluoroquinolones typically have good cell penetration and are stable to a wide range of chemical transformations, which in part accounts for their success in the clinic to date.[243] There is also a wealth of literature available on the structure-activity-relationships of different fluoroquinolone analogues that can guide conjugate design. Finally, many fluoroquinolones are themselves dual-targeting, inhibiting both DNA topoisomerase IV and II (DNA gyrase).[244] This means that if the chemical modification necessary for conjugation reduces the affinity of the fluoroquinolone scaffold for one of these enzymes, it may still retain activity towards the other.

A conjugate of the fluoroquinolone moxifloxacin and the aminoglycoside tobramycin clearly illustrates the advantages of covalent conjugation (A, Figure 48).[240] The hybrid antibiotic displayed improved outer membrane permeability and reduced efflux in *P. aeruginosa* compared to the individual components. Under conditions designed to subject the bacteria to selective pressure, the MIC values for tobramycin and moxifloxacin increased by 512- and 16-fold respectively, whereas the MIC for the hybrid conjugate only increased by 2-fold, indicating that it delays the development of resistance.

Hybrid antimicrobials have been tested in the clinic, for example TD-1792, a conjugate of the glycopeptide vancomycin and the cephalosporin ceftazidime, both targeting different aspects of cell wall biosynthesis, developed by Theravance Biopharma (B, Figure 48). TD-1792 displays synergistic activity against MDR Gram-positive bacterial strains that cannot be achieved with a combination of the individual drugs.[245] TD-1792 completed Phase II clinical trials for the treatment of Gram-positive skin infections in 2007, but no clinical trials have been listed since.[246]

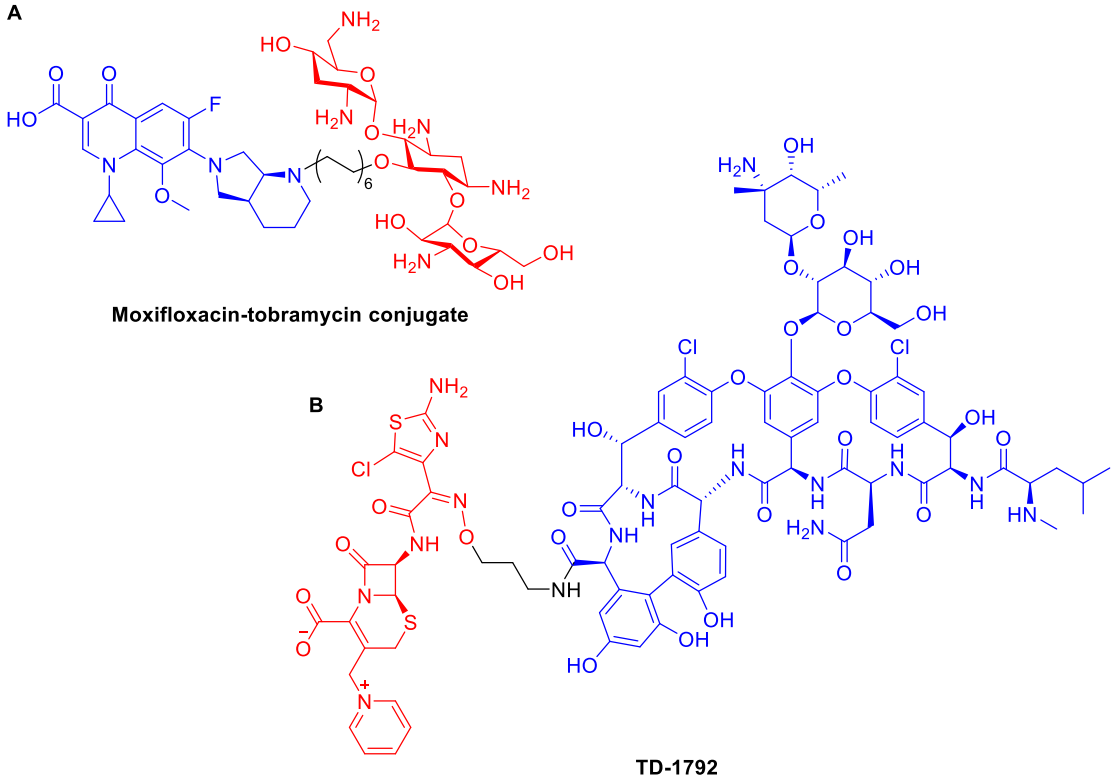

Figure 48 The structures of two hybrid antimicrobials. A) A drug-drug conjugate consisting of moxifloxacin (blue) and tobramycin (red).[240] B) TD-1792, consisting of vancomycin (blue) and ceftazidime (red).[245]

Drug-drug conjugates are not the only class of hybrid drug that have been reported. In addition, conjugates consisting of antibiotics attached to chemicals which either promote their uptake, target the drug to the bacteria or sensitise the bacteria to the drug have been investigated.

3.1.4.3 Siderophore-drug conjugates

Chemicals that promote the uptake of compounds into bacterial cells are found in nature and can be exploited to facilitate the absorption of cytotoxic synthetic compounds: siderophores are one such example. Iron is essential for bacteria, however, Fe(III) has an extremely low aqueous solubility and therefore is not bioavailable to most microorganisms.[247] Consequently bacteria have developed strategies for iron uptake, one of which is the production of iron-

binding siderophores. Typical siderophore structural motifs include catecholates, carboxylates, phenolates and hydroxamates.[248] Natural siderophore-antibiotic conjugates exist, called sideromycins. Albomycin is one example, comprising a hydroxamate iron-binding motif attached to a thioribosyl pyrimidine antibiotic moiety (Figure 49). Once inside the bacteria, the peptide linker is cleaved, releasing the antibiotic.[249]

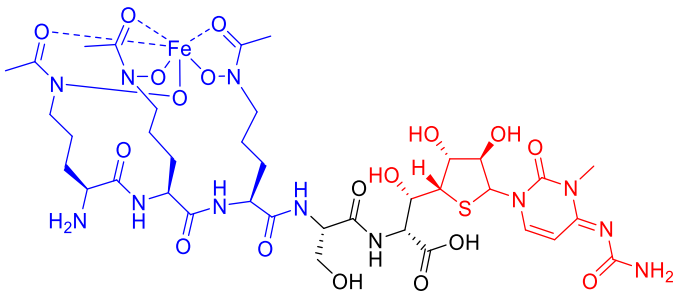

Figure 49 The structure of albomycin, a natural antibiotic (red)-siderophore (blue) conjugate.

Inspired by this natural siderophore-antibiotic conjugate, synthetic conjugates have been synthesised with many different combinations of siderophore and antibiotic.[238] The Nolan group have contributed widely to this field, developing ciprofloxacin- and β-lactam-siderophore conjugates. Their initial work focused on developing β-lactam-siderophore conjugates that were selectively taken up by IroN, a siderophore receptor associated with increased virulence.[250] Conjugates of penicillins ampicillin and amoxicillin were synthesised, incorporating a derivative of natural siderophore enterobactin, a cachecolate that is common in Gram-positive bacteria and displays one of the highest affinities for iron (Figure 50).[251] It was found that the β-lactam-siderophore conjugates displayed a 100-fold increase in antibacterial activity compared to the parent drugs.

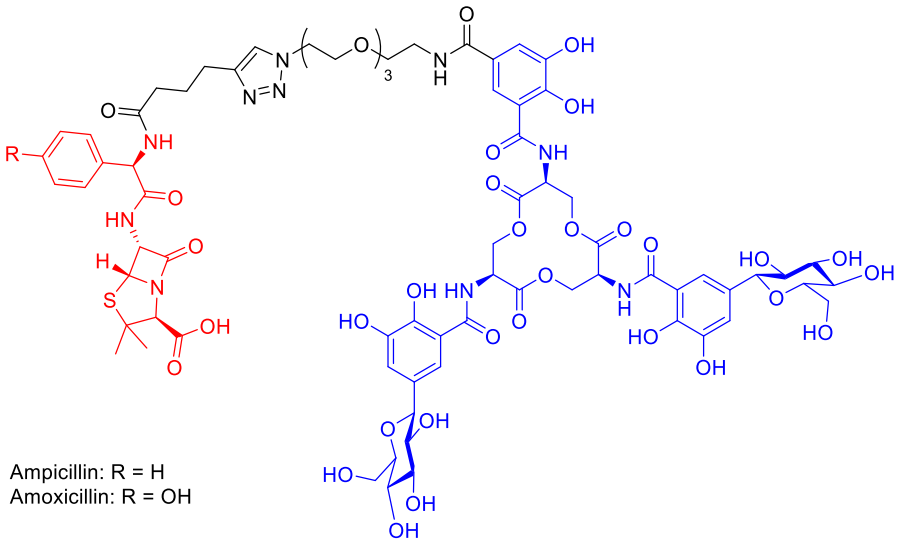

Figure 50 The structure of an antibiotic-siderophore conjugate comprised of a β-lactam (red) and enterobactin analogue (blue).[250]

More recently, the Nolan group conjugated ciprofloxacin to a siderophore to improve cellular uptake (Figure 51).[252] The conjugate acts as an inactive prodrug, and is selectively taken up by bacteria which express the uptake machinery for enterobactin. The free drug is released intracellularly after hydrolysis of the siderophore. The conjugate shows comparable activity to free ciprofloxacin, however the highlight of this work lies in the mechanism of release. Studies found that hydrolysis of the enterobactin moiety is mediated by IroD, a cytoplasmic hydrolase which is expressed in pathogenic strains of *E. coli*. This demonstrates, therefore, that siderophore-antibiotic 'prodrugs' could be designed which are selectively taken up and hydrolysed only in pathogenic bacteria.

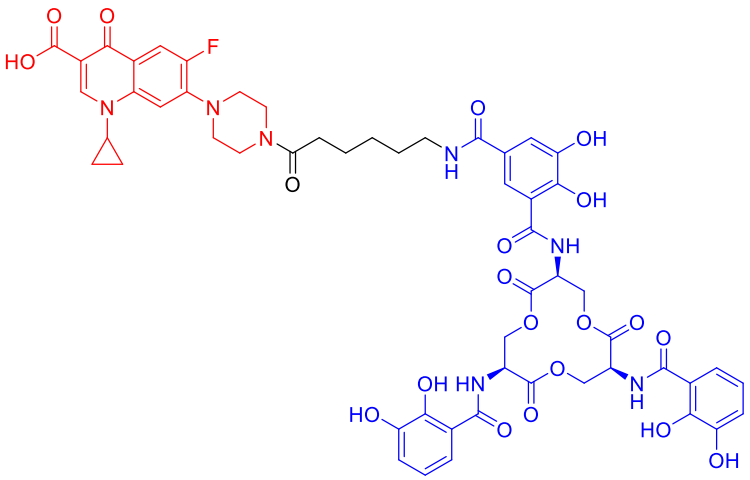

Figure 51 The structure of a ciprofloxacin (red)-siderophore (blue) conjugate.[252]

3.1.4.4 Cell-penetrating peptide-drug conjugates

Another approach to improving the accumulation of antibiotics inside bacteria is the attachment of cell-penetrating peptides (CPPs). Some CPPs are able to translocate bacterial membranes with no bacteriostatic or bactericidal activity, others display toxicity towards the bacteria, and many CPPs sit between these two extremes in activity. The exact role of the CPP in a CPP-drug conjugate varies depending on the example and the target bacteria. Deshayes *et al*. published a drug-CPP conjugate consisting of the aminoglycoside tobramycin conjugated to the protein-derived CPP penetratin,[253] which has no antimicrobial activity and therefore serves only to improve the cellular uptake of the drug in this instance. The conjugate displayed improved antibacterial activity and significantly increased inner membrane permeability compared to the individual components and higher antibacterial activity against so-called 'persister cells' compared to tobramycin alone (Figure 52).

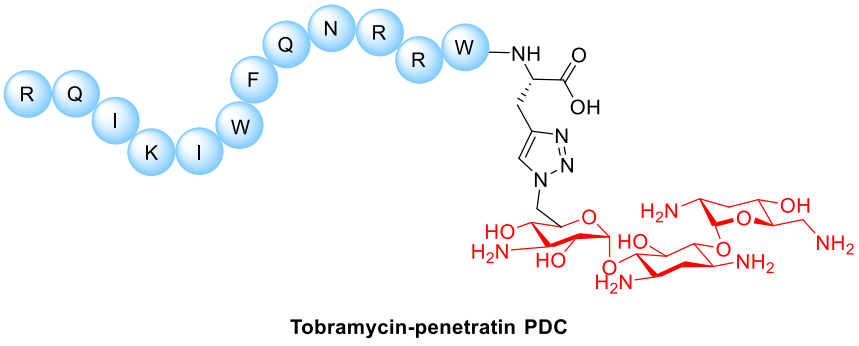

Figure 52 The structure of a penetratin (blue spheres)-tobramycin (red) conjugate.[253]

Riahifard *et al*. developed a conjugate comprised of cyclic [R_4W_4K] peptide and fluoroquinolone levofloxacin Q (Figure 53).[254] The cyclic CPP [R_4W_4K] displays antibacterial activity, and when conjugated to levofloxacin Q, the resulting CPP-drug conjugate displayed a significant improvement in antibacterial activity against methicillin-resistant *S. aureus* (MRSA) and *Klebsiella pneumoniae*, where the parent drug had been inactive.

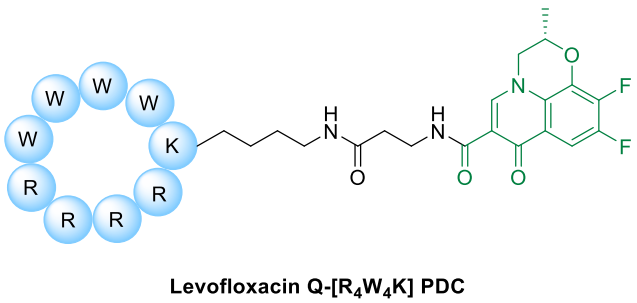

Figure 53 The structure of a cyclic PDC consisting of c[R_4W_4K] (blue spheres) and levofloxacin Q (green).[254]

More recently, a polyarginine CPP was attached to vancomycin in an effort to restore antibacterial activity against vancomycin-resistant bacterial strains.[255] The lead candidate which displayed a significantly improved antibacterial activity compared to vancomycin alone, and was active against several vancomycin-resistant strains (Figure 54). An *in vivo* study of *S. aureus*-infected mice showed that the conjugate reduced the number of colony-forming units whilst maintaining a stable body weight.

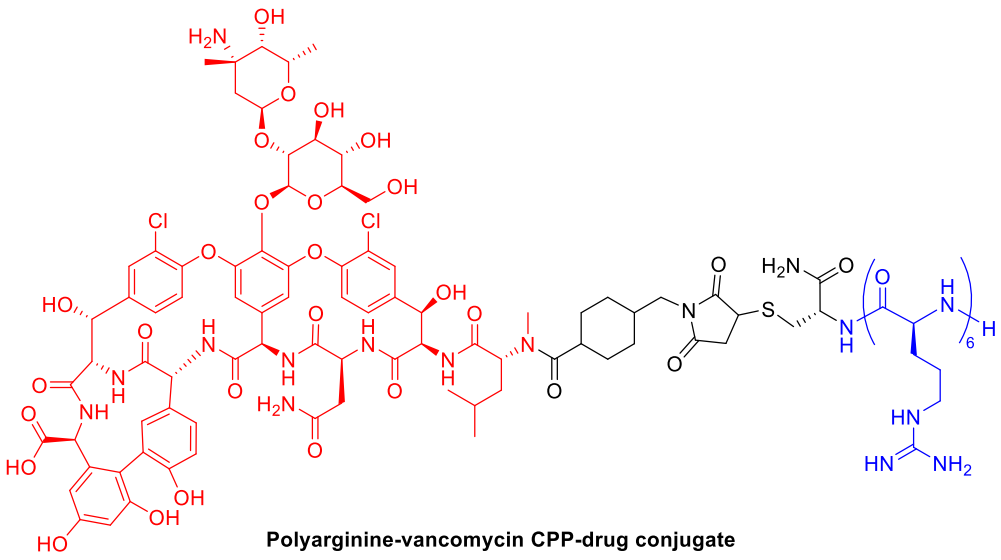

Figure 54 The structure of a vancomycin (red)-polyarginine (blue) conjugate.[255]

3.1.4.5 Selective release strategies

Selective release strategies allow a biologically active chemical to be released or revealed under specific environmental conditions. These strategies are usually paired with approaches that have already been discussed, such as prodrugs, peptide-drug conjugates (PDCs), and siderophore-drug conjugates. In the context of antimicrobial therapeutics, the use of a selective release moiety which is sensitive to the presence of the infecting microbe yields an 'infection-activated' system.[216] These systems can have advantages including improved antimicrobial activity, fewer side effects and the reduced emergence of drug-resistance mechanisms. As BLs are produced by resistant bacteria, the BL-sensitive cephalosporin moiety can be employed as an infection-activated system. A possible application of such a release mechanism is in drug delivery *via* enzyme-sensitive polymeric vesicles. To this end, Li *et al.* synthesised enzyme-sensitive polymeric vesicles encapsulating vancomycin.[256] The polymers incorporated a cephalosporin moiety, and BL hydrolysis of this group revealed a self-immolative linker. Subsequent immolation caused degradation of the polymeric vesicle, releasing the encapsulated drug (Figure 55). The authors observed that the BL-sensitive vesicles enabled selective delivery of antimicrobial agents to BL-producing bacterial strains:

vesicles containing vancomycin were able to inhibit the growth of MRSA whilst pro-biotic strains such as *Enterococcus faecalis* were unaffected.

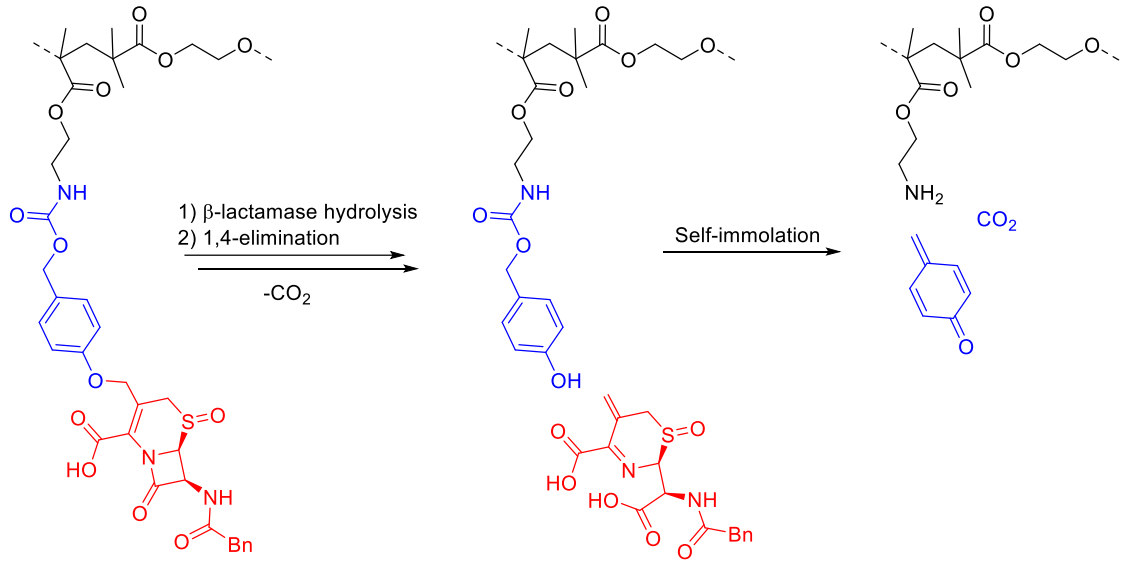

Figure 55 An overview of the release mechanism of BL-sensitive polymeric vesicles. The cephalosporin moiety is shown in red, the self-immolative linker in blue and a fragment of the polymer back-bone in black.[256]

Inspired by the intracellular release of an antibiotic component from natural sideromycins such as albomycin, Miller *et al.* combined the approaches of siderophore conjugation and selective release through incorporating a cephalosporin linker between a siderophore and an oxazolidinone antibiotic (Figure 56).[257] The siderophore allowed intracellular delivery of the conjugate, which was cleaved by BL hydrolysis of the cephalosporin linker, releasing the free oxazolidinone warhead. Whilst oxazolidinones are typically active against Gram-positive bacteria, the conjugate was active against Gram-negative bacteria, illustrating that this strategy allows the repurposing and retargeting of existing antibiotics. Additionally, the studies showed that the BL cleavage was necessary for activity, as the non-cleavable analogues displayed no antibacterial effect.

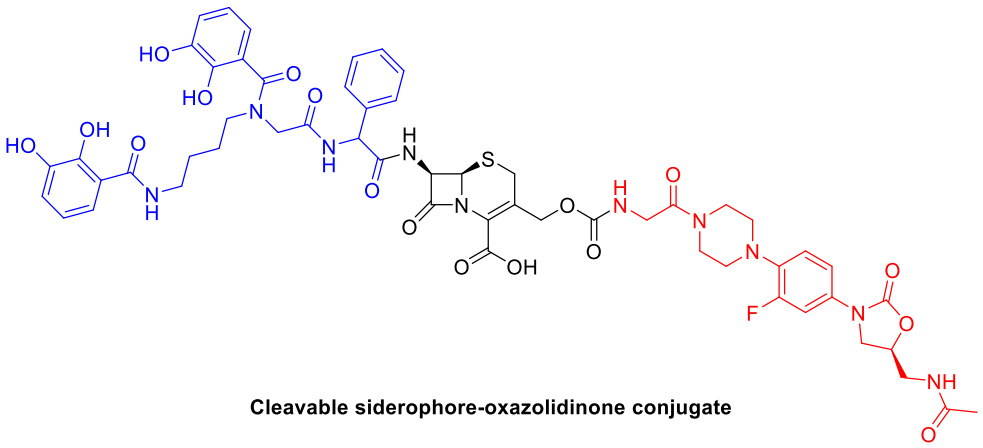

Figure 56 The structure of a cleavable siderophore-oxazolidinone conjugate reported by Miller et al.[257] *The siderophore is shown in blue, the cephalosporin in black and the oxazolidinone in red.*

CPP-drug conjugates have already been discussed as a strategy to improve the bacterial penetration of a drug. However, infections due to mycobacteria pose an additional challenge, as the bacteria are able to reside in intracellular compartments of the host organism's cells, meaning that a drug must cross both the eukaryotic and bacterial membranes to reach its intended target. Kelley and co-workers incorporated a cephalosporin release mechanism in an unusual drug delivery strategy for targeting mycobacteria.[258] Methotrexate is a dihydrofolate reductase inhibitor which could be used to treat infections of *Mycobacterium tuberculosis*, however, it is unable to penetrate the cell wall of the mycobacteria. Additionally, the drug must penetrate the eukaryotic cell and enter the phagosomes in which the mycobacteria are residing. To overcome this issue, Kelley and co-workers conjugated methotrexate to a cationic, lipophilic peptide (called the 'delivery peptide'); this PDC was capable of entering the mycobacteria, and was in turn appended *via* a cephalosporin moiety to an anionic peptide which promotes phagocytosis. The resulting conjugate was able to enter eukaryotic cells *via* phagocytosis and, when in the vicinity of the infecting mycobacteria, the cephalosporin linker was hydrolysed releasing the delivery PDC, which could enter the mycobacteria and reach its intracellular target (Figure 57).

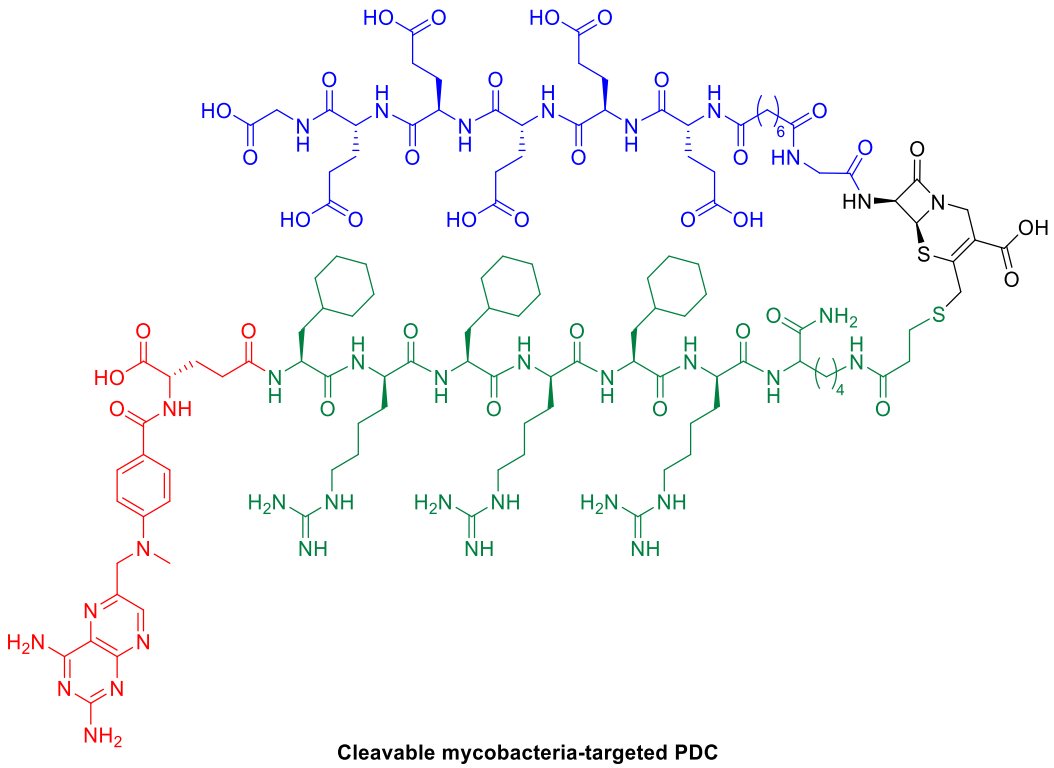

Figure 57 The structure of a methotrexate-peptide conjugate developed by Kelley and co-workers. Methotrexate and the cationic delivery peptide are shown in blue, the cephalosporin linker in red and the anionic peptide in green. Adapted from Pereira et al.[258]

Another example of a cleavable PDC targeting intracellular pathogens was published by Brezden *et al*.[259] Aminoglycosides are ineffective against bacteria that can reside in macrophages, such as *Mycobacteria*, *Salmonella* and *Brucella* spp., as they are unable to penetrate eukaryotic cell membranes. Brezden *et al*. conjugated aminoglycoside kanamycin to a CPP, P14LRR (Figure 58). P14LRR improved the cellular penetration of kanamycin and exerted an antimicrobial effect itself *via* membrane disruption. The authors synthesised and tested both a hydrocarbon non-cleavable and a disulfide cleavable analogue. The cleavable disulfide analogue could be reduced once the construct was inside the eukaryotic cell, releasing the peptide and drug as separate species. The intracellular antimicrobial activity of the conjugates was assessed, and it was found that the peptide and drug on their own were incapable of clearing an intracellular population of various *Mycobacteria*, *Salmonella* and *Brucella* strains from a macrophage cell line. The non-cleavable conjugate showed similar activity to a combination of the drug and peptide, however, the cleavable conjugate showed a significantly improved activity against all of the bacteria. In *M. tuberculosis*, 93% of the intracellular bacteria were cleared with the cleavable conjugate at 10 μM.

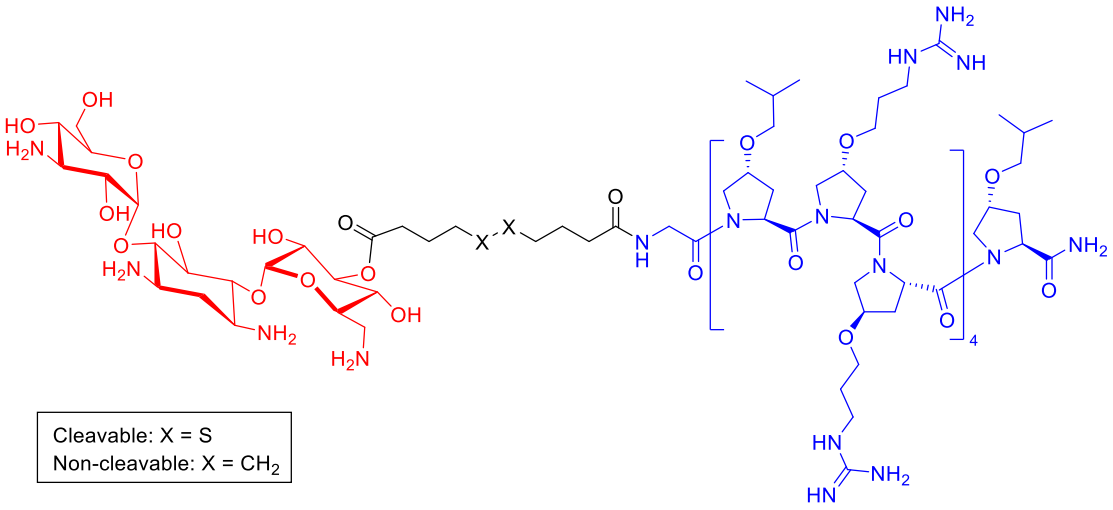

Figure 58 The structure of the cleavable and non-cleavable PDCs developed by Brezden et al.[260] The drug, kanamycin, is shown in red, the linker in black and the CPP, P14LRR, in blue. Adapted from Brezden et al.[260,261]

3.1.5 Antimicrobial peptides

Antimicrobial peptides (AMPs) are an emerging class of antimicrobial compounds with great potential as new antibacterial therapeutics. AMPs are also referred to as host defence peptides as they modulate a wide range of biological functions in the host organism, including the innate immune system.[262,263] The literature defines AMPs as a subset of CPPs as they are cationic and amphipathic, allowing them to interact with cell membranes. Unlike most CPPs, however, AMPs cause significant membrane disruption and by this mechanism exert bactericidal and bacteriostatic effects. As very few drugs interact with lipid membranes as their target, AMPs represent an interesting and unique class of antimicrobial agents.[187] Another attractive feature of AMPs is that the cellular membranes of pathogens (e.g. bacteria, yeast, fungi) vary from the host's cellular membranes, enabling selective targeting of the infectious species.[264] For these reasons, AMPs are receiving increased interest as potential therapeutics.[265]

Indeed, the data repository of AMPs (DRAMP) database lists over 3,800 AMPs, whilst increasing numbers of novel AMPs are published every year.[266,267] Moreover, in 2018 there were 70 AMPs in clinical trials, thus, representing an expanding and exciting new field of antibiotic discovery.[268] A 2016 review by the Wellcome Trust listed AMPs in the top 10 'alternative approaches to antibiotics'.[186]

3.1.5.1 Mechanisms of action

AMPs can have various bacterial targets including efflux pumps,[269] specific outer membrane proteins,[270] and intracellular targets,[271] however, the most common mechanism of action by far is membrane disruption. Significant bacterial membrane disruption leads to increased flow of water and ions and destroys the transmembrane electrochemical gradient, causing cell swelling and osmolysis and resulting in cell death.[272] AMPs often show selectivity for Gram-negative bacteria as the thick cell wall of Gram-positive bacteria represents a significant barrier to the bacterial cell membrane.[187]

AMPs can have different secondary structures, including β-turns and random coils (or 'extended peptides') but by far the most predominant structural motif is the α-helix.[266,273] AMPs typically have an overall cationic charge and are amphipathic, and it is these distinct biophysical properties that enable their interaction with bacterial membranes.[274] As both the outer leaflet of the Gram-negative outer membrane and the outer surface of the cell wall in Gram-positive bacteria are negatively charged, interactions with AMPs are guided by electrostatic interactions. Secondly, AMPs must be water-soluble and able to penetrate hydrophobic lipid membranes, which requires them to adopt a conformation that enables both; for most AMPs this is an amphipathic α-helix. The α-helicity and amphipathicity enables the formation of oligomers, wherein each AMP is arranged with the hydrophobic face pointing inwards and the hydrophilic face solvent-exposed.[272]

These properties have led to the proposal of two main mechanisms by which membrane disruption occurs: the barrel-stave and carpet model. The barrel-stave mechanism involves the association of AMPs (either as monomers or oligomers) with the bacterial membrane, then the formation of pore-like structures where the hydrophobic faces of the peptides face outwards (A, Figure 59).[275] These structures are then able to penetrate the membrane (B, Figure 59). The toroidal-pore mechanism is related and involves the same steps in a different order: the same pore-like structures form within the membrane, rather than prior to insertion.[276]

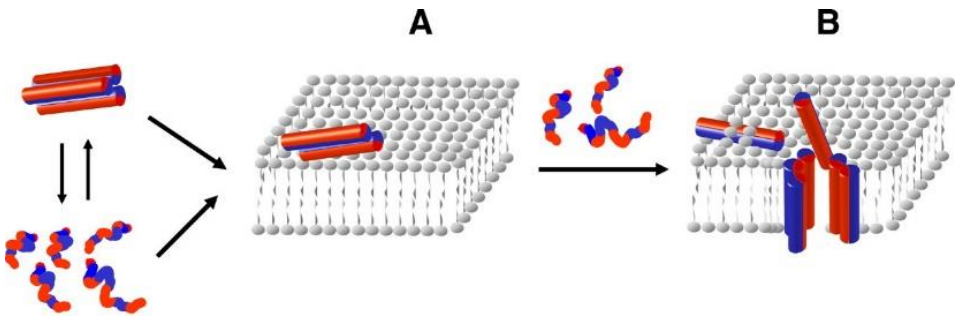

Figure 59 A cartoon representing the barrel-stave model of membrane disruption. A: Peptides associate with the membrane either as monomers or oligomers. B: Additional peptides associate and insert into the membrane. The

peptides are shown as red and blue cylinders or lines and the membrane lipids as grey spheres. Reprinted with permission from Brogden.[272] (Copyright Springer Nature 1969).

The carpet model involves AMP monomers or oligomers interacting with the phospholipids on the outer membrane and covering it in a carpet-like manner (A, Figure 60).[277] Once a particular threshold AMP concentration is reached, the natural curvature of the membrane is significantly disrupted, causing disintegration (B, Figure 60).

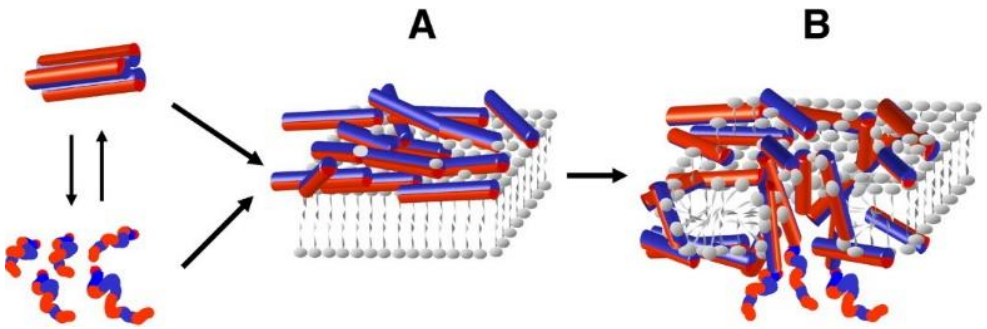

Figure 60 A cartoon representing the carpel model of membrane disruption. A: Peptides associate with the membrane as monomers or oligomers. B: Once a threshold concentration has been achieved transient pores are formed. The peptides are shown as red and blue cylinders or lines and the membrane lipids as grey spheres. Reprinted with permission from Brogden.[272] (Copyright Springer Nature 1969).

AMPs can interact with other antibiotics, with numerous synergistic combinations featuring AMPs now reported in the literature. Although as yet unproven, it is largely accepted that the mechanism by which this synergy arises is *via* AMP-mediated membrane disruption allowing the other antibiotic increased access to its target.[278] By using antibiotics in synergy with AMPs, lower doses of these toxic chemicals can be administered. Additionally, the synergistic action can allow a broad spectrum of activity for the drug, which enables the treatment of a wider range of bacterial infections and decreases the chances of resistance developing.[223]

If not synergistic, drugs can have an additive effect, and act as permeabilisers or sensitisers for other antibiotics. Typically, this involves one compound targeting intrinsic or acquired antibiotic resistance mechanisms, thus improving the permeability of a second drug, or re-sensitising the bacteria to this drug. AMPs can act in this way by targeting the outer membrane, which is a major cause of drug resistance in Gram-negative bacteria.[278]

3.1.5.2 Bacterial resistance to antimicrobial peptides

Bacteria have developed resistance mechanisms to AMPs, although the underrepresentation of AMPs on the market often means that these resistance mechanisms are overlooked when discussing the potential for AMPs as novel therapeutics. A fundamental resistance mechanism is the production of enzymes such as proteases, predominantly associated with the outer

membrane. Other AMP-sequestering proteins are produced which bind to AMPs and render them inactive, for example Staphylokinase produced by *S. aureus*.[279]

Other mechanisms of resistance involve modifications to the outer surface of the bacteria. For example, some Gram-negative bacteria can reduce the overall negative charge of their outer membrane, thus reducing the electrostatic attraction of cationic AMPs.[280] Gram-positive bacteria can modify the composition of their cell wall to achieve the same effect. Additionally, some pathogenic strains, including *P. aeruginosa*, can produce an anionic polysaccharide capsule that surrounds the cell. It is believed that this capsule is capable of sequestering AMPs before they are able to reach the outer membrane.[279]

As previously discussed, biofilm formation reduces the activity of antibiotics; this is also the case for AMPs. This is in part due to the reduced penetration of AMPs through the extracellular matrix and partly due to the presence of extracellular polysaccharides which can bind to and sequester AMPs.[279] A final key feature of AMP resistance in bacteria is efflux: there are many efflux pumps in bacteria for which AMPs are substrates, for example the resistance-nodulation-cell division family transporters present in many Gram-negative bacteria. Additionally, many strains of bacteria that produce and secrete AMPs as part of their own defences have AMP-specific efflux pumps which can contribute to the efflux of non-endogenous AMPs.[279]

3.1.5.3 Macrocyclic antimicrobial peptides

As previously discussed in Chapter 1, macrocyclic peptides have a number of advantages over their linear counterparts, including increased serum stability and reduced conformational flexibility. In the context of therapeutic AMPs, performing macrocyclisation for these reasons is also relevant. A therapeutic AMP must survive both eukaryotic and prokaryotic proteases before reaching its target. Additionally, as many AMPs must adopt an α-helical, amphipathic structure to exert their antibacterial activity, conformational rigidity may improve the activity. The α-helicity of AMPs is dependent on their environment, in particular the pH and salt concentration.[281] In CF patients, who are at risk from opportunistic pathogens like *P. aeruginosa*, often chronic infections occur in the pulmonary mucus. This is an environment with a high salt concentration that renders many AMPs ineffective,[282] however, conformationally locking AMPs can improve their salt-stability.[281] Finally, AMPs suffer from poor bioavailability which can limit their use to topical applications. Macrocyclisation provides an opportunity to add functionality or modify the properties of the peptide to improve bioavailability.[283]

There are many examples of both natural and synthetic macrocyclic AMPs in the literature, that use a variety of macrocyclisation chemistries.[202,283–285] This thesis is concerned with macrocyclisation by peptide stapling, and so particular attention will be afforded to stapled antimicrobial peptides (STAMPs) here.

3.1.5.4 Stapled antimicrobial peptides

Reports of STAMPs are dominated by one technique, ring-closing metathesis (RCM). Literature examples of stapled AMPs include linear AMPs isolated from natural sources which have been stapled to improve their properties, *de novo* designed stapled AMPs, and AMPs featuring more than one staple ('stitched peptides').[283] Examples of these three types of stapled AMPs will be discussed in this section.

Luong *et al*. investigated the effect of introducing a hydrocarbon staple to polybia-MP1, a linear AMP isolated from wasp venom, alongside specific amino acid substitutions which increased the overall positive charge.[286] One of the analogues, MP1S-Q12K, displayed significantly improved MIC values against Gram-positive bacterial strains over the wild-type sequence (Figure 61), and, unlike the wild-type peptide, MP1S-Q12K displayed no activity towards Gram-negative strains. The stapled peptide was more helical than the wild-type sequence, and significantly more stable in a trypsin digestion assay: over 97% of unmodified MP1S-Q12K was present after incubation for 60 minutes compared to only 15% for the wild-type peptide.

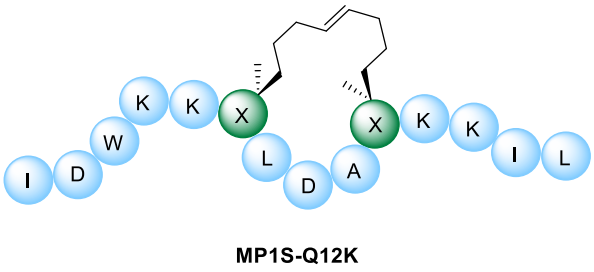

MP1S-Q12K

Figure 61 The structure of an all-hydrocarbon stapled analogue of polybia-MP1, MP1S-Q12K, reported by Luong et al.[286] The amino acid residues are represented by blue spheres, the unnatural amino acids by green spheres and X = alkenyl unnatural amino acids.

Dinh *et al.* investigated the *de novo* design of short, amphipathic all-hydrocarbon STAMPs.[287] Starting from a heptapeptide scaffold, they placed the all-hydrocarbon bridge between *i,i*+4 positions and inserted amino acid residues in the remaining places to maximise the amphipathicity; lysine residues on the hydrophilic face and alanine and tryptophan on the hydrophobic face, an example is given in Figure 62. All of the STAMPs displayed an increased α-helical content compared to the unstapled analogues, however, it is interesting to note that the most helical peptide did not give the highest level of growth inhibition when tested against a panel of different Gram-positive and -negative strains, and the two peptides which displayed

the most potent activity against *S. aureus* and *E. coli* also displayed the highest levels of haemolysis.

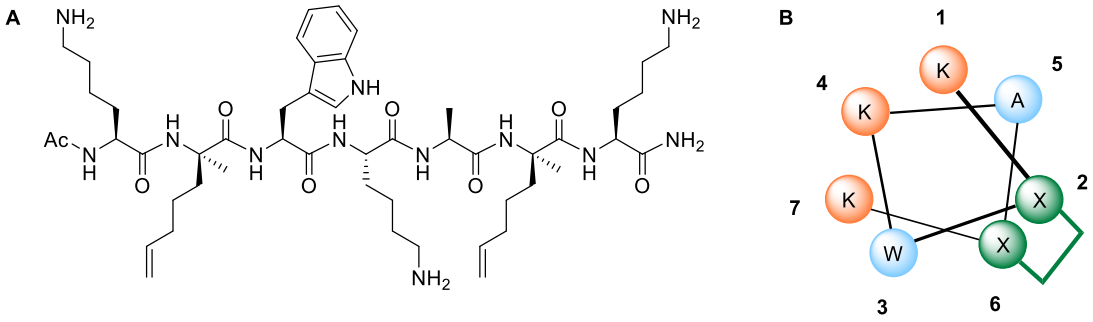

Figure 62 A: The linear sequence of an all-hydrocarbon STAMP designed by Dinh et al.[287] B: A helical wheel representation of the STAMP. The hydrophobic amino acid residues are represented by blue spheres, the hydrophilic residues by orange spheres and the unnatural amino acids by green spheres. X = the unnatural amino acids, the oct-4-enyl linker is represented by a green line.

Chapuis *et al*. investigated the effect of introducing two hydrocarbon staples into AMPs lasioglossin and melectin, both isolated from bee venom, to investigate how the double staple architecture affected the peptides' pharmacological properties.[288] Alkenyl amino acids were introduced into the hydrophobic portion of the peptide so that the number of cationic residues remained constant. A series of lasioglossin and melectin analogues were synthesised with either one or two hydrocarbon staples of different lengths and positions, and it was found that the introduction of two staples into the peptides gave mixed results. For example, one doubly-stapled analogue of lasioglossin, LL-IIIs-4, showed significantly reduced activity compared to the wild-type peptide (Figure 63). However, the double staple conferred a high level of α-helicity and proteolytical stability; LL-IIIs-4 showed minimal degradation in a trypsin digestion assay.

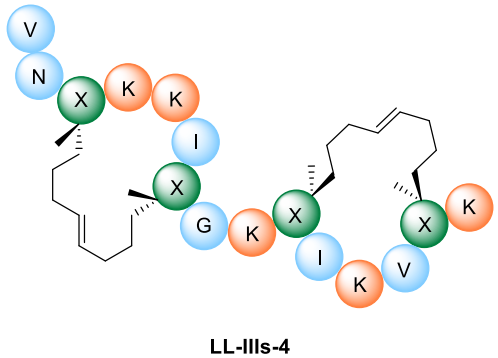

LL-IIIs-4

Figure 63 The structure of a 'stitched' peptide, LL-IIIs-4 reported by Chapuis et al.[288] The hydrophobic amino acid residues are represented by blue spheres, the hydrophilic residues by orange spheres and the unnatural amino acids by green spheres. X = alkenyl unnatural amino acids.

These examples show the complicated relationship between α-helicity, conformational flexibility, amphipathicity, antibacterial activity and haemolysis. Whilst there are many examples of all-hydrocarbon stapled AMPs with improved proteolytic stability and α-helicity,

these peptides can also display higher levels of haemolysis and lowered antibacterial activity.[283] To address this potential minefield when designing new stapled AMPs, Walensky and co-workers undertook a systematic screening approach to determine design guidelines, using all-hydrocarbon stapled analogues of AMP magainin II as a model system.[289] A key finding was that the staple must be incorporated into pre-existing regions of hydrophobicity to avoid undesirable haemolysis. Taking their findings from magainin II, an algorithm for stapled AMP design was constructed; using this algorithm the authors were able to rapidly design stapled AMPs with high levels of antibacterial activity and negligible haemolysis without the need for a systematic library screen for each different AMP. Following on from this work, Walensky and co-workers have filed a patent for all-hydrocarbon stapled AMPs based on the sequence of magainin II.[40]

Whilst the overwhelming majority of literature STAMPs make use of RCM stapling, there are examples where other macrocyclisation techniques have been employed. One example is a bicyclic peptide developed by the Reymond group.[290] The addition of a 3,5-bis(chloromethyl)toluoyl group at the *N*-terminus of the peptide allowed alkylation with two cysteine residues to give a thioether linkage (Figure 64). The linear 'tail' of the peptide was found to be unstable in serum, however the enantiomeric peptide containing all D-amino acids was significantly more stable and gave comparable MIC values to polymyxin B against MDR strains of *Acinetobacter baumannii*. The bicyclic peptide also inhibited biofilm formation of *P. aeruginosa*, *E. coli* and *A. baumannii*.

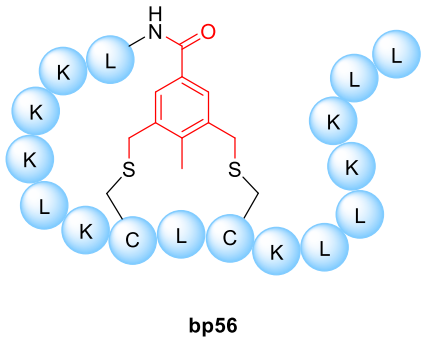

bp56

Figure 64 The structure of the bicyclic, thioether bridged peptide developed by the Reymond group.[290] The amino acids are represented by blue spheres, and the letters represent the D enantiomers of the amino acids. The cyclisation linker is highlighted in red.

The Pentelute group investigated various macrocyclic AMPs which were conjugated to an antibody targeting *E. coli,* creating an antibody-antibiotic conjugate.[291] Analogues of the AMP cathelicidin were stapled with a perfluoroalkyl linker *via* an S_NAr reaction (Figure 65). The stapled peptides all displayed improved serum stability compared to their linear counterparts, minimal haemolysis, and MIC values in the micromolar range for *E. coli* and *P. aeruginosa*.

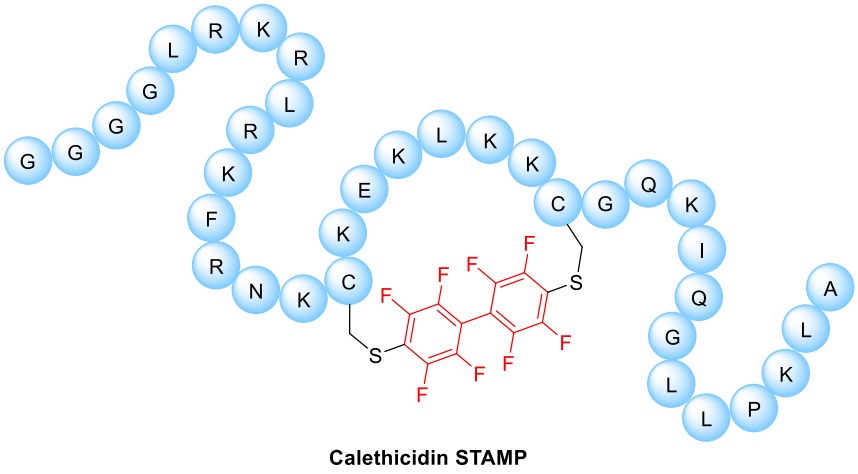

Figure 65 The structure of one of the perfluoroalkyl stapled peptides developed by Pentelute et al. for use in a peptide-antibody conjugate.[291]

3.1.6 Peptide-drug conjugates

PDCs contain a covalently-linked peptide and pharmaceutical drug, natural product or toxin. Antimicrobial PDCs belong to the class of 'hybrid drugs', which were discussed in Section 3.1.4. The role of the peptide in a PDC can be either:

1. To act as a targeting agent
2. To provide an alternative and additional mechanism of action
3. To improve cellular uptake of the drug

Examples of PDCs where the peptide is assuming each of these roles will be discussed in this section except for the last. The appendage of CPPs to drugs to improve their cellular uptake was discussed in Section 3.1.4.4 and in Chapter 2, and will not be discussed further here.

3.1.6.1 Homing peptide-drug conjugates

To date, the most advanced PDCs are all in the field of cancer therapies, which typically consist of drugs conjugated to homing peptides, which specifically bind to cell-surface receptors that are overexpressed on cancer cells.[292] Lutathera® is currently the only marketed PDC, consisting of octreotate (a disulfide-bridged peptide which mimics the pharmacological effect of somatostatin) covalently linked to a chelated radionuclide lutetium-177 (Figure 66).[293] It was approved by the FDA in 2018 for the treatment of gastroenteropancreatic neuroendocrine tumours. Somatostatin receptors are overexpressed in most neuroendocrine tumours, allowing selective binding and internalization of Lutathera®. Once internalised, the radionuclide ^{177}Lu causes DNA damage, leading to cell death.

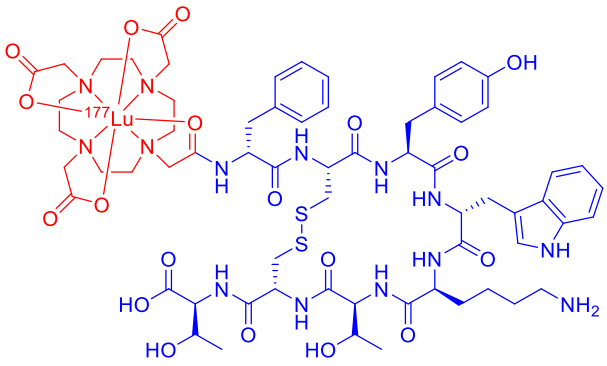

Figure 66 The structure of marketed PDC Lutathera®. The targeting peptide, octreotate, is shown in blue and the drug, radionuclide ^{177}Lu, in red.

There are currently three chemotherapeutic PDCs in clinical trials, which have all been developed by Bicycle Therapeutics. They all consist of a bicyclic peptide, a cleavable linker, and a cytotoxic drug. The bicyclic peptides, BT1718, BT5528 and BT8009, were discovered using phage display and CLIPS cyclisation, then further optimised through the introduction of unnatural amino acids to improve binding and replace metabolically-labile residues.[105] BT1718 was developed for the treatment of lung cancer, and the peptide component binds with high affinity to membrane type-1 matrix metalloprotease which is over-expressed in triple-negative breast cancer and non-small cell lung cancer. Its cytotoxic payload is tubulin-binder mertansine, which is attached to the targeting bicyclic peptide *via* a disulfide cleavable linker (Figure 67). BT1718 is currently in Phase I/IIa clinical trials due for completion in 2022.[294,295]

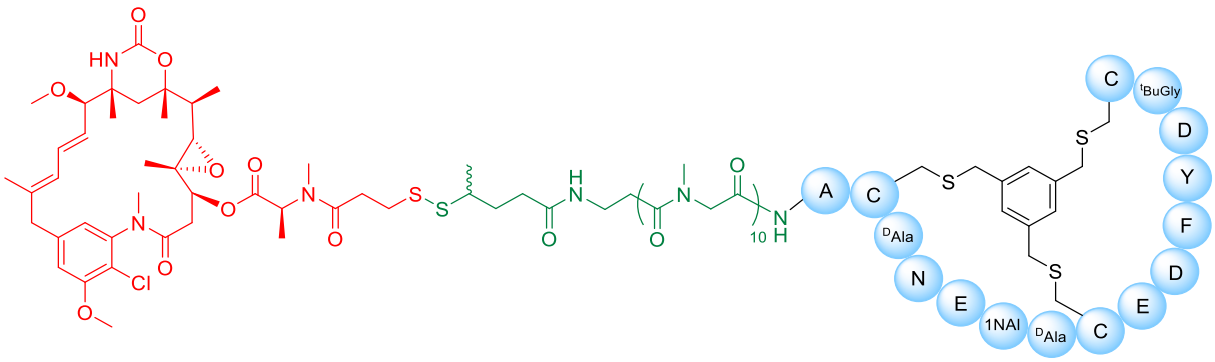

Figure 67 The structure of BT1718, a PDC consisting of cytotoxin mertansine (red) linked to a bicyclic peptide (blue spheres) via a disulfide cleavable linker (green). 1NAl = 1-naphthyl-L-alanine, ^{t}BuGly = L-tert-leucine.

BT5528 targets Ephrin receptor A2, which is overexpressed in many cancers including ovarian and pancreatic. It is comprised of monomethyl auristatin E, a cytotoxin which prevents the polymerisation of tubulin, bound to a bicyclic peptide through a cathepsin-cleavable linker (Figure 68).[105] BT5528 entered Phase I/II clinical trials in 2019.[296] Another PDC, BT8009 has the same drug-cleavable linker structure as BT5528 but differs in the peptide moiety, instead

incorporating a peptide which targets Nectin-4, a cell adhesion molecule overexpressed in lung and bladder cancer (Figure 68).[297]

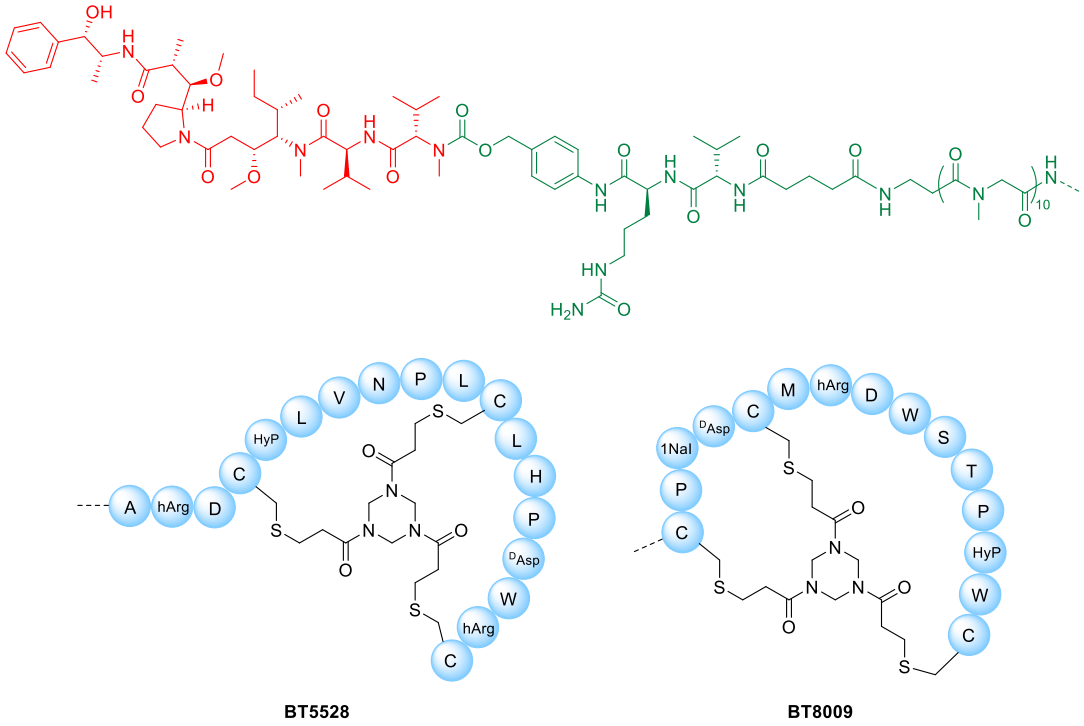

Figure 68 The structures of BT5528 and BT8009, two PDCs consisting of bicyclic peptides (blue spheres) linked to cytotoxin monomethyl auristatin E (red) via a cathepsin cleavable linker (green). 1NAl = 1-naphthyl-L-alanine, HyP = 4-hydroxyproline, hArg = homoarginine.

3.1.6.2 AMP-drug conjugates

Aside from targeting a specific cell-type, another role for a peptide in a PDC is to provide an additional and alternative mechanism of action. When incorporated into a PDC, a membrane-disrupting AMP exerts an antimicrobial effect in its own right, but also increases the uptake and the traditional drug component of the PDC.[298] Whilst there are no AMP-containing PDCs in the clinic, many have been reported in the literature.[276,299,300] An illustrative example is a chloramphenicol PDC reported by Chen *et al*.[301] Chloramphenicol has a high antimicrobial activity, however, it suffers from nonspecific distribution and severe side effects *in vivo*. UBI_{29-41} is a cationic AMP that had previously been used for imaging and diagnosis of bacterial infections. The conjugation of chloramphenicol and UBI_{29-41} lowered the cytotoxicity of the drug whilst maintaining the broad-spectrum bactericidal effects (Figure 69).

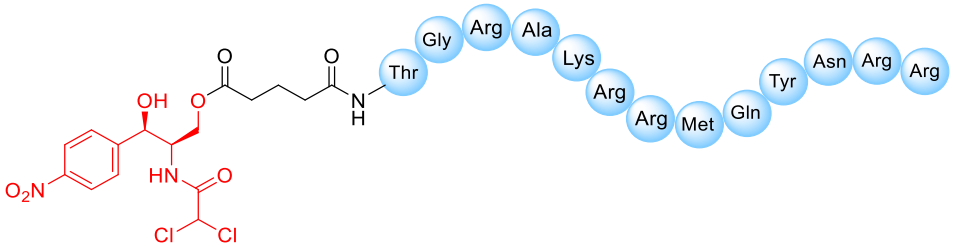

UBI$_{29-41}$-chloramphenicol PDC

Figure 69 The structure of a PDC developed by Chen et al.[301] Chloramphenicol is shown in red, the linker in black and AMP UBI$_{29-41}$ as blue spheres.

Ptaszyńska *et al.* investigated conjugates of levofloxacin and ciprofloxacin with AMPs based on a fragment of human lactoferrin, which distorts the bacterial outer membrane.[302] One of the PDCs investigated featured a human lactoferrin-derived peptide, HLopt2, conjugated to ciprofloxacin *via* a disulfide linker (Figure 70). The resulting PDC displayed the highest antimicrobial activity out of all the PDCs screened against *S. aureus, E. coli* and *P. aeruginosa*. Further studies confirmed that the disulfide was reduced intracellularly, releasing the peptide and a ciprofloxacin-cysteine species; the authors hypothesised that this contributed to the elevated antimicrobial activity.

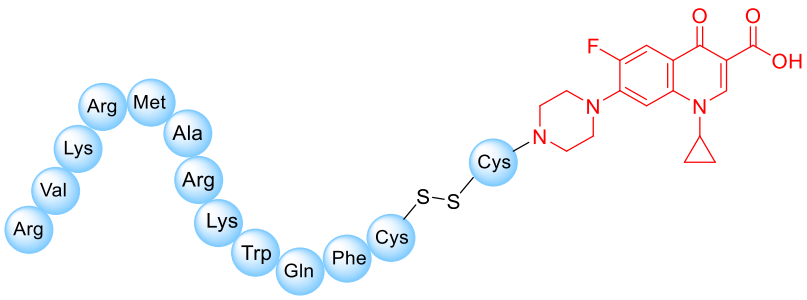

HLopt2-ciprofloxacin PDC

Figure 70 The structure of a disulfide-linked ciprofloxacin-HLopt2 conjugate reported by Ptaszyńska et al.[302] Ciprofloxacin is highlighted in red and the peptide HLopt2 is represented by blue spheres.

PDCs have been reported which incorporate STAMPs. In 2017, a patent application was filed by the Walensky research group describing RCM stapled analogues of the AMP magainin II. The patent mentions conjugation of the peptides to 'appropriate antimicrobial agents' and discusses the conjugation of the STAMPs to carrier proteins to enable their cellular permeability, although no structural information about the conjugates is given.[271,303]

It is clear from the examples discussed in this section that inventive combinations of alternative antimicrobial strategies are being explored, for example cleavable STAMP-drug conjugates,[260,302] and infection-controlled release of antibiotics from siderophores,[257] prodrugs,[235] and polymeric vesicles.[256] Simultaneously, whilst peptide stapling is improving the therapeutic potential of AMPs, the benefits of two-component peptide stapling, particularly

with respect to the development of functionalised peptides, is yet to be fully realised for AMPs. This section describes the development of an innovative antimicrobial PDC which draws inspiration from these fields and aims to yield a therapeutic which is advantageous over each of these technologies in isolation.

3.2 Project overview and aims

The primary aim of this project was to develop a novel PDC comprised of a STAMP, a selective release moiety, and an antibiotic drug. Based on literature reports of other alternative antimicrobial strategies (*vide supra*), it was hypothesised that the PDC would have several unique features that would be advantageous over current antimicrobial therapies:

- As the STAMP and small molecule antibiotic would have different mechanisms of action, this would be a dual-targeting conjugate; the many advantages of such 'hybrid antibiotics' were discussed in the introduction (Sections 3.1.4 and 3.1.5).
- It was envisioned that the AMP would be selective for *P. aeruginosa*, allowing the conjugate to be targeted to this species of bacteria. This could reduce the side effects associated with some broad-spectrum small-molecule antibiotics.
- An enzyme-cleavable moiety between the AMP and the drug would enable selective release of the free drug. This would avoid issues of the conjugation position negatively affecting the antibiotic activity of the drug. By incorporating a moiety that could be selectively cleaved by pathogenic bacteria, reduced off-target toxicity could be achieved.

The work described in this section can be divided into two sections. The first part details the selection of a suitable stapled peptide. This was done by identifying AMPs from the literature and screening stapled analogues for antimicrobial activity. For the peptide screen 24 peptides were synthesised, and from this library one STAMP (**AMP2-17**, Figure 71) was selected that gave good antimicrobial activity and selectivity for *P. aeruginosa* over *S. aureus*.

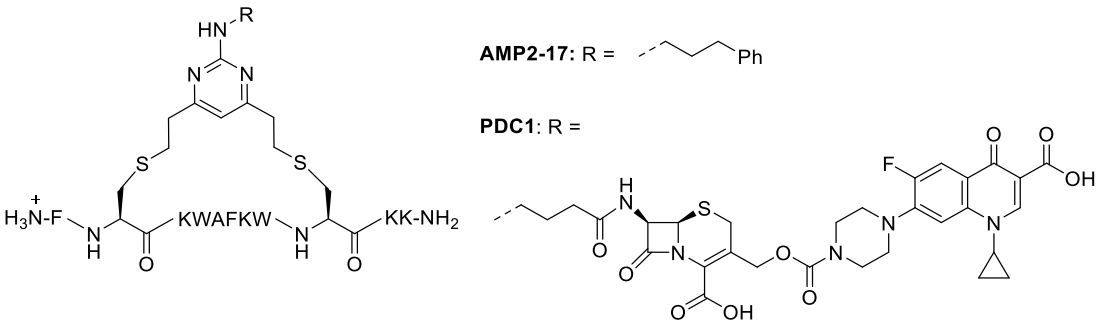

*Figure 71 The structure of **AMP2-17**, the two-component STAMP chosen from the peptide screen performed in Section 3.3.2 and **PDC1**.*

The second section describes the selection of each component, and the overall design of **PDC1** (Figure 71). The synthesis of the first-generation linkers required for **PDC1** is detailed in Section 3.3.6, and in Section 3.3.7 the second-generation linkers are discussed, including the full route towards the most advanced intermediate.

3.3 Results and discussion

3.3.1 Synthesis of unfunctionalised STAMPs

3.3.1.1 Peptide selection and design

There are two possible approaches to the development of a novel STAMP: *de novo* design or by applying a stapling strategy to a literature AMP. It was decided that the second approach would be more efficient for this project as the aim was to develop novel a PDC rather than a novel AMP. Additionally, it would be revealing to apply a novel stapling strategy to AMPs, as any stapling methodologies outside of RCM have been underexplored in the literature. First, a panel of literature AMPs (both linear and RCM stapled) with the desired properties were identified. The criteria used to select these peptides included good antimicrobial activity towards *P. aeruginosa*, little or no haemolysis and sequences long enough to accommodate a stapling linker. Once suitable peptides had been identified, stapled analogues would be designed and synthesised. The resulting panel of stapled AMPs would then be screened to determine their minimum inhibitory concentration (MIC) against *P. aeruginosa*; the stapled peptide(s) displaying the best MIC values would then be taken on to constitute the peptide fragment of the full cleavable PDC.

To this end, a panel of 8 AMPs were selected from the literature, which were derived from a wide range of sources, including bacteria (**AMP3**),[304] humans (**AMP6** and **AMP7**),[305,306] and several from animal sources (Table 14). **AMP1** and **AMP2** were originally derived from AMPs isolated from the Korean frog, *Rana rugosa*.[307,308,309] Additionally, **AMP4** originated from a peptide found in porcine myeloid cells and **AMP5** is derived from Anoplin, an AMP isolated from the solitary wasp *Anoplius samariensis*.[310,311] The AMPs chosen spanned a range of different lengths (from 10-20 amino acids) and compositions, some with free *N*-termini and some with lipidated *N*-termini. It was envisioned that this structural diversity would increase the chances of a potent peptide being identified during the screening process downstream.

Table 14 The peptides selected for the initial screen, their literature sequences and the novel sequences determined for cys-DVH stapling. All peptides are C-terminal amides, and all are N-terminal amines unless otherwise indicated. Ac = acetyl capped, C8 = capped with octanoyl chloride.

Peptide	Sequence (Original sequence)	Reference
AMP1 **AMP1a**	Ac-TLKQF**C**KGVGKW**C**VK (Ac-TLKQFAKGVGKWLVK)	307,308
AMP2 **AMP2a**	F**C**KWAFKW**C**KK (FAKWAFKWLKK)	309
AMP3 **AMP3a**	Ac-W**C**LKKFRG**C**F (Ac-WMLKKFRGMF)	304
AMP4 **AMP4a**	RFRRL**C**KKWRKR**C**KKI (RFRRLRKKWRKRLKKI)	310
AMP5 **AMP5a**	C8-G**C**LKFIKK**C**L C8-GLLKFIKKLL)	311
AMP6 **AMP6a**	KWVQNY**C**KHLGRK**C**HTLKT (KWVQNYMKHLGRKAHTLKT)	305
AMP7 **AMP7a**	NLFRKL**C**HRLFRR**C**FGYTLR (NLFRKLTHRLFRRNFGYTLR)	306

With respect to their antimicrobial activity, a direct comparison of the chosen AMPs could not be performed due to the use of different assays and bacterial strains by each group. Broadly, **AMP1a** is an analogue of gaegurin-4, which has an intermediate MIC value (100 μg/mL) for *P. aeruginosa*; this peptide was chosen to investigate whether stapling could improve the MIC value to afford a more potent peptide. **AMP2a** was highly active towards all Gram-negative and Gram-positive strains tested and **AMP3a** rapidly killed *P. aeruginosa* (NCTC 6750 strain) following treatment. **AMP4a** displayed good lethal concentrations against a wide range of *P. aeruginosa* strains including MDR strains, and comparable time-kill kinetics to polymyxin B for *P. aeruginosa* (LCCI strain). **AMP5a** showed some selectivity for *P. aeruginosa* (PAO1 strain) over other Gram-negative and -positive strains and a 6-fold selectivity for *P. aeruginosa* over *E. coli*. Both **AMP6a** and **-7a** displayed promising *in vivo* properties: **AMP6a** was shown to be highly effective *in vivo*, reducing lung injury and bacterial load in *P. aeruginosa* infected mice, and **AMP7a** displayed a good MIC against *P. aeruginosa* (ATCC 27853 strain) and even better MIC values against some clinical isolates. In a mouse model of sepsis, **AMP7a** gave reduced mortality and improved survival rates. With respect to cytotoxicity, **AMP2a**, **AMP4a** and **AMP6a** gave undetectable haemolysis under the respective assay conditions and **AMP3a** and **-7a** only gave minimal haemolysis at the minimum lethal concentration (MLC). No data regarding haemolysis was reported in the literature for **AMP1a** or **AMP5a**.

To make stapled analogues of these AMPs, cysteine-divinylheterocycle (Cys-DVH) stapling was chosen, due to the advantages discussed in Chapter 1.[67] DVH stapling is highly chemoselectivity towards cysteine residues, and the native cysteine amino acids are cheaper

and give more efficient SPPS compared to the preparation of sequences containing unnatural amino acids, such as the azido amino acids used for CuAAC stapling. Additionally, the DVH stapling linkers offer the same opportunities for functionalisation as the bis-alkynyl linkers required for CuAAC stapling. For Cys-DVH stapling, the AMPs needed to contain two cysteine residues, and it was decided to place the cysteine residues at *i,i*+7 positions in the peptide sequences, as it is widely accepted that stapling between these positions can improve the α-helicity.[15,42] It was desirable for the STAMPs to have reasonable levels of α-helicity, as for many AMPs increased α-helicity can lead to greater antimicrobial activity.[283] Consequently, a key requirement for the selected AMPs was that cysteine residues could be inserted at *i,i*+7 positions in the peptide sequence without disrupting the predicted α-helicity, amphipathicity or overall cationic charge, all of which are important for antimicrobial activity.

The optimal staple position was guided by *in silico* experimentation performed by Dr. Yaw Sing Tan (A* Institute, Singapore). Briefly, structures of **AMP1-7** were modelled, assuming they formed a perfect α-helix, and the staple was placed so that the overall cationic charge and amphipathicity (both of which are linked to antimicrobial activity) were preserved.[98,312] Additionally, any potentially unstable residues such as methionine were replaced by the staple where possible. Molecular dynamics simulations were performed on the linear and stapled versions of **AMP1** and **-2** to predict the ability of the staple to maintain peptide helicity. After the selection of suitable peptides from the literature and the *in silico*-guided design of cysteine analogues, seven linear cysteine-containing AMPs, **AMP1**-**AMP7**, were selected for stapling (Table 14).

3.3.1.2 Synthesis of linear peptides

AMP1-**AMP7** were synthesised using microwave-assisted Fmoc-SPPS. Low-loading Rink amide MBHA resin was used as the *C*-terminal amide was desired, and low-loading resin would assist in the prevention of on-resin aggregation. All of the peptides were cleaved from the resin without acetyl capping, leaving an *N*-terminal amine, except **AMP1** and **-3** which were capped with an acetyl group, and **AMP5** which was capped with octanoyl chloride in keeping with the literature sequences for these peptides.[304,307,311] For the cleavage of the peptides from the resin, often EDT is added to the cleavage cocktail for thiol-containing peptides to prevent unwanted oxidation and alkylation.[313] Trial reactions were performed using both standard cleavage conditions (TFA/TIPS/H_2O/CH_2Cl_2 (92.5:2.5:2.5:2.5), 40 °C, 45 min) and EDT conditions (TFA/TIPS/H_2O/EDT (94:1:2.5:2.5), 40 °C, 45 min). It was found that for **AMP1**-**AMP7**, the purity of the crude peptide was the same regardless of the cleavage cocktail

used so for practical simplicity the standard cleavage conditions were used. The crude peptides were purified by preparative reverse phase HPLC prior to peptide stapling.

3.3.1.3 Synthesis of DVH linkers **14** and **17**

Both DVT and DVPs have been used in peptide stapling methodologies.[67,69] Trial stapling reactions were performed to ascertain whether a DVT or DVP linker would give the best stapling reaction with **AMP1**-**AMP7**. The key factors were the solubility of the linker and the stapled peptide product and the reaction profile. For these trial reactions, simple DVT and DVP linkers were synthesised. The DVT linker was synthesised according to the literature synthetic route shown below (Scheme 12).[67] Briefly, an S_NAr reaction between sarcosine ethyl ester and 2,4,6-trichloro-1,3,5-triazine gave **12** in an excellent yield. A bis-Suzuki-Miyaura cross-coupling with potassium vinyl trifluoroborate gave the ester **13** in a moderate yield, and a final step of basic ester hydrolysis generated the desired linker **14** in a 56% yield after trituration.

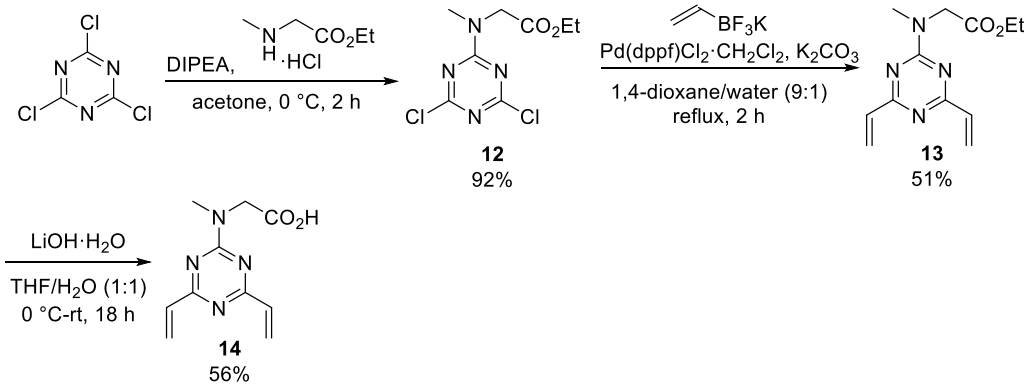

*Scheme 12 The synthesis of peptide stapling linker **14** from commercially available 2,4,6-trichloro-1,3,5-triazine.*

A simple phenyl-propyl DVP linker **17** was synthesised following the same synthetic route as the DVT linker. From commercially available starting material 2,4,6-trichlopyrimidine, the initial S_NAr reaction with 3-phenylpropan-1-amine gave the incorrect regioisomer **16** as a by-product, resulting in a moderate yield of **15** (Scheme 13). The isomers were chromatographically separable.

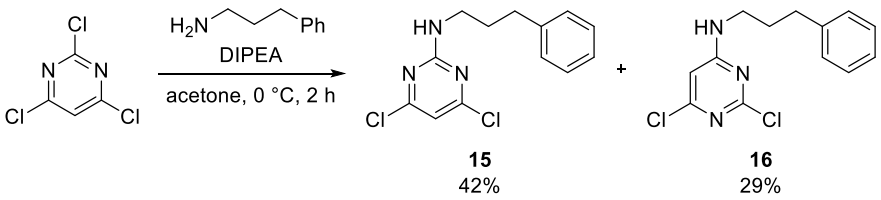

*Scheme 13 The synthesis of desired product **15** and unwanted regioisomer **16** via an S_NAr reaction of 2,4,6-trichlopyrimidine and 3-phenylpropan-1-amine.*

Next, the bis-Suzuki-Miyaura cross-coupling gave the desired product **17** in a 70% yield (Scheme 14).

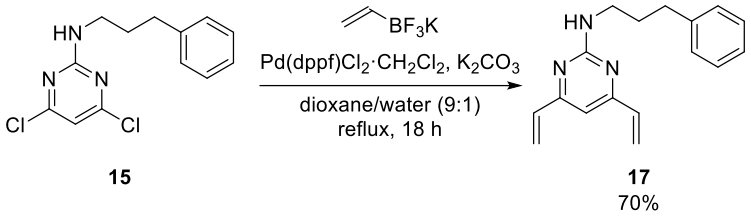

*Scheme 14 The synthesis of **17** from **15** via a bis-Suzuki-Miyaura cross-coupling.*

3.3.1.4 Test stapling reactions and optimisation

With the linear peptides **AMP1**-**AMP7** and simple linkers **14** and **17** in hand, test stapling reactions were performed with **AMP4** as a model peptide, using the literature conditions for Cys-DVT stapling (Scheme 15).[67] Analytical HPLC and LCMS were used to monitor the reaction mixtures and compare the performance of the DVH linkers.

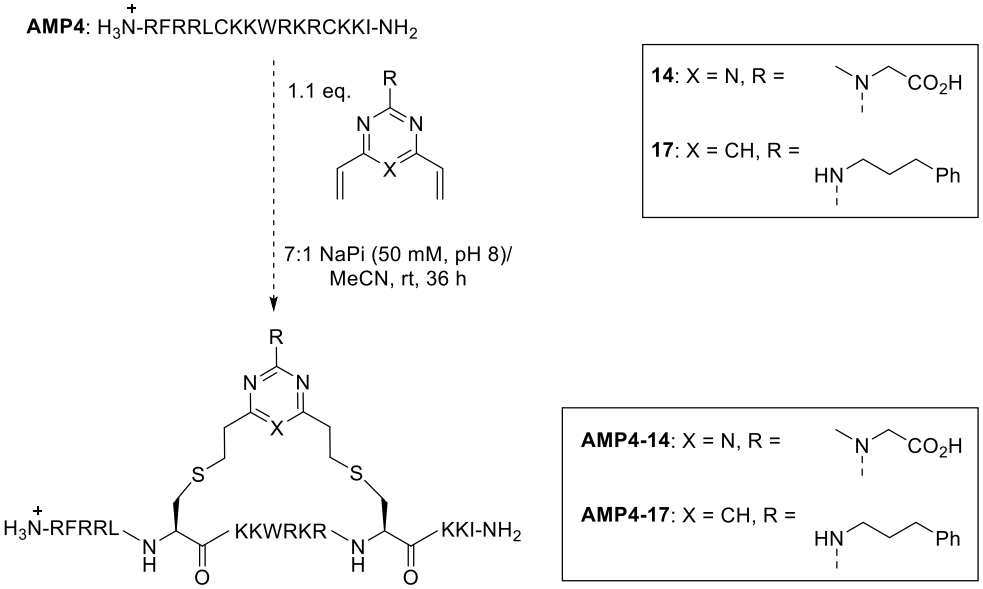

*Scheme 15 The trial peptide stapling reactions performed with peptides **AMP4** and linkers **14** and **17** under the literature conditions for Cys-DVT stapling.*[67]

For the stapling reaction with DVT **14**, the analytical HPLC traces of the reaction mixture at 0 hours showed a complex reaction profile and after 18 hours only the mass corresponding to the starting material was observed when analysed by LCMS. When an additional 0.5 equivalents of linker **14** was added and the reaction left for 18 hours, still no product was observed. Conversely, with DVP **17** after 36 hours a species with the correct mass for the stapled peptide was observed by LCMS analysis. However, the reaction mixture went cloudy on addition of the linker (as a stock solution in DMSO), indicating that either the linker or stapled peptide were insoluble in the reaction solvent system. Based on the preliminary results

from these trial reactions, the DVT linker was discontinued and subsequent optimisation focused on the DVP linker.

Alternative reaction conditions were trialled with **AMP2** and linker **17** which included a much higher proportion of organic solvent, and pH 6 buffer rather than pH 8 (Scheme 16). Under these conditions, with the peptide and linker concentrations as before, it appeared that the solubility issues had been solved as the reaction proceeded cleanly to the desired product with full conversion after 2 hours. However, when this reaction was attempted on a larger scale,[o] it was found that the addition of the linker as a stock solution in DMSO still resulted in limited solubility.

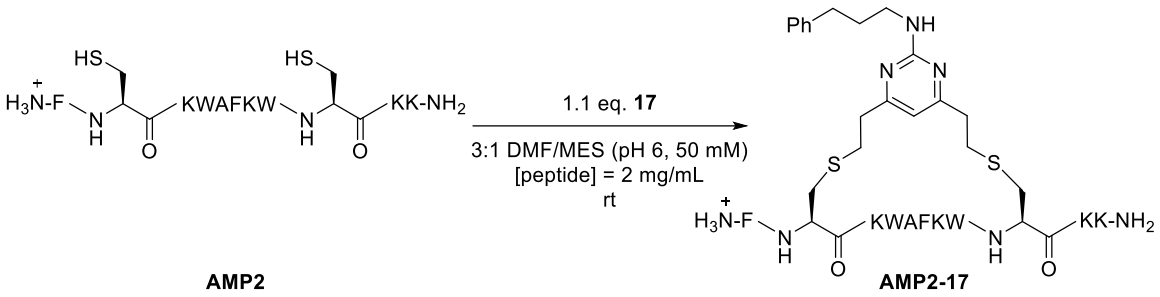

*Scheme 16 The conditions trialled for the stapling of peptide **AMP2** with linker **17**.*

As a result, the effect of both the reaction solvent system and the linker stock solution composition was investigated using **AMP2** and **17** (Table 15). Different solvent combinations were trialled, and the transparency of the reaction mixture (as determined by eye) after the addition of the linker was monitored.

*Table 15 The result of investigations into different combinations of solvent systems and stock solutions of linker **17** for the stapling of peptide **AMP2** under the conditions shown.*

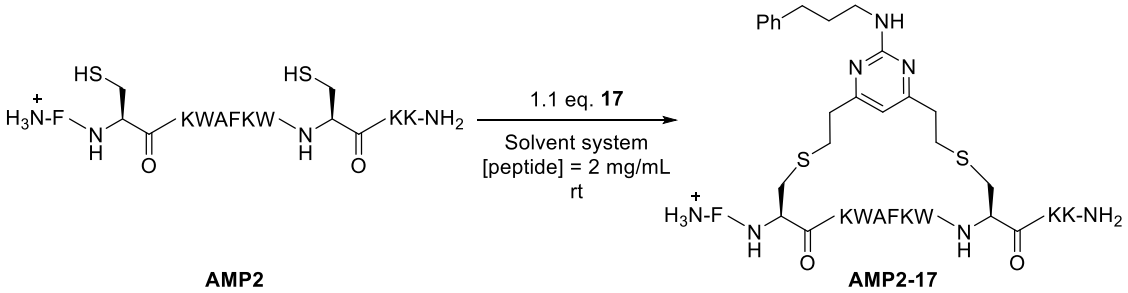

Entry	Solvent system	Solution of linker 17[†]	Outcome on addition of linker to reaction mixture[††]
1	40% MeCN/NaPi (pH 8, 50 mM)	DMF/MeCN (1:1)	Cloudy
2	3:1 MES (pH 6, 50 mM)/DMF	DMF	Cloudy
3	3:1 DMF/MES (pH 6, 50 mM)	DMF/MeCN (1:1)	Clear
4	3:1 NaPi (pH 6, 50 mM)/DMF	DMF/MeCN (1:1)	Cloudy

[†]All stock solutions of linker **17** = [50 mg/mL]
[††]Outcome measured by judging transparency of reaction mixture by eye

[o] 'Larger scale' = 0.034 mmol *cf.* 0.00068 mmol scale for the previously described trial reactions

It was found that a solvent system of 3:1 DMF/MES (pH 6, 50 mM), with the linker added as a DMF/MeCN stock solution (entry 3, Table 15) gave a clear reaction mixture. These conditions were taken forwards for subsequent peptide stapling using DVP linker **17** and will be referred to as the 'standard conditions' from hereon.

3.3.1.5 Synthesis of unfunctionalised STAMPs

Using the optimised conditions, stapling reactions were performed with **AMP1**-**AMP7** (Table 16). The stapling reactions all proceeded smoothly under the standard conditions to give the desired stapled peptides.

*Table 16 The sequences of **AMP1**-**AMP7**, and the conversion of the stapling reactions of these peptides and linker **17** under the conditions shown. Amino acids are shown as blue spheres. % Conversion determined by LCMS analysis of the reaction mixtures after 18 h.*

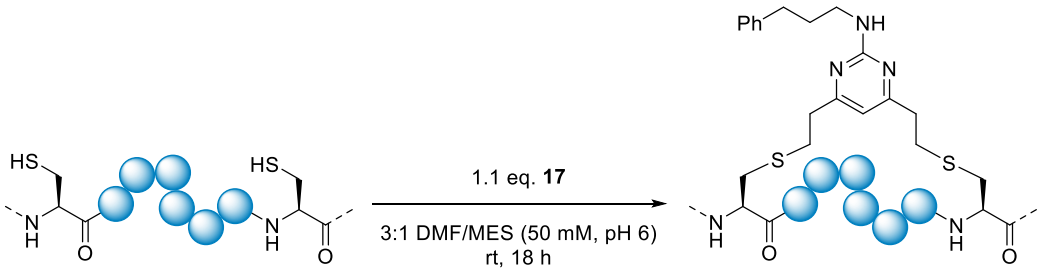

Peptide	Sequence	Stapled peptide	Conversion (%)
AMP1	Ac-TLKQF**C**KGVGKW**C**VK	**AMP1-17**	96
AMP2	F**C**KWAFKW**C**KK	**AMP2-17**	>99
AMP3	Ac-W**C**LKKFRG**C**F	**AMP3-17**	>99
AMP4	RFRRL**C**KKWRKR**C**KKI	**AMP4-17**	97
AMP5	C8-G**C**LKFIKK**C**L	**AMP5-17**	>99
AMP6	KWVQNY**C**KHLGRK**C**HTLKT	**AMP6-17**	>99
AMP7	NLFRKL**C**HRLFRR**C**FGYTLR	**AMP7-17**	96

3.3.1.6 Synthesis of capped 'control peptides'

Control peptides were required to compare to the STAMPs in biological testing, to analyse the impact of cyclisation on antimicrobial activity. In the literature, cysteine-stapled peptides are often compared to their linear counterparts, however to ensure that no disulfide bonds form during the storage or testing of the peptides, capped control peptides were synthesised using a mono-vinyl pyrimidine 'capping reagent'.[314] The capping reagent **18** was synthesised *via* a Suzuki-Miyaura cross-coupling between commercially available 2-amino-4-chloropyrimidine and potassium vinyl trifluoroborate under literature conditions (Scheme 17).[315] The reaction proceeded cleanly in a high conversion, however a significant amount of mass was lost during the chromatographic purification due to product streaking.

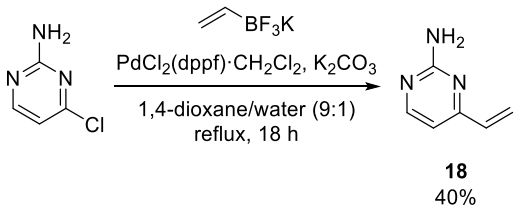

*Scheme 17 The synthesis of **18** via a Suzuki-Miyaura cross-coupling reaction.*

The linear cysteine-containing peptide **AMP1**-**AMP7** were reacted with **18** to give the desired capped peptides. Due to the superior solubility of **18** and the resulting capped peptides compared to linker **17** and the stapled peptides, alternative coupling conditions with a lower proportion of organic solvent could be used, allowing direct injection of the reaction mixtures for HPLC purification (Table 17). Under these conditions, the stapling reactions all proceeded in full conversion to give the desired products, which were purified by preparatory HPLC.

*Table 17 The sequences of **AMP1**-**AMP7**, and the conversion of the capping reactions of these peptides and capping reagent **18** under the conditions shown. Amino acids are shown as blue spheres. % Conversion determined by LCMS analysis of the reaction mixtures after 18 h.*

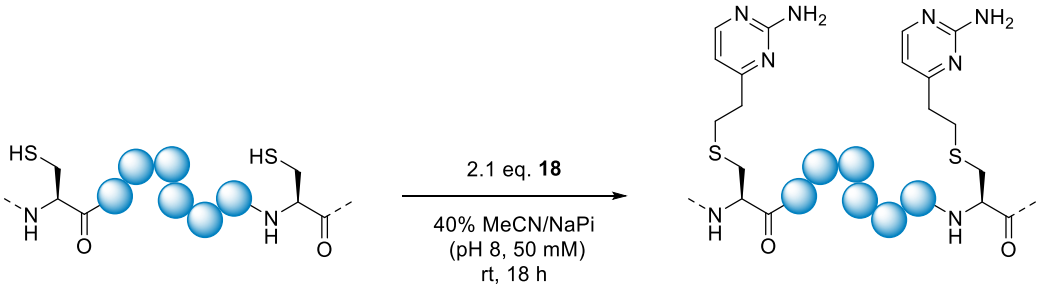

Peptide	Sequence	Capped peptide	Conversion (%)
AMP1	Ac-TLKQF**C**KGVGKW**C**VK	**AMP1-18**	>99
AMP2	F**C**KWAFKW**C**KK	**AMP2-18**	98
AMP3	Ac-W**C**LKKFRG**C**F	**AMP3-18**	98
AMP4	RFRRL**C**KKWRKR**C**KKI	**AMP4-18**	>99
AMP5	C8-G**C**LKFIKK**C**L	**AMP5-18**	97
AMP6	KWVQNY**C**KHLGRK**C**HTLKT	**AMP6-18**	>99
AMP7	NLFRKL**C**HRLFRR**C**FGYTLR	**AMP7-18**	>99

3.3.1.7 Summary of peptide synthesis

In total, 21 peptides were synthesised for the initial biological screen: seven linear cysteine-containing AMPs, seven unfunctionalised STAMPs and seven capped AMPs as control peptides (Figure 72).

AMPX-17 **AMPX-18**

*Figure 72 The general structures of **AMPX-17** and **AMPX-18**, where X = 1-7. For peptide sequences see Table 16 and Table 17.*

3.3.2 Biological testing of unfunctionalised STAMPs

A rapid and facile assessment of antibacterial activity was desired, so that a suitable peptide could be identified for incorporation into the cleavable PDC. To this end the linear peptides **AMP1**-**AMP7**, stapled peptides and capped peptides were screened to assess their antimicrobial activity in a broth dilution minimum inhibitory concentration (MIC) assay, which compares the growth of bacteria both in the presence and absence of antimicrobial agents after incubation for 24 hours.[316] The turbidity of a bacterial suspension increases when the bacterial growth occurs, and changes in the optical density (OD) of the growth medium can be used to assess growth inhibition. If complete inhibition of growth has been achieved the growth media will be clear; if the bacteria are unaffected then the media will have become cloudy during the incubation period. The difference in turbidity of the media can be analysed *via* measuring the OD at 600 nm (OD_{600}).

For **AMP1-17** to **AMP7-17**, it was hoped that there would be no significant loss of inhibitory activity upon cyclisation. At this stage of the project it was unknown what the specific role of the peptide would be in the conjugate, and therefore whether a high level of antibacterial activity would be necessary. The peptide itself could act as a bactericidal agent, requiring a high level of antimicrobial activity. Alternatively, the peptide could be acting as a sensitiser and/or targeting moiety for ciprofloxacin, meaning that a lower level of antibacterial activity would suffice.

3.3.2.1 Inhibition of growth: Initial screen at 256 μg/mL

An initial screen to determine the antimicrobial activity of the peptides was performed with all the peptides at a concentration of 256 μg/mL.[p] For peptides that inhibited growth at 256 μg/mL, serial dilution assays were performed to determine a more precise MIC value. The following strains were used in the MIC assay: *P. aeruginosa* PAO1 (wild-type reference strain),[317] YM64 (PAO1 derivative strain lacking the four major outer membrane efflux pumps),[318] and *S. aureus* 25923 (a commonly used Gram-positive laboratory reference strain). Strain YM64 was included to assess whether the peptides were actively effluxed from the bacteria; if this were the case a lower MIC would be expected for YM64 than PAO1. *S. aureus* was included to see if the peptides displayed activity towards a Gram-positive species, or whether they displayed selective activity against Gram-negative bacteria only.

As a positive control, colistin (polymyxin E) was selected. The polymyxin family of macrocyclic AMPs were discovered in the 1940s and display potent and specific activity towards Gram-negative bacteria.[217] Colistin was used clinically for several decades but was ultimately withdrawn due to nephrotoxicity and neurological side effects, however it is still a last resort drug for the treatment of *P. aeruginosa* infections.[188] The mechanism of action for the polymyxins is not fully understood, but it is believed to involve binding of the cationic peptide to the negatively charged lipid A portion of the lipopolysaccharide on the external cell wall of Gram-negative bacteria.[319] Colistin was chosen as a positive control as it is cheap, commercially available and inhibits growth through disruption of the membrane, the anticipated mechanism of action for the STAMPs. In addition to this, as colistin has been thoroughly researched, literature values for the MIC against various bacterial strains are available.[320]

The growth-inhibiting activity of the stapled peptides, capped peptides, linear cysteine-containing peptides, and linkers 14 and 17 were assessed at 256 μg/mL, and this initial screen identified two STAMPs (**AMP2-17** and **AMP4-17**) that inhibited the growth of PAO1 and **AMP6-17** that showed partial growth inhibition (Table 19). These STAMPs selectively inhibited both PAO1 and YM64 and there was no effect on the growth of *S. aureus*: the full data for these peptides is shown in Table 18. For all of the other peptides, no inhibition of growth was observed at 256 μg/mL and these peptides were therefore deemed to be inactive.

[p] According to the European Committee on Antimicrobial Susceptibility Testing (EUCAST), bacteria are deemed 'resistant' to a compound if no antimicrobial activity is observed at 256 μg/mL.[374]

*Table 18 The results from the initial screen of antimicrobial activity at 256 µg/mL against P. aeruginosa strains PAO1 and YM64 and S. aureus for **AMP2-17**, **AMP4-17**, **AMP6-17** and related analogues. All other peptides displayed no antimicrobial activity at 256 µg/mL. 'Inhibition' refers to growth media with a comparable OD_{600} to the control wells containing just broth. 'No inhibition' refers to growth media which has a comparable OD_{600} to the control wells containing bacterial suspension. 'Partial inhibition' refers to a well which has an OD_{600} between these two extremes.*

Peptide	Bacterial strain		
	PAO1	**YM64**	***S. aureus***
AMP2a	No inhibition	Inhibition	No inhibition
AMP2	No inhibition	No inhibition	No inhibition
AMP2-18	No inhibition	No inhibition	No inhibition
AMP2-17	Inhibition	No inhibition	No inhibition
AMP4a	Inhibition	Inhibition	No inhibition
AMP4	No inhibition	No inhibition	No inhibition
AMP4-18	Inhibition	Inhibition	No inhibition
AMP4-17	Inhibition	No inhibition	No inhibition
AMP6a	Inhibition	Inhibition	No inhibition
AMP6	No inhibition	No inhibition	No inhibition
AMP6-18	No inhibition	No inhibition	No inhibition
AMP6-17	Inhibition	Inhibition	No inhibition
17	No inhibition	No inhibition	No inhibition
18	Partial inhibition	Partial inhibition	Partial inhibition

The stapling reagent **17** displayed no antimicrobial activity, however capping reagent **18** displayed partial inhibition of all of the strains tested against. As the same moiety was not going to be present in the final cleavable PDC, it was decided that this result was not relevant.

3.3.2.2 Inhibition of growth: Serial dilution MIC assay

The peptides that displayed inhibition of growth at 256 µg/mL were analysed further in a serial dilution MIC assay to determine approximate MIC values. For this, the literature sequences were desired as additional control peptides, and so **AMP2a**, **-4a** and **-6a** were synthesised by SPPS and purified by preparative HPLC (for sequences see Table 14).

The serial dilution assay follows the same set up as previously described, however each compound is serially diluted by two-fold along each well of a row on a 96-well plate, allowing growth inhibition to be assayed at concentrations between 256 and 0.5 µg/mL. The results from this assay are given in Table 19. Data for **AMP2**, **-4** and **-6** from the initial screen at 256 µg/mL have been included to allow comparison of all analogues within a given set of AMPs.

*Table 19 The results from the serial dilution MIC assay for peptides that were identified in the previous screen. The inhibition of peptides at concentrations between 256-0.5 µg/mL were tested against bacterial strains PAO1, YM64 and S. aureus for **AMP2-17**, **AMP4-17**, **AMP6-17** and related analogues. ND = no data.*

Peptide		Bacterial strain		
		PAO1	**YM64**	***S. aureus***
AMP2	**AMP2-17**	64	64	ND
	AMP2-18	>256*	>256*	>256*
	AMP2a	>256	>256	>256
	AMP2	>256*	>256*	>256*
AMP4	**AMP4-17**	64	64	ND
	AMP4-18	ND	ND	ND
	AMP4a	32	64	>256
	AMP4	>256*	>256*	>256*
AMP6	**AMP6-17**	>256	>256	>256*
	AMP6-18	>256*	>256*	>256*
	AMP6a	>256	>256	>256
	AMP6	>256*	>256*	>256*
Colistin (polymyxin E)		8	8	>256

*Results from 256 µg/mL screen described previously. All other results from serial dilution MIC assay.

The results from the serial dilution MIC assay showed that **AMP6-17** (or related analogues) did not exhibit any antimicrobial activity. This means that the inhibition of growth observed in the screen at 256 µg/mL was not a reliable result and this peptide was subsequently excluded from further investigations. The literature peptide **AMP6a** failed to display any antimicrobial activity under these assay conditions (*cf.* 24-48 µg/mL in the literature), however this disparity could be due to differences in the assay set up and the bacterial strains used.[306,321]

Whilst **AMP4-17** did not have the same high level of antimicrobial activity reported in the literature for **AMP4a** (MIC 2-4 µg/mL),[310] promisingly these peptides show not dissimilar activity under the assay conditions used for the initial screen (**AMP4a** 32 µg/mL, **AMP4-17** 64 µg/mL). Pleasingly, the peptides displayed similar MIC values for *P. aeruginosa* strains PAO1 and YM64, indicating that efflux was not an issue for these antimicrobials (**AMP4-17** 64 µg/mL for PAO1 and YM64). Additionally, no inhibition of growth was observed for *S. aureus*, indicating that the peptides were selectively active against Gram-negative *P. aeruginosa* strains over the Gram-positive *S. aureus*.

For **AMP2**, out of all the analogues tested, the stapled analogue **AMP2-17** had the highest antimicrobial activity (**AMP2-17** 64 µg/mL, all other peptides >256 µg/mL). This could be because the staple is holding the peptide in a more α-helical conformation, thus improving its ability to interact with the bacterial membranes. Interestingly, **AMP2a** did not show any inhibition of growth against PA, (*cf.* 12.5 µg/mL reported in the literature) however again this could be due to differences between the bacterial strains used and the conditions of the

assay.[309] As was the case for **AMP4-17**, no inhibition of growth was observed for *S. aureus* and **AMP2-17** had the same MIC value (64 µg/mL) for PAO1 and YM64.

Both **AMP2-17** and **AMP4-17** showed very reasonable MIC values against *P. aeruginosa*, however, it was decided that, in order to simplify the development of the proof-of-concept PDC, only one peptide sequence would be used. **AMP2-17** was chosen as it showed antimicrobial activity when stapled but not linear, therefore some aspect of the peptide stapling was conferring antimicrobial activity onto the peptide sequence; additional biological testing would be required to fully elucidate this phenomenon. Additionally, **AMP2-17** was shorter than **AMP4-17**, resulting in a faster and more efficient SPPS. If the PDC constructed using **AMP2-17** was promising, then the construction of a PDC using **AMP4-17** could be performed to showcase the modular design.

3.3.2.3 Effect of STAMPs on biofilm formation

The aim of this project was to develop an antimicrobial PDC to treat *P. aeruginosa* infections, therefore for the STAMPs, MIC values for growth-inhibition were used to determine which to incorporate into the PDC design. However, as previously discussed, biofilm formation can contribute greatly to the antibiotic resistance and virulence of *P. aeruginosa*. Antimicrobial agents can prevent biofilm formation and disrupt pre-formed biofilms, however, they can also cause bacterial stress that may induce biofilm formation.[322] The effect of the unfunctionalised, active STAMPs on the formation of *P. aeruginosa* biofilms was assessed using a standard crystal violet staining assay. In this assay, bacteria are incubated with sub-inhibitory concentrations of an antimicrobial agent, then the amount of biofilm present is quantified by crystal violet staining and recording the optical density at 595 nm (OD_{595}).[323] Preliminary investigations were made with **AMP2-17** and **AMP4-17** looking at the effect of sub-inhibitory concentrations of peptide on the formation of *P. aeruginosa* biofilms over 24 hours using polymyxin E as a positive control (Figure 73). This assay gave interesting initial results, however these data need repeating for further validation, and therefore did not influence the overall PDC design. Near-inhibitory concentrations of **AMP2-17** caused an increase in biofilm formation compared to untreated PAO1 bacteria, indicating a bacterial stress response, whereas near-inhibitory concentrations of **AMP2a** showed a significant reduction in biofilm formation. **AMP4-17** and the linear analogue **AMP4a** displayed similar effects on biofilm formation, with near-inhibitory concentrations leading to less crystal violet straining than untreated bacteria.

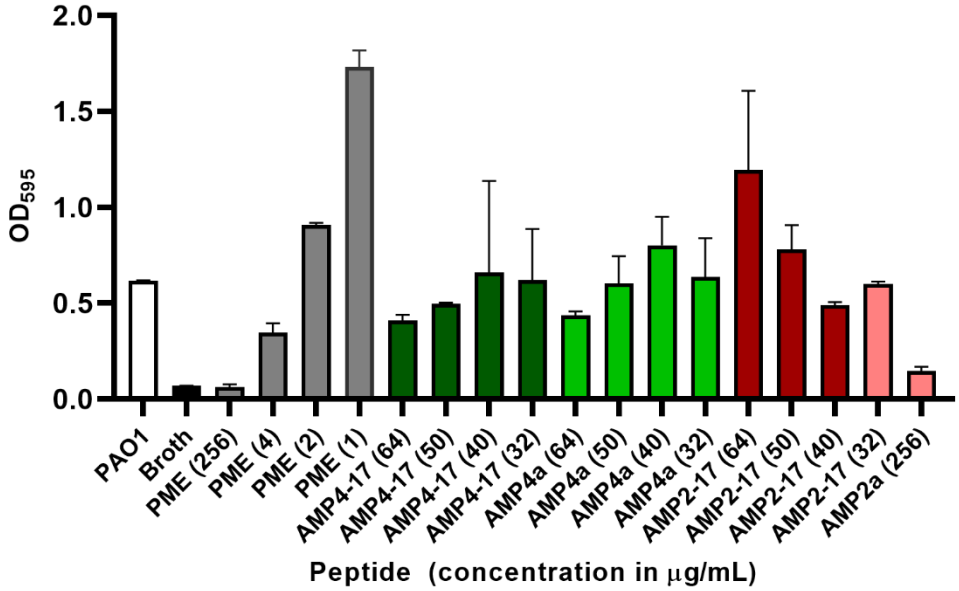

Figure 73 Preliminary results from a crystal violet staining assay to assess the effect of subinhibitory concentrations of growth-inhibiting peptides on the biofilm formation of PAO1. Plotted is the OD_{595} of the growth media after treatment with peptides at the concentration given in brackets. PME = polymyxin E, the positive control. Data is shown as the mean of two repeats ± standard deviation.

At this stage of the project, the assays described in this section were deemed appropriate for the preparation of the complete PDC construct. Further testing would be required to investigate the mechanism of action of the STAMPs, however it was decided to perform more in-depth biological investigations once the full, cleavable PDC had been synthesised and the unfunctionalised STAMP and PDC could be analysed together.

3.3.4 Circular dichroism spectroscopy of AMPs

To determine the effect of stapling on the secondary structure of the peptides, **AMP2-17** and **AMP2a** were analysed using circular dichroism (CD) spectroscopy. Whilst there is no information in the literature regarding the secondary structure of peptide **AMP2a**, there is for the gaegurin-5 peptide[q] from which **AMP2a** is derived.[324] Gaegurin-5 displayed a random coil in aqueous buffer, and it was only in the presence of either 2,2,2-trifluoroethanol (TFE), a known helix-stabiliser,[325] or a bacterial membrane-mimicking environment such as sodium dodecyl sulfate (SDS) or dodecylphosphocholine (DPC) micelles that helicity was observed.[326] This conformational disparity between aqueous and membrane-mimicking environments has been widely observed for membrane-disrupting peptides, and supports the proposed carpet and barrel-stave mechanisms of action.[277]

Samples of **AMP2-17**, **AMP2** and **AMP2a** in MeCN/H_2O (1:1) were analysed by CD spectroscopy (A, Figure 74). As expected, the literature sequence **AMP2a** displayed a low α-

[q] GGN5 sequence = FLGALFKVASKVLPSVKCAITKKC.[324]

helical content (11%), and pleasingly the stapled peptide, whilst still displaying a relatively low percentage helicity, had a much higher percentage helicity (**AMP2-17**, 26%). This indicates that the staple is able to fix the peptide in a more α-helical conformation. To investigate how the helical content of the parent peptide sequence varied in different environments, CD spectroscopy was performed with **AMP2a** in aqueous buffer, and in the presence of TFE and SDS (B, Figure 74). In keeping with the literature reports for the gaegurin-5, it was found that **AMP2a** displayed a random coil structure in NaPi buffer (8% α-helicity), and the α-helical content was significantly improved in the presence of SDS (18%) and TFE (36%).[324]

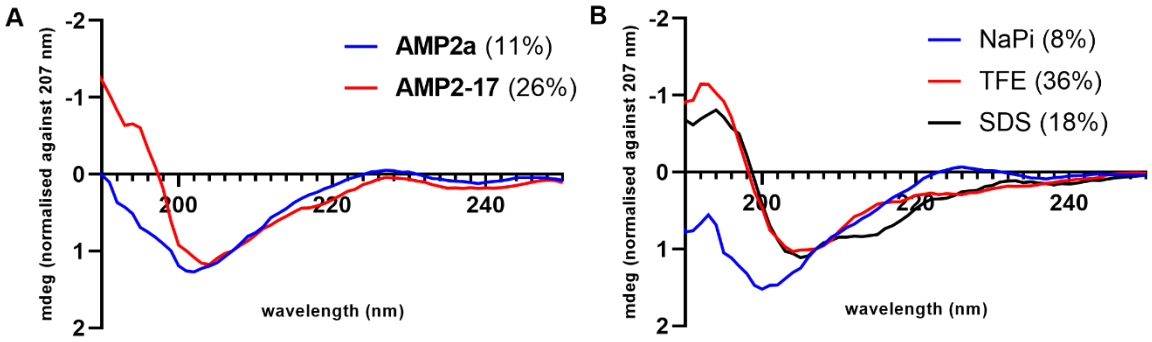

*Figure 74 CD spectra for AMPs A) The CD spectra of **AMP2-17** and **AMP2a** in MeCN/H_2O (1:1). B) The CD spectra of **AMP2a** in different solutions: TFE = 50% aq. TFE solution, SDS = 30 mM SDS solution and NaPi = 10 mM, pH 7.4 NaPi buffer. The % helicity is given in brackets in the legend.*

3.3.5 Design of peptide-drug conjugate

The cleavable PDC described in this thesis is composed of a STAMP, a cleavable linker and an antimicrobial drug (A, Figure 75). For a proof-of-concept PDC, each component must be carefully and rationally selected to maximise the probability of success, whilst validating the proposed biological mechanism of action. The selection of the stapled peptide component was described in the previous section (B, Figure 75). For the construction of the full PDC, the linear peptide sequence validated in **AMP2-17** was used. However, a different staple was required to enable incorporation of the cleavable linker and drug instead of the 3-phenylpropan-1-amino group in **AMP2-17**.

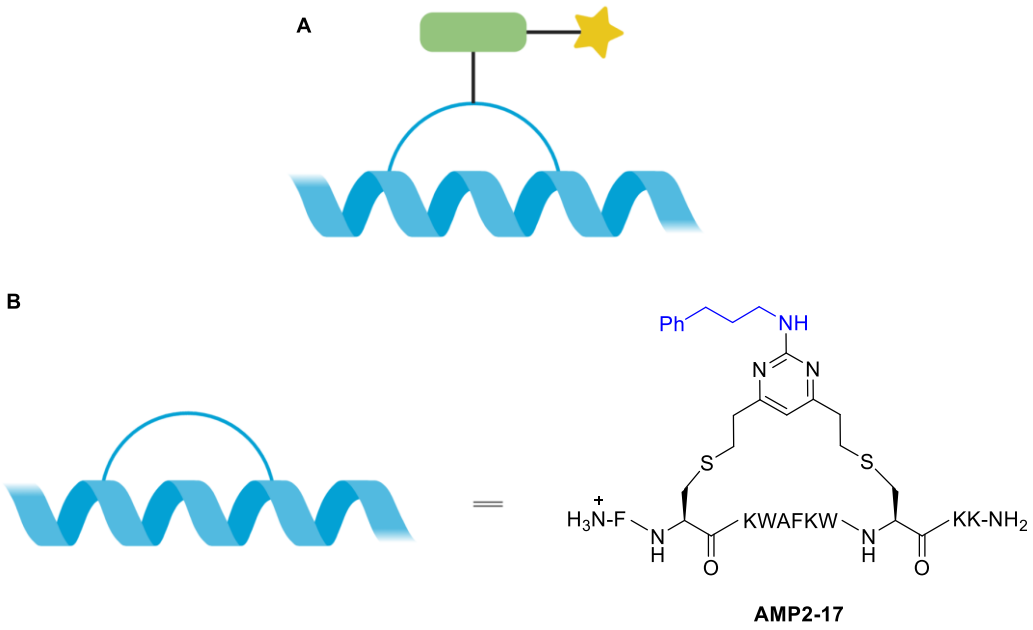

*Figure 75 A: A cartoon depicting a PDC comprising a stapled peptide (blue helix), a cleavable linker (green rectangle) and an antimicrobial drug (yellow star). B: The structure of **AMP2-17**, which forms the basis of the stapled peptide component. The 3-phenylpropan-1amino moiety is highlighted in blue.*

Ciprofloxacin was chosen as the drug, as it is widely used in the clinic to treat *P. aeruginosa* infections (A, Scheme 18).[327] Additionally it is very cheap, stable to a wide range of chemical transformations and contains suitable synthetic handles for the attachment of other groups.[328] For these reasons, it has been widely used in conjugate and pro-drug strategies, thus providing precedence for its application in a cleavable PDC.[242] A cephalosporin scaffold was chosen as the cleavable moiety, as it has been used successfully in various prodrug and selective release strategies.[56,57,77–79] This is primarily due to their relative stability (compared to penicillins) and selective and efficient β-lactam hydrolysis and elimination when exposed to β-lactamase (BL) enzymes (B, Scheme 18).

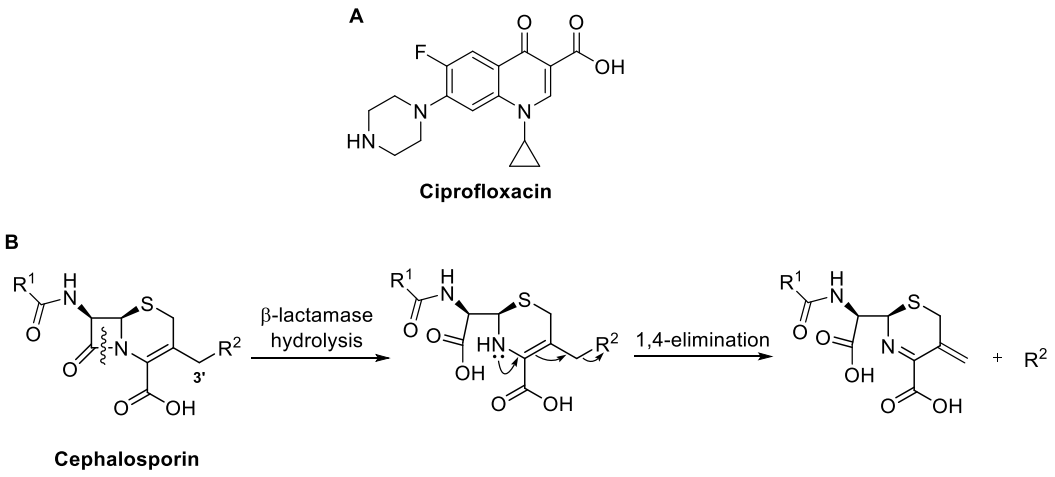

Scheme 18 A) Ciprofloxacin, B) the BL hydrolysis of the β-lactam ring in a cephalosporin. This is followed by 1,4-elimination and subsequent release of a leaving group, R^2. R^1 is a variable group on the cephalosporin.

With the individual components confirmed, the attachment strategy was considered. As a proof-of-concept PDC, a simple synthetic route was desired so that the final construct could be rapidly synthesised and tested. Starting with the cleavable linker, the chosen cephalosporin moiety contains two chemical handles for attachment: the amine at position C-7 and the methylene at position C-10 (R^1 and R^2 respectively, B, Scheme 18). Amides formed at position 7 are stable to BL hydrolysis, making this a suitable attachment point for the stapled peptide. The group attached to position 10 is ultimately eliminated after BL hydrolysis, hence it was decided that the drug, ciprofloxacin, would be connected at this position (R^2, B, Scheme 18).

Ciprofloxacin can be conjugated either *via* the carboxylic acid (e.g. A, Figure 76)[235] or piperazine amine (e.g. B, Figure 76)[252] and examples of both exist in the literature. The carboxylic acid is necessary for antibacterial activity, therefore conjugation at this position would mask the activity of ciprofloxacin until cleavage of the cephalosporin, resulting in a pro-drug effect.[329,212] Conversely, conjugation *via* the piperazine amine could have a less marked effect on the activity. As it was unknown whether masking the effect of ciprofloxacin would be necessary, it was decided that both attachment points would be investigated.

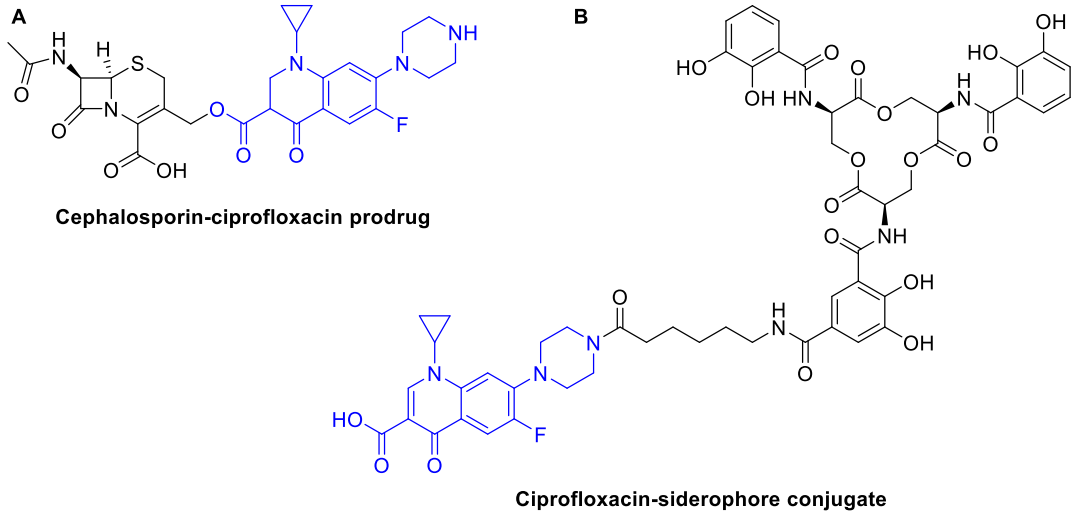

Figure 76 The structures of two literature ciprofloxacin conjugates. A: A cleavable ciprofloxacin prodrug with conjugation via the carboxylic acid,[235] and B: A ciprofloxacin-siderophore conjugate, where ciprofloxacin is attached via the amine.[252] Ciprofloxacin is highlighted in blue.

The synthetic route was designed using the cheapest and most widely available starting material, 7-aminocephalosporanic acid (7-ACA). Possible chemical conjugation strategies for the connection of the three components are shown in Figure 77. For the attachment of the DVP to the cephalosporin, two robust linkage strategies are CuAAC (A, Figure 77) or amide coupling (B, Figure 77). These strategies were considered as CuAAC is known to be highly chemoselective and modular, whereas amide coupling is often high yielding and practically simple. For both approaches, the building blocks are widely available and easily accessible.

Amide coupling would require the introduction of a carboxylic acid moiety onto the DVP staple, although no modification would be needed on the cephalosporin. A CuAAC strategy would require modification of both the DVP staple and cephalosporin to introduce the azide and alkyne moieties. For the conjugation of the cephalosporin to the ciprofloxacin, attachment *via* the piperazine amine would necessitate carbamate formation at position C-10 of the cephalosporin (C, Figure 77). Attachment *via* the carboxylic acid would require displacement of the acetate group in 7-ACA with the ciprofloxacin carboxylate (D, Figure 77); literature routes existed for these transformations.

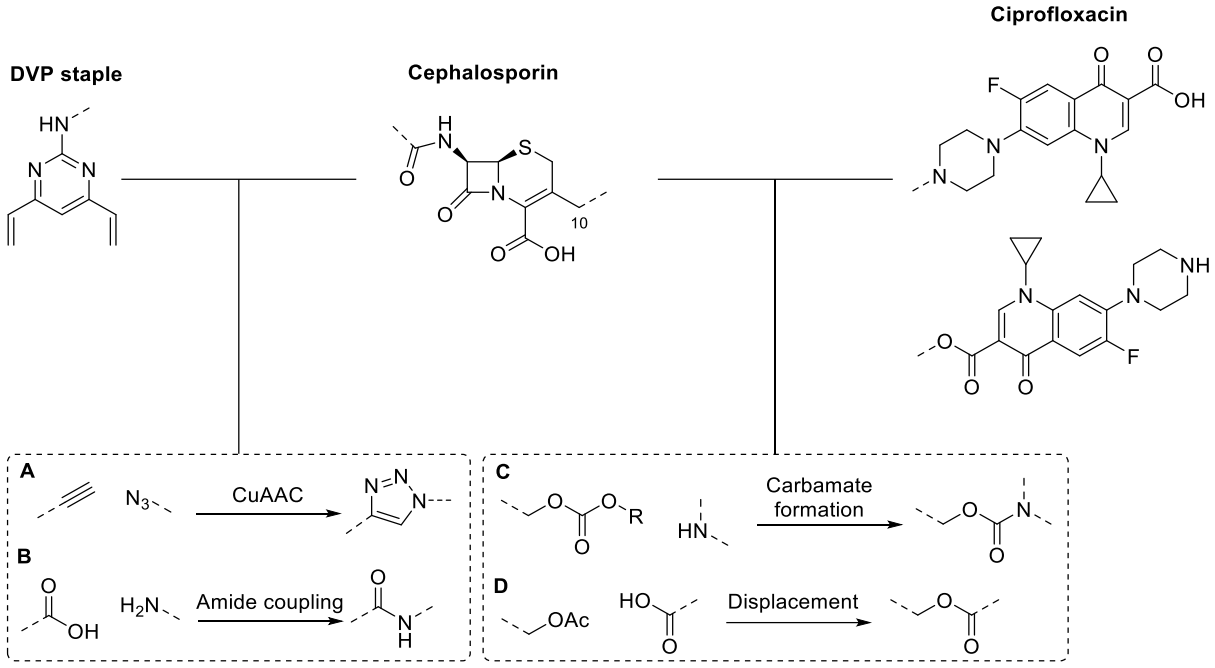

Figure 77 An overview of possible connections between the three different portions of the cleavage linkers (non-exhaustive). The DVP and cephalosporin could be attached via A) CuAAC B) or amidation. Ciprofloxacin could be attached at position 10 of the cephalosporin via C) carbamate formation with the piperazine amine or D) via displacement with the carboxylic acid.

The attachment strategies highlighted in Figure 77 represent just a few possibilities from a vast number of potential approaches. It was noted that the nature of the linkage between the components of the PDC may affect the biological activity, for example their length, conformational flexibility, and lipophilicity. However, with no information in the literature available to guide the design, the main design consideration for the initial proof-of-concept PDC was synthetic tractability. Optimisation of the linkages to maximise the antimicrobial activity could be performed at a later stage.

3.3.6 Synthesis of first-generation linkers

The design of the first-generation linkers **19** and **20** are shown in Figure 78. CuAAC was chosen for the attachment of the DVP to the cephalosporin as this reaction proceeds under

mild conditions, is highly chemoselective and modular. In this manner, the modular CuAAC strategy would enable rapid and efficient synthesis of multiple compounds using the key DVP fragment, including biological controls. It was envisioned that 4-azidobenzoic acid would be used to introduce an azide moiety to the cephalosporin as it was cheap and commercially available. Ciprofloxacin could then be attached *via* the piperazine nitrogen in **19**, and *via* the carboxylic acid in **20**.

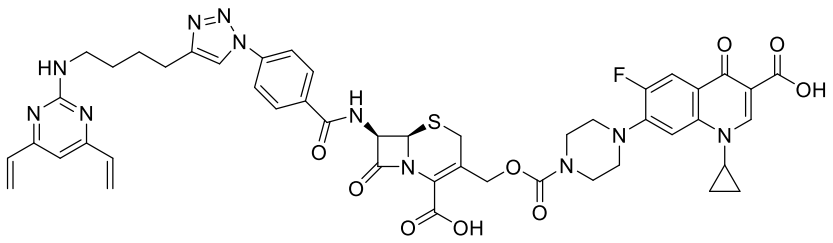

19

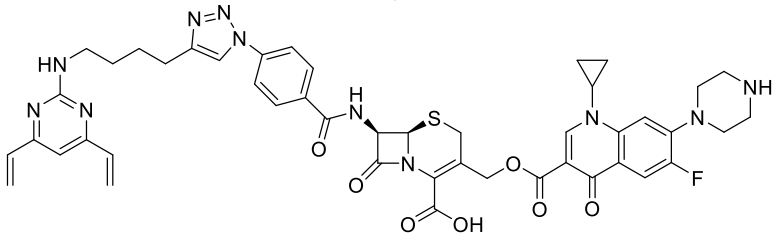

20

*Figure 78 The structure of generation 1 cleavable linkers **19** and **20**.*

Focus was next placed on determining the synthetic strategy. Retrosynthetic analysis of both **19** and **20** involved disconnection of the 1,4-triazole *via* a CuAAC, giving common alkyne **21** and the azides **22** and **23** (Scheme 19).

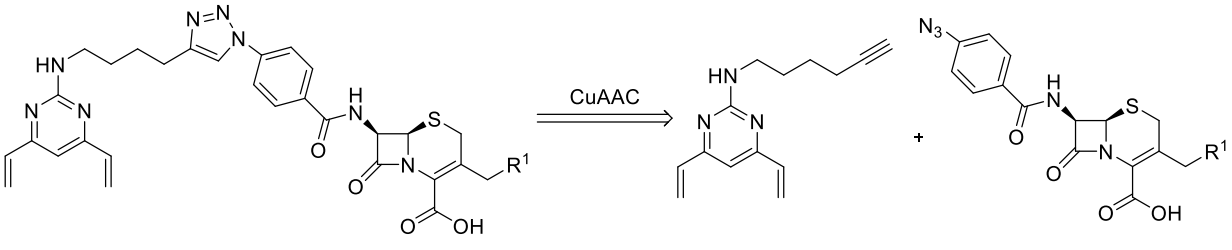

*Scheme 19 The retrosynthetic analysis of proposed linkers **19** and **20**.*

Synthesis of **21** followed a literature procedure (Scheme 20).[68] From commercially available 2-amino-4,6-dichloropyrimidine, the vinyl groups could be introduced to give **24**, *via* a Suzuki-

Miyaura cross-coupling as was described for the synthesis of **17**. Subsequent alkylation of the amine in **24** would install the alkyne moiety to give the desired staple, **21**.

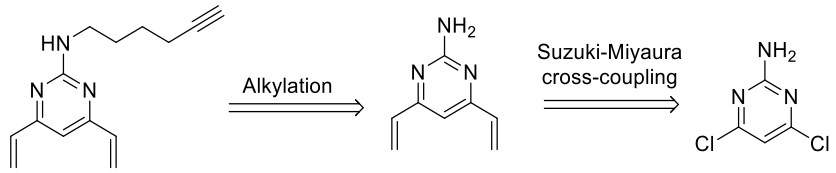

21 **24**

*Scheme 20 The retrosynthetic analysis of **21** to a commercially available starting material.*

For **22**, disconnection of the carbamate gives ciprofloxacin and an activated carbonate at position 10 on the cephalosporin ring; the choice of 4-nitrophenyl carbonate will be discussed in Section 3.3.6.2 (**25**, Scheme 21). Formation of this activated carbonate would require an alcohol at this position, **26**, which could be generated *via* deacetylation of **27**. The final step involved an amide coupling between commercially available starting materials 4-azidobenzoic acid and 7-ACA.

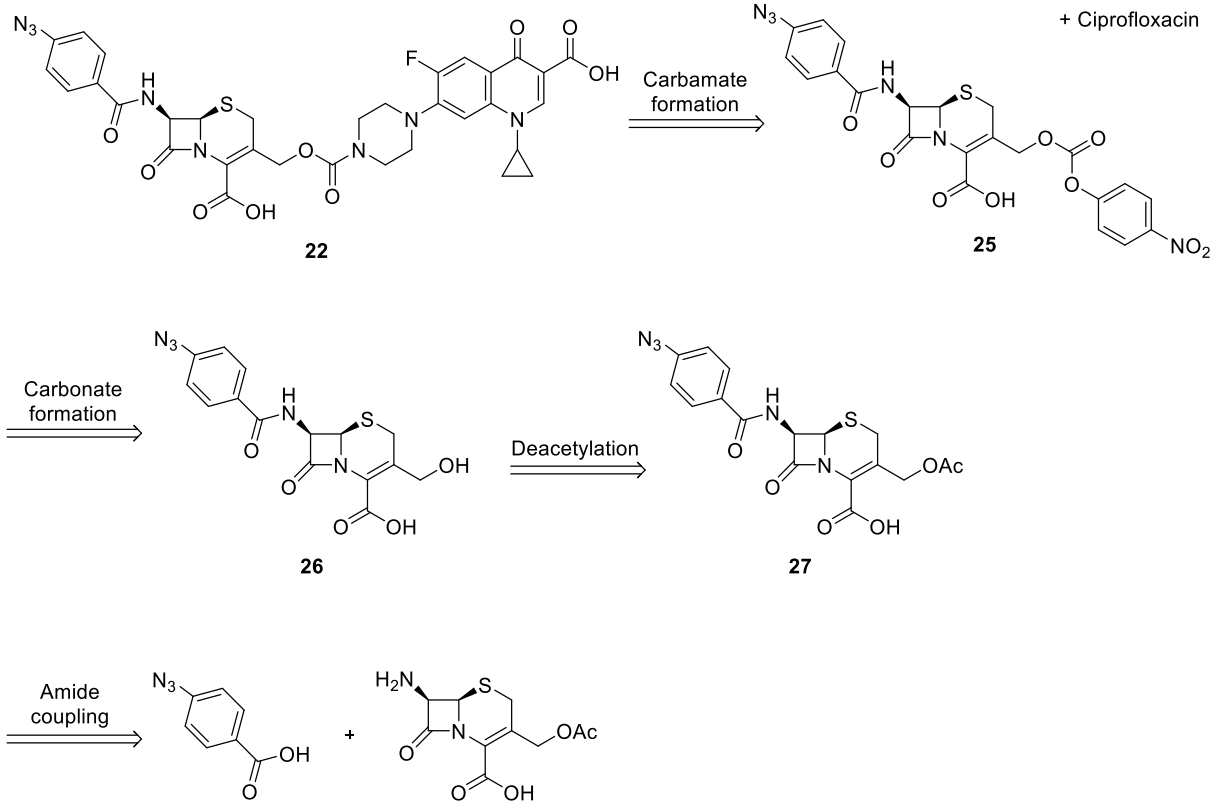

22 **25** **26** **27**

*Scheme 21 The retrosynthetic analysis of **22** to commercially available starting materials.*

For **23**, disconnection at the ester gives ciprofloxacin and **27**, the same intermediate as found in the retrosynthetic analysis for **22** (Scheme 22). The literature synthesis of similar conjugates

as **23** involves displacement of the C10 acetate group on the cephalosporin by *N*-Boc protected ciprofloxacin.[235]

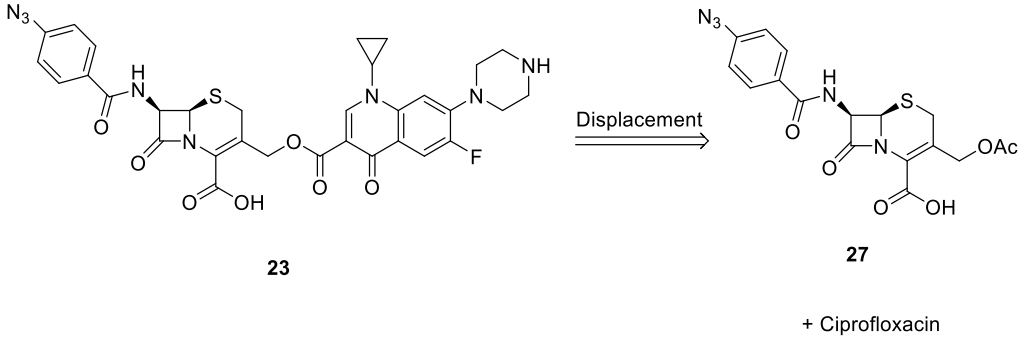

*Scheme 22 The retrosynthetic analysis of **23** to **27** and ciprofloxacin.*

3.3.6.1 Synthesis of **21**

Following the above proposed protocols, investigations towards the synthesis of the PDC commenced. Firstly, DVP **21** was synthesised according to the literature procedure (Scheme 23).[68] Commercially available 2-amino-4,6-dichloropyrimidine was subjected to Suzuki-Miyaura cross-coupling conditions to install the two vinyl groups. This proceeded in a moderate yield to give **24**; despite complete conversion, substantial mass was lost during chromatographic purification due to significant product streaking. Subsequent alkylation with 6-iodo-1-hexyne gave **21** in a low yield, albeit with enough material to pursue the remaining synthesis.

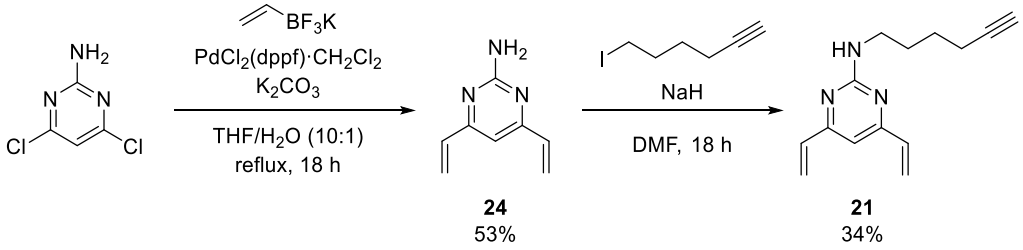

*Scheme 23 The synthesis of **21** via Suzuki-Miyaura cross-coupling and alkylation via the literature route.*[68]

3.3.6.2 Synthesis of **19:** Route 1

The first step in the synthesis of linker **19** was the deacetylation of commercially available 7-ACA to give **28**. Literature approaches to this transformation included hydrolysis with tetrabutylammonium hydroxide (TBAOH)[236] or sodium hydroxide.[330] Both of these conditions were trialled; it was found that using sodium hydroxide gave a higher isolated yield (40% compared to 29% with TBAOH), and there were issues with the isolation of the product using

TBAOH (Scheme 24). Sodium hydroxide-mediated hydrolysis still gave a low-moderate yield, and the resulting product was extremely difficult to analyse due to poor solubility.

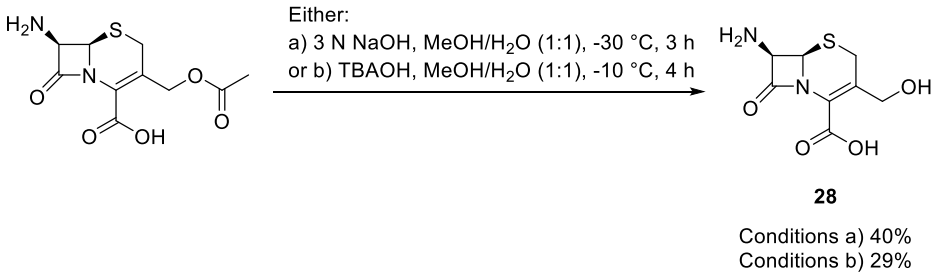

*Scheme 24 The base hydrolysis of 7-ACA to give **28** using either a) NaOH,[330] or b) TBAOH.[236]*

The next step in the synthesis involved amide bond formation with the amine at position 7 of **28**. 4-Azidobenzoic acid was converted into acid chloride **29** under the conditions shown in a quantitative yield (Scheme 25). Coupling of **29** and **28** using conditions reported by Desgranges *et al.*[236] gave the desired product **26**, as confirmed by LCMS and ^{1}H NMR analysis of the reaction mixture. However, chromatographic isolation of the desired product was not possible due to the co-elution of a significant side-product, which itself could not be isolated or characterised (Scheme 25). The crude reaction mixture was used to trial the formation of the activated carbonate. Several activated carbonates of cephalosporins have been reported in the literature, including 1,2,2,2-tetrachloroethyl and 4-nitrophenyl:[236,257] the 4-nitrophenyl carbonate was initially chosen as the reagents required were more widely available. Crude **26** was treated with 4-nitrophenyl chloroformate, however a complex mixture was formed and after chromatographic purification no product was isolated (Scheme 25).

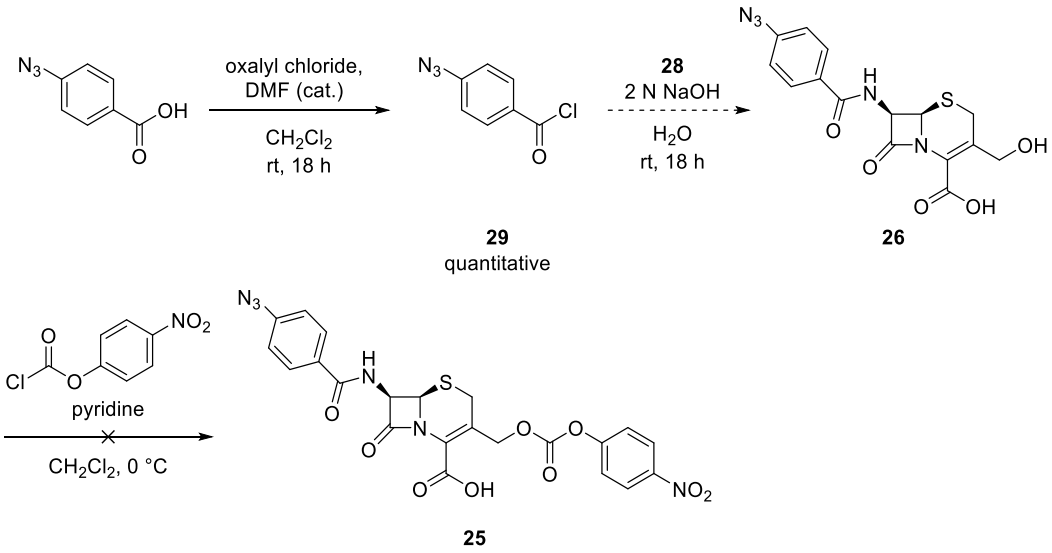

*Scheme 25 The attempted synthesis of **25** via formation of acid chloride **29**, subsequent acylation of **28** and reaction with 4-nitrophenylchloroformate.*

Given the problems with this route, including consistent low yields, problems with isolating **28** and lack of success in the formation of **25**, an alternative route was sought. It was decided that protecting the carboxylic acid of 7-ACA could improve the solubility of the intermediates to circumvent the significant handling issues faced in route 1.

3.3.6.3 Synthesis of **19**: Route 2

Route 1 had followed the synthesis reported by Desgranges *et al.*, involving basic hydrolysis of 7-ACA followed by acylation with **29** (Scheme 26).[236] Route 2 was based on the synthesis of BL cleavable siderophore-ciprofloxacin conjugates reported by Liu *et al*. (Scheme 26).[257] This synthetic route involved protection of the **7-ACA** carboxylic acid in the first step, forming a much more soluble intermediate for the following steps. A step in route 2 was a selective lipase-catalysed deacetylation at the 10 position on the cephalosporin ring; this reaction was developed by the Miller group specifically for the generation of cephalosporin analogues.[331]

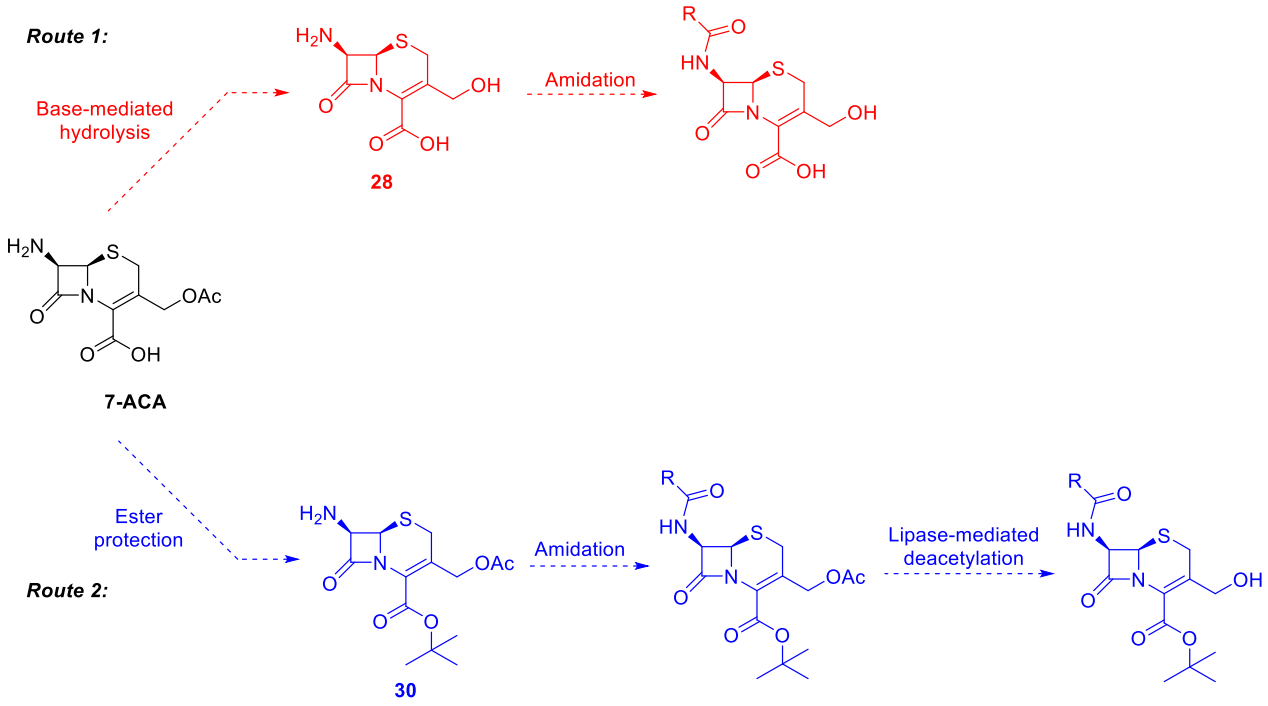

*Scheme 26 An overview of the two possible synthetic routes to **19** investigated.*

3.3.6.3.1 Ester protection and amide coupling

Route 2 commenced with the protection of 7-ACA as a *tert*-butyl ester, which proceeded smoothly and in a high yield under the literature conditions to give **30** (Scheme 27).[332] The desired product, whilst requiring no purification, was extremely hygroscopic, hence **3**0 was immediately subjected to the subsequent amide coupling in order to maximise the yield.

Acylation of **30** with **29** under amidation conditions reported by Miller *et al*. gave **31** in a 52% yield after purification by FCC.[257]

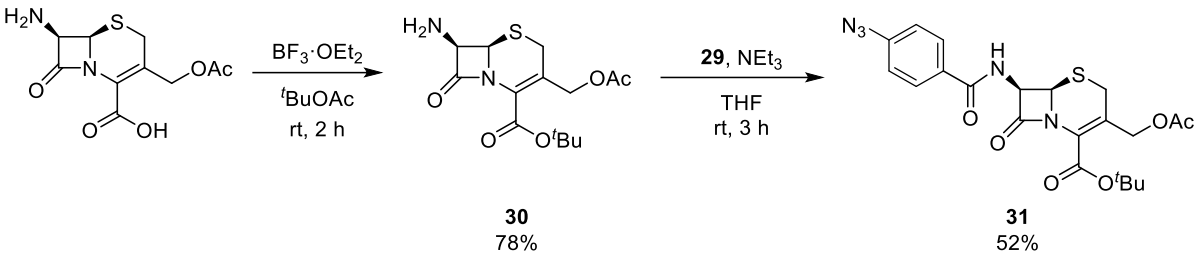

*Scheme 27 The synthesis of **31** under the literature conditions.*[257]

3.3.6.4 Investigations toward the synthesis of **23**

With **31** in-hand, a key transformation in the synthesis of isomeric linker **23** was investigated. The displacement of the C-10 acetate group on **31** with *N*-Boc-ciprofloxacin, **32**, is achieved in the literature by treatment with trimethylsilyl iodide (TMSI) to form an intermediate iodo species, **33**.[235] *N*-Boc-ciprofloxacin was synthesised from commercially available ciprofloxacin in a high yield *via* treatment with Boc anhydride and formation of the sodium salt **32** (Scheme 28).[333]

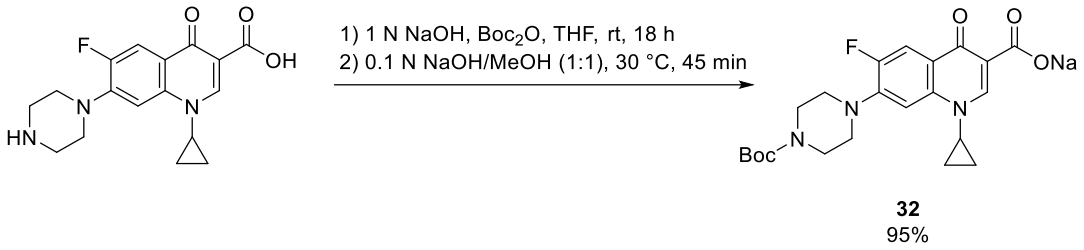

*Scheme 28 The synthesis of **32** from commercially available ciprofloxacin under the literature conditions.*[333]

The displacement reaction was attempted with **32** and **31** (Scheme 29). Unfortunately, under the literature conditions only **32** was recovered from the reaction mixture and there was no evidence of desired product **34** by LCMS and NMR analysis of the crude reaction mixture.

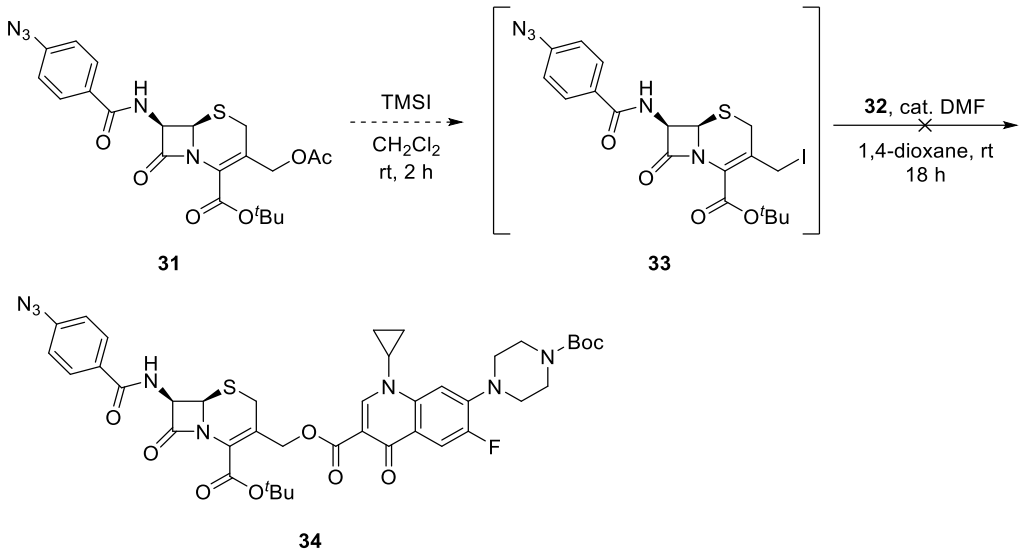

*Scheme 29 The attempted synthesis of **34** under the conditions reported by Evans et al.*[235]

Alternative conditions were investigated for this reaction (Table 20). Using sodium iodide instead of TMSI to activate the acetate group towards displacement gave a complex mixture, as did the use of $BF_3.OEt_2$ (entries 2 and 3 respectively, Table 20).

*Table 20 The conditions trialled for the reaction of **31** with **32**.*

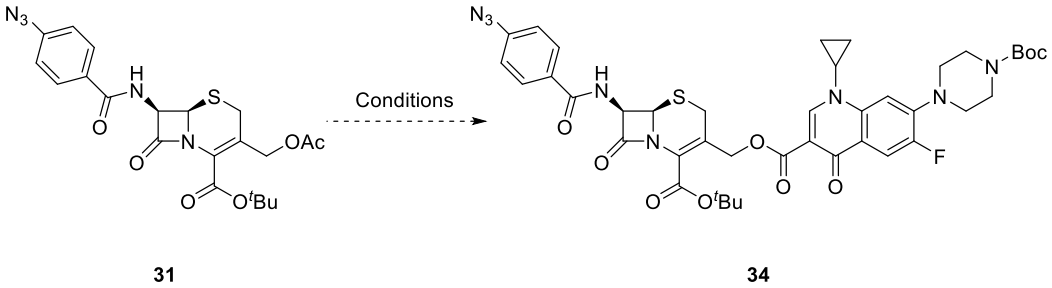

Entry	Conditions	Outcome
1	TMSI in CH_2Cl_2 then **32** and cat. DMF in 1,4-dioxane	No desired product isolated, **32** recovered
2	NaI in CH_2Cl_2, then **32**	Complex mixture, no desired product isolated
3	$BF_3.OEt_2$ in CH_2Cl_2, then **32**	Complex mixture, no desired product isolated

It is possible that **34** could be synthesised *via* a displacement reaction with an alternative alkyl halide intermediate to **33**, for example alkyl bromide **35**, which can be accessed *via* allylic bromination of commercially available 7-aminodesacetoxycephalosporanic acid (7-ADCA). A trial reaction was performed with 7-ADCA and *N*-bromo succinimide (NBS) under irradiation by visible light (Scheme 30).[334] Although the mass of **35** was observed by LCMS analysis, the conversion was low and none was isolated after purification.

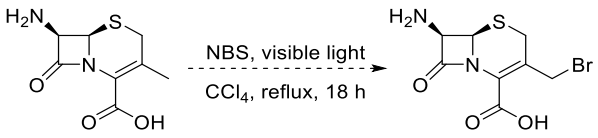

35

*Scheme 30 The attempted allylic bromination of 7-ADCA to give **35**.*

Due to the challenges encountered in the synthesis of first-generation linkers, **19** and **20**, in addition to newly published information that indicated the proposed linker design was not optimal, it was decided to abandon the proposed strategy. This information, and the subsequent changes made are discussed in the following section.

3.3.7 Synthesis of second-generation linkers

In 2019, Evans *et al*. published a series of ciprofloxacin prodrugs that utilised the cephalosporin moiety for selective unmasking of the active drug.[235] During the development of these prodrugs, the authors investigated the effect of different groups at the cephalosporin C7 amide on the rate of BL-mediated hydrolysis using whole-cell NMR assays (Table 21). A range of analogues were synthesised and the MIC values were assessed against a clinically relevant *E. coli* strain, CTF073, both with and without the expression of an extended spectrum BL, CTX-M-1. Using the drug cephalothin for comparison (entry 1, Table 21), the authors found that direct attachment of aromatic groups to the C7 amide was not tolerated and a low percentage of hydrolysis was observed (entries 2-5, Table 21), whereas aliphatic substituents led to more substantial hydrolysis, particularly for shorter alkyl chains (entries 6-8, Table 21). An additional *in vitro* assay, using recombinant BL AmpC, indicated that the low levels of hydrolysis observed in the whole-cell assay for the longer chain analogues was due to poor cellular penetration. Based on the data gathered from all the analogues tested, the authors chose to incorporate a simple acetyl amide at the C7 position (entry 8, Table 21) in the candidate prodrug.

Table 21 Selected examples of prodrugs synthesised and tested by Evans et al., including MIC values and % hydrolysis.[235] BL = CTX-M-1.

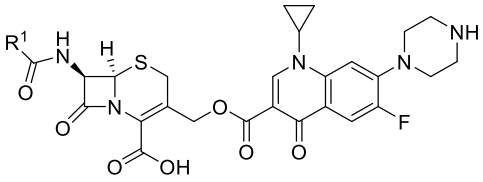

Entry	R^1	MIC (μM in CFT073)		% hydrolysis in CFT073 + BL[a]
		+ BL	- BL	
1	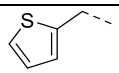	25	>400	68
2	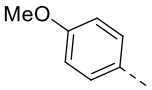	>400	>400	3
3	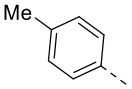	>400	>400	3
4	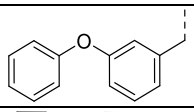	>400	>400	0
5	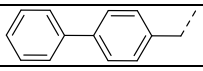	>400	>400	4
6	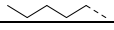	100	>400	7
7		200	>400	25
8		400	>400	67

[a]Hydrolysis of 100 μM of compound after 1 h, as measured by a whole cell NMR assay.

This information provided useful insights that could be applied to the first-generation linkers **19**. This linker contains a quaternary carbon at the C7 amide position (Figure 79), however the data reported by Evans *et al.* suggest that this would not be optimal for hydrolysis (see 0-4% hydrolysis for entries 2-5 respectively, Table 21). Although the assays reported in the paper were performed in *E. coli* and not *P. aeruginosa*, the BLs CTX-M-1 and AmpC used in the reported assays are present in clinical isolates of *P. aeruginosa*.[335–337]

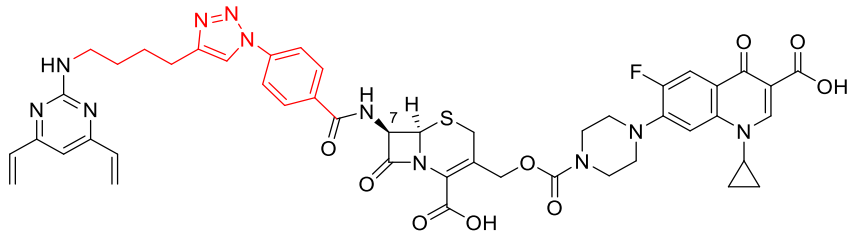

19

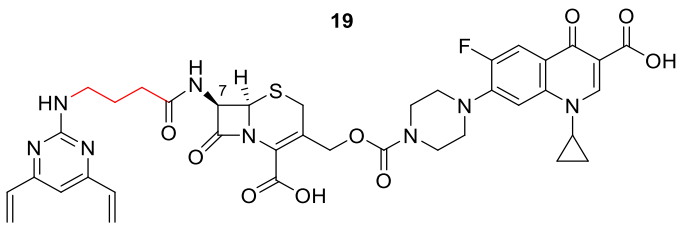

36

*Figure 79 The structure of first-generation linker **19** and second-generation linker **36**. The change in linker design is highlighted in red.*

To make the necessary design alterations whilst retaining the synthetic strategy used in route 2, the azide moiety could be changed from 4-azidobenzoic acid to 2-azidoacetic acid. This substitution would replace the quaternary carbon with a two-carbon aliphatic chain, however 2-azidoacetic acid was deemed too expensive to use, considering the low yields associated with the previously described synthetic route. Instead, a simpler strategy would be to directly couple the cephalosporin to the DVP *via* an aliphatic linker, removing the CuAAC step. From the study by Evans *et al.*, alkyl chains of intermediate length gave reasonable levels of hydrolysis, therefore a 3-carbon linker would be placed between the DVT and cephalosporin.[235] Additionally, it was decided to focus on the carbamate-linked ciprofloxacin design given the challenges faced with the synthesis of the carboxylic acid-linked design (Section 3.3.6.4).

3.3.7.1 Retrosynthetic analysis of second-generation linkers

The retrosynthetic analysis of second-generation linker **36** followed the same procedures as the synthesis of the first-generation linker **19**, in a different order (Scheme 31). With the *tert*-butyl ester protecting group in place throughout the synthesis, the carbamate **37** could be synthesised *via* displacement of an activated carbonate **38** with ciprofloxacin. The activated carbonate could be synthesised from the alcohol **39**, which in turn could be derived from the deacetylation of **40**. Finally, disconnection of the amide bond at the C-7 position would give DVP linker **41** and commercially available 7-ACA.

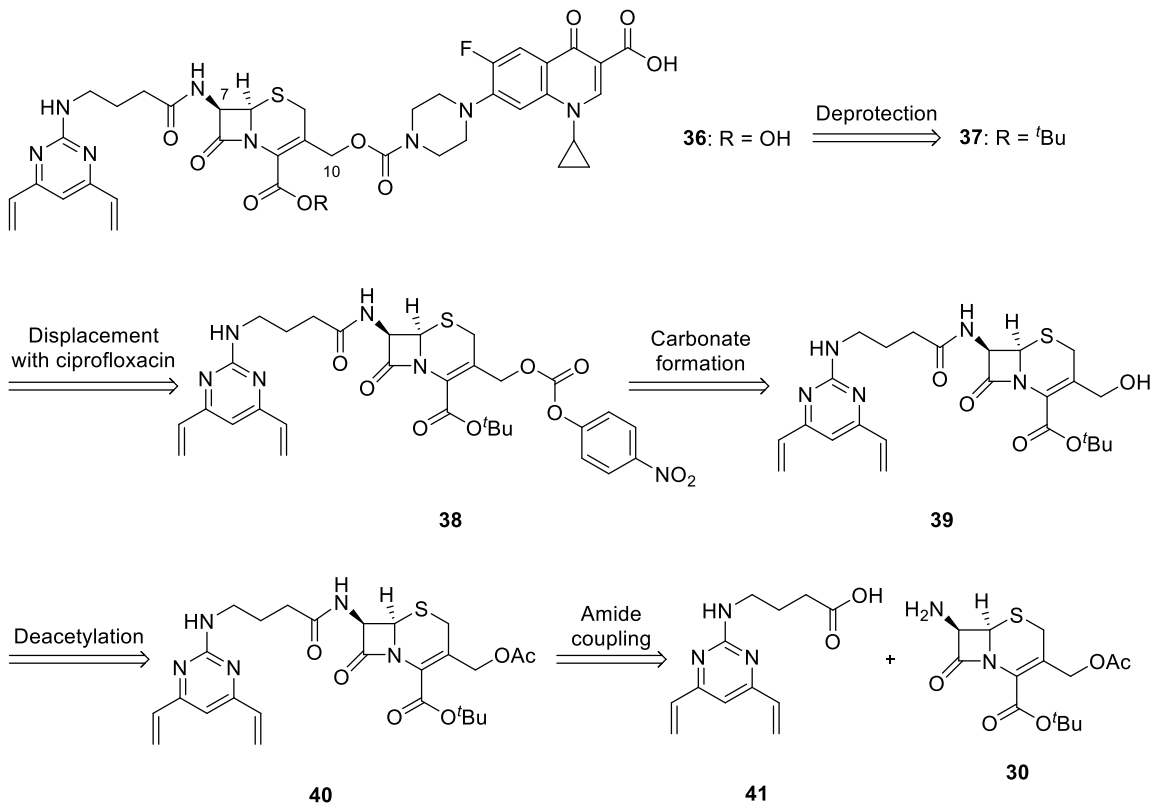

*Scheme 31 The retrosynthetic analysis of linker **36** to **41** and previously described intermediate **30**.*

Retrosynthetic analysis of **41** followed the same literature route as **17**, with an additional final step of ester hydrolysis (Scheme 32).[338] Suzuki-Miyaura cross-coupling would install the two vinyl groups, and an S_NAr reaction between commercially available 2,4,6-trichloropyrimidine and ethyl 4-aminobutanoate would introduce the aliphatic linker and ester moiety.

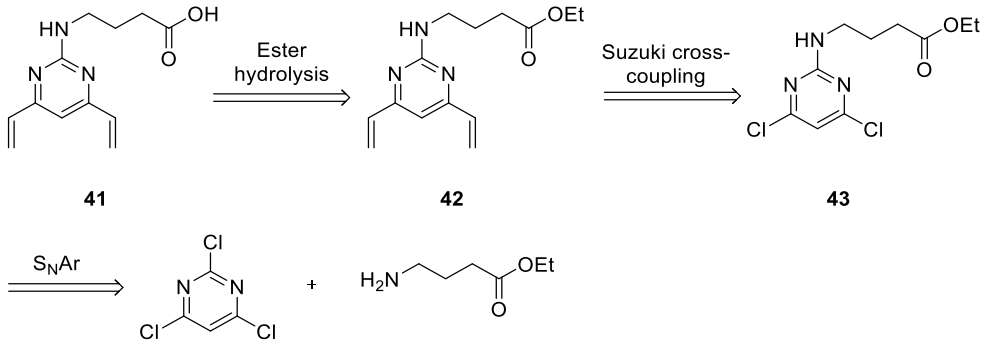

*Scheme 32 The retrosynthetic analysis of **41** to commercially available starting materials.*

3.3.7.2 Synthesis of **41**

41 was synthesised using a route analogous to **17** (Scheme 33) under literature conditions.[69] An S_NAr reaction was performed with commercially available 2,4,6-trichloropyrimidine and ethyl 4-aminobutyrate to give **43** in a 31% yield after chromatographic purification, due to poor

regioselectivity. Suzuki-Miyaura cross-coupling installed the two divinyl groups to give **42** in a quantitative yield, and hydrolysis of the ethyl ester gave the desired DVP staple **41** in a reasonable 60% yield, in a sufficient purity that further purification was not required.

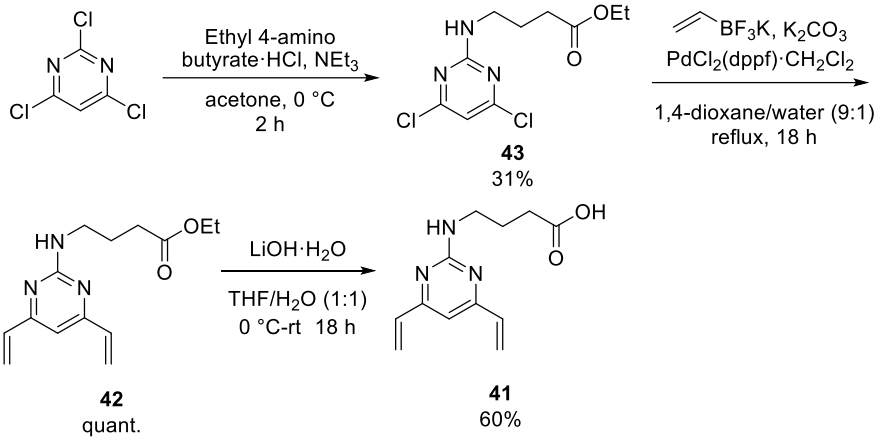

*Scheme 33 The synthesis of **41** from commercially available starting materials, according to the literature route.*[69]

3.3.7.3 Amide coupling of **30** and **41**

Next, conditions for the amide coupling of **30** and **41** were investigated (Table 22). Standard amide coupling reagents such as HATU, EDC·HCl and propylphosphonic anhydride solution (T3P, 50% in DMF) were trialled. Additionally, DMT-MM and DCC were trialled as there is literature precedence of these reagents being employed for amide coupling reactions performed on cephalosporin systems.[339,340]

*Table 22 The results of different reaction conditions for the amide coupling reaction of **30** and **41** to give **40**.*

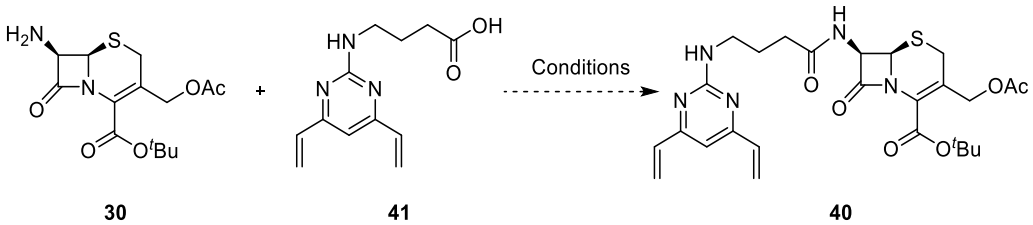

Entry	Conditions	Outcome
1	DMT-MM in MeOH	No reaction
2	HATU, DIPEA in DMF	47% isolated yield of **40**
3	T3P, NEt_3 in DMF	39% conversion to **40** by LCMS
4	EDC·HCl in CH_2Cl_2	Complex mixture
5	DCC in THF	9% conversion to **40** by LCMS

Despite literature precedence for their success in amide couplings of cephalosporins, DMT-MM gave no reaction (entry 1, Table 22) and DCC gave poor conversion (entry 5, Table 22). EDC·HCl (entry 4, Table 22) gave a complex mixture. Both HATU (entry 2, Table 22) and T3P (entry 3, Table 22) resulted in higher conversion by LCMS analysis of the crude reaction

mixtures, however there were side products present in the reaction with T3P that were challenging to remove by FCC. Coupling with HATU gave a cleaner reaction and 47% isolated yield of **40**. For these reasons, these conditions were selected.

3.3.7.4 Lipase deacetylation

In the literature, the base-mediated hydrolysis of a cephalosporin C-10 acetate group has been shown to form the undesired alkene-isomer or lactone, either as the only product or as a major side-product.[331] In the synthesis of **28**, the use of NaOH or TBAOH to effect this transformation was low-yielding (Section 3.3.6.2). Hydrolysis by lipase enzymes is a milder and more efficient alternative, and for this reason Patterson and Miller investigated different lipases and reaction conditions for the selective hydrolysis of cephalosporin C-10 acetate groups.[331] They found that the acrylic resin-bound *Candida antarctica* lipase B (CAL B) gave a high yielding and clean deacetylation. **40** was subjected to the literature conditions, and the hydrolysis was found to be high-yielding, giving **39** as the only product, which was advanced without purification (Scheme 34).

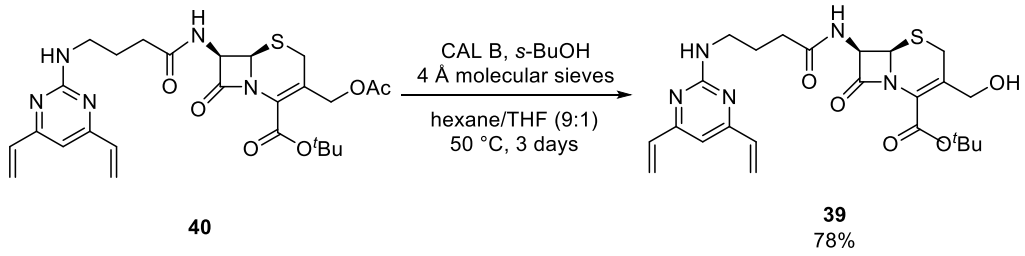

*Scheme 34 The synthesis of **39** via lipase deacetylation of **40** under the literature conditions.*[331]

Upon reaction scale-up, several observations were made with respect to how the reaction set-up affected the final yield of **39**. Firstly, the order of solvent addition was important, as **40** was soluble in THF but not hexane. Therefore, the addition of THF dissolved the starting material, and subsequent addition of hexane to this solution created a fine suspension. If the order was reversed, and hexane added first, **40** remained stuck to the bottom of the reaction vessel and was then partially degraded during the reaction to unknown species. Secondly, to reduce the amount of starting material that degraded during the reaction, it was necessary to reduce the reaction times to 3 days from over 10 days. Consequently, performing the small-scale reaction multiple times in parallel gave improved results over conventional scale-up.

3.3.7.5 Carbamate synthesis *via* the activated carbonate

The next stage in the synthesis involved the formation of an activated carbonate using alcohol **39**. The conditions previously described for this transformation from the synthesis of the generation 1 linkers were trialled, using 4-nitrophenyl chloroformate, however no desired product was formed and starting material was returned (Scheme 35).

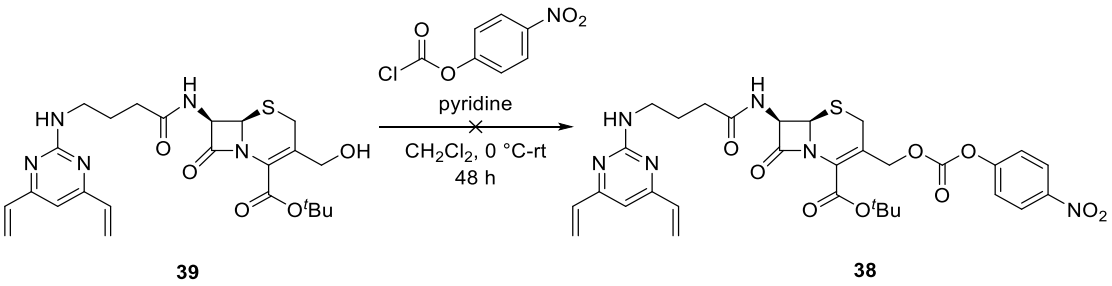

*Scheme 35 The attempted formation of **38** under the conditions shown. No reaction occurred.*

Alternative conditions were trialled using bis(4-nitrophenyl)carbonate and DIPEA in DMF (Scheme 36), and under these conditions the starting material was consumed and the desired product **38** was observed by LCMS analysis of the reaction mixture.[315] As two equivalents of bis(4-nitrophenyl)carbonate were required for full conversion, the reaction was difficult to monitor and purify due the presence of highly UV-active by-products containing the 4-nitrophenol moiety. Therefore, after a mild basic work-up, crude **38** was taken on crude to the next step in the synthesis.

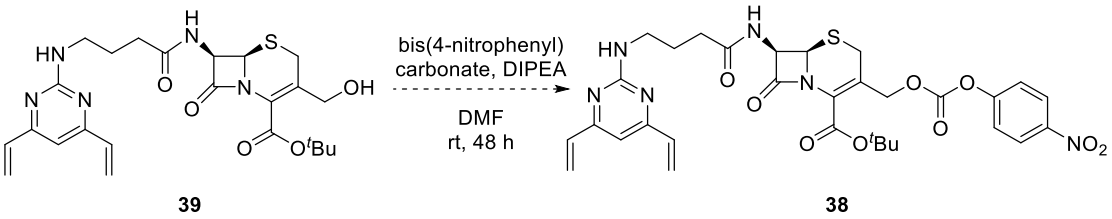

*Scheme 36 The successful formation of **38** under the conditions shown.*[315]

The synthesis of carbamate **37** required the displacement of the 4-nitrophenol moiety of **38** with the piperazine amine of ciprofloxacin. Various conditions were trialled to achieve this transformation: initially, HOAt and DIPEA in a pyridine/DMF solvent system were attempted,[r] however after 48 h no reaction was observed upon LCMS analysis of the reaction mixture (entry 1, Table 23). To ensure that the free carboxylic acid of ciprofloxacin was not hindering the reaction, these conditions were repeated using ethyl ester-protected ciprofloxacin. For this, **44** was synthesised by treatment of ciprofloxacin with sulfuric acid in ethanol, according to the

[r] Jiraborrirak Charoenpattarapreeda, University of Cambridge, unpublished work.

literature procedure.[341] The desired product, **44**, was isolated in a 67% yield without the need for purification.

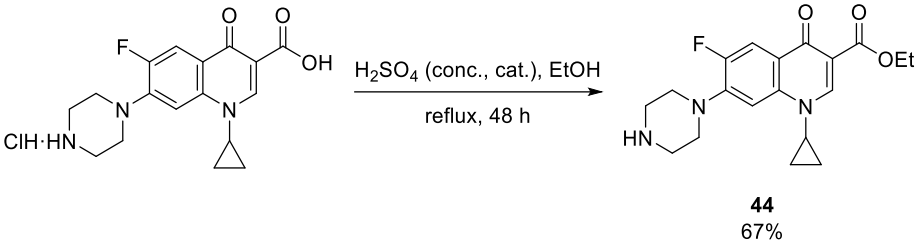

44
67%

*Scheme 37 The esterification of ciprofloxacin to give **44** under the literature conditions.*[341]

44 was trialled under the displacement conditions with **38** however no desired product was formed (entry 2, Table 23). Under the reaction conditions, ciprofloxacin (as either the free acid or ethyl ester) was insoluble and remained as a suspension in the reaction mixture, which could explain the lack of desired reactivity. Alternative conditions were trialled wherein ciprofloxacin was heated in aqueous base, to form a dispersed suspension, prior to the addition of the carbonate (entry 3, Table 23).[342] Under these conditions, consumption of **38** and the formation of the desired product, **37**, were observed by LCMS analysis of the reaction mixture.

*Table 23 The conditions trialled for the formation of carbamate **37** from **38**.*

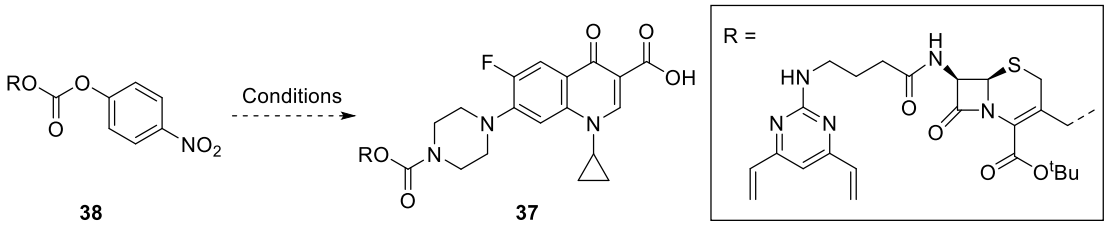

38 **37**

Entry	Conditions	Outcome (LCMS)
1	HOAt, DIPEA, ciprofloxacin Pyridine/DMF (1:6), rt, 48 h	No reaction
2	HOAt, DIPEA, **44** Pyridine/DMF (1:6), rt, 48 h	No reaction
3	Ciprofloxacin, $NaHCO_3$, H_2O, 40 °C then **38** in 1,4-dioxane, rt, 2 h	SM consumed, DP formed as part of mixture

Overall, the synthesis of carbamate **37** from alcohol **39** proceeded *via* formation of the mixed carbonate **38**, which was added as a crude mixture to a suspension of ciprofloxacin in aqueous base, yielding the desired carbamate, **37** (Scheme 38). This transformation was extremely low yielding, giving only a 4% yield of **37** from **39**. The low yield was in part due to mass loss in the final purification step of reverse-phase FCC. Additionally, this reaction was only performed once on a small scale, and it was anticipated that on a larger scale, and with some optimisation of the reaction conditions, this yield could be improved.

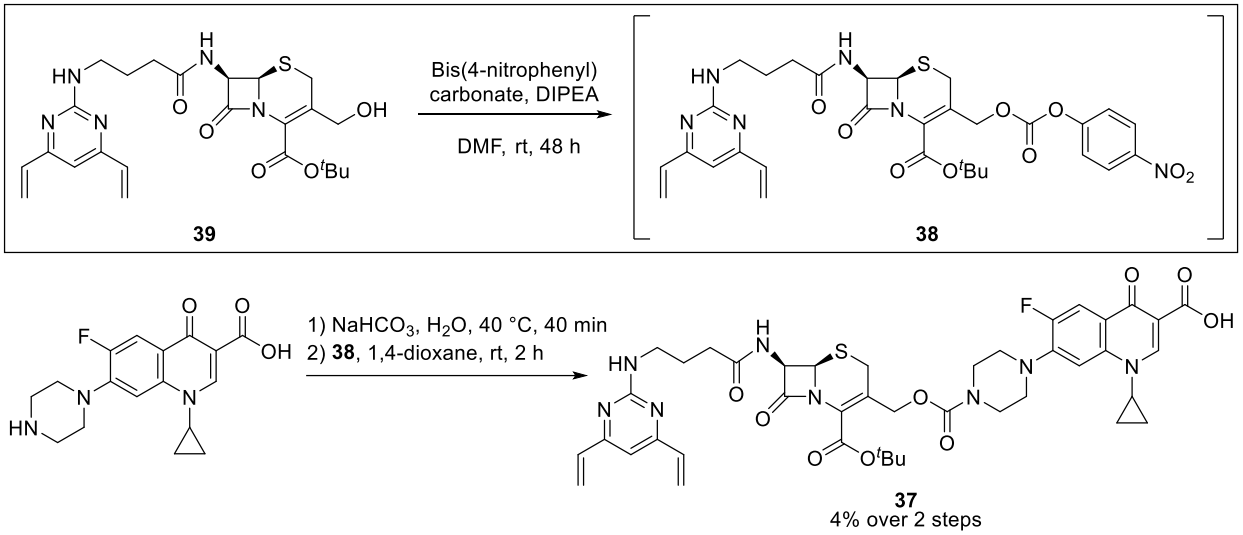

*Scheme 38 The synthesis of carbamate **37** from alcohol **39** via the mixed carbonate **38**.*

3.3.7.6 Peptide stapling and ester deprotection

Looking forward, the final synthetic steps towards the complete PDC require deprotection of the *tert*-butyl ester protecting group of **37** and peptide stapling with **AMP2**. The literature conditions for the ester deprotection involve treatment with TFA in CH_2Cl_2.[235,257] However, poor stability of the DVP motif under acidic conditions has been observed,[s] therefore, it was decided that the best strategy would be to perform the peptide stapling prior to the ester deprotection, thus removing the potentially unstable vinyl groups. A trial peptide stapling reaction was performed with **37** and **AMP2** under the standard conditions (Scheme 39), and the mass of the desired stapled peptide, **AMP2-37**, was observed by LCMS analysis of the crude reaction mixture. Investigations are ongoing with respect to a larger scale peptide stapling reaction and subsequent ester deprotection.

[s] Dr. Stephen Walsh, University of Cambridge, unpublished work.

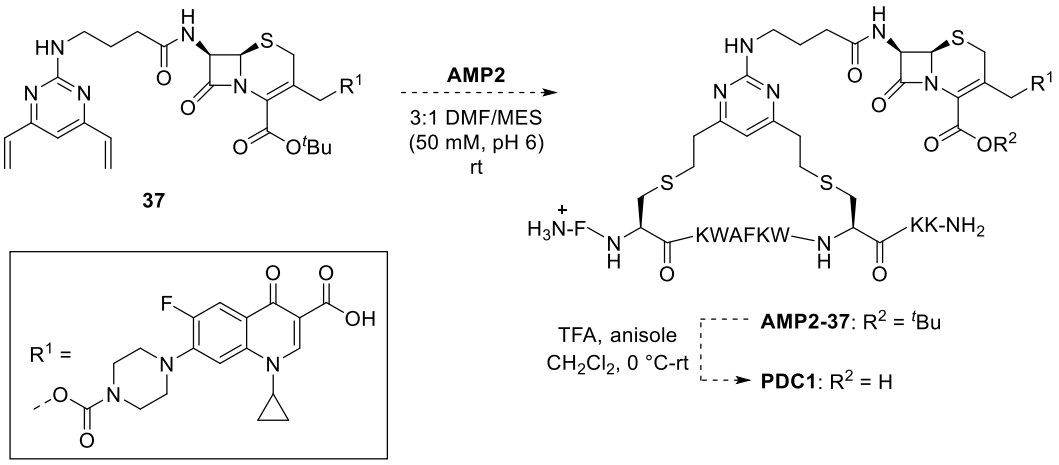

*Scheme 39 The trial peptide stapling of **AMP2** with linker **37** under the standard conditions, and the proposed ester deprotection of the resulting stapled peptide **AMP2-17**.*

3.3.8 Synthesis of control linkers

To provide further insights into the mechanism of action of the proposed PDC, control stapled peptides were required. For the initial biological testing, a non-cleavable analogue of **PDC1** was desired to highlight the effect of BL hydrolysis on the activity of the PDC. Additionally, a control compound containing the stapled peptide and cephalosporin motif was desired to confirm that the cephalosporin gave no additional toxicity, and therefore attribute any change in antimicrobial activity to the presence of ciprofloxacin in the conjugate. Control peptides **AMP2-45** and **AMP2-46** were designed, which required linkers **45** and **46** respectively (Figure 80). The simplest route to **45** was a direct amide coupling between **41**, an intermediate in the synthesis of **37**, and ciprofloxacin. To synthesise **AMP2-46**, **46** was required for the peptide stapling which could be accessed *via* **40**, an intermediate in the synthesis of **37**.

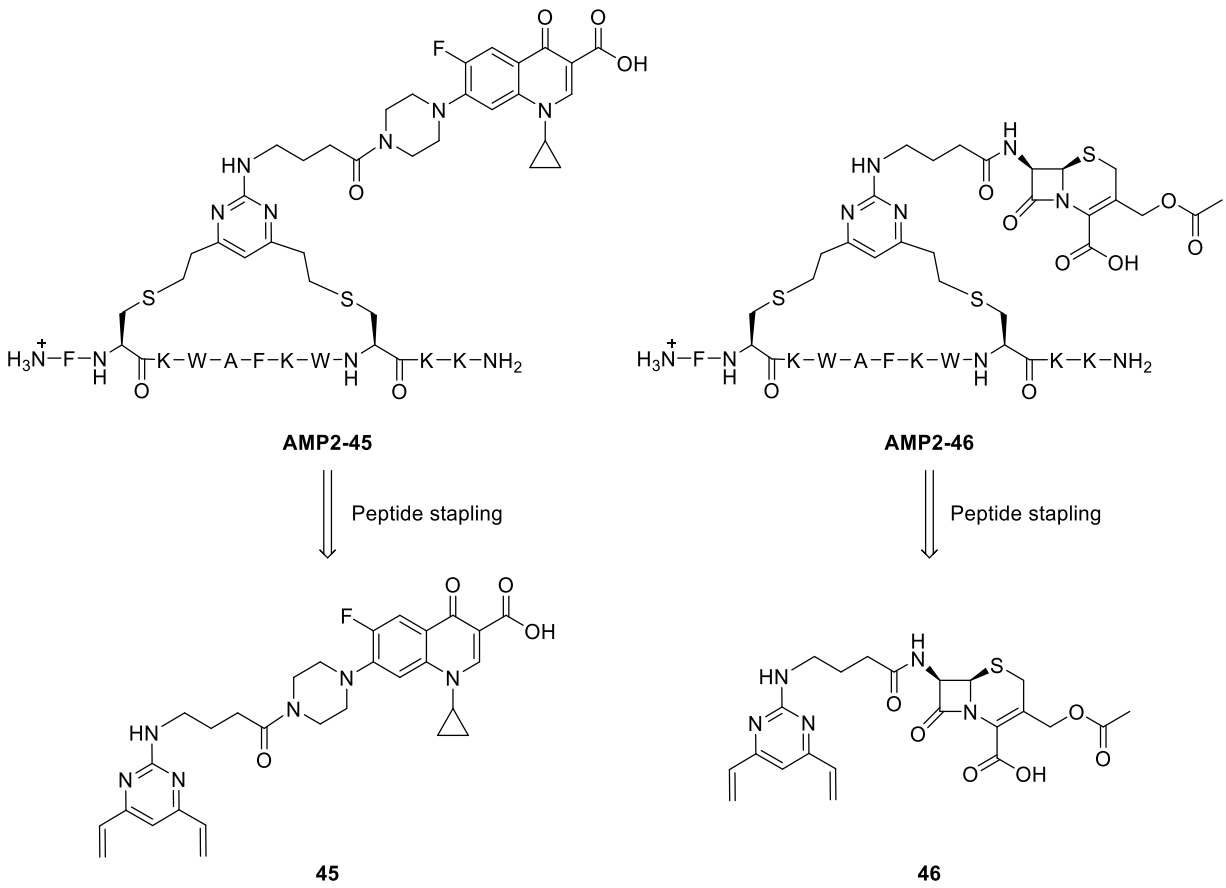

*Figure 80 The structures of the control peptides, **AMP2-45** and **AMP2-46**, and the linkers required for the peptide stapling, **45** and **46** respectively.*

3.3.8.1 Synthesis of control linker **45**

An amide coupling was performed with **41** and **44** with T3P to give **47** (Scheme 40). It was found that **47** streaked during chromatographic purification leading to significant mass loss, however upon repeating the reaction the crude product was of sufficient purity to continue without purification to the next step in the synthesis. Crude **47** was subjected to base-mediated hydrolysis to give the desired linker **45** without the need for purification. **45** was obtained in a low 46% yield; although the reaction reached full conversion and only **45** was formed, the desired product was found to have a high aqueous solubility, leading to significant mass loss during work up.

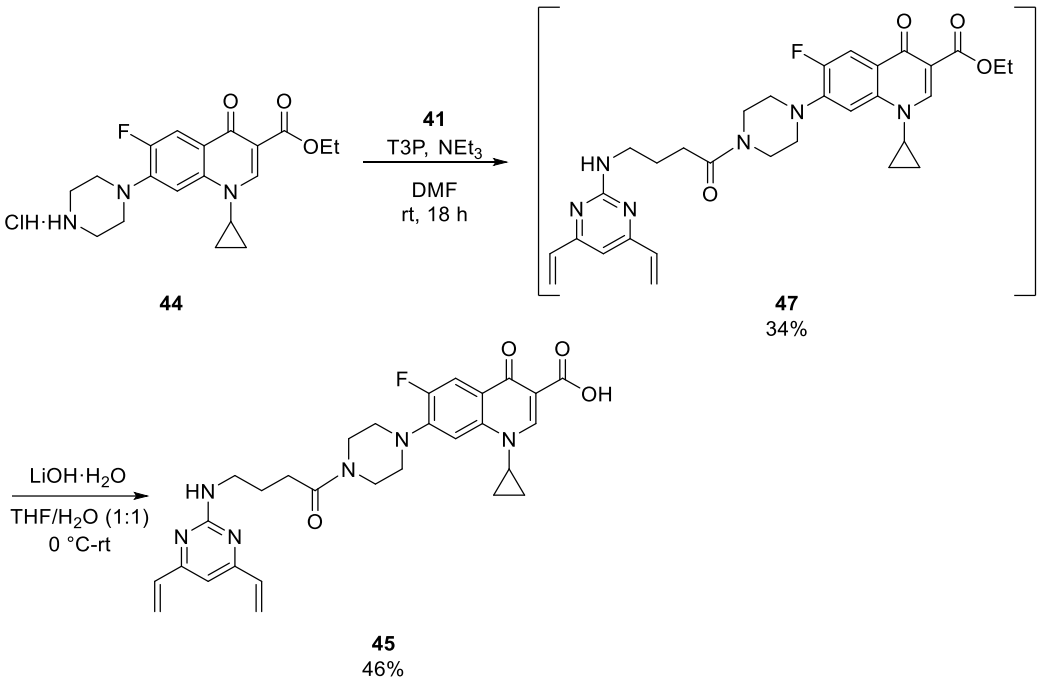

*Scheme 40 The synthesis of control linker **45** via an amide coupling and ester hydrolysis.*

Peptide stapling of **AMP2** with linker **45** was performed, with a minor modification due to the poor solubility of **45** when preparing a stock solution of the linker. Typically, linker stock solutions were prepared in DMF/MeCN (1:1), however it was found that a solvent system of equivalent volumes of DMF, DMSO and MES buffer (pH 6, 50 mM) were necessary to solubilise **45**. Pleasingly, it was found that **45** had good solubility in the reaction solvent system (3:1 DMF/MES), and the stapling proceeded under the standard conditions to give **AMP2-45** after HPLC purification (Scheme 41).

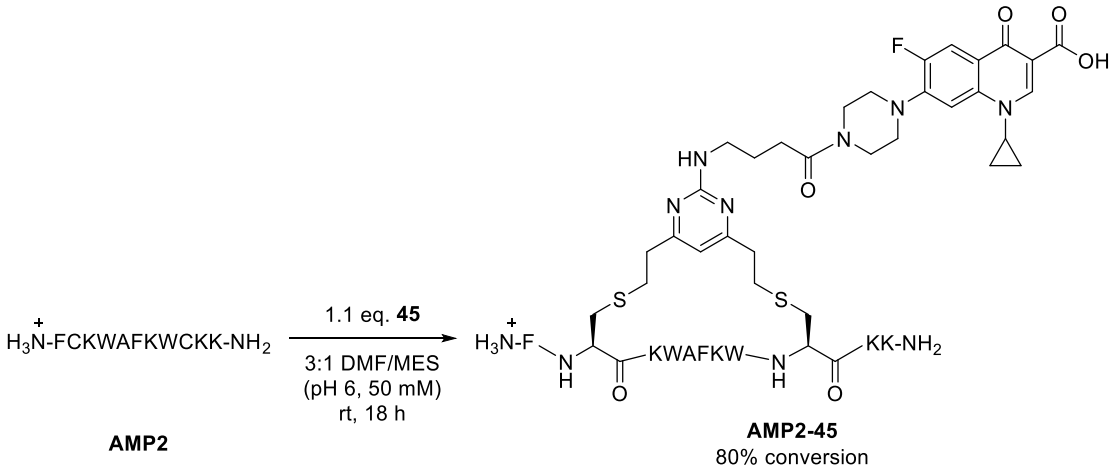

*Scheme 41 The peptide stapling of **AMP2** with **45** to give control peptide **AMP2-45** under the standard conditions.*

3.4 Conclusions

A novel, cleavable PDC was devised to target *P. aeruginosa*. The concept capitalised on the therapeutic potential of membrane-disrupting AMPs and drew inspiration from the fields of functionalised two-component STAMPs, and cleavable linkers which enable infection-activated drug release. The final design of the PDC consisted of a STAMP, which was functionalised with a BL cleavable cephalosporin linker and small-molecule antibiotic ciprofloxacin.

For the development of the PDC, literature reported AMPs were identified for an initial peptide screen. For this screen, an unfunctionalised model linker was synthesised, the stapling reaction conditions were optimised, and seven novel STAMPs were generated. A minimum inhibitory concentration (MIC) assay against *P. aeruginosa* strains and *S. aureus* showed that two peptides, **AMP2-17** and **AMP4-17** (Figure 81), displayed good MICs against *P. aeruginosa*, and gave selectivity over the Gram-positive strain *S. aureus*.

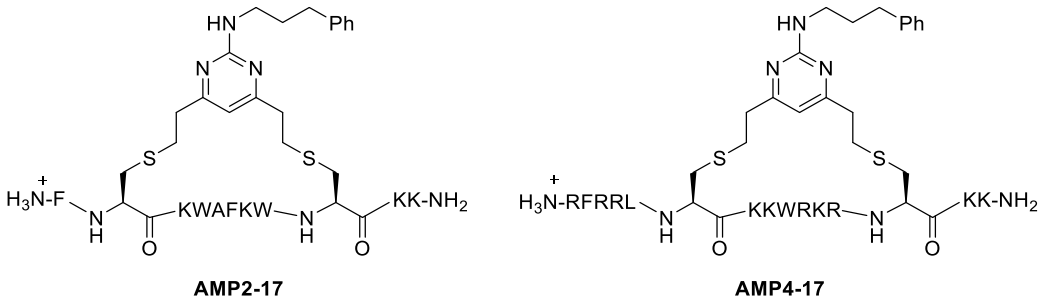

*Figure 81 The structures of novel peptides **AMP2-17** and **AMP4-17**, identified as having good MIC values towards P. aeruginosa and selectivity over S. aureus in the initial peptide screen.*

Next, the synthesis of the PDC was explored. An initial route was developed towards the first generation PDC, and the possibility of connecting the DVP stapling moiety and the cephalosporin linker *via* CuAAC was investigated. In response to new information in the literature, the PDC design and synthesis was adapted, leading to the second generation **PDC1**, accessed *via* a shorter synthetic route. A key step in the synthesis of the desired stapling linker was a lipase-mediated deacetylation that proceeded in high conversion and gave only the desired product **39**, requiring no purification. Overall, a 7-step synthesis generated the most advanced intermediate **37** (Scheme 42). Furthermore, investigations were made into the peptide stapling of **AMP2** and **37**. Synthesis of the target compound **PDC1** is ongoing.

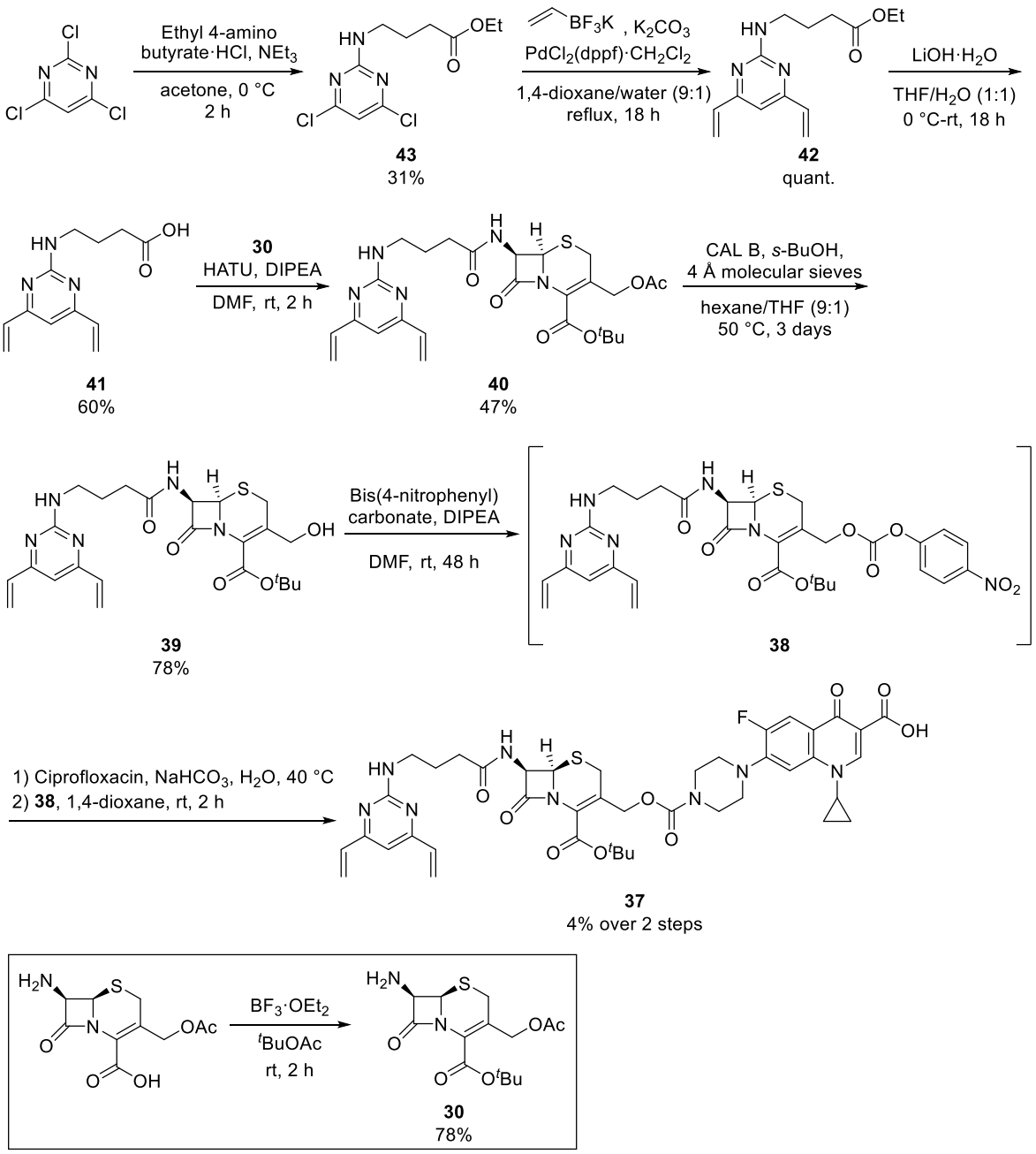

*Scheme 42 The full synthetic route towards the most advanced intermediate, linker **37.***

3.5 Future work

3.5.1 Synthesis and peptide characterisation

To complete the synthesis of **PDC1**, the peptide stapling must be performed on a larger scale, and the *tert*-butyl ester deprotection performed under the literature conditions (Scheme 43).[235,257] The synthesis of control peptide **AMP2-46** will proceed in the same manner.

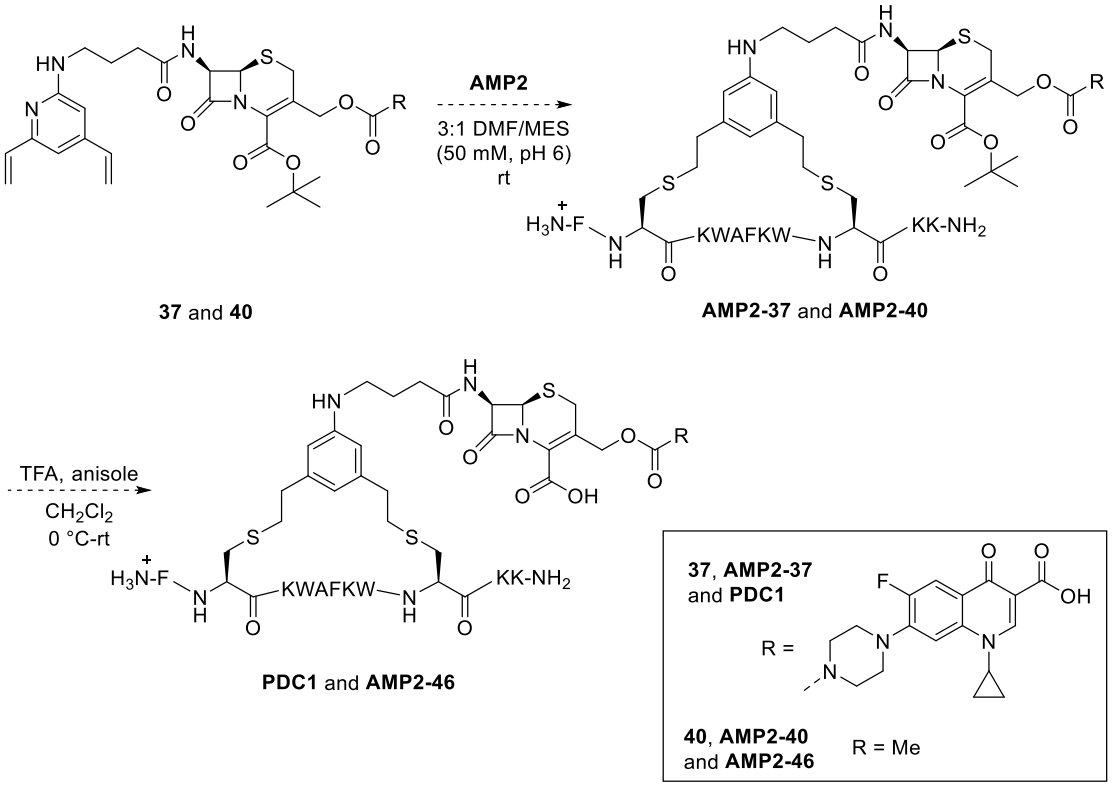

*Scheme 43 The proposed synthetic route towards **PDC1** and control peptide **AMP2-46**. **AMP2** is stapled with intermediate **37** or **40**. The tert-butyl ester protecting group can then be removed under the literature conditions.*

CD spectroscopy will be performed with **PDC1** and the literature peptide sequence, **AMP2**, to ascertain the effect of peptide stapling on the α-helicity. The plasma stability of **PDC1** and the linear analogue **AMP2** will be determined; it is anticipated that the stapled peptide will have a greatly increased half-life, as the staple conformationally locks the peptide and increases resistance to proteolytic hydrolysis.[67] Furthermore, an assay will be developed to analyse the BL hydrolysis of **PDC1** *in vitro* with commercially available *P. aeruginosa* BLs. Using HPLC and LCMS the kinetics of hydrolysis can be determined, and the hydrolysis products confirmed.

3.5.2 Biological testing

For the assays described in this section, control peptides **AMP2-45** and **AMP2-46** will be included alongside **PDC1** to identify how the cleavable linker and the conjugation of ciprofloxacin affects the activity. Biological testing of **PDC1** will commence with a minimum inhibitory concentration (MIC) assay, as described in Section 3.3.2, and additionally the effect on bacterial growth will be assessed by measuring the OD_{600} continuously over 24 hours. To compare the activity of **PDC1** with different concentrations of its constituent parts, **AMP2-17** and ciprofloxacin, a checkerboard assay will be performed.[343] In a checkerboard assay, two compounds are serially-diluted along the rows and columns of a multi-well plate, leading to combinations of different concentrations which are incubated with bacteria and the inhibition of growth measured as previously described.[344] To assess bacterial killing, rather than growth inhibition, the number of colony-forming units present after incubating bacteria with **PDC1** will be measured.[345]

Ideally, **PDC1** will display activity towards *P. aeruginosa* but will be inert towards bacterial strains commonly found in the gut microbiota.[346] To further determine the selectivity of **PDC1**, screening for growth inhibition against several clinical isolates of *P. aeruginosa* and standard strains of *Enterococcus faecalis* and *Enterococcus coli* (as representative gut microbes) will be performed.[235] A wider screen against the ESKAPE pathogens,[347] and other common Gram-negative and -positive bacteria will be performed, to identify the spectrum of activity for **PDC1**. For AMPs, haemolysis often represents a significant barrier to their clinical utility as novel antimicrobials, and it has been shown in the literature that this problem can be exacerbated by RCM peptide stapling due to the lipophilic nature of the alkenyl staple increasing the overall lipophilicity of the STAMP.[283,348] The haemolytic activity of **PDC1** will be ascertained using a standard assay wherein the peptide is incubated with red blood cells at various concentrations, and haemoglobin release measured spectrophotometrically.[349]

The sequence of unfunctionalised STAMP **AMP2-17** is derived from a literature peptide, **AMP2a**.[309] It has been shown in the literature that analogues of **AMP2a** disrupt bacterial membranes, however this has yet to be confirmed for **AMP2a** and **AMP2-17**.[350] Membrane depolarisation assays will be performed to validate this proposed mechanism of action for **AMP2-17** and **PDC1**, *via* measuring the uptake of fluorescent intercalating agent propidium iodide into bacterial cells.[351] Specific disruption of the outer membrane can be assessed by monitoring the uptake of fluorescent probe *N*-phenyl-1-naphthylamine, and depolarisation of the inner membrane assessed by measuring the release of dye $DiSC_3(5)$.[352] Additionally, the Owens group have published lipid monolayers which mimic bacterial membranes, and are able to quantitatively measure the membrane-disruption of antimicrobials using organic

electrochemical transistor technology.[353] A collaboration has been set up with the Owens group, wherein the membrane-disruption of **AMP2**, **AMP2-17** and **PDC1** will be measured using their published novel biomimetic electronic devices. If these assays confirm that **AMP2-17** and **PDC1** cause membrane disruption, this can be visualised using transmission electron microscopy.[310]

The ability of the unfunctionalised peptides **AMP2-17** and **AMP4-17** to prevent the formation of *P. aeruginosa* biofilms was assessed and discussed in Section 3.3.2. These data will be repeated to ensure the reliability of the data, and the effect of **PDC1** and **AMP2-17** on the disruption of pre-formed biofilms will be measured. It is anticipated that **PDC1** will have a greater effect on biofilm formation than the unfunctionalised analogue **AMP2-17**, as ciprofloxacin provides an additional antibiotic effect.

One potential application of **PDC1** is to treat bacterial infections in the pulmonary fluid of cystic fibrosis patients, where there is typically a high salt concentration.[281] This environment can reduce the activity of AMPs, so the MIC of **AMP2-17** and **PDC1** will be measured in different concentrations of NaCl and compared to the literature peptide **AMP2a**; it is anticipated that peptide stapling will improve the activity of the peptide in high salt environments.[354]

3.5.3 Peptide-drug conjugate analogues

The modular design of **PDC1** provides a flexible platform for the targeting of different bacteria. To illustrate this modularity, the individual components (peptide, drug, release mechanism) can be varied to alter the mode of action of the PDC.

3.5.3.1 Alternative antimicrobial peptides

At the start of this project, there were no cysteine-stapled AMPs in the literature, only one component all-hydrocarbon STAMPs. Hence a screening approach was used to identify an active two-component stapled peptide. From the initial peptide screen, **AMP2-17** was identified with a MIC of 64 μg/mL towards *P. aeruginosa* strains PAO1 and YM64. Whilst this was a reasonable MIC for *P. aeruginosa*, more active peptides amenable to cysteine stapling have since been reported in the literature. Further elucidation of the mechanism of action of the peptide is required prior to PDC optimisation, as the peptide may sensitise the bacteria to ciprofloxacin, or the two could a synergistic relationship. However, a more active peptide may be required for the success of **PDC1**.

DJK5 and DJK6 are short, cationic linear peptides[t] that eradicate *P. aeruginosa* biofilms and were reported in a patent in 2019: they have an MIC of 16 μg/mL against *P. aeruginosa* and a broad spectrum of activity, with lower MIC values against ESKAPE pathogens *A. baumannii* and *K. pneumoniae*.[355] These peptides both displayed a synergistic relationship with ciprofloxacin and were shown to increase survival in an *in vivo* infection model. Another example is a two-component stapled peptide based on the sequence of CAP-1, a member of the cathelicidin AMP family published in 2018 (discussed in Section 3.1.4).[291] This peptide was stapled between two cysteine residues with a perfluoroaryl linker, and inhibited the growth of *P. aeruginosa* at a concentration of 4 μM (~16 μg/mL).[u] As this linear sequence already contains cysteine residues at *i,i*+7 positions, it could easily be incorporated into the PDC by stapling the same linear peptide with linker **37**.

3.5.3.2 Alternative release mechanisms

Various bacterial enzymes that selectively and efficiently modify or cleave a chemical motif have been explored for chemotherapy and prodrug applications.[356] Accordingly, any of these chemical motifs that have two suitable handles for attachment of the stapling motif and antibiotic drug could be incorporated into the PDC design. By using different enzyme-cleavable linkers, the properties of the PDC can be 'tuned' as desired.

One example are aryl nitro compounds, which are selectively reduced by bacterial nitroreductases, and have been paired with self-immolative motifs in ciprofloxacin prodrugs.[357] One potential advantage of incorporating a nitroreductase-cleavable linker into the PDC design is that bacterial nitroreductases have wide substrate scopes and highly plastic active sites, therefore they are able to accommodate and cleave large species.[358] Another possibility is the incorporation of cleavable, self-immolative linkers which are sensitive to mammalian β-glucuronidases and aryl sulfatases, and have been used previously in antibody-drug conjugates.[359,360] Bacterial β-glucuronidases have been shown to successfully release a glucuronide prodrug of anti-cancer drug 9-aminocamtothecin,[361] and, as β-glucuronide prodrugs are actively transported into *E. coli*, incorporating a β-glucuronide-cleavable motif into the PDC design could promote cell penetration.[362] Sulfatase activity has been documented in many different bacteria,[363] including *P. aeruginosa*,[364] and the utility of these enzymes has been illustrated by the development of sulfatase-activated fluorophores as diagnostic tools for identifying infections of mycobacteria.[365] As the expression of sulfatases and β-lactamases differs depending on the bacterial strain and species, the two linkers provide

[t] DJK5 and DKJ6 sequences: VQWRAIRVRVIR and VQWRRIRVWVIR respectively
[u] Sequence: GGGLRKRLRKFRNKCKEKLKKCGQKIQGLLPKLA

differing specificities. Chemical motifs that are sensitive to these enzymes could be incorporated into the PDC design with a self-immolative linker, as shown in Scheme 44. Additionally, bacterial lipases represent another class of enzymes that could provide a different release mechanism, which will be discussed below.

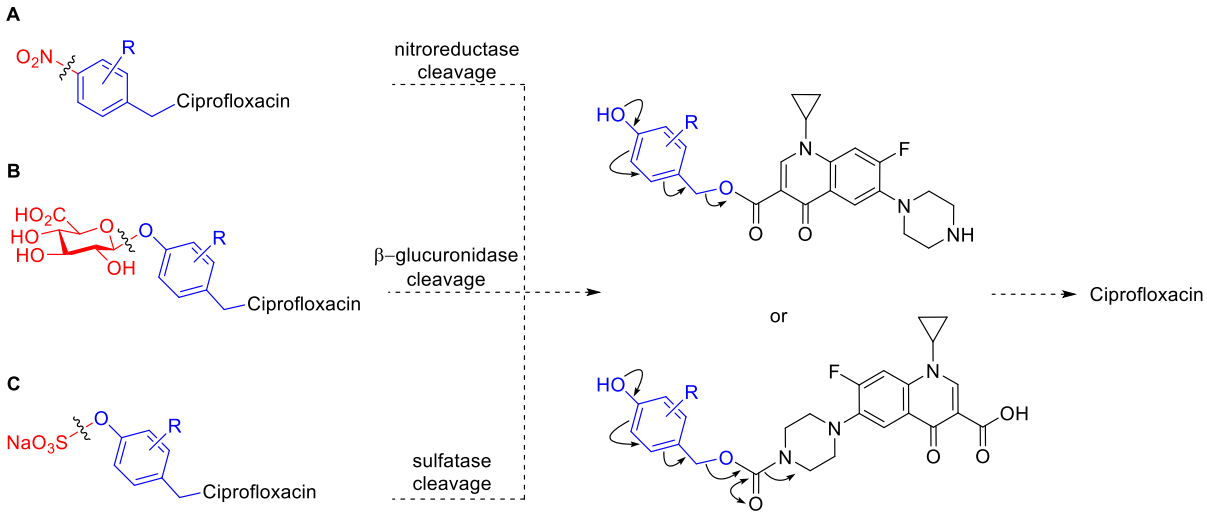

*Scheme 44 The proposed structures of alternative enzyme-cleavable motifs (highlighted in red) which would be incorporated into **PDC1**. All could be linked to ciprofloxacin (shown in black) via a self-immolative linker (shown in blue). A) Nitroaryls are reduced by nitroreductases. B) β-Glucuronidase hydrolyses β-glucuronic acid. C) Sulfatases hydrolyse aryl sulfates. R = variable group.*

3.5.3.3 Alternative small-molecule antibiotics

Due to the rapid development of AMR, it is necessary to investigate novel antimicrobial scaffolds as potential therapeutics, for example quorum sensing molecules. QS is a mechanism by which bacteria can orchestrate group behaviours, including those governing virulence and antibiotic resistance (e.g. the formation of biofilms).[366] Quorum sensing inhibitors (QSIs) disrupt cell-to-cell communication, and due to the increasing prevalence of AMR they are being explored as potential therapeutics. QSIs are often based on the same scaffolds as the endogenous QS molecules. A key group of QSI are the acyl homoserine lactones (AHLs), which were shown to inhibit the formation of *P. aeruginosa* biofilms, for example the AHL analogues 7h and 7o reported by Blackwell and co-workers (Figure 82).[367]

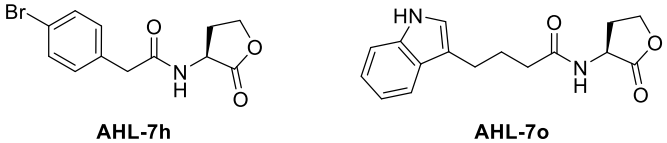

Figure 82 Selected examples of AHLs that affect biofilm formation and QS.[367]

Nielsen and co-workers developed functionalised PEG resins that release AHL QS molecules upon exposure to bacterial lipases, for applications in medical implants.[368] Additionally, functionalised PEG resin beads were reported, which, upon exposure to bacterial lipases released ciprofloxacin; these resin beads were shown to significantly reduce the viability of wild-type *P. aeruginosa*.[368] It is envisioned that the same cleavable motif could also be incorporated into an antimicrobial PDC (**PDC-A**, Scheme 45). Lipase hydrolysis would release ciprofloxacin and a functionalised STAMP (**PDC-B**), which can self-immolate to release an AHL QSI and an unfunctionalised STAMP (**PDC-C**). The proposed PDC would have similar advantages as **PDC1**: the STAMP targets specific bacteria and provides an additional mechanism of action, and the lipase-cleavable motif allows selective release of the QSI and ciprofloxacin. This species would have three distinct mechanisms of action as the STAMP disrupts bacterial membranes, ciprofloxacin targets DNA topoisomerases, and the QSI disrupts biofilm formation. As a proof-of-concept conjugate, **PDC-A** could be synthesised by incorporating the stapled peptide **AMP2-17** reported in this section and a QSI with known *P. aeruginosa* activity. However, the modular nature of the design provides an opportunity to vary the peptide and QSI allowing different bacteria to be targeted, enabled by the wide substrate scope of bacterial lipases.

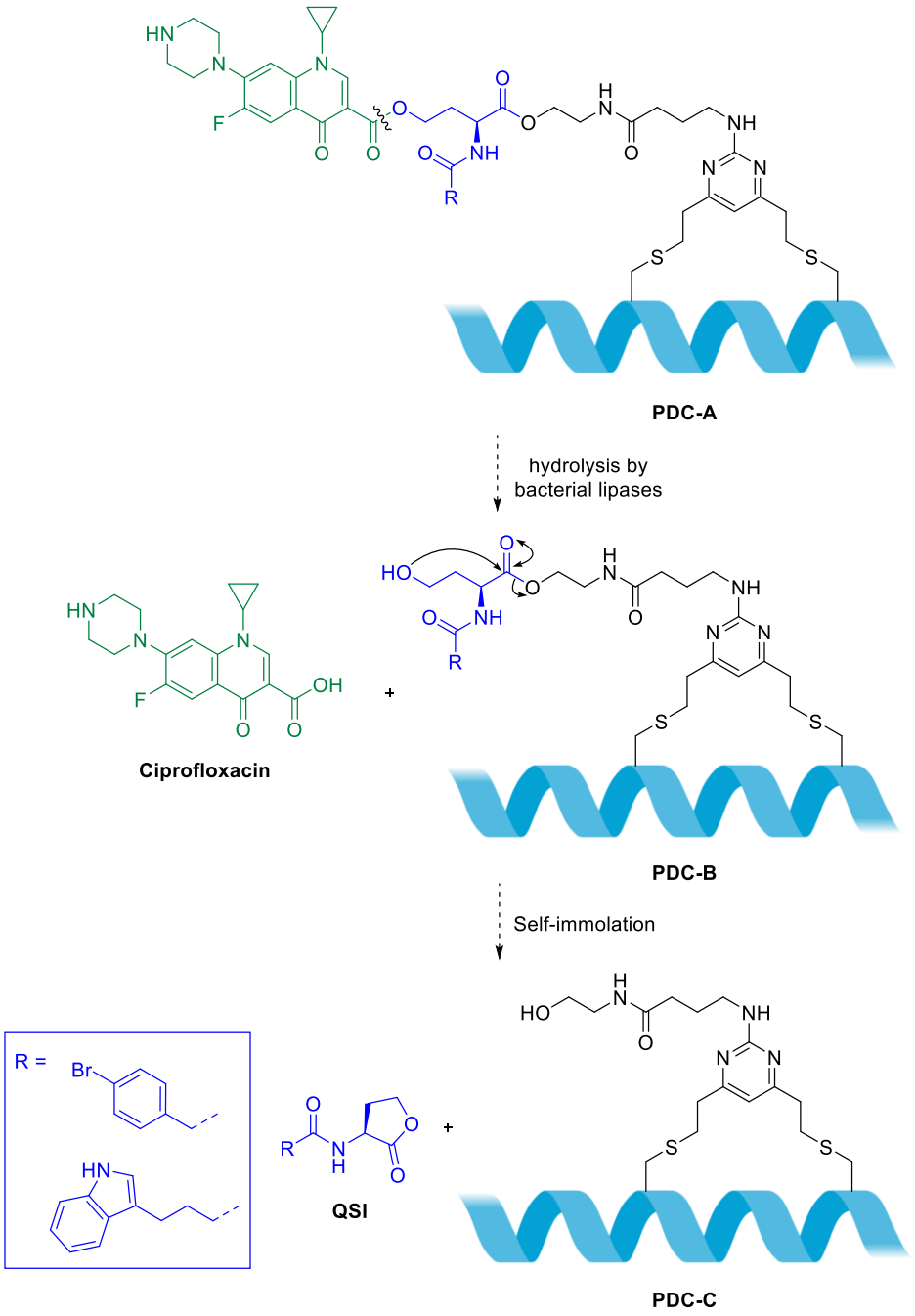

*Scheme 45 The proposed structure and mechanism of release for the dual-functionalised STAMP, **PDC-A**. Exposure to bacterial lipase cleaves the ester linkage, releasing ciprofloxacin and **PDC-B**. **PDC-B** undergoes self-immolation releasing the AHL QSI and unfunctionalised STAMP **PDC-C**. Ciprofloxacin is highlighted in green, the AHL QSI in blue, the lipase cleavable moiety in red, the staple in black and the peptide is represented by a blue helix.*

Chapter 4

Experimental details

4. Chapter 4 - Experimental details

4.1 Chemistry experimental procedures

All experiments were carried out in oven-dried glassware under an atmosphere of N_2 unless otherwise stated. Reaction temperatures of 0 °C were maintained using an ice-water bath and those below 0 °C using dry-ice and acetone; room temperature (rt) refers to 20-25 °C.

Solvents: Distilled solvents were used unless otherwise stated. Diethyl ether was distilled from calcium hydride and lithium aluminium hydride. Tetrahydrofuran (THF) was dried over sodium wire and distilled from a mixture of lithium aluminium hydride and calcium hydride with triphenylmethane as the indicator. Acetonitrile (MeCN), CH_2Cl_2, hexane, methanol (MeOH), and toluene were all distilled from calcium hydride. Petroleum ether 40-60 (PE 40-60) refers to the petroleum fraction with boiling point of 40–60 ˚C.

Reagents: Chemicals were purchased from commercial sources and used without further purification.

Yield: refer to chromatographically and spectroscopically pure compounds unless otherwise stated and are reported as follows: mass, moles, percentage.

Flash chromatography: Analytical thin layer chromatography was carried out on SiO_2 Merck Kieselgel 60 F254 plates with visualisation either by UV light or staining with potassium permanganate or ninhydrin dips made using standard procedures. Retention factors (R_f) are quoted to 0.01. FCC was performed under a positive pressure of N_2 or compressed air using slurry-packed Merck 9385 Kieselgel 60 SiO_2 (230-400 mesh), or with a Combiflash Rf200 automated chromatography system using Redisep® reverse-phase C18-silica flash columns (20-40 µm).

Nuclear Magnetic Resonance (NMR): ^{1}H, ^{13}C and ^{19}F NMR spectra were recorded using an internal deuterium lock at ambient probe temperatures on the following instruments: Bruker Avance III 400 MHz HD Smart Probe Spectrometer, Bruker Avance III 400 MHz HD Spectrometer, Bruker 400 MHz QNP Cryoprobe Spectrometer, Bruker 500 MHz DCH Cryoprobe Spectrometer, Bruker Avance III 500 MHz HD Smart Probe Spectrometer. The following deuterated solvents were used: chloroform ($CDCl_3$) and dimethylsulfoxide (DMSO-d_6). ^{1}H-NMR chemical shifts (δ) are quoted in ppm to the nearest 0.01 ppm, relative to the residual non-deuterated solvent peak and coupling constants (*J*) are quoted to the nearest 0.1 Hertz (Hz). ^{13}C NMR chemical shifts are quoted to the nearest 0.1 ppm, relative to the solvent peak and coupling constants are quoted to the nearest 0.1 Hz. ^{19}F NMR chemical shifts are quoted to the nearest 0.1 ppm and coupling constants (*J*) are quoted to the nearest 0.1 Hertz

(Hz). Spectral data is reported as follows: chemical shift, integration, multiplicity (s, singlet; d, doublet; t, triplet; q, quartet; p, pentet; sept, septet; m, multiplet; br., broad; appt., apparent; (or a combination thereof), coupling constant(s) and assignment. The numbering system used in the assignments does not necessarily follow the IUPAC convention. Assignment of all spectra is supported by DEPT, COSY, HSQC and HMBC or done by analogy to fully assigned spectra of closely related compounds.

Liquid chromatography-mass spectrometry (LCMS): LCMS was carried out using a Waters ACQUITY H-Class UPLC with an ESCi Multi-Mode Ionisation Waters SQ Detector 2 spectrometer using MassLynx 4.1 software; ESI refers to the electrospray ionisation technique; LC system: solvent A: 2 mM NH_4OAc in H_2O/MeCN (95:5); solvent B: MeCN; solvent C: 2% formic acid; column: ACQUITY UPLC® CSH C18 (2.1 mm × 50 mm, 1.7 µm, 130 Å) at 40 °C; gradient: 5 – 95% B with constant 5% C over 1 min at flow rate of 0.6 mL/min; Injection volume: 5 µL. Chromatographs were monitored by absorbance using diode array detection at a wavelength range of 190-600 nm, interval 1.2 nm.

High resolution mass spectrometry (HRMS): HRMS was carried out using a Waters LCT Premier® Time of Flight mass spectrometer or the Waters Vion IMS Qtof mass spectrometer. Reported mass values are within the error limits of ± 5 ppm mass units. ESI refers to the electrospray ionisation technique.

Analytical high-performance LC: Chromatographs were obtained on an Agilent 1260 Infinity® using a reversed-phase Supelcosil ABZ+PLUS column (150 mm x 4.6 mm, 3 µm) eluting with a linear gradient system (solvent A: 0.05% (v/v) TFA in H_2O, solvent B: 0.05% (v/v) TFA in MeCN) over 15 min, unless otherwise stated, at a flow rate of 1 mL/min. HPLC was monitored by UV absorbance at 220 and 254 nm.

Preparative HPLC: Preparative HPLC was carried out on an Agilent 1260 Infinity® using a reversed-phase Supelcosil ABZ+PLUS column (250 mm x 21.2 mm, 5 µm) eluting with a linear gradient system (solvent A: 0.1% (v/v) TFA in H_2O, solvent B: 0.05% (v/v) TFA in MeCN) over 20 min at a flow rate of 20 mL/min. HPLC was monitored by UV absorbance at 220 and 254 nm.

Melting points: Melting points (mp) were measured using a Büchi melting point B545 apparatus and are uncorrected.

Infra-red spectroscopy (IR): Infra-red spectra were recorded neat on a Perkin Elmer Spectrum One FT-IR spectrometer fitted with an Attenuated Total Reflectance (ATR) sampling accessory. Selected absorption maxima (ν_{max}) are quoted in wavenumbers (cm^{-1}) with the following abbreviation: br, broad.

Optical rotations: Optical rotations were recorded on an Anton Parr MCD 100 Polarimeter. $[\alpha]_D^{25}$ values are reported in 10^{-1} deg cm^2 g^{-1} at 589 nm, concentration (c) is given in g dL^{-1}.

4.1.1 Chemistry experimental procedures for Chapter 2

3-Azidosulfonyl-3*H*-imidazol-1-ium hydrogen sulfate (1)

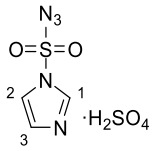

To a suspension of sodium azide (13.0 g, 200 mmol, 1.01 eq.) in MeCN (160 mL) was added sulfuryl chloride (16.1 mL, 199 mmol) dropwise with ice cooling. The reaction mixture was stirred at rt for 16 h. Imidazole (25.9 g, 380 mmol, 1.91 eq.) was added portion-wise to the reaction mixture with ice cooling and the resulting slurry was stirred at rt for 5 h. The mixture was diluted with EtOAc (400 mL) and H_2O (400 mL). The organic phase was washed with H_2O (400 mL) and sat. aq. $NaHCO_3$ solution (2 × 400 mL), then dried ($MgSO_4$) and concentrated to 200 mL *in vacuo*. A solution of sulfuric acid (conc., 11 mL, 200 mmol, 1.01 eq.) in EtOAc (100 mL) was added dropwise with ice cooling over 30 min and the reaction mixture was stirred at rt for 16 h. The precipitate was filtered, washed with EtOAc (3 × 50 mL) and dried *in vacuo* to give the title compound as a white solid (32.7 g, 121 mmol, 61%).

^{1}H NMR (400 MHz, DMSO-d_6) δ 8.57 (1H, s, H1), 7.96 (1H, s, H2), 7.32 (1H, s, H3); **^{13}C NMR** (101 MHz, DMSO-d_6) δ 138.3 (CH, C1), 130.2 (CH, C2), 119.5 (CH, C3); **IR** (neat, cm^{-1}) ν_{max} 2177 (strong, N=N=N stretch), 1586 (C=C bend), 1151 (S=O); **HRMS** (ESI): $[M+Na]^+$ calcd. for $[C_3H_5N_5O_6S_2Na]^+$ 293.9579, observed 293.9583 (Δ = -2.0 ppm).

Data in accordance with previous literature reports.[168]

(*S*)-4-((((9*H*-Fluoren-9-yl)methoxy)carbonyl)amino)-4-carboxybutan-1-aminium chloride (2)

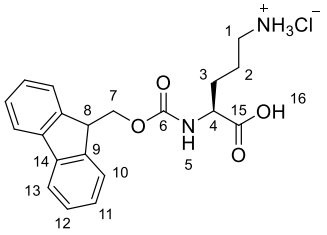

To a stirred solution of Fmoc-Orn(Boc)-OH (2.50 g, 5.50 mmol) in 1,4-dioxane (8 mL) was added HCl (4 M in 1,4-dioxane, 4.00 mL, 16.00 mmol, 2.9 eq.). The reaction was stirred at rt for 21 h. The reaction mixture was diluted with diethyl ether (100 mL) and the precipitate was

filtered. The precipitate was washed with diethyl ether (4 × 50 mL) and dried *in vacuo* to give the title compound as a white powder (1.94 g, 4.96 mmol, 90%).

^{1}H NMR (400 MHz, DMSO-d_6) δ 7.90 (5H, m, H13 and NH_3), 7.74-7.68 (3H, m, H10 and H5), 7.42 (2H, appt. t, *J* = 7.4 Hz, H12), 7.33 (2H, appt. t, *J* = 7.4 Hz, H11), 4.31-4.21 (3H, m, H7 and H4), 3.97-3.93 (1H, m, H8), 2.83-2.72 (2H, m, H1), 1.86-1.71 (1H, m, H3), 1.70-1.53 (3H, m, H3 and H2); **^{13}C NMR** (101 MHz, DMSO-d_6), 174.0 (C=O, C15), 156.6 (C=O, C6), 144.3 (C, C9), 141.2 (C, C14), 128.1 (CH, C12), 127.6 (CH, C11), 125.7 (CH, C13), 120.6 (CH, C10), 66.1 (CH_2, C7), 53.9 (CH, C8), 47.1 (CH, C4), 38.9 (CH_2, C1), 28.2 (CH_2, C3), 24.4 (CH_2, C2); **IR** (neat, cm^{-1}) ν_{max} 3015 (br, OH), 1730 (C=O), 1691 (C=O); **HRMS** (ESI): $[M+H]^+$ calcd. for $[C_{20}H_{23}N_2O_4]^+$ 355.1652, observed 355.1567 (Δ = -1.4 ppm); **$[\alpha]_D^{25}$** -1.00 (c = 1, DMSO).

Data in accordance with previous literature reports.[23]

(*S*)-2-((((9*H*-Fluoren-9-yl)methoxy)carbonyl)amino)-5-azidopentanoic acid (3)

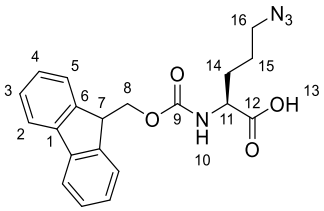

2 (1.94 g, 5.00 mmol) was dissolved in a biphasic mixture of H_2O (25 mL), MeOH (75 mL) and CH_2Cl_2 (50 mL). To the reaction mixture was added $CuSO_4 \cdot 5H_2O$ (7.00 mg, 2.98 µmol, 0.006 eq.) and **1** (4.31 g, 15.9 mmol, 3.18 eq.). The reaction mixture was adjusted to pH 9 with sat. aq. K_2CO_3 solution, then stirred vigorously at rt for 18 h. The reaction mixture was diluted with CH_2Cl_2 (50 mL) and the aqueous phase was separated. The organic phase was extracted with sat. $NaHCO_3$ solution (2 × 60 mL). The combined aqueous extracts were washed with diethyl ether (2 × 60 mL). The ethereal extracts were discarded, and the aqueous layer was acidified to pH 2 with conc. HCl and extracted with diethyl ether (3 × 60 mL). The combined ethereal extracts were dried ($MgSO_4$) and the solvent was removed *in vacuo* to give the title compound as a white solid (1.41 g, 3.71 mmol, 75%).

R_f 0.38 (1% MeOH and 1% AcOH in CH_2Cl_2); **^{1}H NMR** (400 MHz, DMSO-d_6) δ 7.92-7.87 (2H, d, *J* = 7.4 Hz, H2), 7.74-7.65 (3H, m, H5 and H10), 7.43 (2H, appt. t, *J* = 7.4 Hz, H3), 7.34 (2H, appt. dt, *J* = 7.4, 1.0 Hz, H4), 4.34-4.27 (2H, m, H8), 4.26-4.21 (1H, m, H11), 4.02-3.95 (1H, m, H7), 3.34 (2H, appt. t, *J* = 8.0 Hz, H15), 1.85-1.75 (1H, m, H14), 1.73-1.53 (3H, m, H14 and H16); **^{13}C NMR** (101 MHz, DMSO-d_6) δ 174.1 (C=O, C12), 156.6 (C=O, C9), 144.3 (C, C6 or C1), 141.2 (C, C6 or C1), 128.1 (CH, C3), 127.5 (CH, C4), 125.7 (CH, C5), 120.6 (CH, C2), 66.1 (CH_2, C8), 53.8 (CH, C7), 50.7 (CH_2, C11), 47.1 (CH, C16), 28.5 (CH_2, C15), 25.6

(CH_2, C14); **IR** (neat, cm^{-1}) v_{max} 3065 (br. OH), 2095 (N=N=N stretch), 1700 (C=O), 1697 (C=O), 1522 (C-C stretch); **HRMS** (ESI): $[M+H]^+$ calcd. for $[C_{20}H_{21}N_4O_4]^+$: 381.1518, observed 381.1573 (Δ = 2.6 ppm); **$[\alpha]_D^{25}$** -3.6 (c = 1, MeOH, lit. $[\alpha]_D$ -2.3).[369]

Data in accordance with previous literature reports.[369]

3,6-Dibromo-9*H*-carbazole (4)

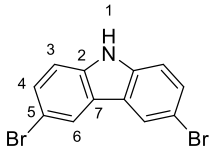

A solution of *N*-bromosuccinimide (23.1 g, 130 mmol, 2.17 eq.) in DMF (150 mL) was added dropwise to an ice-cold suspension of carbazole (10.0 g, 59.8 mmol) in toluene (50 mL). The reaction mixture was warmed to rt, stirred for 30 min then poured onto H_2O (500 mL). The precipitate that formed was washed with H_2O (100 mL) and cold MeOH (100 mL). The crude product was triturated with cold MeOH/hexanes (1:1) to give the title compound as a cream solid (12.8 g, 39.6 mmol, 66%).

R_f 0.31 (20:80 EtOAc/Hexanes); **^{1}H NMR** (500 MHz, DMSO-d_6) δ 11.60 (1H, s, NH, H1), 8.44 (2H, d, *J* = 1.8 Hz, H6), 7.54 (2H, dd, *J* = 8.6, 1.8 Hz, H4), 7.48 (2H, d, *J* = 8.6 Hz, H3); **^{13}C NMR** (101 MHz, DMSO-d_6) δ 139.3 (C, C2), 129.2 (CH, C6), 123.8 (CH, C4), 123.8 (C, C5), 113.7 (CH, C3), 111.5 (C, C7); **IR** (neat, cm^{-1}) v_{max} 3420 (NH stretch), 1430 (C=C stretch); **HRMS** (ESI): $[M+H]^+$ calcd. for $[C_{12}H_8{}^{79}Br_2N]^+$ 325.9003, observed 325.1504 (Δ = -0.9 ppm).

Data in accordance with previous literature reports.[369]

3,6-Bis((trimethylsilyl)ethynyl)-9*H*-carbazole (5)

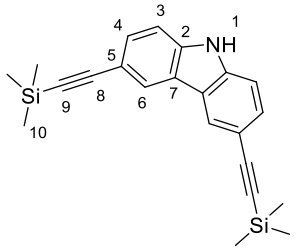

A suspension of **4** (5.0.0 g, 15.5 mmol), $Pd(PPh_3)_2Cl_2$ (500 mg, 0.775 mmol, 0.05 eq.), CuI (100 mg, 0.465 mmol, 0.026 eq.), trimethylsilylacetylene (10.0 mL, 69.8 mmol, 4.5 eq.), and PPh_3 (100 mg, 0.388 mmol, 0.025 eq.) in NEt_3 (160 mL) was heated to reflux for 18 h. The reaction mixture was filtered through Celite®, washed with H_2O (50 mL) and brine (50 mL),

dried (Na_2SO_4) and concentrated *in vacuo*. The residue was purified by FCC on SiO_2 (0-60% EtOAc in PE 40-60) to give the title compound as an orange solid (4.02 g, 11.2 mmol, 72%).

R_f 0.37 (15% EtOAc/PE 40-60); **^{1}H NMR** (400 MHz, $CDCl_3$) δ 8.19-8.16 (3H, m, H1 and H6), 7.54 (2H, dd, *J* = 8.4, 1.5 Hz, H4), 7.32 (2H, d, *J* = 8.4 Hz, H3), 0.29 (18H, s, H10); **^{13}C NMR** (101 MHz, $CDCl_3$) δ 139.6 (C, C2), 130.4 (CH, C4), 124.8 (CH, C6), 122.9 (C, C7), 114.6 (C, C5), 110.8 (CH, C3), 106.3 (C, C8), 92.3 (C, C9), 0.28 (CH_3, C10); **IR** (neat, cm^{-1}) ν_{max} 3362 (NH stretch), 2956 (C-H aromatic stretch), 2138 (C≡C stretch), 1481 (C=C stretch); **HRMS** (ESI): $[M+H]^+$ calcd. for $[C_{22}H_{26}NSi_2]^+$ 360.1604, observed 360.1604 (Δ = -4.7 ppm).

Data in accordance with previous literature reports.[370]

3,6-Diethynyl-9*H*-carbazole (6)

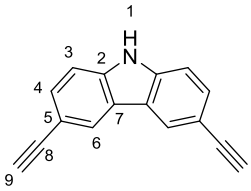

A suspension of **5** (321 mg, 0.892 mmol) and K_2CO_3 (469 mg, 3.39 mmol, 3.8 eq.) in MeOH (30 mL) was stirred at rt for 18 h. The reaction mixture was evaporated *in vacuo* and the residue purified by FCC on SiO_2 (40% CH_2Cl_2 in PE 40-60) to give the title compound as a beige solid (156 mg, 0.725 mmol, 81%).

R_f 0.28 (25% EtOAc/hexanes); **^{1}H NMR** (400 MHz, DMSO) δ 11.70 (1H, s, H1), 8.37 (2H, s, H6), 7.51-7.48 (4H, m, H3 and H4), 4.04 (2H, s, H8); **^{13}C NMR** (101 MHz, DMSO-d_6) δ 140.4 (C, C2), 130.1 (CH, C4), 125.0 (CH, C6), 122.4 (C, C7), 112.6 (C, C5), 112.0 (CH, C3), 85.4 (C, C8), 79.0 (CH, C9); **IR** (neat, cm^{-1}) ν_{max} 3404 (NH stretch), 3269 (C≡C-H stretch), 2103 (C≡C stretch), 1601 (C=C stretch); **HRMS** (ESI): $[M+H]^+$ calcd. for $[C_{16}H_{10}N]^+$ 216.0813, observed 216.0818 (Δ = 2.3 ppm).

Data in accordance with previous literature reports.[370]

6-(3,6-Diethynyl-9*H*-carbazol-9-yl)hexanoic acid (7)

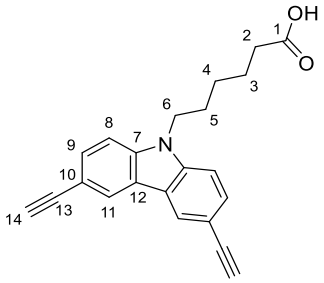

Freshly ground KOH (1.25 g, 22.2 mmol, 7.9 eq.) was suspended in DMF/DMSO (1:1, 5.6 mL) and stirred for 1.5 h. **6** (1.00 g, 2.80 mmol) was added and the reaction mixture was stirred at rt for 20 min. 6-Bromohexanoic acid (1.09 g, 5.60 mmol, 2.0 eq.) was added and the reaction mixture was stirred at rt for 20 min then irradiated with 37 kHz ultrasonic waves for 1.5 h. The reaction mixture was acidified to pH 4 with 2 N HCl and the aqueous phase was extracted with EtOAc (3 × 10 mL). The combined organics were dried ($MgSO_4$) and concentrated *in vacuo*. The residue was purified by FCC on SiO_2 (0-100% EtOAc in hexane, then 0-10% MeOH in EtOAc) to yield the title compound as an orange oil which solidified on standing (580 mg, 1.76 mmol, 63%).

R_f 0.12 (50% EtOAc/hexanes); **^{1}H NMR** (400 MHz, $CDCl_3$) δ 8.21 (2H, s, H11), 7.60 (2H, d, *J* = 8.5 Hz, H9), 7.32 (2H, d, *J* = 8.5 Hz, H8), 4.28 (2H, t, *J* = 7.2 Hz, H6), 3.09 (2H, s, H14), 2.32 (2H, t, *J* = 7.4 Hz, H2), 1.88 (2H, appt. p, *J* = 7.6 Hz, H5), 1.67 (2H, appt. p, *J* = 7.5 Hz, H3), 1.46-1.37 (2H, m, H4); **^{13}C NMR** (101 MHz, $CDCl_3$) δ 178.9 (C, C1), 140.6 (C, C7), 130.2 (CH, C9), 124.8 (CH, C11), 122.3 (C, C12), 112.8 (C, C10), 108.9 (CH, C8), 84.7 (C, C13), 75.5 (CH, C14), 43.0 (CH_2, C6), 33.6 (CH_2, C2), 28.6 (CH_2, C5), 26.6 (CH_2, C3), 24.3 (CH_2, C4); **IR** (neat, cm^{-1}) ν_{max} 3260 (C≡C-H stretch), 2926 (OH stretch), 1699 (CO carbonyl stretch), 1480 (C=C aromatic stretch); **HRMS** (ESI): $[M+H]^+$ calcd. for $[C_{22}H_{20}NO_2]^+$ 330.1494, observed 330.1489 (Δ = -1.5 ppm).

Methyl 3,5-bis((trimethylsilyl)ethynyl)benzoate (9)

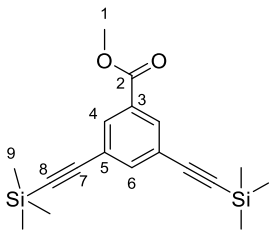

To a solution of methyl 3,5-dibromobenzoate (900 mg, 3.10 mmol), tris(dibenzylideneacetone)dipalladium(0) (54.0 mg, 59.0 µmol, 0.19 eq.), CuI (11.5 mg, 6.00 µmol, 0.0019 eq.) and PPh_3 (77.5 mg, 0.290 mmol, 0.094 eq.) in anhydrous NEt_3 (15 mL) was

added trimethylsilylacetylene (6.00 mL, 42.2 mmol, 13.6 eq.). The reaction was heated to reflux for 18 h. The solvent was removed under N_2 and the crude product was purified by FCC on SiO_2 (0-5% EtOAc/PE 40-60) to yield the title compound as an orange oil which solidified on standing (977 mg, 2.97 mmol, 96%).

R_f 0.45 (1% EtOAc/PE 40-60); **^{1}H NMR** (400 MHz, $CDCl_3$) δ 8.04 (2H, d, *J* = 1.6 Hz, H4), 7.72 (1H, t, *J* = 1.6 Hz, H6), 3.91 (3H, s, H1), 0.24 (18H, s, H9); **^{13}C NMR** (101 MHz, CDCl3) δ 165.7 (C, C2), 139.1 (CH, C6), 132.7 (CH, C4), 130.7 (C, C3), 124.0 (C, C5), 103.1 (C, C7), 96.2 (C, C8), 52.5 (CH_3, C1), -0.1 (CH_3, C9)**; IR** (neat, cm^{-1}) ν_{max} 2956 (C-H aromatic stretch), 2155 (C≡C stretch), 1730 (C=O, carbonyl stretch), 1588 (C=C aromatic stretch); **HRMS** (ESI): $[M+H]^+$ calcd. for $[C_{18}H_{25}Si_2O_2]^+$ 329.1393, found: 329.1474 (Δ = 3.3 ppm).

Data in accordance with previous literature reports.[23]

3,5-Diethynylbenzoic acid (10)

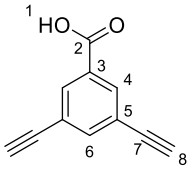

To a solution of **9** (2.85 g, 8.68 mmol) in THF (50 mL) was added 6 N KOH solution (8.50 mL, 50 mmol, 5.76 eq.). The reaction was stirred at rt for 48 h. The volatile solvents were removed *in vacuo* and the remaining aqueous solution was diluted with H_2O (20 mL) and acidified to pH 2 using 2 N HCl. The mixture was extracted with diethyl ether (3 × 30 mL) and the combined organics were dried ($MgSO_4$) and evaporated *in vacuo*. The crude product was recrystallised from $CHCl_3$ to give the title compound as pale orange crystals (1.25 g, 7.35 mmol, 84% yield).

R_f 0.40 (1% MeOH/CH_2Cl_2 with 1% AcOH); **Mp** ($CHCl_3$) 200 °C decomp. (lit. mp 250 °C decomp.);[23] **^{1}H NMR** (400 MHz, DMSO-d_6) δ 7.95 (2H, d, *J* = 1.4 Hz, H4), 7.80 (1H, t, *J* = 1.5 Hz, H6), 4.40 (2H, s, H8); **^{13}C NMR** (101 MHz, DMSO-d_6) δ 170.8 (C, C2), 143.4 (C, C6), 137.6 (CH, C4), 128.9 (C, C3), 128.1 (C, C5), 87.9 (C, C7), 86.7 (CH, C8); **IR** (neat, cm^{-1}) ν_{max} 3286 (C≡C-H stretch), 2599 (OH), 1684 (C=O carbonyl stretch), 1443 (C=C aromatic stretch); **HRMS** (ESI): $[M-H]^-$ calcd. for $[C_{11}H_5O_2]^-$ 169.0295, observed 169.0290 (Δ = -2.9 ppm).

Data in accordance with previous literature reports.[23]

4.1.2 Chemistry experimental procedures for Chapter 3

General method 1 - S_NAr reaction: To a solution of chloro-aryl (1.0 eq.) and amine (1.2 eq.) in acetone was added NEt_3 (2.5 eq.) with ice cooling. The reaction was stirred with ice cooling for 2 h and then warmed to rt and stirred for 1 h. The reaction mixture was diluted with EtOAc, washed with H_2O (× 3), dried ($MgSO_4$) and evaporated *in vacuo.* The residue was purified by FCC on SiO_2 to give the title compound.

General method 2 - Suzuki-Miyaura coupling[67]: A suspension of di-chloroaryl (1.0 eq.), potassium vinyltrifluoroborate (3.0 eq.) and K_2CO_3 (6.0 eq.) in 1,4-dioxane/H_2O (9:1) was degassed under N_2 for 5 min. $PdCl_2(dppf)\cdot CH_2Cl_2$ (0.1 eq.) was added to the reaction mixture at rt and the reaction was heated to reflux for 18 h. The reaction mixture was filtered through Celite® and evaporated *in vacuo* to give the crude product which was purified by FCC to give the desired product.

General method 3 - Ethyl ester hydrolysis: To a solution of ethyl ester (1.0 eq.) in THF/H_2O (1:1, reaction molarity 0.07 M) at 0 °C was added $LiOH\cdot H_2O$ (1.1 eq.) and the reaction was stirred at rt until the starting material was fully consumed. The reaction mixture was diluted with H_2O, washed with Et_2O (× 1) and the pH was adjusted with 1N HCl. The aqueous was extracted with CH_2Cl_2 (× 4) and the combined organics were dried (Na_2SO_4) to give the crude product.

Ethyl *N*-(2,6-dichloropyrimidin-4-yl)-*N*-methylglycinate (12)

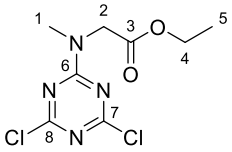

To a solution of cyanuric chloride (5.00 g, 27.1 mmol) and sarcosine ethyl ester hydrochloride (4.16 g, 27.1 mmol, 1.0 eq.) in acetone (100 mL) at 0 °C was added DIPEA (9.45 mL, 54.2 mmol, 2.0 eq.) dropwise. The reaction was stirred at 0 °C for 2 h, then poured onto ice water (100 mL). The aqueous was extracted with CH_2Cl_2 (3 × 50 mL), dried ($MgSO_4$) and evaporated *in vacuo* to give the title compound as a yellow solid (6.57 g, 24.9 mmol, 92%) which was taken on without further purification.

R_f 0.26 (20% EtOAc/PE 40-60); **^{1}H NMR** (400 MHz, $CDCl_3$) δ 4.35 (2H, s, H2), 4.22 (2H, q, *J* = 7.2 Hz, H4), 3.25 (3H, s, H1), 1.28 (3H, t, *J* = 7.2 Hz, H5); **^{13}C NMR** (101 MHz, $CDCl_3$) δ 170.4 (C=O, C3), 170.0 (C, C6), 167.9 (C, C7), 165.5 (C, C8), 61.8 (CH_2, C2), 50.8 (CH_2, C4), 36.5 (CH_3, C1), 14.2 (CH_3, C5); **IR** (neat, cm^{-1}) ν_{max} 2992 (aliphatic C-H, stretch), 1735 (ester C=O, stretch), 1480 (aliphatic C-H, bend), 1215 (ester C-O, stretch), 794 (aromatic C-Cl,

stretch); **HRMS** (ESI): $[M+H]^+$ calcd. for $[C_8H_{11}Cl_2N_4O_2]^+$ 265.0259, observed 265.0249 (Δ = -3.8 ppm).

Data in accordance with previous literature reports.[67]

Ethyl *N*-(4,6-divinyl-1,3,5-triazin-2-yl)-*N*-methylglycinate (13)

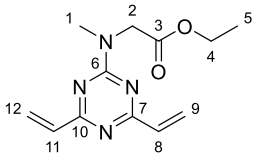

Prepared following *general method 2* using **12** (2.50 g, 9.43 mmol), potassium vinyltrifluoroborate (3.80 g, 28.4 mmol, 3.0 eq.), K_2CO_3 (7.80 g, 56.7 mmol, 6.0 eq.) and $PdCl_2(dppf)\cdot CH_2Cl_2$ (770 mg, 0.945 mmol, 0.1 eq.) in 1,4-dioxane/H_2O (9:1, 128 mL). The reaction was complete after 2 h. The crude product was purified by FCC on SiO_2 (0-25% EtOAc in PE 40-60) to give the title compound as a clear oil (1.20 g, 4.83 mmol, 51%).

R_f 0.52 (25% EtOAc/PE 40-60); **^{1}H NMR** (400 MHz, $CDCl_3$) δ 6.78-6.52 (4H, m, H9 and H12), 5.75 (2H, dd, *J* = 2.1, 10.2 Hz, H8 and H11), 4.38 (2H, s, H2), 4.18 (2H, q, *J* = 7.2 Hz, H4), 3.29 (3H, s, H1), 1.25 (3H, t, *J* = 7.2 Hz, H5); **^{13}C NMR** (101 MHz, $CDCl_3$) δ 170.7 (C=O, C3), 170.2 (C, C6), 169.6 (C, C7 or C10), 165.5 (C, C7 or C10), 136.2 (CH, C8 or C11), 136.0 (CH, C8 or C11), 126.2 (CH_2, C9 or C12), 126.0 (CH_2, C9 or C12), 61.1 (CH_2, C2), 50.7 (CH_2, C4), 35.7 (CH_3, C1), 14.2 (CH_3, C5); **IR** (neat, cm^{-1}) ν_{max} 2983 (alkene C-H, stretch), 1742 (ester C=O, stretch), 1637 (alkene C=C, stretch), 1186 (ester C-O, stretch), alkene C-H, bend); **HRMS** (ESI) $[M+H]^+$ calcd. for $[C_{12}H_{17}N_4O_2]^+$ 249.1352, observed 249.1352 (Δ = -0.4 ppm).

Data in accordance with previous literature reports.[67]

***N*-(4,6-Divinyl-1,3,5-triazin-2-yl)-*N*-methylglycine (14)**

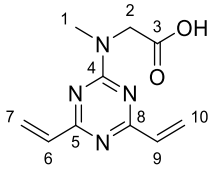

Prepared following *general method 3*, using **13** (100 mg, 0.403 mmol) and $LiOH\cdot H_2O$ (19.0 mg, 0.453 mmol, 1.1 eq.) in THF/H_2O (1:1, 6 mL). The starting material was consumed after 18 h. After washing with Et_2O (1 × 5 mL), the pH was adjusted to 7 with 1N HCl and the aqueous was extracted with CH_2Cl_2 (4 × 5 mL). The combined organics were dried (Na_2SO_4),

evaporated and triturated with cold PE 40-60 to give the title compound as a white solid (50.0 mg, 22.7 mmol, 56%).

R_f 0.17 (10% MeOH/CH_2Cl_2); **^{1}H NMR** (400 MHz, DMSO-d_6) δ 6.74-6.49 (4H, m, H7 and 10), 5.89-5.81 (2H, m, H6 and 9), 4.36 (2H, s, H2), 3.21 (3H, s, H1); **^{13}C NMR** (101 MHz, DMSO-d_6) δ 171.1 (C=O, C3), 170.4 (C, C4), 170.0 (C, C5 or C8), 165.6 (C, C5 or C8), 136.4 (CH_2, C7 or 10), 136.3 (CH_2, C7 or 10), 127.3 (CH, C6 or 9), 127.3 (CH, C6 or 9), 50.5 (CH_3, C1), 35.9 (CH_2, C2); **IR** (neat, cm^{-1}) ν_{max} 2495 (alkene C-H, stretch), 1711 (acid C=O, stretch), 1640 (alkene C=C, stretch), 1224 (acid C-O, stretch); **LRMS** (ESI) $[M+H]^+$ calcd. for $[C_{10}H_{13}N_4O_2]^+$ 221.1 observed 221.2.

Data in accordance with previous literature reports.[67]

4,6-Dichloro-*N*-(3-phenylpropyl)pyrimidin-2-amine (15)

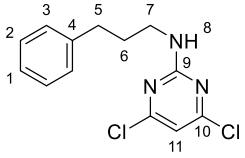

Prepared following *general method 1* using 2,4,6-trichloropyrimidine (1.57 mL, 13.6 mmol), 3-phenyl-1-propylamine (2.30 mL, 16.4 mmol, 1.2 eq.) and NEt_3 (4.80 mL, 34.2 mmol, 2.5 eq.) in acetone (70 mL). The crude product was purified by FCC on SiO_2 (25% EtOAc in PE 40-60) to give the title compound as a yellow solid (1.62 g, 5.74 mmol, 42%).

R_f 0.63 (25% EtOAc/PE 40-60); **^{1}H NMR** (400 MHz, $CDCl_3$) δ 7.34-7.21 (5H, m, H1 and H2 and H3), 6.62 (1H, s, H11), 5.45 (1H, appt. s, H8), 3.48 (2H, q, *J* = 6.8 Hz, H7), 2.72 (2H, t, *J* = 7.5 Hz, H5), 1.97 (2H, p, *J* = 7.5 Hz, H6); **^{13}C NMR** (101 MHz, $CDCl_3$) δ 161.6 (C, C9 and C10), 141.1 (C, C4), 128.5 (CH, C2), 128.3 (CH, C3), 126.1 (CH, C1), 108.9 (CH, C11), 41.1 (CH_2, C7), 33.0 (CH_2, C5), 30.8 (CH_2, C6); **IR** (neat, cm^{-1}) ν_{max} 3271 (N-H, stretch), 3122 (aromatic C-H, stretch), 2934 (aliphatic C-H, stretch), 1600 (N-H, bend), 1518 (aromatic C=C, stretch), 1450 (aliphatic C-H, bend), 696 (C-Cl, stretch); **HRMS** (ESI) $[M+H]^+$ calcd. for $[C_{13}H_{14}N_3{}^{35}Cl_2]^+$ 282.0565 observed 282.0557 (Δ = -1.0 ppm).

_N_-(3-phenylpropyl)-4,6-divinylpyrimidin-2-amine (17)

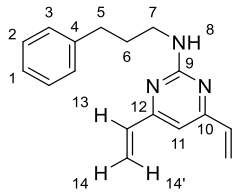

Prepared following *general method 2* using **15** (1.00 g, 3.55 mmol), potassium vinyltrifluoroborate (1.42 g, 10.6 mmol, 3.0 eq.), K_2CO_3 (2.94 g, 21.2 mmol, 6.0 eq.) and $PdCl_2(dppf)\cdot CH_2Cl_2$ (290 mg, 0.346 mmol, 0.1 eq.) in 1,4-dioxane/H_2O (9:1, 50 mL). The crude product was purified by FCC on SiO_2 (0-25% EtOAc in PE 40-60) to give the title compound as a pale yellow oil (659 mg, 2.49 mmol, 70%).

R_f 0.44 (25% EtOAc/PE 40-60); **^{1}H NMR** (400 MHz, $CDCl_3$) δ 7.33-7.18 (5H, m, H1 and H2 and H3), 6.61 (2H, dd, *J* = 17.4, 10.6 Hz, H13), 6.56 (1H, s, H11), 6.38 (2H, dd, *J* = 17.3, 0.8 Hz, H14'), 5.59 (2H, dd, *J* = 10.6, 1.4 Hz, H14), 5.24 (1H, appt. s, H8), 3.54 (2H, q, *J* = 6.8 Hz, H7), 2.75 (2H, t, *J* = 7.5 Hz, H5), 1.99 (2H, p, *J* = 7.4 Hz, H6); **^{13}C NMR** (101 MHz, $CDCl_3$) δ 163.8 (C, C10 and C12), 162.7 (C, C9), 142.0 (C, C4), 136.0 (CH, C13), 128.6 (CH, C2 or C3), 128.5 (CH, C2 or C3), 126.0 (CH, C1), 121.6 (CH_2, C14), 105.7 (CH, C11), 41.1 (CH_2, C7), 33.4 (CH_2, C5), 31.5 (CH_2, C6); **IR** (neat, cm^{-1}) ν_{max} 3027 (aromatic C-H, stretch), 2937 (alkene C-H, stretch), 1636 (alkene C=C, stretch), 1541 (aromatic C=C, stretch), 1325 (C-N, stretch), 907 (alkene C=C, bend); **HRMS** (ESI) $[M+H]^+$ calcd. for $[C_{17}H_{20}N_3]^+$ 266.1657, observed 266.1645 (Δ = -4.5 ppm).

4-Vinylpyrimidin-2-amine (18)

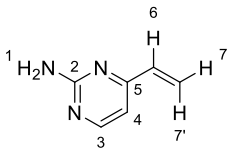

Prepared following *general method 2* using 2-amino-4-chloropyrimidine (200 mg, 1.54 mmol), K_2CO_3 (1.28 g, 9.24 mmol, 6.0 eq.), potassium vinyltrifluoroborate (620 mg, 4.63 mmol, 3.0 eq.), and $PdCl_2(dppf)\cdot CH_2Cl_2$ (126 mg, 0.154 mmol, 0.1 eq.) in 1,4-dioxane/H_2O (9:1, 26 mL). The crude product was adsorbed onto Fluorosil® and purified by FCC on SiO_2 (1% NEt_3 in EtOAc) to give the title compound as a beige solid (75.0 mg, 0.619 mmol, 40%).

R_f 0.46 (1% NEt_3/EtOAc); **^{1}H NMR** (400 MHz, $CDCl_3$) δ 8.26 (1H, d, *J* = 5.1 Hz, H3), 6.63 (1H, d, *J* = 5.1 Hz, H4), 6.57 (1H, dd, *J* = 17.4, 10.6 Hz, H6), 6.34 (1H, dd, *J* = 17.4, 1.0 Hz, H7'), 5.61 (1H, dd, *J* = 10.6, 1.0 Hz, H7), 5.12 (2H, br. s, H1); **^{13}C NMR** (101 MHz, $CDCl_3$) δ 164.4 (C, C5), 162.3 (C, C2), 157.4 (CH, C3), 135.4 (CH, C6), 123.2 (CH_2, C7), 108.7 (CH, C4); **IR**

(neat, cm^{-1}) ν_{max} 3328, 3168, 2352, 1650, 1548, 1451, 1337, 1217; **HRMS** (ESI) $[M+H]^+$ calcd. for $[C_6H_8N_3]^+$ 122.0718 observed 122.0715 (Δ = 1.5 ppm).

Data in accordance with previous literature reports.[371]

4,6-Divinylpyrimidin-2-amine (24)

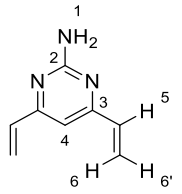

A suspension of 2-amino-4,6-dichloropyrimidine (400 mg, 2.44 mmol, 1.0 eq.), potassium vinyltrifluoroborate (980 mg, 7.32 mmol, 3.0 eq.), $Pd(dppf)Cl_2 \cdot CH_2Cl_2$ (200 mg, 0.244 mmol, 0.01 eq.) and K_2CO_3 (2.02 g, 14.64 mmol, 6.0 eq.) in THF/H_2O (10:1, 6.6 mL) was heated to 70 °C for 18 h. The reaction mixture was filtered through Celite® and concentrated *in vacuo*. The crude residue was purified by FCC on SiO_2 (20-40% EtOAc/PE 40-60) to give the title compound as a yellow solid (190 mg, 1.29 mmol, 53%).

R_f 0.33 (50% EtOAc/PE 40-60); **^{1}H NMR** (400 MHz, $CDCl_3$) δ 6.67 (1H, s, H4), 6.61 (2H, dd, *J* = 17.4, 10.7 Hz, H5), 6.36 (2H, dd, *J* = 17.4, 1.3 Hz, H6), 5.62 (2H, dd, J = 10.7, 1.3 Hz, H6'); **^{13}C NMR** (101 MHz, $CDCl_3$) δ 164.2 (C, C3), 163.2 (C, C2), 135.6 (CH, C5), 122.0 (CH_2, C6), 106.2 (CH, C4); **IR** (neat, cm^{-1}) ν_{max} 3329 (N-H, stretch), 1648 (C=C stretch, alkene), 1558 (N-H bending), 1457 (C=C aromatic, stretch), 1223 (C-N stretch); **LRMS** (ESI) $[M+H]^+$ calcd. for $[C_8H_{10}N_3]^+$ 148.1 observed 148.2.

Data in accordance with previous literature reports.[371]

***N*-(Hex-5-yn-1-yl)-4,6-divinylpyrimidin-2-amine (21)**

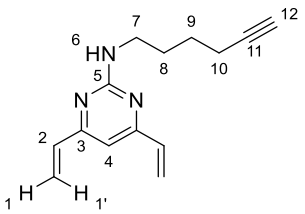

To a solution of **24** (190 mg, 1.29 mmol) in DMF (5.6 mL) was added 6-iodo-1-hexyne (850 µL, 6.45 mmol, 5.0 eq.). To the reaction mixture was added sodium hydride (60% in mineral oil, 260 mg, 6.45 mmol, 5.0 eq.) portion-wise. The reaction mixture was stirred at rt for 18 h, then diluted with H_2O (50 mL) and extracted with CH_2Cl_2 (3 × 20 mL). The combined organics were dried ($MgSO_4$) and the solvent removed *in vacuo*. The crude product was purified by

FCC on SiO_2 (20-40% EtOAc/PE 40-60) to give the title compound as an orange oil (100 mg, 0.440 mmol, 34%).

R_f 0.4 (30% EtOAc/PE 40-60); **^{1}H NMR** (400 MHz, $CDCl_3$) δ 6.60 (2H, dd, *J* = 17.4, 10.6 Hz, H2), 6.54 (1H, s, H4), 6.37 (2H, appt. d, *J* = 17.4 Hz, H1'), 5.57 (2H, dd, *J* = 10.6, 1.4 Hz, H1), 5.20 (1H, br. s, H6), 3.51 (2H, q, *J* = 6.7 Hz, H7), 2.28-2.24 (2H, m, H12), 1.97 (2H, t, *J* = 2.6 Hz, H10), 1.79-1.72 (2H, m, H8 or H9), 1.68-1.63 (2H, m, H8 or H9); **^{13}C NMR** (101 MHz, $CDCl_3$) δ 163.7 (C, C3), 162.7 (C, C5), 136.0 (CH, C2), 121.3 (CH_2, C1), 105.5 (CH, C4), 84.3 (C, C11), 68.5 (CH, C12), 40.8 (CH_2, C7), 28.8 (CH_2, C8), 25.8 (CH_2, C9), 18.2 (CH_2, C10); **IR** (neat, cm^{-1}) v_{max} 3349 (N-H, stretch), 3211 (C-C alkyne, stretch), 1632 (C=C stretch, conjugated alkene), 1558 (N-H bending), 1219 (C-N stretch); **LRMS** (ESI) $[M+H]^+$ calcd. for $C_{14}H_{18}N_3^+$ 228.1 observed 228.3.

Data in accordance with previous literature reports.[371]

(6R,7R)-7-Amino-3-(hydroxymethyl)-8-oxo-5-thia-1-azabicyclo[4.2.0]oct-2-ene-2-carboxylic acid (28)

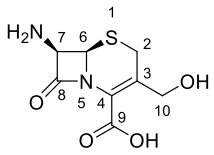

To a suspension of 7-ACA (184 mg, 0.676 mmol) in MeOH/H_2O (2 mL, 1:1) at -30 °C was added sodium hydroxide (3 N, 0.3 mL, 1.3 eq.) dropwise. The reaction mixture was stirred at -30 °C for 4 h then warmed to 0 °C and acidified to pH 2 with 1 N HCl. The resulting precipitate was filtered and washed with MeOH to give the title compound as an orange solid (63.0 mg, 0.274 mmol, 40%).

^{1}H NMR (400 MHz, DMSO-d_6) δ 4.93 (1H, d, *J* = 4.0 Hz, H7), 4.73 (1H, d, *J* = 4.0 Hz, H6), 4.21-4.20 (2H, m, H10), 3.56 (1H, d, *J* = 18, H2), 3.48 (1H, d, *J* = 18 Hz, H2); **^{13}C NMR** (400 MHz, DMSO-d_6) 170.0 (C=O, C8), 163.8 (C=O, C9), 129.5 (C, C3), 79.6 (C, C4), 63.5 (CH, C6), 60.0 (CH_2, C10), 59.0 (CH, C7), 25.2 (CH_2, C2); **IR** (neat, cm^{-1}) v_{max} 3377 (O-H, stretch), 3146 (N-H, stretch), 1783 (C=O lactam, stretch), 1616 (C=O acid, stretch), 1535 (alkene C=C, stretch).

Data in accordance with previous literature reports.[330]

4-Azidobenzoyl chloride (29)

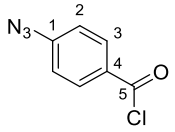

To a suspension of 4-azidobenzoic acid (720 mg, 4.41 mmol) in CH_2Cl_2 (3 mL) at rt was added oxalyl chloride (225 µL, 2.66 mmol, 0.6 eq.). The reaction mixture was stirred for 20 min then DMF (15 µL, cat.) was added dropwise. The reaction mixture was stirred at rt for 18 h, then the solvent removed *in vacuo* to give the crude product as a beige solid (786 mg, 4.33 mmol, 98%) which was used without further purification.

R_f 0.29 (2% MeOH/CH_2Cl_2); **^{1}H NMR** (400 MHz, DMSO-d_6) δ 7.97-7.95 (2H, m, H2), 7.22-7.19 (2H, m, H3); **^{13}C NMR** (101 MHz, DMSO-d_6) δ 167.0 (C=O, C5), 144.4 (C, C4), 131.7 (CH, C2), 127.7 (C, C1), 119.6 (CH, C3); **IR** (neat, cm^{-1}) v_{max} cm^{-1} 2122 (N=N=N), 1762 (C=O, stretch), 1572 (aromatic C-H, bend).

Data in accordance with previous literature reports.[372]

***Tert*-butyl (6*R*,7*R*)-3-(acetoxymethyl)-7-amino-8-oxo-5-thia-1-azabicyclo[4.2.0]oct-2-ene-2-carboxylate (30)**

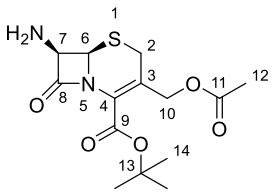

tert-Butyl acetate (9.25 mL) was sparged for 5 min then 7-ACA (500 mg, 1.84 mmol) was added. $BF_3.OEt_2$ (1.40 mL, 11.0 mmol, 6.0 eq.) was added dropwise and the reaction mixture was stirred at rt for 2 h. Upon the formation of a homogenous solution the reaction mixture was poured into ice water (50 mL) and extracted with EtOAc (4 x 30 mL). The combined organics were dried ($MgSO_4$) and the solvent was removed *in vacuo* to yield the crude product (473 mg, 1.44 mmol, 78%) as a beige gum which was used without further purification.

R_f 0.29 (50% EtOAc/PE with 1% NEt_3); **^{1}H NMR** (400 MHz, DMSO-d_6) δ 4.98 (1H, d, *J* = 5.1 Hz, H7), 4.89 (1H, d, *J* = 12.6 Hz, H10), 4.79 (1H, d, *J* = 5.1 Hz, H6), 4.60 (1H, d, *J* = 12.6 Hz, H10'), 3.58 (1H, d, *J* = 18.2 Hz, H2), 3.43 (1H, d, *J* = 18.1 Hz, H2'), 2.02 (3H, s, H12), 1.46 (9H, s, H14); **^{13}C NMR** (101 MHz, DMSO-d_6) δ 170.3 (C=O, C9), 170.1 (C=O, C11), 160.8 (C=O, C8), 127.1 (C, C3), 122.1 (C, C4), 82.6 (C, C13), 63.8 (CH, C6), 62.8 (CH_2, C10), 59.3 (CH, C7), 27.5 (CH_3, C14), 25.4 (CH_2, C2), 20.7 (CH_3, C12); **IR** (neat, cm^{-1}) v_{max} 2957 (N-H stretch), 1777 (C=O lactam, stretch), 1699 (C=O ester, stretch), 1678 (C=O ester, stretch),

1150 (C-O ester, stretch); **LRMS** (ESI) $[M+H]^+$ calcd. for $[C_{14}H_{20}N_2O_5SNa]^+$ 351.1 observed 351.4.

Data in accordance with previous literature reports.[373]

Tert-butyl (6*R*,7*R*)-3-(acetoxymethyl)-7-(4-azidobenzamido)-8-oxo-5-thia-1-azabicyclo[4.2.0]oct-2-ene-2-carboxylate (31)

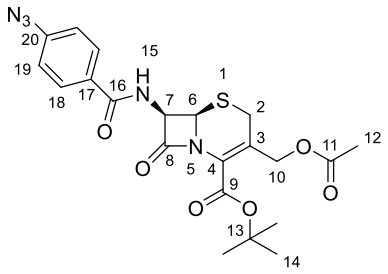

To a solution of **30** (416 mg, 1.27 mmol) in THF (31.2 mL) was added **29** (291 mg, 1.61 mmol, 1.2 eq.) and NEt_3 (229 µL, 1.61 mmol, 1.2 eq.). The reaction was stirred at rt for 2 h then a further 0.5 eq. of **29** (121 mg, 0.670 mmol, 0.5 eq.) was added to the reaction mixture. The reaction mixture was stirred for 1 h then the solvent was removed under reduced pressure. The crude product was purified by FCC on SiO_2 (0-50% EtOAc in PE 40-60) to give the title compound (315 mg, 0.665 mmol, 52%) as a yellow oil.

R_f 0.53 (50% EtOAc/PE 40-60); **^{1}H NMR** ($CDCl_3$, 400 MHz) δ 7.83 (2H, d, *J* = 8.6 Hz, H19 or 18), 7.08 (2H, d, *J* = 8.6 Hz, H19 or 18), 6.99 (1H, d, *J* = 8.7 Hz, H15), 6.01 (1H, dd, *J* = 4.8, 8.7 Hz, H7), 5.12 (1H, d, *J* = 13.3 Hz, H10), 5.07 (1H, d, *J* = 4.9 Hz, H6), 4.81 (1H, d, *J* = 13.3 Hz, H10), 3.59 (1H, d, *J* = 18.5 Hz, H2), 3.39 (1H, d, *J* = 18.5 Hz, H2), 2.09 (3H, s, H12), 1.53 (9H, s, H14); **^{13}C NMR** (101 MHz, $CDCl_3$) δ 170.7 (C=O, C9), 166.4 (C=O, C11), 164.5 (C=O, C16), 160.3 (C=O, C8), 144.3 (C, C20), 129.2 (CH, C19), 129.1 (C, C17), 127.3 (C, C3), 123.9 (C, C4), 119.2 (CH, C18), 83.9 (C, C13), 63.1 (CH_2, C10), 59.7 (CH, C6), 57.5 (CH, C7), 27.8 (CH_3, C14), 26.4 (CH_2, C2), 20.8 (CH_3, C12); **IR** (neat, cm^{-1}) ν_{max} 2987 (N-H, stretch), 2124 (N=N=N), 1776 (C=O lactam, stretch), 1735 (C=O, stretch), 1704 (C=O, stretch), 1646 (C=O, stretch), 1603 (aromatic C-H, stretch), 1148 (C-O ester, stretch); **HRMS** (ESI) $[M+Na]^+$ calcd. for $[C_{21}H_{23}N_5O_6SNa]^+$ 496.1270 observed 496.1269 (Δ = -0.2 ppm).

1-Azaneyl 7-(4-(*tert*-butoxycarbonyl)piperazin-1-yl)-1-cyclopropyl-6-fluoro-4-oxo-1,4-dihydroquinoline-3-carboxylate (32)

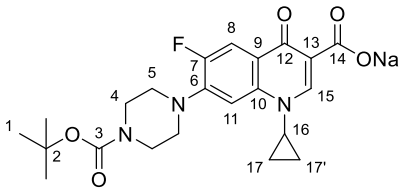

To a suspension of ciprofloxacin (1.00 g, 3.02 mmol) in 1 N NaOH (10 mL) and THF (20 mL) was added a solution of di-*tert*-butyl dicarbonate (720 mg, 3.32 mmol, 1.1 eq.) in THF (20 mL) dropwise at rt. The reaction mixture was stirred at rt for 18 h, then the solvent was removed under reduced pressure. The residue was taken up in H_2O (20 mL) and the pH adjusted to 7 with sat. aq. NH_4Cl solution. The resulting precipitate was filtered and washed with H_2O (1 × 10 mL) to give a white solid. The solid was suspended in MeOH/0.1 N NaOH (60 mL, 1:1) and heated to 30 °C for 45 min. The solvent was removed under reduced pressure, and the residue taken up in EtOH/H_2O (20 mL, 99:1) and evaporated 3 times. The solid was taken up in CH_2Cl_2 (20 mL) and the solvent removed under reduced pressure to give the title compound as a white solid (1.30 g, 2.87 mmol, 95%).

^{1}H NMR (400 MHz, $CDCl_3$) δ 8.76 (1H, s, H15), 8.02 (1H, d, *J* = 12.8 Hz, H8), 7.36 (1H, d, *J* = 7.0 Hz, H11), 3.67 (4H, appt. br. s, H4), 3.53 (1H, appt. br. s, H16), 3.29 (4H, appt. br. s, H5), 1.50 (9H, s, H1), 1.40-1.39 (2H, m, H17 or H17'), 1.21-1.23 (2H, m, H17 or H17'); **^{13}C NMR** (125 MHz, $CDCl_3$) δ 177.1 (C, C12), 166.9 (C, C14), 154.5 (C, C3), 153.6 (C, d, *J* = 250.4 Hz, C7), 147.5 (CH, C15), 145.8 (C, d, *J* = 11.25 Hz, C6), 139.0 (C, C10), 120.2 (C, d, *J* = 6.8 Hz, C9), 112.6 (CH, d, *J* = 23.6 Hz, C8), 108.2 (C, C13), 105.0 (CH, C11), 80.4 (C, C2), 49.8 (CH_2, C4 and C5), 35.3 (CH, C16), 28.4 (CH_3, C1), 8.3 (CH_2, C17 and C17'); **^{19}F NMR** (376 MHz, $CDCl_3$) δ -121.0; **IR** (neat, cm^{-1}) ν_{max} 2977 (carboxylic acid O-H, stretch), 1777 (C=O unsaturated, stretch), 1701 (C=O, stretch), 1681 (C=O, stretch), 1455 (O-H, bend), 1367 (aromatic C-N, stretch); **LRMS** (ESI) $[M+H]^+$ calcd. for $[C_{22}H_{27}{}^{19}FN_3O_5]^+$ 432.2 observed 432.1.

Data in accordance with previous literature reports.[333]

Ethyl 4-((4,6-dichloropyrimidin-2-yl)amino)butanoate (43)

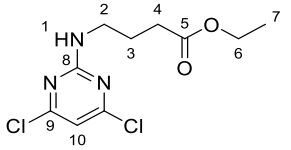

Prepared following *general method 1*, using 2,4,6-trichloropyrimidine (1.00 g, 5.45 mmol), ethyl-4-aminobutyrate hydrochloride (1.10 g, 6.54 mmol, 1.2 eq.) and NEt_3 (1.90 mL, 13.6

mmol, 2.5 eq.) in acetone (34 mL). The crude product was purified by FCC on SiO_2 (20-70% EtOAc in PE 40-60) to give the title compound as a light yellow solid (469 mg, 1.69 mmol, 31%).

R_f 0.48 (25% EtOAc/PE 40-60); **^{1}H NMR** (400 MHz, $CDCl_3$) δ 6.59 (1H, s, H10), 5.87 (1H, br. s, H1), 4.14 (2H, q, *J* = 7.1 Hz, H6), 3.49 (2H, q, *J* = 6.7 Hz, H2), 2.39 (2H, t, *J* = 7.2 Hz, H4), 1.94 (2H, p, *J* = 7.1 Hz, H3), 1.25 (3H, t, *J* = 7.1 Hz, H7); **^{13}C NMR** (101 MHz, $CDCl_3$) δ 173.2 (C, C5), 161.9 (C, C8), 161.8 (C, C9), 109.1 (CH, C10), 60.7 (CH_2, C6), 41.1 (CH_2, C2), 31.6 (CH_2, C4), 24.7 (CH_2, C3), 14.3 (CH_3, C7); **IR** (neat, cm^{-1}) ν_{max} cm^{-1} 2980 (aliphatic C-H stretch), 1705 (ester C=O stretch), (aliphatic C-H bend), 1375 (C-N stretch), 788 (aromatic C-Cl stretch); **HRMS** (ESI) $[M+H]^+$ calcd. for $[C_{10}H_{14}{}^{35}Cl_2N_3O_2]^+$ 278.0463 observed 278.0456 (Δ = -2.5 ppm)

Data in accordance with previous literature reports.[69]

Ethyl 4-((4,6-divinylpyrimidin-2-yl)amino)butanoate (42)

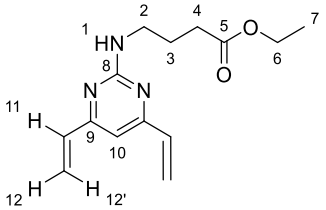

Prepared following *general method 2*, using **43** (301 mg, 1.08 mmol), K_2CO_3 (897 mg, 6.50 mmol, 6.0 eq.), potassium vinyl trifluoroborate (434 mg, 3.24 mmol, 3.0 eq.) and $PdCl_2(dppf)\cdot CH_2Cl_2$ (90.0 mg, 0.110 mmol, 0.1 eq.) in 1,4-dioxane (13 mL) and H_2O (1.4 mL). The crude product was purified by FCC on SiO_2 (25-50% EtOAc in PE 40-60) to give the title compound as a yellow oil (283 mg, 1.08 mmol, quant.).

R_f 0.58 (25% EtOAc/PE 40-60); **^{1}H NMR** (400 MHz, $CDCl_3$) δ 6.56 (2H, dd, *J* = 17.4, 10.6 Hz, H11), 6.51 (1H, s, H10), 6.34 (2H, d, *J* = 17.4 Hz, H12'), 5.54 (2H, dd, *J* = 10.6, 1.3 Hz, H12), 5.14 (1H, br. s, H1), 4.11 (2H, q, *J* = 7.2 Hz, H6), 3.52 (2H, q, *J* = 6.6 Hz, H2), 2.40 (2H, t, *J* = 7.4 Hz, H4), 1.95 (2H, p, *J* = 7.1 Hz, H3), 1.23 (3H, t, *J* = 7.2 Hz, H7); **^{13}C NMR** (101 MHz, $CDCl_3$) δ 173.5 (C, C5), 163.7 (C, C8), 162.6 (C, C9), 135.9 (CH, C11), 121.4 (CH_2, C12), 105.7 (CH, C10), 60.4 (CH_2, C6), 40.7 (CH_2, C2), 31.8 (CH_2, C4), 25.1 (CH_2, C3), 14.2 (CH_3, C7); **IR** (neat, cm^{-1}) ν_{max} 2977 (aromatic C-H, stretch), 2901 (alkene C-H, stretch), 1728 (C=O ester), 1539 (aromatic C=C, stretch), 936 (alkene C=C, bend); **HRMS** (ESI) $[M+H]^+$ calc. for $[C_{14}H_{20}N_3O_2]^+$ 262.1556 observed 262.1554 (Δ = – 0.8 ppm).

Data in accordance with previous literature reports.[69]

4-((4,6-Divinylpyrimidin-2-yl)amino)butanoic acid (41)

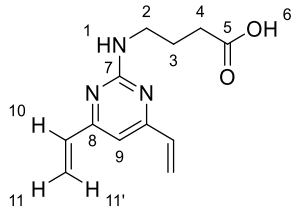

Prepared following *general method 3*, using **42** (190 mg, 0.727 mmol) and $LiOH{\cdot}H_2O$ (93.0 mg, 2.18 mmol, 3.0 eq.) in THF/H_2O (10 mL, 1:1). The reaction mixture was diluted with H_2O (5 mL), acidified to pH 5 with 1 N HCl and extracted with CH_2Cl_2 (3 × 10 mL). The combined organics were dried ($MgSO_4$) and evaporated under reduced pressure to give the title compound as a cream solid (100 mg, 0.430 mmol, 60%).

R_f 0.27 (EtOAc); **^{1}H NMR** (400 MHz, $CDCl_3$) δ 6.84-6.76 (1H, m, H1), 6.60-6.48 (3H, m, H9 and H10), 6.35-6.17 (2H, m, H11'), 5.59-5.57 (2H, m, H11), 3.59 (2H, q, *J* = 6.0 Hz, H4), 2.46 (2H, t, *J* = 6.8 Hz, H2), 2.02 (2H, p, *J* = 6.7 Hz, H3); **^{13}C NMR** (101 MHz, $CDCl_3$) 177.7 (C, C5), 163.9 (C, C8), 162.2 (C, C7), 135.3 (CH, C10), 122.4 (CH_2, C11), 104.0 (CH, C9), 40.9 (CH_2, C2), 32.4 (CH_2, C4), 25.0 (CH_2, C3); **IR** (neat, cm^{-1}) ν_{max} 3279 (N-H, stretch), 2929 (aromatic C-H stretch), 1702 (C=O ester, stretch), 1562 (aromatic C=C, stretch), 928 (alkene C=C, bend); **LRMS** (ESI) $[M-H]^-$ calc. for $[C_{12}H_{14}N_3O_2]^-$ 232.4 observed 232.1.

Data in accordance with previous literature reports.[69]

***Tert*-butyl (6*R*,7*R*)-3-(acetoxymethyl)-7-(4-((4,6-divinylpyrimidin-2-yl)amino)butanamido)-8-oxo-5-thia-1-azabicyclo[4.2.0]oct-2-ene-2-carboxylate (40)**

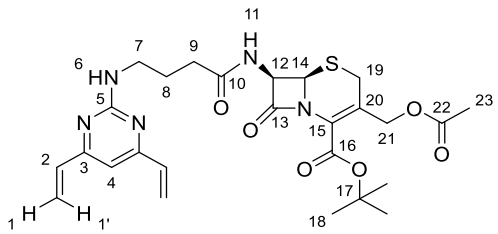

To a solution of **41** (808 mg, 3.47 mmol) in DMF (50 µL) was added DIPEA (1.205 mL, 6.94 mmol, 2.0 eq.) and HATU (2.415 g, 4.16 mmol, 1.2 eq.). To this was added **30** (1.138 g, 3.47 mmol, 1.0 eq.), and the reaction mixture was stirred at rt for 2 h. The reaction mixture was diluted with H_2O and the organic layer was washed with brine, then dried ($MgSO_4$) and concentrated *in vacuo* to give the crude product. The crude product was purified by FCC (C18 silica, eluted with 5-95% acetonitrile in 0.1 M NH_4OH) to give the title compound as a yellow oil (614 mg, 1.13 mmol, 47%).

R_f 0.24 (2% MeOH/CH_2Cl_2); **^{1}H NMR** (400 MHz, $CDCl_3$) δ 6.96 (1H, s, H4), 6.73 (2H, dd, *J* = 17.3, 10.6 Hz, H2), 6.50 (2H, dd, *J* = 17.3, 1.1 Hz, H1'), 5.68 (2H, dd, *J* = 10.6, 1.1 Hz, H1), 5.04 (1H, d, *J* = 12.8 Hz, H21), 4.94 (1H, d, *J* = 5.2 Hz, H12), 4.85-4.74 (3H, m, H21' and H14), 4.16-4.10 (2H, m, H7), 3.55 (1H, d, *J* = 18.2 Hz, H19), 3.35 (1H, d, *J* = 18.2 Hz, H19'), 2.70-2.62 (2H, m, H9), 2.15-2.10 (2H, m, H8), 2.08 (3H, s, H23), 1.54 (9H, s, H18); **^{13}C NMR** (101 MHz, $CDCl_3$) δ 174.2 (C=O), 173.3 (C=O), 171.2 (C=O), 170.6 (C=O), 164.0 (C, C3), 162.5 (C, C5), 135.2 (CH, C2), 127.4 (C, C20), 123.0 (CH_2, C1), 121.5 (C, C15), 110.6 (CH, C4), 83.8 (C, C17), 63.1 (CH_2, C21), 59.3 (CH, C14), 57.5 (CH, C12), 48.1 (CH_2, C7), 33.7 (CH2, C9), 27.8 (CH_3, C18), 26.5 (CH2, C8), 25.6 (CH_2, C19), 20.8 (CH_3, C23); **IR** (neat, cm^{-1}) ν_{max} 2971 (aromatic, C-H stretch), 2923 (N-H, stretch), 1780 (C=O, stretch), 1719 (C=O, stretch), 1684 (C=O, stretch), 1635 (conjugated C=C, stretch); **HRMS** (ESI) $[M+H]^+$ calcd. for $[C_{26}H_{34}N_5O_6S]^+$ 544.2230 observed 544.2216 (Δ = -2.6 ppm).

Tert-butyl (6*R*,7*R*)-7-(4-((4,6-divinylpyrimidin-2-yl)amino)butanamido)-3-(hydroxymethyl)-8-oxo-5-thia-1-azabicyclo[4.2.0]oct-2-ene-2-carboxylate (39)

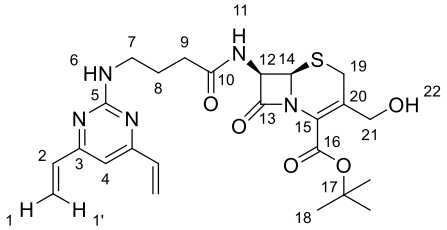

40 (65 mg, 0.120 mmol) was dissolved in anhydrous THF (640 µL) and anhydrous hexanes (5.77 mL) were added to make a suspension. To this was added *s*-BuOH (213 µL, 2.28 mmol, 19.0 eq.), CAL B lipase (267 mg) and 4 Å molecular sieves (54 mg). The reaction mixture was heated to 50 °C in a heated incubator for 3 days. The reaction mixture was diluted with CH_2Cl_2 (1 mL), filtered and the filtrate was evaporated under reduced pressure to give the crude product as an orange oil (47 mg, 0.0934 mmol, 78%) which was taken on without further purification.

R_f 0.45 (25% EtOAc/PE 40-60); **^{1}H NMR** (400 MHz, MeOD) δ 6.72 (1H, s, H4), 6.64 (2H, dd, *J* = 17.4, 10.7 Hz, H2), 6.39 (2H, appt. d, *J* = 16.8 Hz, H1'), 5.74-5.4 (3H, m, H1 and H14), 5.13-5.27 (1H, m, H22), 5.07-4.94 (1H, m, H12), 4.43-4.08 (2H, m, H21), 3.54-3.48 (2H, m, H7), 3.55-3.47 (2H, m, H19), 2.45-2.37 (2H, m, H9), 2.09-1.93 (2H, m, H8); **^{13}C NMR** (125 MHz, $CDCl_3$) δ 169.9 (C=O),168.0 (C=O), 166.6 (C=O), 164.7 (C, C3), 164.0 (C, C5), 135.1 (CH, C2), 129.7 (C, C20), 123.5 (C, C15), 123.3 (CH_2, C1), 110.6 (CH, C4), 84.2 (C, C17), 65.1 (CH, C14), 60.2 (CH, C12), 53.5 (C19), 48.1 (CH_2, C7), 33.7 (CH_2, C9), 29.7 (CH_3, C18), 28.0 (CH_2, C8), 22.7 (CH_2, C19); **IR** (neat, cm^{-1}) ν_{max} 2925 (aromatic, C-H stretch), 2920 (N-H, stretch), 1757 (C=O, stretch), 1681 (C=O, stretch), 1660 (C=O, stretch), 1640 (conjugated

C=C, stretch); **HRMS** (ESI) $[M+H]^+$ calcd. for $[C_{24}H_{32}N_5O_5S]^+$ 502.2124 observed 502.2122 (Δ = -0.40 ppm).

Ethyl 1-cyclopropyl-6-fluoro-4-oxo-7-(piperazin-1-yl)-1,4-dihydroquinoline-3-carboxylate (44)

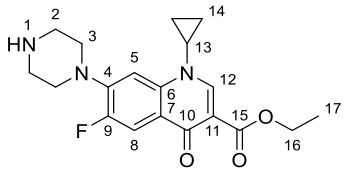

Ciprofloxacin hydrochloride (500 mg, 1.36 mmol) was dissolved in EtOH (9 mL) and sulfuric acid (conc., 200 µL, cat.) was added dropwise. The reaction mixture was heated to reflux for 48 h then cooled to rt. The solvent was removed under N_2 and the residue taken up in sat. aq. $NaHCO_3$ and extracted with CH_2Cl_2 (4 × 5 mL). The combined organics were dried ($MgSO_4$) and evaporated under reduced pressure to give the title compound as a cream solid (328 mg, 0.913 mmol, 67%)

^{1}H NMR (400 MHz, $CDCl_3$) δ 8.49 (1H, s, H12), 7.98 (1H, d, *J* = 13.4 Hz, H8), 7.25 (1H, d, *J* = 7.2 Hz, H5), 4.37 (2H, q, *J* = 7.2 Hz, H16), 3.44 (1H, sept., *J* = 4.0 Hz, H13), 3.26-3.21 (4H, m, H3), 3.13-3.07 (4H, m, H2), 1.40 (3H, t, *J* = 7.2 Hz, H17), 1.35-1.29 (2H, m, H14), 1.17-1.11 (2H, m, H14); **^{13}C NMR** (101 MHz, $CDCl_3$) δ 173.1 (C=O, *d*, *J* = 2.2 Hz, C10), 165.7 (C=O, C15), 153.3 (C, d, *J* = 249.5 Hz, C9), 148.0 (CH, C12) 144.9 (C, d, *J* = 10.6 Hz, C4), 137.9 (C, d, *J* = 1.2 Hz, C6), 122.8 (C, d, *J* = 7.1 Hz, C7), 113.1 (CH, d, *J* = 23.3 Hz, C8), 110.2 (C, C11), 104.7 (CH, d, *J* = 3.2 Hz, C5), 60.7 (CH_2, C16), 51.0 (CH_2, d, *J* = 4.5 Hz, C3), 45.9 (CH_2, C2), 34.4 (CH, C13), 14.4 (CH_3, C17), 8.0 (CH_2, C14); **^{19}F NMR** (376 MHz, $CDCl_3$) δ -123.6; **IR** (neat, cm^{-1}) ν_{max} cm^{-1} 2988 (alkene C-H, stretch), 2901 (N-H, stretch), 1718 (C=O, stretch), 1617 (C=O, stretch), 1589 (C=C, stretch), 1254 (ester C-O, stretch); **LRMS** (ESI) $[M+H]^+$ calcd. for $[C_{19}H_{23}FN_3O_3]^+$ 360.2 observed 360.5.

Data in accordance with previous literature reports.[341]

7-(4-((((6*R*,7*R*)-2-(*tert*-butoxycarbonyl)-7-(4-((4,6-divinylpyrimidin-2-yl)amino)butanamido)-8-oxo-5-thia-1-azabicyclo[4.2.0]oct-2-en-3-yl)methoxy)carbonyl)piperazin-1-yl)-1-cyclopropyl-6-fluoro-4-oxo-1,4-dihydroquinoline-3-carboxylic acid (37)

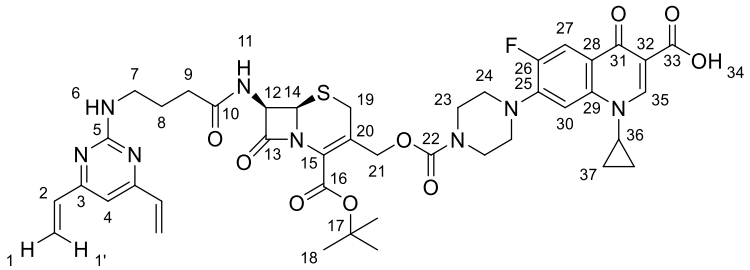

Step 1: **39** (145 mg, 0.290 mmol) was dissolved in DMF (1.4 mL) and DIPEA (252 mL, 1.97 mmol, 5.0 eq.) and bis(4-nitrophenyl)carbonate (176 mg, 0.580 mmol, 2.0 eq.) were added. The reaction mixture was stirred at rt for 48 h then diluted with H_2O. The organic layer was washed with brine, sat. aq. $NaHCO_3$, 1 N KOH (1 × 1 mL each), the organic layer was dried ($MgSO_4$) and concentrated *in vacuo* to give a dark brown residue.

Step 2: A suspension of ciprofloxacin (101 mg, 0.305 mmol, 1.05 eq.) and $NaHCO_3$ (122 mg, 1.45 mmol, 5.0 eq.) in H_2O (1.8 mL) was heated to 45 °C for 40 min then cooled to rt. To this was added a solution of the dark brown residue from step 1 in 1,4-dioxane (1.8 mL). The reaction was stirred at rt for 2 h then H_2O (1 mL) and diethyl ether (1 mL) were added. The aqueous portion was extracted with diethyl ether, CH_2Cl_2 and EtOAc (2 × 1 mL of each), and the combined organics were dried ($MgSO_4$) and evaporated *in vacuo*. The resulting residue was purified by FCC on C18 silica (eluted with 5-95% MeCN in 0.1 N NH_4OH) and lyophilised to give the title compound as a cream solid (10.0 mg, 0.0116 mmol, 4%).

R_f 0.55 (25% EtOAc/PE 40-60); **^{1}H NMR** (400 MHz, $CDCl_3$) δ 8.81-8.76 (1H, m, H35), 8.30-8.22 (1H, m, H27), 8.12-8.02 (1H, m, H27), 7.35-7.28 (1H, m, H30), 6.63-6.46 (3H, m, H2 and H4), 6.40-6.30 (3H, m, H1b and H30), 5.69-5.62 (1H, m, H12), 5.61-5.54 (2H, m, H1'), 5.32-5.28 (1H, m, H14), 5.09-4.90 (2H, m, H19 or 21), 4.75-4.55 (2H, m, H19 or 21), 3.76-3.66 (1H, br. s, H36), 3.61-3.49 (4H, m, H23), 3.50-3.02 (4H, m, H24), 2.41-2.35 (2H, m, H7), 2.09-1.94 (2H, m, H9); 1.54-15.1 (9H, m, H18); 1.44-1.35 (2H, m, H37), 1.30-1.20 (2H, m, H37); **^{13}C NMR** (101 MHz, $CDCl_3$) δ 173.0 (C=O, C31), 172.7 (C10), 170.5 (C=O, C16), 166.0 (C=O, C33), 165.9 (C=O, C13), 164.9 (C, C3), 164.4 (C, C5), 160.4 (C=O, C22), 154.5 (C, C26), 148.2 (CH, C35), 145.6 (C, C25), 135.7 (C, C29), 135.7 (CH, C2), 125.2 (C, C20), 125.0 (C, C15), 122.2 (C, C28), 121.5 (CH_2, C1), 119.6 (CH, C27), 108.3 (C, C32), 105.5 (CH, C4), 105.4 (CH, C30), 83.9 (C, C17), 65.5 (CH_2, C21), 60.4 (CH, C12 or C14), 53.5 (CH, C12 or C14), 50.8 (CH_2, C24), 50.7 (CH_2, C24), 40.5 (CH_2, C7), 40.5 (CH_2, C23), 35.3 (CH, C36), 33.3 (CH_2, C9), 27.9 (CH_3, C18), 26.4 (CH_2, C19), 25.5 (CH_2, C8), 8.2 (CH_2, C37); **IR** (neat, cm^{-1}) ν_{max} 3121 (O-H stretch), 2937 (N-H, stretch), 1779 (C=O, stretch), 1723 (C=O, stretch),

1719 (C=O, stretch), 1626 (C=O, stretch), 1545 (C=C, stretch), 1457 (O-H, bend), 1209 (C-F, stretch); **HRMS** (ESI) $[M+H]^+$ calcd. for $C_{42}H_{48}FN_8O_9S$ 859.3249 observed 859.3271 (Δ = 2.6 ppm).

Ethyl 1-cyclopropyl-7-(4-(4-((4,6-divinylpyrimidin-2-yl)amino)butanoyl)piperazin-1-yl)-6-fluoro-4-oxo-1,4-dihydroquinoline-3-carboxylate (47)

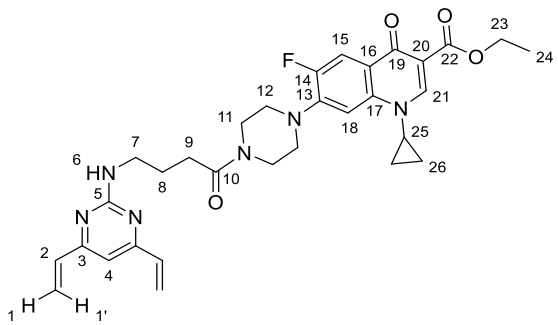

To a suspension of **41** (50.0 mg, 0.215 mmol), **44** (69.0 mg, 0.193 mmol, 0.9 eq.) and NEt_3 (75 µL, 0.539 mmol, 2.0 eq.) in DMF (2.2 mL) was added T3P (50% in DMF, 192 µL, 0.323 mmol, 1.5 eq.). The reaction mixture was stirred at rt for 18 h. The reaction mixture was poured onto H_2O (30 mL) and washed with sat. aq. $NaHCO_3$ solution (1 × 5 mL), 10% aq. citric acid solution (1 × 5 mL), 5% aq. LiCl solution (10 × 5 mL). The organic layer was dried ($MgSO_4$) and evaporated *in vacuo* to give the crude product as a cream solid (42.0 mg, 0.0731 mmol, 34%), which was used without further purification.

R_f 0.10 (2% MeOH/CH_2Cl_2); **^{1}H NMR** (400 MHz, $CDCl_3$) δ 8.53 (1H, s, H21), 8.06 (1H, d, *J* = 13.2 Hz, H15), 7.24 (1H, d, *J* = 7.0 Hz, H18), 6.60-6.52 (3H, m, H4 and H2), 6.35 (2H, d, *J* = 17.3 Hz, H1'), 5.55 (2H, dd, *J* = 10.6, 1.4 Hz, H1), 5.26-5.19 (1H, m, H6), 4.39 (2H, q, *J* = 7.12 Hz, H23), 3.84 (2H, t, *J* = 4.6 Hz, H11), 3.64 (2H, t, *J* = 4.2 Hz, H11), 3.57 (2H, q, *J* = 6.4 Hz, H7), 3.40 (1H, appt. s, *J* = 3.2 Hz, H25), 3.20 (4H, t, *J* = 4.9 Hz, H12), 2.50 (2H, t, *J* = 7.3 Hz, H9), 2.03 (2H, p, *J* = 6.8 Hz, H8), 1.40 (3H, t, *J* = 7.1 Hz, H24), 1.35-1.27 (2H, m, H26), 1.16-1.10 (2H, m, H26); **^{13}C NMR** (125 MHz, $CDCl_3$) δ 173.1 (C=O, C19), 171.3 (C=O, C10), 165.9 (C=O, C22), 163.7 (C, C3), 162.7 (C, C5), 153.3 (C, d, *J* = 247.1 Hz, C14), 148.2 (CH, C21), 144.0 (C, d, *J* = 10.6 Hz, C13), 138.0 (C, d, *J* = 1.1 Hz, C17), 135.9 (CH, C2), 123.6 (C, d, *J* = 7.0 Hz, C16), 121.5 (CH_2, C1), 113.6 (CH, d, *J* = 22.9 Hz, C15), 110.7 (C, C20), 105.7 (CH, C4), 105.0 (CH, d, *J* = 2.6 Hz, C18), 61.0 (CH_2, C23), 50.5 (CH_2, d, *J* = 5.6 Hz, C12), 49.6 (CH_2, d, *J* = 2.9 Hz, C12), 45.4 (CH_2, C11), 41.3 (CH_2, C11), 41.0 (CH_2, C7), 34.5 (CH, C25), 30.6 (CH_2, C9), 25.2 (CH_2, C8), 14.4 (CH_3, C24), 8.2 (CH_2, C26); **^{19}F NMR** (376 MHz, $CDCl_3$) δ -123.9; **IR** (neat, cm^{-1}) ν_{max} 2988 (aromatic C-H, stretch), 2901 (N-H, stretch), 1777 (C=O, stretch), 1735 (C=O, stretch), 1709 (C=O, stretch), 1647 (conjugated C=C, stretch), 1380 (C-

F, stretch); **HRMS** (ESI) $[M+H]^+$ calcd. for $[C_{31}H_{36}{}^{19}FN_6O_4]^+$ 575.2782 observed 575.2765 (Δ = -2.1 ppm).

1-Cyclopropyl-7-(4-(4-((4,6-divinylpyrimidin-2-yl)amino)butanoyl)piperazin-1-yl)-6-fluoro-4-oxo-1,4-dihydroquinoline-3-carboxylic acid (45)

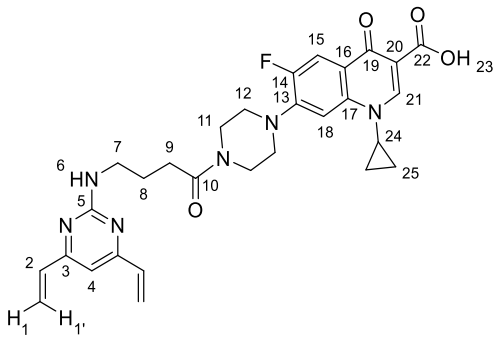

Prepared following *general method 3*, with **47** (25.0 mg, 0.0436 mmol) and $LiOH{\cdot}H_2O$ (2.00 mg, 0.0477 mmol, 1.1 eq.) in THF/H_2O (1:1, 588 µL). The reaction mixture was washed with diethyl ether (1 × 1 mL), the aqueous phase acidified to pH 4 using 1 N HCl and extracted with CH_2Cl_2 (5 × 2 mL). The combined organics were dried and evaporated to give the title compound as a cream solid (11.0 mg, 0.0201 mmol, 46%).

R_f 0.08 (2% MeOH/CH_2Cl_2); **^{1}H NMR** (400 MHz, $CDCl_3$) δ 14.91 (1H, s, H23), 8.79 (1H, s, H21), 8.06 (1H, d, *J* = 12.9 Hz, H15), 7.34 (1H, d, *J* = 6.6 Hz, H18), 6.61-6.52 (3H, dd and s, *J* = 17.4, 10.7 Hz, H2 and H4), 6.35 (2H, d, *J* = 17.0 Hz, H1'), 5.56 (2H, dd, *J* = 10.6, 1.4 Hz, H1), 5.40-5.33 (1H, m, H6), 3.89-3.83 (2H, m, H11), 3.70-3.64 (2H, m, H11), 3.58 (2H, q, *J* = 6.4 Hz, H7), 3.55-3.49 (1H, m, H24), 3.32-3.24 (4H, m, H12), 2.51 (2H, t, *J* = 7.3 Hz, H9), 2.04 (2H, p, *J* = 6.9 Hz, H8), 1.43-1.53 (2H, m, H25), 1.23-1.17 (2H, m, H25); **^{13}C NMR** (101 MHz, $CDCl_3$) δ 177.2 (C=O, C19), 171.3 (C=O, C10), 166.9 (C=O, C22), 163.7 (C, C3), 162.6 (C, C5), 153.6 (C, d, *J* = 249.2 Hz, C14), 147.6 (CH, C21), 145.4 (C, d, *J* = 10.1 Hz, C13), 139.0 (C, d, *J* = 1.0 Hz, C17), 135.8 (CH, C2) 121.6 (C, C16), 120.5 (CH_2, C1), 112.7 (CH, d, *J* = 23.7 Hz, C15), 108.4 (C, C20), 105.6 (CH, C4), 105.0 (CH, d, *J* = 3.3 Hz, C18), 50.2 (CH_2, d, *J* = 6.3 Hz, C12), 49.4 (CH_2, d, *J* = 2.7 Hz, C12) 45.2 (CH_2, C11), 41.2 (CH_2, C11), 41.0 (CH_2, C7), 35.3 (CH, C24) 30.5 (CH_2, C9), 25.1 (CH_2, C8), 8.3 (CH_2, C25); **^{19}F NMR** (376 MHz, $CDCl_3$) δ -121.16; **IR** (neat, cm^{-1}) ν_{max} 3038 (aromatic C-H, stretch), 2922 (N-H, stretch), 1732 (C=O, stretch), 1728 (C=O, stretch), 1625 (C=O, stretch), 1556 (C=C, stretch), 1212 (C-F, stretch); **HRMS** (ESI) $[M+H]^+$ calcd. for $[C_{29}H_{32}{}^{19}FN_6O_4]^+$ 547.2469 observed 547.2470 (Δ = 1.2 ppm).

4.1.3 Peptide synthesis and stapling procedures

Solid Phase Peptide Synthesis (SPPS): For all peptides, a Rink Amide MBHA low-loading resin (0.19-0.51 mmol/g, 100−200 mesh) was used to afford *C*-terminal amides upon cleavage from the resin. Fmoc-protected amino acids were employed and the following side chain protecting groups were used: 2,2,4,6,7-pentamethyldihydrobenzofuran-5-sulfonyl (Arg), triphenylmethyl (Asn, Gln, Cys), *tert*-butyl (Asp, Glu, Ser, Thr, Tyr) and Boc (His, Lys, Trp). The chloranil qualitative amine test was used to assess the completion of coupling and deprotection reactions: colourless resin indicated an Fmoc-protected peptide, a blue/green resin colour indicated a free *N*-terminus.[170]

Manual SPPS: Amide coupling was conducted using Fmoc-protected amino acids (5.0 eq.), HATU (5.0 eq.), DIPEA (10.0 eq.) in the minimum amount of DMF at rt with agitation. Fmoc deprotection was carried out with 20% piperidine in DMF at rt with agitation. If required, *N*-terminal capping was performed with acetic anhydride or octanoyl chloride (5.0 eq.) and DIPEA (10.0 eq.) in CH_2Cl_2 at rt with agitation.

Automated SPPS: Automated SPPS was carried out on solid-phase using a Fmoc-protecting group strategy on a CEM Liberty Blue® automated microwave peptide synthesiser. Arginine was coupled using double couplings for 15 min each without microwave irradiation. All other amino acids were coupled using double couplings with 25 W power at 75 ^{o}C for 15 min. Fmoc deprotection was carried out with 20% piperidine in DMF, using 45 W power at 75 ^{o}C over 3 min. If required, the *N*-terminus of the peptide was capped by acetylation using 20% acetic anhydride or octanoyl chloride solution in DMF solution at rt for 20 min.

Resin cleavage: Peptides were cleaved from the resin in either a TFA cocktail containing TFA/H_2O/TIPS/CH_2Cl_2 (92.5:2.5:2.5:2.5) or TFA/TIPS/H_2O/EDT (94:1:2.5:2.5). Cleavage was performed at 40 ˚C for 45 min, and the resin filtered. The eluate was dried, and the cleaved peptide was precipitated with cold diethyl ether and dried. The crude peptide was purified by preparative HPLC. The purified peptides were lyophilised, the mass analysed by LCMS and the purity determined by analytical HPLC.

General procedure for two-component CuAAC peptide stapling: The double-click reaction was used to cross-link the azido functionalised peptides with dialkynyl functionalised linkers. All solvents for the reaction were degassed with N_2 for 30 min before use. The dialkynyl linker (1.1 eq.) was added to the diazido peptide in H_2O/*tert*-butanol (1:1) under N_2 before the addition of a solution of $CuSO_4 \cdot 5H_2O$ (1.0 eq.), tris(3-hydroxypropyltriazolylmethyl)amine (THPTA, 1.0 eq.), and sodium ascorbate (3.0 eq.) in H_2O. The reaction mixture was stirred at rt and monitored by LCMS and HPLC. One the starting material had been consumed, the

reaction was lyophilised, and the crude product purified by preparative HPLC. The purified stapled peptide was lyophilised and analysed by LCMS and analytical HPLC.

General procedure for Cys-DVP peptide stapling: The Cys-DVP reaction was used to cross-link the cysteine-containing peptides with DVP linkers. The peptide was dissolved in MES buffer (pH 6, 50 mM) and DMF (1:3, 2 mg/mL of peptide). The DVP linker (1.1 eq.) was added as a stock solution (5- mg/mL, DMF/MES buffer (pH 6, 50 mM), 1:1). The reaction was stirred at rt and monitored by analytical HPLC and LCMS. Additional linker was added if necessary. Once the starting material had been consumed the solvent was removed under N_2, and the crude product purified by preparative HPLC. The purified stapled peptide was lyophilised and analysed by LCMS and analytical HPLC.

4.1.4 Peptide analysis

4.1.4.1 Peptide mass spectrometry data

*Table 24 Peptide sequence, mass spectrometry and analytical HPLC data for Chapter 2 peptides. All peptides are C-terminal amides and acetyl capped. X = Orn(N_3), X_6, X_{10} and X_{11} = stapled between Orn(N_3) with linkers **6**, **10** and **11** respectively. ND = purity not determined.*

Peptide	Sequence	Mass	m/z found	m/z calcd.	Species	% Purity†	Retention time (min)†
P1	Ac-IARKLQCIADQFHRL	1853.2	927.6	927.6	$[M+2H]^{2+}$	>99	7.9
P2	Ac-IGAQLRRMADDLNAQY	1876.1	939.0	939.1	$[M+2H]^{2+}$	>99	7.9
P3	Ac-CATQLRRFGDKLNFR	1866.1	934.0	934.1	$[M+2H]^{2+}$	>99	6.9
P4	Ac-IAXKLQCIADQFHXL	1819.9	911.6	911.0	$[M+2H]^{2+}$	>99	9.3
P5	Ac-IGXQLRRMADDLNXQY	2013.0	2013.4	2013.0	$[M+H]^{+}$	94	8.3
P6	Ac-CAXQLRRFGDKLNXR	1897.0	950.3	949.5	$[M+2H]^{2+}$	>99	9.3
P4-6	Ac-IAX_6KLQCIADQFHX_6L	1993.0	997.7	997.5	$[M+2H]^{2+}$	92	9.3
P5-6	Ac-IGX_6QLRRMADDLNX_6QY	2229.5	1115.8	1115.5	$[M+2H]^{2+}$	90	8.5
P6-6	Ac-CAX_6QLRRFGDKLNX_6R	2113.4	1057.7	1057.5	$[M+2H]^{2+}$	ND††	7.3
P8	Ac-IARKLQXIADQFHXL	1874.2	1875.0	1875.2	$[M+H]^{+}$	>99	8.6
P9	Ac-IGAXLRRMADXLNAQY	1913.2	957.7	957.5	$[M+2H]^{2+}$	94	9.6
P10	Ac-CATQLRXFGDKLNXR	1843.1	922.5	922.5	$[M+2H]^{2+}$	95	9.6
P11	Ac-IATQLRXFGDKLNXR	1853.1	1854.6	1854.1	$[M+H]^{+}$	92	8.5
P8-10	Ac-IARKLQX_{10}IADQFHX_{10}L	2044.4	1023.4	1023.2	$[M+2H]^{2+}$	>99	10.4
P9-10	Ac-IGAX_{10}LRRMADX_{10}LNAQY	2083.4	1042.9	1042.7	$[M+2H]^{2+}$	97	8.9
P11-10	Ac-IATQLRX_{10}FGDKLNX_{10}R	2023.3	1012.7	1012.6	$[M+2H]^{2+}$	94	8.0
P8-11	Ac-IARKLQX_{11}IADQFHX_{11}L	2739.3	1370.6	1370.5	$[M+2H]^{2+}$	92	8.4
P9-11	Ac-IGAX_{11}LRRMADX_{11}LNAQY	2777.3	1390.0	1389.6	$[M+2H]^{2+}$	91	8.3
P11-11	Ac-IATQLRX_{11}FGDKLNX_{11}R	2717.2	907.1	906.7	$[M+3H]^{3+}$	>99	7.5
11	**10**-Ahx-Ahx-(D)R-(D)R-(D)R	864.1	864.9	864.0	$[M+H]^{+}$	97	7.4

†Purity and retention time determined by analytical HPLC (5-95% MeCN in H_2O run over 15 min).
††Due to the broad signal an accurate purity could not be determined. See Appendix 2 for HPLC spectrum.

*Table 25 Peptide sequence, mass spectrometry and analytical HPLC data for Chapter 3 peptides. All peptides are C-terminal amides and have an uncapped N-terminus unless otherwise specified; Ac = acetyl capped, C8 = capped with octanoyl chloride. C_{17} = stapled with linker **17**. C_{18} = Cys capped with reagent **18**, C_{45} = stapled with linker **45**.*

Peptide	Sequence	Mass	m/z found	m/z calcd.	Species	% Purity†	Retention time (min)†
AMP1	Ac-TLKQFCKGVGKWCVK	1766.2	884.4	884.1	$[M+2H]^{2+}$	84	6.9
AMP2	FCKWAFKWCKK	1473.9	738.1	738.0	$[M+2H]^{2+}$	86	9.9
AMP3	Ac-WCLKKFRGCF	1328.7	665.4	665.3	$[M+2H]^{2+}$	85	7.9
AMP4	RFRRLCKKWRKRCKKI	2204.8	735.9	735.9	$[M+3H]^{3+}$	>99	5.9
AMP5	C8-GCLKFIKKCL	1277.7	1278.8	1278.7	$[M+H]^{+}$	95	10.2
AMP6	KWVQNYCKHLGRKCHTLKT	2341.2	1171.6	1171.4	$[M+2H]^{2+}$	>99	6.0
AMP7	NLFRKLCHRLFRRCFGYTLR	2599.2	867.2	867.4	$[M+3H]^{3+}$	95	5.7
AMP1-17	Ac-TLKQFC$_{17}$KGVGKWC$_{17}$VK	2031.1	1016.7	1016.6	$[M+2H]^{2+}$	94	8.5
AMP2-17	FC$_{17}$KWAFKWC$_{17}$KK	1737.9	1739.8	1739.2	$[M+H]^{+}$	97	7.6
AMP3-17	Ac-WC$_{17}$LKKFRGC$_{17}$F	1592.8	1594.5	1594.0	$[M+H]^{+}$	98	9.0
AMP4-17	RFRRLC$_{17}$KKWRKRC$_{17}$KKI	2470.2	1236.3	1236.1	$[M+2H]^{2+}$	95	9.4
AMP5-17	C8-GC$_{17}$LKFIKKC$_{17}$L	1541.9	1543.5	1543.1	$[M+H]^{+}$	98	7.0
AMP6-17	KWVQNYC$_{17}$KHLGRKC$_{17}$HTLKT	2607.4	2608.8	2608.2	$[M+H]^{+}$	82	7.8
AMP7-17	NLFRKLC$_{17}$HRLFRRC$_{17}$FGYTLR	2864.5	1433.3	1433.3	$[M+2H]^{2+}$	>99	8.9
AMP1-18	Ac-TLKQFC$_{18}$KGVGKWC$_{18}$VK	2008.5	1005.2	1005.0	$[M+2H]^{2+}$	>99	6.9
AMP2-18	FC$_{18}$KWAFKWC$_{18}$KK	1716.2	858.9	858.4	$[M+2H]^{2+}$	>99	6.7
AMP3-18	Ac-WC$_{18}$LKKFRGC$_{18}$F	1571.0	786.2	786.5	$[M+2H]^{2+}$	87	7.2
AMP4-18	RFRRLC$_{18}$KKWRKRC$_{18}$KKI	2447.1	816.6	816.3	$[M+3H]^{3+}$	>99	6.0
AMP5-18	C8-GC$_{18}$LKFIKKC$_{18}$L	1520.0	1518.8	1518.9	$[M-H]^{-}$	>99	7.5
AMP6-18	KWVQNYC$_{18}$KHLGRKC$_{18}$HTLKT	2583.4	1291.3	1291.6	$[M-2H]^{2-}$	>99	6.0
AMP7-18	NLFRKLC$_{18}$HRLFRRC$_{18}$FGYTLR	2841.5	711.3	711.4	$[M+4H]^{4+}$	96	7.8
AMP2a	FAKWAFKWLKK	1451.9	1452.8	1452.8	$[M+H]^{+}$	93	4.8
AMP4a	RFRRLRKKWRKRLKKI	2268.9	757.1	757.3	$[M+3H]^{+}$	90	6.3
AMP6a	KWVQNYMKHLGRKAHTLKT	2339.8	1170.9	1170.5	$[M+2H]^{2+}$	96	6.4
AMP2-45	FC$_{45}$KWAFKWC$_{45}$KK	2021.5	2021.0	2021	$[M+H]^{+}$	>99	7.5

†Purity determined by analytical HPLC (5-95% MeCN in H_2O run over 15 min).

Table 26 SPPS yields for linear peptides after HPLC purification.

Peptide	Amount of resin used (mg)	Amount of resin used (mmol)	Yield of peptide (mg)	Yield of peptide (%)
P1	294	0.1	21*	22*
P2	294	0.1	19*	20*
P3	294	0.1	25	13
P4	301	0.1	15	8
P5	301	0.1	20	10
P6	400	0.1	4.2	2
P8	735	0.25	81	17
P9	735	0.25	154	22
P10	735	0.25	9.2	2
P11	301	0.1	15	8
11	758	0.25	52*	48*
AMP1	490	0.25	57	13
AMP2	490	0.25	78	21
AMP3	490	0.25	51	15
AMP4	490	0.25	30	5
AMP5	490	0.25	29	9
AMP6	490	0.25	14	2
AMP7	490	0.25	35	5
AMP2a	196	0.1	21*	28*
AMP4a	196	0.1	19*	16*
AMP6a	196	0.1	13*	11*

*Yield of peptide cleaved and purified from half of the resin. The % yield has been multiplied by 2 to correct for this.

4.1.4.2 Circular dichroism spectroscopy

Circular dichroism spectroscopy was performed with an Aviv 410 circular dichroism spectropolarimeter. Data was collected between 185-250 nm at 298 K with the following parameters: 1.0 nm bandwidth, 0.5 s averaging time, 1.0 nm wavelength step in a quartz cuvette with a 1 mm path length. Pure, lyophilised peptides were dissolved in either MeCN/H_2O (1:1), SDS (30 mM), TFE (50% aq. solution) or NaPi (10 mM, pH 7.4) to an approximate concentration of 100 µL. The recorded spectra are a smoothed average of three scans, normalised against the solvent used.

The ellipticity recorded was normalised against the ellipticity recorded at 207 nm, and the α-helicity calculated using the following equation, where E_{193} and E_{211} are the ellipticities recorded at these wavelengths (in nm):[176,175]

$$\%\,\alpha\,helicity = 27.58 - (14.46 \times E_{193}) + \left(1.86 \times {E_{193}}^2\right) - (5.66 \times E_{211}) - (14.72 \times {E_{211}}^2)$$

4.2 General biological procedures

4.2.1 Flow cytometry assay procedures

Ethical approval was obtained from the Faculty Research Ethics Committee at Anglia Ruskin University, Cambridge, UK where the experiments were carried out. Unless otherwise stated, the experiments were performed on no fewer than three separate occasions using platelets from different donors. Data were analysed using AccuriC6 BD Software and GraphPad Prism. The following reagents were used: Annexin-V-PE (BD Biosciences, UK), anti-PAC-1 (BD Biosciences, UK), anti-CD62P (BD Pharmingen, UK), or anti-CD63 (BD Pharmingen, UK). Peptides and ABT737 were stored as 1 mM DMSO stock solutions.

Preparation of washed platelet suspension:[v] Human blood was collected from healthy volunteers, who had not taken medication for two weeks, following informed consent in accordance with the Declaration of Helsinki. Blood was collected into 11 mM sodium citrate and washed platelets were prepared as follows: Platelet-rich plasma was obtained by centrifugation (240 g, 15 min). Prostaglandin E1 (2 µM) was added to prevent premature platelet activation, and the plasma was centrifuged at 640 g for 15 min. Platelets were suspended in calcium-free Tyrode's buffer (CFT buffer, containing: 140 mM NaCl, 5 mM KCl, 10 mM HEPES, 5 mM glucose, 0.42 mM NaH_2PO_4, 12 mM $NaHCO_3$, titrated to pH 7.4 with NaOH) to a final concentration of 2×10^8 platelet/mL and rested at 37 °C for 1 h.

Flow cytometry: Treated washed platelet suspensions were analysed by flow cytometry using a C6 Accuri Flow Cytometer (Beckton Dickinson, UK). At least 10,000 events were acquired per experiment. In all the experiments, the entire platelet population was primarily gated by forward scatter (FSC). Untreated platelets (no fluorescent markers, no compounds) were analysed by flow cytometer on the laser of interest and the measurement used as *zero*. The shift of the peak of treated platelets towards the right was normalised against untreated platelets.

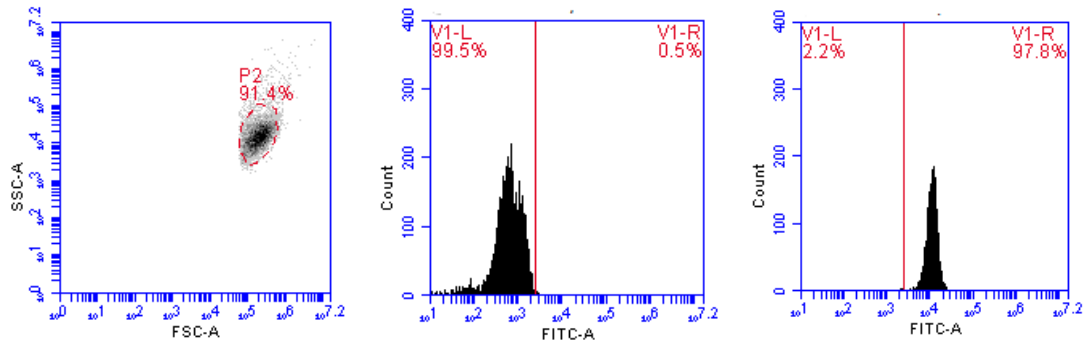

[v] Performed by Dr. Niaz Ahmed, Anglia Ruskin University.

Figure 83 Data normalisation for flow cytometry of washed platelet suspensions. A) An example of untreated platelets with gating applied. B) A threshold is set using the fluorescence of untreated platelets. C) After treatment, 'positive platelets' are defined as platelet populations that appear to the right of the threshold.

Phosphatidyl serine (PS) exposure: PS exposure was assessed after incubation of washed platelet suspensions (50 µL) at 37 °C in Tyrode's solution (pH 7.4, 445 µL) with either the peptide (5 µL of 1 mM stock solution in DMSO), DMSO (5 µL) or ABT737 (5 µL of 1 mM stock solution in DMSO). At t = 1, 2 and 3 h, 25 µL of the suspension was added to 25 µL of an annexin V solution (10% in Tyrode's solution), and the sample was protected from direct light and analysed by flow cytometry.

Platelet activation markers: Platelet activation markers (PAC-1, CD62P and anti-CD63) were assessed after incubation of washed platelet suspensions (3 µL) in CFT buffer (pH 7.4, 105 µL) with the desired antibody (1.2 µL) and peptide (1.1 µL of 1 mM DMSO stock solution) at 37 °C for 1 h. The suspensions were analysed by flow cytometry at t = 1 h.

4.2.2 Microbiology assay procedures

All compounds were stored as 25.6 mg/mL stock solutions in DMSO/H_2O (1:1). Colistin was used as a positive control and was stored as a 25.6 mg/mL stock solution in water. Antimicrobial testing was performed according to EUCAST guidelines in microdilution.[316] Compounds were tested against *P. aeruginosa* strains PAO1,[317] YM64,[318] and *Staphylococcus aureus*. Unless otherwise stated, each result was duplicated on the same plate and each test repeated in triplicate on separate days.

Initial MIC testing: Bacterial cultures were grown overnight at 37 °C in Lysogeny broth (LB).[w] The suspension was diluted to OD_{600} 0.1 in cation-adjusted Muller-Hinton broth (MH-B). Into each well of a 96-well plate was added 99 µL of bacterial suspension, leaving the outer columns empty in case of evaporation. To the desired wells 1 µL of compound stock solution was added. Some wells left untreated as a negative control, colistin was added to some wells as a positive control, and some wells contained only cation-adjusted MH-B to check for contamination of the broth. The plate was sealed with a gas-permeable membrane and incubated at 37 °C with 50 revolutions per minute (rpm) shaking for 18 h. The optical density at 600 nm (OD_{600}) was measured, and the MIC was determined as the lowest concentration of compound which prevented visible growth.

Serial dilution MIC testing: Bacterial suspensions were made up to OD_{600} 0.1 in MH-B as previously described. Into the first well of a 96-well plate was added 99 µL of broth and 1 µL

[w] Preparation of bacterial cultures performed by Thomas O'Brien, University of Cambridge.

of compound (stock solution = 25.6 mg/mL in DMSO/H_2O 1:1). Into the second well was added 199 µL of broth and 1 µL of compound (stock solution = 25.6 mg/mL in DMSO/H_2O 1:1). To the remaining wells was added 99 µL of broth. 100 µL of solution was taken from the second well and added to the third with mixing and this was continued along the row until the minimum desired concentration was achieved: the excess 100 µL was discarded. Each well was inoculated with 50 µL of bacterial suspension. The same controls were included as previously described. The plate was sealed with a gas-permeable membrane and incubated at 37 °C with 50 rpm shaking for 18 h. The absorbance at 600 nm was measured, and the MIC was determined as the lowest concentration of compound which prevented visible growth.

Biofilm crystal violet assay: The protocol for 'Initial MIC testing' was followed, with sub-inhibitory concentrations of the desired peptides. Untreated bacteria and bacteria treated with inhibitory and sub-inhibitory concentrations of colistin were included as controls. The bacterial supernatant was aspirated off, and the cells were washed with deionised H_2O (2 × 120 µL). Crystal violet (0.1% aq. solution, 120 µL) was added to each well and the plate was incubated at rt for 15 min. The crystal violet was aspirated off, the wells washed with deionised H_2O (3 × 120 µL) and the plate was inverted and dried in the oven for 10 min. To each well was added acetic acid (30% aq. solution, 120 µL) and the plate was vortexed gently. The absorbance at 595 nm of each well was measured.

4.2.3 Computational methods[x]

Peptides were modelled using Chimera. For peptides in Chapter 3, the staple was placed so that the overall cationic charge and amphipathicity, both of which are linked to antimicrobial activity, were preserved.[98,312] Additionally, any potentially unstable residues (Met) were replaced by the staple where possible. Where possible, molecular dynamics simulations were performed using AMBER 14 on the linear and stapled peptides to predict the ability of the staple to maintain peptide helicity. The force fields ff14SB and GAFF were used to describe the peptide and staple respectively during the simulations.

[x] All computational experiments described in this dissertation were performed by Dr. Yaw Sing Tan, A*STAR Institute, Singapore.

5. References

1 D. S. Dimitrov, *Methods Mol. Biol.*, 2012, **899**, 1–26.

2 J. L. Lau and M. K. Dunn, *Bioorg. Med. Chem.*, 2017, **26**, 2700–2707.

3 D. E. Scott, A. R. Bayly, C. Abell and J. Skidmore, *Nat. Rev. Drug Discov.*, 2016, **15**, 533–550.

4 T. Passioura, *Biochemistry*, 2020, **59**, 139–145.

5 A. Henninot, J. C. Collins and J. M. Nuss, *J. Med. Chem.*, 2018, **61**, 1382–1414.

6 A. Pessi, S. L. Bixler, V. Soloveva, S. Radoshitzky, C. Retterer, T. Kenny, R. Zamani, G. Gomba, D. Gharabeih, J. Wells, K. S. Wetzel, T. K. Warren, G. Donnelly, S. A. Van Tongeren, J. Steffens, A. J. Duplantier, C. D. Kane, P. Vicat, V. Couturier, K. E. Kester, J. Shiver, K. Carter and S. Bavari, *Antiviral Res.*, 2019, **171**, 104592.

7 G. L. Verdine and G. J. Hilinski, in *Methods in Enzymology*, Elsevier Inc., 1st edn., 2012, vol. 503, pp. 3–33.

8 T. A. F. Cardote and A. Ciulli, *ChemMedChem*, 2016, **11**, 787–794.

9 G. H. Bird, N. Madani, A. F. Perry, A. M. Princiotto, J. G. Supko, X. He, E. Gavathiotis, J. G. Sodroski and L. D. Walensky, *Proc. Natl. Acad. Sci. USA*, 2010, **107**, 14093–14098.

10 K. Fosgerau and T. Hoffmann, *Drug Discov. Today*, 2015, **20**, 122–128.

11 L. Di, *J. Am. Assoc. Pharm. Sci.*, 2015, **17**, 134–143.

12 L. B. Knudsen and J. Lau, *Front. Endocrinol.*, 2019, **10**, 155.

13 D. J. Craik, D. P. Fairlie, S. Liras and D. Price, *Chem. Biol. Drug Des.*, 2013, **81**, 136–147.

14 J. M. Carton and W. R. Strohl, in *Introduction to Biological and Small Molecule Drug Research and Development: Theory and Case Studies*, eds. C. R. Ganellin, R. Jefferies and S. M. Roberts, Academic Press, 2013, pp. 127–159.

15 M. Pelay-Gimeno, A. Glas, O. Koch and T. N. Grossmann, *Angew. Chemie - Int. Ed.*, 2015, **54**, 8896–8927.

16 T. A. Stone and C. M. Deber, *Biochim. Biophys. Acta - Biomembr.*, 2017, **1859**, 577–585.

17 C. J. White and A. K. Yudin, *Nat. Chem.*, 2011, **3**, 509–524.

18 L. D. Walensky and G. H. Bird, *J. Med. Chem.*, 2014, **57**, 6275–6288.

19 W. A. Loughlin, J. D. A. Tyndall, M. P. Glenn and D. P. Fairlie, *Chem. Rev.*, 2004, **104**, 6085–6117.

20 A. Luther, C. Bisang and D. Obrecht, *Bioorg. Med. Chem.*, 2018, **26**, 2850–2858.

21 J. D. A. Tyndall, T. Nall and D. P. Fairlie, *Chem. Rev.*, 2005, **105**, 973–1000.

22 Y. Q. Long, S. X. Huang, Z. Zawahir, Z. L. Xu, H. Li, T. W. Sanchez, Y. Zhi, S. De Houwer, F. Christ, Z. Debyser and N. Neamati, *J. Med. Chem.*, 2013, **56**, 5601–5612.

23 Y. H. Lau, P. de Andrade, S.-T. Quah, M. Rossmann, L. Laraia, N. Sköld, T. J. Sum, P. J. E. Rowling, T. L. Joseph, C. Verma, M. Hyvönen, L. S. Itzhaki, A. R. Venkitaraman, C. J. Brown, D. P. Lane and D. R. Spring, *Chem. Sci.*, 2014, **5**, 1804–

1809.

24 Y. Wu, L. B. Olsen, Y. H. Lau, C. H. Jensen, M. Rossmann, Y. R. Baker, H. F. Sore, S. Collins and D. R. Spring, *ChemBioChem*, 2016, **17**, 689–692.

25 J. Iegre, P. Brear, D. J. Baker, Y. S. Tan, E. L. Atkinson, H. F. Sore, D. H. O'Donovan, C. S. Verma, M. Hyvönen and D. R. Spring, *Chem. Sci.*, 2019, **10**, 5056–5063.

26 O. Koch, J. Cole, P. Block and G. Klebe, *J. Chem. Inf. Model.*, 2009, **49**, 2388–2402.

27 B. N. Bullock, A. L. Jochim and P. S. Arora, *J. Am. Chem. Soc.*, 2011, **133**, 14220–14223.

28 J. C. Phelan, N. J. Skelton, A. C. Braisted and R. S. McDowell, *J. Am. Chem. Soc.*, 1997, **119**, 455–460.

29 D. Y. Jackson, D. S. King, J. Chmielewski, S. Singh and P. G. Schultz, *J. Am. Chem. Soc.*, 1991, **113**, 9391–9392.

30 H. E. Blackwell and R. H. Grubbs, *Angew. Chemie - Int. Ed.*, 1998, **37**, 3281–3284.

31 C. E. Schafmeister, J. Po and G. L. Verdine, *J. Am. Chem. Soc.*, 2000, **122**, 5891–5892.

32 S. A. Kawamoto, A. Coleska, X. Ran, H. Yi, C. Y. Yang and S. Wang, *J. Med. Chem.*, 2012, **55**, 1137–1146.

33 M. M. Madden, A. Muppidi, Z. Li, X. Li, J. Chen and Q. Lin, *Bioorg. Med. Chem. Lett.*, 2011, **21**, 1472–1475.

34 Y. Wang and D. H. C. Chou, *Angew. Chemie - Int. Ed.*, 2015, **54**, 10931–10934.

35 C. M. Haney, M. T. Loch and W. S. Horne, *Chem. Commun.*, 2011, **47**, 10915.

36 F. M. Brunel and P. E. Dawson, *Chem. Commun.*, 2005, **2005**, 2552–2554.

37 L. Mendive-Tapia, S. Preciado, J. García, R. Ramón, N. Kielland, F. Albericio and R. Lavilla, *Nat. Commun.*, 2015, **6**, 1–9.

38 J. Tang, Y. He, H. Chen, W. Sheng and H. Wang, *Chem. Sci.*, 2017, **8**, 4565–4570.

39 G. H. Bird, F. Bernal, K. Pitter and L. D. Walensky, *Methods Enzymol.*, 2008, **446**, 369–386.

40 US20170015716, 2016.

41 J. Iegre, J. S. Gaynord, N. S. Robertson, H. F. Sore, M. Hyvönen and D. R. Spring, *Adv. Ther.*, 2018, **1**, 1800052.

42 Y. H. Lau, P. de Andrade, Y. Wu and D. R. Spring, *Chem. Soc. Rev.*, 2015, **44**, 91–102.

43 O. Torres, D. Yüksel, M. Bernardina, K. Kumar and D. Bong, *ChemBioChem*, 2008, **9**, 1701–1705.

44 Y. H. Lau, Y. Wu, P. de Andrade, W. R. J. D. Galloway and D. R. Spring, *Nat. Protoc.*, 2015, **10**, 585–94.

45 P. T. Tran, C. Ø. Larsen, T. Røndbjerg, M. De Foresta, M. B. A. Kunze, A. Marek, J. H. Løper, L. E. Boyhus, A. Knuhtsen, K. Lindorff-Larsen and D. S. Pedersen, *Chem. - A Eur. J.*, 2017, **23**, 3490–3495.

46 L. Zhang, T. Navaratna, J. Liao and G. M. Thurber, *Bioconjug. Chem.*, 2015, **26**, 329–

337.

47 Y. H. Lau, Y. Wu, M. Rossmann, B. X. Tan, P. De Andrade, Y. S. Tan, C. Verma, G. J. Mckenzie, A. R. Venkitaraman, M. Hyvönen and D. R. Spring, *Angew. Chemie - Int. Ed.*, 2015, **54**, 15410–15413.

48 I. Z. Siemion, *BioSystems*, 1994, **32**, 163–170.

49 P. Timmerman, J. Beld, W. C. Puijk and R. H. Meloen, *ChemBioChem*, 2005, **6**, 821–824.

50 D. Bernhagen, V. Jungbluth, N. G. Quilis, J. Dostalek, P. B. White, K. Jalink and P. Timmerman, *ACS Comb. Sci.*, 2019, **21**, 198–206.

51 L. E. J. Smeenk, N. Dailly, H. Hiemstra, J. H. Van Maarseveen and P. Timmerman, *Org. Lett.*, 2012, **14**, 1194–1197.

52 G. J. J. Richelle, S. Ori, H. Hiemstra, J. H. van Maarseveen and P. Timmerman, *Angew. Chemie - Int. Ed.*, 2018, **57**, 501–505.

53 D. E. Streefkerk, M. Schmidt, J. H. Ippel, T. M. Hackeng, T. Nuijens, P. Timmerman and J. H. Van Maarseveen, *Org. Lett.*, 2019, **21**, 2095–2100.

54 C. Heinis, T. Rutherford, S. Freund and G. Winter, *Nat. Chem. Biol.*, 2009, **5**, 502–507.

55 F. Zhang, O. Sadovski, S. J. Xin and G. A. Woolley, *J. Am. Chem. Soc.*, 2007, **129**, 14154–14155.

56 D. G. Flint, J. R. Kumita, O. S. Smart and G. A. Woolley, *Chem. Biol.*, 2002, **9**, 391–397.

57 J. R. Kumita, O. S. Smart and G. A. Woolley, *Proc. Natl. Acad. Sci.*, 2000, **97**, 3803–3808.

58 C. M. B. K. Kourra and N. Cramer, *Chem. Sci.*, 2016, **7**, 7007–7012.

59 N. Assem, D. J. Ferreira, D. W. Wolan and P. E. Dawson, *Angew. Chemie - Int. Ed.*, 2015, **54**, 8665–8668.

60 S. Sun, I. Compañón, N. Martínez-Sáez, J. D. Seixas, O. Boutureira, F. Corzana and G. J. L. Bernardes, *ChemBioChem*, 2018, **19**, 48–52.

61 A. M. Spokoyny, Y. Zou, J. J. Ling, H. Yu, Y. S. Lin and B. L. Pentelute, *J. Am. Chem. Soc.*, 2013, **135**, 5946–5949.

62 C. M. Fadzen, J. M. Wolfe, C. F. Cho, E. A. Chiocca, S. E. Lawler and B. L. Pentelute, *J. Am. Chem. Soc.*, 2017, **139**, 15628–15631.

63 S. Kalhor-Monfared, M. R. Jafari, J. T. Patterson, P. I. Kitov, J. J. Dwyer, J. M. Nuss and R. Derda, *Chem. Sci.*, 2016, **7**, 3785–3790.

64 S. P. Brown and A. B. Smith, *J. Am. Chem. Soc.*, 2015, **137**, 4034–4037.

65 J. Guy, R. Castonguay, N. B. Campos-Reales Pineda, V. Jacquier, K. Caron, S. W. Michnick and J. W. Keillor, *Mol. Biosyst.*, 2010, **6**, 976.

66 C. M. Grison, G. M. Burslem, J. A. Miles, L. K. A. Pilsl, D. J. Yeo, Z. Imani, S. L. Warriner, M. E. Webb and A. J. Wilson, *Chem. Sci.*, 2017, **8**, 5166–5171.

67 N. S. Robertson, S. J. Walsh, E. Fowler, M. Yoshida, S. M. Rowe, Y. Wu, H. F. Sore, J. S. Parker and D. R. Spring, *Chem. Commun.*, 2019, **55**, 9499–9502.

68 S. J. Walsh, S. Omarjee, W. R. J. D. Galloway, T. T. L. Kwan, H. F. Sore, J. S. Parker, M. Hyvönen, J. S. Carroll and D. R. Spring, *Chem. Sci.*, 2019, **10**, 694–700.

69 S. J. Walsh, J. Iegre, H. Seki, J. D. Bargh, H. F. Sore, J. S. Parker, J. S. Carroll and D. R. Spring, *Org. Biomol. Chem.*, 2020, **18**, 4224–4230.

70 E. V. Vinogradova, C. Zhang, A. M. Spokoyny, B. L. Pentelute and S. L. Buchwald, *Nature*, 2015, **526**, 687–691.

71 A. J. Rojas, B. L. Pentelute and S. L. Buchwald, *Org. Lett.*, 2017, **19**, 4263–4266.

72 A. J. Rojas, C. Zhang, E. V. Vinogradova, N. H. Buchwald, J. Reilly, B. L. Pentelute and S. L. Buchwald, *Chem. Sci.*, 2017, **8**, 4257–4263.

73 K. Fujimoto, M. Kajino and M. Inouye, *Chem. - A Eur. J.*, 2008, **14**, 857–863.

74 K. Kubota, P. Dai, B. L. Pentelute and S. L. Buchwald, *J. Am. Chem. Soc.*, 2018, **140**, 3128–3133.

75 E. Y.-L. Hui, B. Rout, Y. S. Tan, C. S. Verma, K.-P. Chan and C. W. Johannes, *Org. Biomol. Chem.*, 2018, **1**, 389–392.

76 G. K. Dewkar, P. B. Carneiro and M. C. T. Hartman, *Org. Lett.*, 2009, **11**, 4708–4711.

77 J. Iegre, N. S. Ahmed, J. S. Gaynord, Y. Wu, K. M. Herlihy, Y. S. Tan, M. E. Lopes-Pires, R. Jha, Y. H. Lau, H. F. Sore, C. Verma, D. H. O' Donovan, N. Pugh and D. R. Spring, *Chem. Sci.*, 2018, **9**, 4638–4643.

78 W. Xu, Y. H. Lau, G. Fischer, Y. S. Tan, A. Chattopadhyay, M. De La Roche, M. Hyvönen, C. Verma, D. R. Spring and L. S. Itzhaki, *J. Am. Chem. Soc.*, 2017, **139**, 2245–2256.

79 C. R. Braun, J. Mintseris, E. Gavathiotis, G. H. Bird, S. P. Gygi and L. D. Walensky, *Chem. Biol.*, 2010, **17**, 1325–1333.

80 E. P. Harvey, H.-S. Seo, R. M. Guerra, G. H. Bird, S. Dhe-Paganon and L. D. Walensky, *Structure*, 2017, **26**, 153–160.

81 J. Charoenpattarapreeda, Y. S. Tan, J. Iegre, S. J. Walsh, E. Fowler, R. S. Eapen, Y. Wu, H. F. Sore, C. S. Verma, L. Itzhaki and D. R. Spring, *Chem. Commun.*, 2019, **55**, 7914–7917.

82 H. Kleinkauf and H. Von Döhren, in *Biotechnology, Second, Completely Revised Edition, Volume 7: Products of Secondary Metabolism*, Wiley-VCH, 2008, vol. 43, pp. 277–322.

83 N. Tsomaia, *Eur. J. Med. Chem.*, 2015, **94**, 459–470.

84 *21st Model List of Essential Medicines, World Health Organisation*, 2019.

85 C. Sohrabi, A. Foster and A. Tavassoli, *Nat. Rev. Chem.*, 2020, **4**, 90–101.

86 S. S. Sidhu and G. A. Weiss, in *Anticancer Drug Development*, Academic Press, 2002, pp. 237–248.

87 O. B. C. Monty, P. Nyshadham, K. M. Bohren, M. Palaniappan, M. M. Matzuk, D. W. Young and N. Simmons, *ACS Comb. Sci.*, 2020, **22**, 80–88.

88 M. Ohuchi, H. Murakami and H. Suga, *Curr. Opin. Chem. Biol.*, 2007, **11**, 537–542.

89 T. Passioura and H. Suga, *Chem. - A Eur. J.*, 2013, **19**, 6530–6536.

90 C. Heinis and G. Winter, *Curr. Opin. Chem. Biol.*, 2015, **26**, 89–98.

91 K. Deyle, X. D. Kong and C. Heinis, *Acc. Chem. Res.*, 2017, **50**, 1866–1874.

92 A. Tavassoli and S. J. Benkovic, *Angew. Chemie - Int. Ed.*, 2005, **44**, 2760–2763.

93 A. Tavassoli, *Curr. Opin. Chem. Biol.*, 2017, **38**, 30–35.

94 E. Valeur, S. M. Guéret, H. Adihou, R. Gopalakrishnan, M. Lemurell, H. Waldmann, T. N. Grossmann and A. T. Plowright, *Angew. Chemie - Int. Ed.*, 2017, **56**, 10294–10323.

95 R. D. Taylor, M. Rey-Carrizo, T. Passioura and H. Suga, *Drug Discov. Today Technol.*, 2017, **26**, 17–23.

96 Bicycle Therapeutics: Approach, https://www.bicycletherapeutics.com/approach/#platform, (accessed 19 February 2020).

97 K. Deyle and C. Heinis, *Chimia*, 2018, **72**, 426–427.

98 Y. S. Tan, D. P. Lane and C. S. Verma, *Drug Discov. Today*, 2016, **21**, 1642–1653.

99 ALRN-6924 in Patients With Advanced Solid Tumors or Lymphomas, https://clinicaltrials.gov/ct2/show/NCT02264613, (accessed 19 February 2020).

100 J. S. Choi and S. H. Joo, *Biomol. Ther.*, 2020, **28**, 18–24.

101 V. Baeriswyl and C. Heinis, *ChemMedChem*, 2013, **8**, 377–384.

102 P. B. Molinoff, A. M. Shadiack, D. Earle, L. E. Diamond and C. Y. Quaon, *Ann. N. Y. Acad. Sci.*, 2003, **994**, 96–102.

103 E. Marsault and M. L. Peterson, in *Practical Medicinal Chemistry with Macrocycles: Design, Synthesis, and Case Studies*, John Wiley & Sons, Inc., 2016.

104 Phase 1 Safety Study of ALRN-5281 in Healthy Subjects, https://clinicaltrials.gov/ct2/show/NCT01775358, (accessed 19 February 2020).

105 G. E. Mudd, A. Brown, L. Chen, K. van Rietschoten, S. Watcham, D. P. Teufel, S. Pavan, R. Lani, P. Huxley and G. S. Bennett, *J. Med. Chem.*, 2020, **63**, 4107–4116.

106 V. Azzarito, K. Long, N. S. Murphy and A. J. Wilson, *Nat. Chem.*, 2013, **5**, 161–173.

107 A. Loregian and G. Palù, *J. Cell. Physiol.*, 2005, **204**, 750–762.

108 X. Ran and J. E. Gestwicki, *Curr. Opin. Chem. Biol.*, 2018, **44**, 75–86.

109 A. M. Ali, J. Atmaj, N. Van Oosterwijk, M. R. Groves and A. Dömling, *Comput. Struct. Biotechnol. J.*, 2019, **17**, 263–281.

110 A. D. Cunningham, N. Qvit and D. Mochly-Rosen, *Curr. Opin. Struct. Biol.*, 2017, **44**, 59–66.

111 R. Rezaei Araghi and A. E. Keating, *Curr. Opin. Struct. Biol.*, 2016, **39**, 27–38.

112 S. Elmore, *Toxicol. Pathol.*, 2007, **35**, 495–516.

113 L. Happo, A. Strasser and S. Cory, *J. Cell Sci.*, 2012, **125**, 1081–1087.

114 A. M. Petros, E. T. Olejniczak and S. W. Fesik, *Biochim. Biophys. Acta - Mol. Cell Res.*, 2004, **1644**, 83–94.

115 S. Rajan, M. Choi, K. Baek and H. S. Yoon, *Proteins Struct. Funct. Bioinforma.*, 2015, **83**, 1262–1272.

116 C. Elena, Lomonosova G, *Oncogene*, 2008, **27**, 1–31.

117 B. T. Kile, *Br. J. Haematol.*, 2014, **165**, 217–226.

118 J. E. Chipuk, T. Moldoveanu, F. Llambi, M. J. Parsons and D. R. Green, *Mol. Cell*, 2010, **37**, 299–310.

119 A. Shamas-Din, H. Brahmbhatt, B. Leber and D. W. Andrews, *Biochim. Biophys. Acta - Mol. Cell Res.*, 2011, **1813**, 508–520.

120 M. Vogler, D. Dinsdale, M. J. S. Dyer and G. M. Cohen, *Cell Death Differ.*, 2009, **16**, 360–367.

121 J. C. Reed, S. Yum, C. Stein, C. Subasinghe, J. Cohen, S. Haldar and C. M. Croce, *Cancer Res.*, 1990, **50**, 6565–6570.

122 C. M. Croce and J. C. Reed, *Cancer Res.*, 2016, **76**, 5914–5920.

123 J. C. Reed, *Cell Death Differ.*, 2018, **25**, 3–6.

124 M. Sattler, H. Liang, D. Nettesheim, R. P. Meadows, J. E. Harlan, M. Eberstadt, H. S. Yoon, S. B. Shuker, B. S. Chang, A. J. Minn, C. B. Thompson and S. W. Fesik, *Science*, 1997, **275**, 983–986.

125 A. M. Petros, A. Medek, D. G. Nettesheim, D. H. Kim, H. S. Yoon, K. Swift, E. D. Matayoshi, T. Oltersdorf and S. W. Fesik, *Proc. Natl. Acad. Sci. USA*, 2001, **98**, 3012–3017.

126 S. B. Shuker, P. J. Hajduk, R. P. Meadows and S. W. Fesik, *Science*, 1996, **274**, 1531–1534.

127 T. Oltersdorf, S. W. Elmore, A. R. Shoemaker, R. C. Armstrong, D. J. Augeri, B. A. Belli, M. Bruncko, T. L. Deckwerth, J. Dinges, P. J. Hajduk, M. K. Joseph, S. Kitada, S. J. Korsmeyer, A. R. Kunzer, A. Letai, C. Li, M. J. Mitten, D. G. Nettesheim, S. C. Ng, P. M. Nimmer, J. M. O'Connor, A. Oleksijew, A. M. Petros, J. C. Reed, W. Shen, S. K. Tahir, C. B. Thompson, K. J. Tomaselli, B. Wang, M. D. Wendt, H. Zhang, S. W. Fesik and S. H. Rosenberg, *Nature*, 2005, **435**, 677–681.

128 C. Tse, A. R. Shoemaker, J. Adickes, M. G. Anderson, J. Chen, S. Jin, E. F. Johnson, K. C. Marsh, M. J. Mitten, P. Nimmer, L. Roberts, S. K. Tahir, Y. Xiao, X. Yang, H. Zhang, S. W. Fesik, S. H. Rosenberg and S. W. Elmore, *Cancer Res.*, 2008, **68**, 3421–3428.

129 L. Gandhi, D. R. Camidge, M. R. De Oliveira, P. Bonomi, D. Gandara, D. Khaira, C. L. Hann, E. M. McKeegan, E. Litvinovich, P. M. Hemken, C. Dive, S. H. Enschede, C. Nolan, Y. L. Chiu, T. Busman, H. Xiong, A. P. Krivoshik, R. Humerickhouse, G. I. Shapiro and C. M. Rudin, *J. Clin. Oncol.*, 2011, **29**, 909–916.

130 A. J. Souers, J. D. Leverson, E. R. Boghaert, S. L. Ackler, N. D. Catron, J. Chen, B. D. Dayton, H. Ding, S. H. Enschede, W. J. Fairbrother, D. C. S. Huang, S. G. Hymowitz, S. Jin, S. L. Khaw, P. J. Kovar, L. T. Lam, J. Lee, H. L. Maecker, K. C. Marsh, K. D. Mason, M. J. Mitten, P. M. Nimmer, A. Oleksijew, C. H. Park, C. M. Park, D. C. Phillips, A. W. Roberts, D. Sampath, J. F. Seymour, M. L. Smith, G. M. Sullivan, S. K. Tahir, C. Tse, M. D. Wendt, Y. Xiao, J. C. Xue, H. Zhang, R. A. Humerickhouse, S. H. Rosenberg and S. W. Elmore, *Nat. Med.*, 2013, **19**, 202–208.

131 Food and Drug Authority, *Venclexta®: Highlights of prescribing information*, 2019.

132 P. A. Valiente, D. Becerra and P. M. Kim, *J. Org. Chem.*, 2020, **85**, 1644–1651.

133 T. Moldoveanu, C. R. Grace, F. Llambi, A. Nourse, P. Fitzgerald, K. Gehring, R. W.

Kriwacki and D. R. Green, *Nat. Struct. Mol. Biol.*, 2013, **20**, 589–597.

134 M. L. Stewart, E. Fire, A. E. Keating and L. D. Walensky, *Nat. Chem. Biol.*, 2010, **6**, 595–601.

135 A. J. Huhn, R. M. Guerra, E. P. Harvey, G. H. Bird and L. D. Walensky, *Cell Chem. Biol.*, 2016, **23**, 1123–1134.

136 J. L. LaBelle, S. G. Katz, G. H. Bird, E. Gavathiotis, M. L. Stewart, C. Lawrence, J. K. Fisher, M. Godes, K. Pitter, A. L. Kung and L. D. Walensky, *J. Clin. Invest.*, 2012, **122**, 2018–2031.

137 E. Gavathiotis, M. Suzuki, M. L. Davis, K. Pitter, G. H. Bird, S. G. Katz, H. C. Tu, H. Kim, E. H. Y. Cheng, N. Tjandra and L. D. Walensky, *Nature*, 2008, **455**, 1076–1081.

138 A. L. Edwards, E. Gavathiotis, J. L. Labelle, C. R. Braun, K. A. Opoku-Nsiah, G. H. Bird and L. D. Walensky, *Chem. Biol.*, 2013, **20**, 888–902.

139 L. D. Walensky, K. Pitter, J. Morash, K. J. Oh, S. Barbuto, J. Fisher, E. Smith, G. L. Verdine and S. J. Korsmeyer, *Mol. Cell*, 2006, **24**, 199–210.

140 E. S. Leshchiner, C. R. Braun, G. H. Bird and L. D. Walensky, *Proc. Natl. Acad. Sci. USA*, 2013, **110**, E986–E995.

141 L. D. Walensky, A. L. Kung, I. Escher, T. J. Malia, S. Barbuto, R. D. Wright, G. Wagner, G. L. Verdine and S. J. Korsmeyer, *Science*, 2004, **305**, 1466–1470.

142 L. Vela and I. Marzo, *Curr. Opin. Pharmacol.*, 2015, **23**, 74–81.

143 N. A. Cohen, M. L. Stewart, E. Gavathiotis, J. L. Tepper, S. R. Bruekner, B. Koss, J. T. Opferman and L. D. Walensky, *Chem. Biol.*, 2012, **19**, 1175–1186.

144 G. Lippi, M. Franchini and G. Targher, *Nat. Rev. Cardiol.*, 2011, **8**, 502–512.

145 S. J. Shattil, M. Cunningham and J. Hoxie, *Blood*, 1987, **70**, 307–315.

146 A. J. Gale, *Toxicol. Pathol.*, 2011, **39**, 273–280.

147 J. N. George, *Lancet*, 2000, **355**, 1531–9.

148 B. Nieswandt, I. Pleines and M. Bender, *J. Thromb. Haemost.*, 2011, **9**, 92–104.

149 L. J. Gay and B. Felding-Habermann, *Nat. Rev. Cancer*, 2011, **11**, 123–134.

150 J. Ware, *Thromb. Haemost.*, 2004, **92**, 478–485.

151 F. Rendu and B. Brohard-Bohn, *Platelets*, 2001, **12**, 261–273.

152 S. J. Shattil, H. Kashiwagi and N. Pampori, *Blood*, 1998, **91**, 2645–2657.

153 B. B. Wolf, J. C. Goldstein, H. R. Stennicke, H. Beere, G. P. Amarante-Mendes, G. S. Salvesen and D. R. Green, *Blood*, 1999, **94**, 1683–1692.

154 S. M. Schoenwaelder, Y. Yuan, E. C. Josefsson, M. J. White, Y. Yao, K. D. Mason, L. A. O'Reilly, K. J. Henley, A. Ono, S. Hsiao, A. Willcox, A. W. Roberts, D. C. S. Huang, H. H. Salem, B. T. Kile and S. P. Jackson, *Blood*, 2009, **114**, 663–666.

155 A. Shcherbina and E. Remold-O'Donnell, *Blood*, 1999, **93**, 4222–4231.

156 A. V. Gyulkhandanyan, A. Mutlu, D. J. Allen, J. Freedman and V. Leytin, *Thromb. Res.*, 2014, **133**, 73–79.

157 J. Thachil, *Clin. Med. J. R. Coll. Physicians London*, 2016, **16**, 152–160.

158 G. Passacquale and A. Ferro, *Br. J. Clin. Pharmacol.*, 2011, **72**, 604–618.

159 A. R. D. Delbridge, S. Chappaz, M. E. Ritchie, B. T. Kile, A. Strasser and S. Grabow, *Br. J. Haematol.*, 2016, **174**, 962–969.

160 H. Zhang, P. M. Nimmer, S. K. Tahir, J. Chen, R. M. Fryer, K. R. Hahn, L. A. Iciek, S. J. Morgan, M. C. Nasarre, R. Nelson, L. C. Preusser, G. A. Reinhart, M. L. Smith, S. H. Rosenberg, S. W. Elmore and C. Tse, *Cell Death Differ.*, 2007, **14**, 943–51.

161 T. Kodama, T. Takehara, H. Hikita, S. Shimizu, M. Shigekawa, W. Li, T. Miyagi, A. Hosui, T. Tatsumi, H. Ishida, T. Kanto, N. Hiramatsu, X. M. Yin and N. Hayashi, *J. Biol. Chem.*, 2011, **286**, 13905–13913.

162 K. D. Mason, M. R. Carpinelli, J. I. Fletcher, J. E. Collinge, A. A. Hilton, S. Ellis, P. N. Kelly, P. G. Ekert, D. Metcalf, A. W. Roberts, D. C. S. Huang and B. T. Kile, *Cell*, 2007, **128**, 1173–1186.

163 T. Klymenko, M. Brandenburg, C. Morrow, C. Dive and G. Makin, *Mol. Cancer Ther.*, 2011, **10**, 2373–2383.

164 M. A. Debrincat, I. Pleines, M. Lebois, R. M. Lane, M. L. Holmes, J. Corbin, C. J. Vandenberg, W. S. Alexander, A. P. Ng, A. Strasser, P. Bouillet, M. Sola-Visner, B. T. Kile and E. C. Josefsson, *Cell Death Dis.*, 2015, **6**, e1721.

165 T. Thijs, H. Deckmyn and K. Broos, *Blood*, 2012, **119**, 1634–1642.

166 J. Iegre, PhD Thesis, University of Cambridge, 2019.

167 Y. H. Lau, PhD Thesis, University of Cambridge, 2014.

168 N. Fischer, E. D. Goddard-Borger, R. Greiner, T. M. Klapötke, B. W. Skelton and J. Stierstorfer, *J. Org. Chem.*, 2012, **77**, 1760–1764.

169 Y. H. Lau and D. R. Spring, *Synlett*, 2011, **2011**, 1917–1919.

170 W. C. Chan and P. D. White, *Fmoc Solid Phase Peptide Synthesis: A Practical Approach*, Oxford University Press Inc., 2000.

171 D. J. Mitchell, L. Steinman, D. T. Kim, C. G. Fathman and J. B. Rothbard, *J. Pept. Res.*, 2000, **56**, 318–325.

172 N. J. Greenfield, *Trends Anal. Chem.*, 1999, **18**, 236–244.

173 S. M. Kelly, T. J. Jess and N. C. Price, *Biochim. Biophys. Acta - Proteins Proteomics*, 2005, **1751**, 119–139.

174 T. Okamoto, K. Zobel, A. Fedorova, C. Quan, H. Yang, W. J. Fairbrother, D. C. S. Huang, B. J. Smith, K. Deshayes and P. E. Czabotar, *ACS Chem. Biol.*, 2013, **8**, 297–302.

175 V. Raussens, J. M. Ruysschaert and E. Goormaghtigh, *Anal. Biochem.*, 2003, **319**, 114–121.

176 V. Raussens, J. M. Ruysschaert and E. Goormaghtigh, *Anal. Biochem.*, 2006, **359**, 150.

177 J. Li, Y. Xia, A. M. Bertino, J. P. Coburn and D. J. Kuter, *Transfusion*, 2000, **40**, 1320–1329.

178 S. B. Brown, M. C. H. Clarke, L. Magowan, H. Sanderson and J. Savill, *J. Biol. Chem.*, 2000, **275**, 5987–5996.

179 M. L. Taylor, N. L. A. Misso, G. A. Stewart and P. J. Thompson, *Platelets*, 1995, **6**, 394–401.

180 A. M. Bertino, X. Q. Qi, J. Li, Y. Xia and D. J. Kuter, *Transfusion*, 2003, **43**, 857–866.

181 Sir Alexander Fleming, Nobel Lecture, 'Penicillin', https://www.nobelprize.org/prizes/medicine/1945/fleming/lecture/, (accessed 30 March 2020).

182 M. McKenna, *Nature*, 2013, **499**, 394–396.

183 *No time to wait: securing the future from drug-resistant infections, Interagency Coordination Group on Antimicrobial Resistance*, 2019.

184 *The Pew Charitable Trusts: A Scientific Roadmap for Antibiotic Discovery*, 2016.

185 *Tackling Drug-Resistant Infections Globally: Final Report and Recommendations. The Review on Antimicrobial Resistance, Lord Jim O'Neill*, 2016.

186 L. Czaplewski, R. Bax, M. Clokie, M. Dawson, H. Fairhead, V. A. Fischetti, S. Foster, B. F. Gilmore, R. E. W. Hancock, D. Harper, I. R. Henderson, K. Hilpert, B. V. Jones, A. Kadioglu, D. Knowles, S. Ólafsdóttir, D. Payne, S. Projan, S. Shaunak, J. Silverman, C. M. Thomas, T. J. Trust, P. Warn and J. H. Rex, *Lancet Infect. Dis.*, 2016, **16**, 239–251.

187 G. L. Patrick, *An Introduction to Medicinal Chemistry*, Oxford University Press Inc., New York, 4th edn., 2009.

188 M. Chatterjee, C. P. Anju, L. Biswas, V. Anil Kumar, C. Gopi Mohan and R. Biswas, *Int. J. Med. Microbiol.*, 2016, **306**, 48–58.

189 E. Tacconelli, E. Carrara, A. Savoldi, S. Harbarth, M. Mendelson, D. L. Monnet, C. Pulcini, G. Kahlmeter, J. Kluytmans, Y. Carmeli, M. Ouellette, K. Outterson, J. Patel, M. Cavaleri, E. M. Cox, C. R. Houchens, L. Grayson, P. Hansen, N. Singh, U. Theuretzbacher and N. Magrini, *Lancet Infect. Dis.*, 2018, **18**, 318–327.

190 M. Bassetti, A. Vena, A. Croxatto, E. Righi and B. Guery, *Drugs Context*, 2018, **7**, 1–18.

191 S. Wagner, R. Sommer, S. Hinsberger, C. Lu, R. W. Hartmann, M. Empting and A. Titz, *J. Med. Chem.*, 2016, **59**, 5929–5969.

192 R. M. Donlan and J. W. Costerton, *Clin. Microbiol. Rev.*, 2002, **15**, 167–193.

193 S. J. McConoughey, R. Howlin, J. F. Granger, M. M. Manring, J. H. Calhoun, M. Shirtliff, S. Kathju and P. Stoodley, *Future Microbiol.*, 2014, **9**, 987–1007.

194 D. Sriramulu, *Microbiol. Insights*, 2013, **6**, 29–36.

195 S. Moreau-Marquis, B. A. Stanton and G. A. O'Toole, *Pulm. Pharmacol. Ther.*, 2008, **21**, 595–599.

196 M. C. Walters, F. Roe, A. Bugnicourt, M. J. Franklin and P. S. Stewart, *Antimicrob. Agents Chemother.*, 2003, **47**, 317–323.

197 K. Lewis, *Antimicrob. Agents Chemother.*, 2001, **45**, 999–1007.

198 J. W. Costerton, P. S. Stewart and E. P. Greenberg, *Science*, 1999, **284**, 1318–1322.

199 P. Singelton, *Bacteria in Biology, Biotechnology and Medicine*, John Wiley, 5th edn., 1998.

200 T. Dörr, P. J. Moynihan and C. Mayer, *Front. Microbiol.*, 2019, **10**, 2051.

201 S. I. Miller and N. R. Salama, *PLoS Biol.*, 2018, **16**, e2004935.

202 R. M. Epand, C. Walker, R. F. Epand and N. A. Magarvey, *Biochim. Biophys. Acta - Biomembr.*, 2016, **1858**, 980–987.

203 T. Strateva and D. Yordanov, *J. Med. Microbiol.*, 2009, **58**, 1133–1148.

204 C. Walsh, *Antibiotics: actions, origins, resistance*, ASM Press, 1st edn., 2003.

205 K. Gould, *J. Antimicrob. Chemother.*, 2016, **71**, 572–575.

206 S. A. Alharbi, M. Wainwright, T. A. Alahmadi, H. Bin Salleeh, A. A. Faden and A. Chinnathambi, *Saudi J. Biol. Sci.*, 2014, **21**, 289–293.

207 E. D. Brown and G. D. Wright, *Nature*, 2016, **529**, 336–343.

208 S. J. Baker, D. J. Payne, R. Rappuoli and E. De Gregorio, *Proc. Natl. Acad. Sci.*, 2018, **115**, 12887–12895.

209 T. D. M. Pham, Z. M. Ziora and M. A. T. Blaskovich, *Med. Chem. Commun.*, 2019, **10**, 1719–1739.

210 A. C. Vatopoulos, V. Kalapothaki, N. J. Legakis, G. Antoniadis, E. Arhondidou, S. Chatzipanagiotou, E. Chinou, A. Chrysaki, V. Daniilidis, G. Genimata, H. Gessouli, P. Golemati, E. Kaili-Papadopoulou, A. Kansuzidou, D. Kailis, E. Kaitsa, M. Kanelopoulou, S. Kitsou-Kyriakopoulou, Z. Komninou, E. Kouskouni, C. Koutsia-Karouzou, S. Ktenidou-Kartali, V. Liakou, H. Malamou-Lada, H. Mercuri, C. Nicolopoulou, A. Pagkali, E. Panagiotou, E. Papafragas, A. Perogamvros, C. Poulopoulou, D. Sofianou, G. Theodoropoulou-Rodiou, S. Thermogianni, E. Trikka-Graphakos, O. Vavatsi-Manou, M. Ventouri, E. Vogiatzakis, A. Xanthaki, C. Zagora, E. Chatzidaki, G. Papoutsakis and N. J. Legakis, *Emerg. Infect. Dis.*, 1999, **5**, 471–476.

211 H. Mouneimné, J. Robert, V. Jarlier and E. Cambau, *Antimicrob. Agents Chemother.*, 1999, **43**, 62–66.

212 S. Correia, P. Poeta, M. Hébraud, J. L. Capelo and G. Igrejas, *J. Med. Microbiol.*, 2017, **66**, 551–559.

213 N. Mesaros, P. Nordmann, P. Plésiat, M. Roussel-Delvallez, J. Van Eldere, Y. Glupczynski, Y. Van Laethem, F. Jacobs, P. Lebecque, A. Malfroot, P. M. Tulkens and F. Van Bambeke, *Clin. Microbiol. Infect.*, 2007, **13**, 560–578.

214 M. J. Klein, S. Schmidt, P. Wadhwani, J. Bürck, J. Reichert, S. Afonin, M. Berditsch, T. Schober, R. Brock, M. Kansy and A. S. Ulrich, *J. Med. Chem.*, 2017, **60**, 8071–8082.

215 C. L. Tooke, P. Hinchliffe, E. C. Bragginton, C. K. Colenso, V. H. A. Hirvonen, Y. Takebayashi and J. Spencer, *J. Mol. Biol.*, 2019, **431**, 3472–3500.

216 M. H. Xiong, Y. Bao, X. Z. Yang, Y. H. Zhu and J. Wang, *Adv. Drug Deliv. Rev.*, 2014, **78**, 63–76.

217 M. E. Falagas and S. K. Kasiakou, *Crit. Care*, 2006, **10**, 1–13.

218 FDA updates warnings for fluoroquinolone antibiotics on risks of mental health and low blood sugar adverse reactions, https://www.fda.gov/news-events/press-announcements/fda-updates-warnings-fluoroquinolone-antibiotics-risks-mental-health-and-low-blood-sugar-adverse, (accessed 2 July 2020).

219 K. C. Nicolaou and S. Rigol, *J. Antibiot.*, 2018, **71**, 153–184.

220 C. N. Spaulding, R. D. Klein, H. L. Schreiber, J. W. Janetka and S. J. Hultgren, *Biofilms and Microbiomes*, 2018, **4**, 1–7.

221 *Antimicrobial resistance - Global Report on Surveillance, World Health Organisation*, 2014.

222 M. S. Butler and D. L. Paterson, *J. Antibiot.*, 2020, **73**, 329–364.

223 M. S. Mulani, E. E. Kamble, S. N. Kumkar, M. S. Tawre and K. R. Pardesi, *Front. Microbiol.*, 2019, **10**, 539.

224 F. Von Nussbaum, M. Brands, B. Hinzen, S. Weigand and D. Häbich, *Angew. Chemie - Int. Ed.*, 2006, **45**, 5072–5129.

225 L. L. Silver, *Clin. Microbiol. Rev.*, 2011, **24**, 71–109.

226 *Global Action Plan on Antimicrobial Resistance, World Health Organisation*, 2015.

227 S. Mariathasan and M. W. Tan, *Trends Mol. Med.*, 2017, **23**, 135–149.

228 S. D. Clas, R. I. Sanchez and R. Nofsinger, *Drug Discov. Today*, 2014, **19**, 79–87.

229 E. M. Larsen and R. J. Johnson, *Drug Dev. Res.*, 2019, **80**, 33–7.

230 M. Assali, M. Joulani, R. Awwad, M. Assad, M. Almasri, N. Kittana and A. N. Zaid, *ChemistrySelect*, 2016, **1**, 1132–1135.

231 L. N. Jungheim and T. A. Shepherd, *Chem. Rev.*, 1994, **94**, 1553–1566.

232 M. L. Rodrigues, P. Carter, C. Wirth, S. Mullins, A. Lee and B. K. Blackburn, *Chem. Biol.*, 1995, **2**, 223–227.

233 V. M. Vrudhula, H. P. Svensson and P. D. Senter, *J. Med. Chem.*, 1995, **38**, 1380–1385.

234 L. N. Jungheim, T. A. Shepherd and J. K. Kling, *Heterocycles*, 1993, **35**, 339–348.

235 L. E. Evans, A. Krishna, Y. Ma, T. E. Webb, D. C. Marshall, C. L. Tooke, J. Spencer, T. B. Clarke, A. Armstrong and A. M. Edwards, *J. Med. Chem.*, 2019, **62**, 4411–4425.

236 S. Desgranges, C. C. Ruddle, L. P. Burke, T. M. McFadden, J. E. O'Brien, D. Fitzgerald-Hughes, H. Humphreys, T. P. Smyth and M. Devocelle, *RSC Adv.*, 2012, **2**, 2480–2492.

237 F. C. Odds, *J. Antimicrob. Chemother.*, 2003, **52**, 1.

238 P. Klahn and M. Brönstrup, *Nat. Prod. Rep.*, 2017, **34**, 832–885.

239 P. D. Tamma, S. E. Cosgrove and L. L. Maragakis, *Clin. Microbiol. Rev.*, 2012, **25**, 450–470.

240 B. K. Gorityala, G. Guchhait, S. Goswami, D. M. Fernando, A. Kumar, G. G. Zhanel and F. Schweizer, *J. Med. Chem.*, 2016, **59**, 8441–8455.

241 H. Shiozawa, A. Shimada and S. Takahashi, *J. Antibiot.*, 1997, **50**, 449–452.

242 G. F. Zhang, X. Liu, S. Zhang, B. Pan and M. L. Liu, *Eur. J. Med. Chem.*, 2018, **146**, 599–612.

243 A. H. Delcour, *Biochim. Biophys. Acta - Proteins Proteomics*, 2009, **1794**, 808–816.

244 K. Drlica and X. Zhao, *Microbiol. Mol. Biol. Rev.*, 1997, **61**, 377–392.

245 K. L. Tyrrell, D. M. Citron, Y. A. Warren and E. J. C. Goldstein, *Antimicrob. Agents Chemother.*, 2012, **56**, 2194–2197.

246 TD-1792 in Gram-positive Complicated Skin and Skin Structure Infection, https://clinicaltrials.gov/ct2/show/NCT00442832?term=td+1792&draw=2&rank=1, (accessed 5 May 2020).

247 R. C. Hider and X. Kong, *Nat. Prod. Rep.*, 2010, **27**, 637–657.

248 M. Miethke and M. A. Marahiel, *Microbiol. Mol. Biol. Rev.*, 2007, **71**, 413–451.

249 A. Hartmann, H.-P. Fielder and V. Braun, *Eur. J. Biochem.*, 1979, **99**, 517–524.

250 P. Chairatana, T. Zheng and E. M. Nolan, *Chem. Sci.*, 2015, **6**, 4458–4471.

251 C. J. Carrano and K. N. Raymond, *J. Am. Chem. Soc.*, 1979, **101**, 5401–5404.

252 W. Neumann, M. Sassone-Corsi, M. Raffatellu and E. M. Nolan, *J. Am. Chem. Soc.*, 2018, **140**, 5193–5201.

253 S. Deshayes, W. Xian, N. W. Schmidt, S. Kordbacheh, J. Lieng, J. Wang, S. Zarmer, S. S. Germain, L. Voyen, J. Thulin, G. C. L. Wong and A. M. Kasko, *Bioconjug. Chem.*, 2017, **28**, 793–804.

254 N. Riahifard, K. Tavakoli, J. Yamaki, K. Parang and R. Tiwari, *Molecules*, 2017, **22**, 957.

255 F. Umstätter, C. Domhan, T. Hertlein, K. Ohlsen, E. Mühlberg, C. Kleist, S. Zimmermann, B. Beijer, K. D. Klika, U. Haberkorn, W. Mier and P. Uhl, *Angew. Chemie - Int. Ed.*, 2020, **59**, 8823–8827.

256 Y. Li, G. Liu, X. Wang, J. Hu and S. Liu, *Angew. Chemie - Int. Ed.*, 2016, **55**, 1760–1764.

257 R. Liu, P. A. Miller, S. B. Vakulenko, N. K. Stewart, W. C. Boggess and M. J. Miller, *J. Med. Chem.*, 2018, **61**, 3845–3854.

258 M. P. Pereira, J. Shi and S. O. Kelley, *ACS Infect. Dis.*, 2016, **1**, 586–592.

259 J. Kuriakose, V. Hernandez-Gordillo, M. Nepal, A. Brezden, V. Pozzi, M. N. Seleem and J. Chmielewski, *Angew. Chemie - Int. Ed.*, 2013, **52**, 9664–9667.

260 A. Brezden, M. F. Mohamed, M. Nepal, J. S. Harwood, J. Kuriakose, M. N. Seleem and J. Chmielewski, *J. Am. Chem. Soc.*, 2016, **138**, 10945–10949.

261 A. Brezden, M. F. Mohamed, M. Nepal, J. S. Harwood, J. Kuriakose, M. N. Seleem and J. Chmielewski, *J. Am. Chem. Soc.*, 2018, **140**, 13125–13126.

262 B. B. Finlay and R. E. W. Hancock, *Nat. Rev. Microbiol.*, 2004, **2**, 497–504.

263 E. F. Haney, S. K. Straus and R. E. W. Hancock, *Front. Chem.*, 2019, **7**, 43.

264 M.-P. Mingeot-Leclercq and J.-L. Décout, *Med. Chem. Commun*, 2014, **7**, 611.

265 F. G. Avci, B. S. Akbulut and E. Ozkirimli, *Biomolecules*, 2018, **8**, 1–43.

266 X. Kang, F. Dong, C. Shi and H. Zheng, *Sci. Data*, 2019, **6**, 148.

267 M. Mahlapuu, J. Håkansson, L. Ringstad and C. Björn, *Front. Cell. Infect. Microbiol.*, 2016, **6**, 1–12.

268 H. B. Koo and J. Seo, *Pept. Sci.*, 2019, **111**, e24122.

269 K. Bellmann-Sickert, T. A. Stone, B. E. Poulsen and C. M. Deber, *J. Biol. Chem.*, 2015, **290**, 1752–1759.

270 N. Srinivas, P. Jetter, B. J. Ueberbacher, M. Werneburg, K. Zerbe, J. Steinmann, B. Van Der Meijden, F. Bernardini, A. Lederer, R. L. A. Dias, P. E. Misson, H. Henze, J. Zumbrunn, F. O. Gombert, D. Obrecht, P. Hunziker, S. Schauer, U. Ziegler, A. Käch, L. Eberl, K. Riedel, S. J. Demarco and J. A. Robinson, *Science*, 2010, **327**, 1010–1013.

271 US20170247423, 2017.

272 K. A. Brogden, *Nat. Rev. Microbiol.*, 2005, **3**, 238–250.

273 L. T. Nguyen, E. F. Haney and H. J. Vogel, *Trends Biotechnol.*, 2011, **29**, 464–472.

274 R. E. W. Hancock and H. G. Sahl, *Nat. Biotechnol.*, 2006, **24**, 1551–1557.

275 K. Splith and I. Neundorf, *Eur. Biophys. J.*, 2011, **40**, 387–397.

276 A. Reinhardt and I. Neundorf, *Int. J. Mol. Sci.*, 2016, **17**, 701.

277 Y. Shai, *Biopolym. - Pept. Sci. Sect.*, 2002, **66**, 236–248.

278 D. A. Gray and M. Wenzel, *ACS Infect. Dis.*, 2020, **6**, 1346–1365.

279 H. S. Joo, C. I. Fu and M. Otto, *Phil. Trans. R. Soc. B*, 2016, **371**, 20150292.

280 M. R. Yeaman and N. Y. Yount, *Pharmacol. Rev.*, 2003, **55**, 27–55.

281 I. Y. Park, J. H. Cho, K. S. Kim, Y. B. Kim, M. S. Kim and S. C. Kim, *J. Biol. Chem.*, 2004, **279**, 13896–13901.

282 L. Zhang, J. Parente, S. M. Harris, D. E. Woods, R. E. W. Hancock and T. J. Falla, *Antimicrob. Agents Chemother.*, 2005, **49**, 2921–2927.

283 D. Migoń, D. Neubauer and W. Kamysz, *Protein J.*, 2018, **37**, 2–12.

284 J. McPhee, M. Scott and R. E. W. Hancock, *Comb. Chem. High Throughput Screen.*, 2005, **8**, 257–272.

285 K. Matsuzaki, *Biochim. Biophys. Acta - Biomembr.*, 2009, **1788**, 1687–1692.

286 H. X. Luong, D. H. Kim, B. J. Lee and Y. W. Kim, *Arch. Pharm. Res.*, 2017, **40**, 1414–1419.

287 T. T. T. Dinh, D. H. Kim, B. J. Lee and Y. W. Kim, *Bull. Korean Chem. Soc.*, 2014, **35**, 3632–3636.

288 H. Chapuis, J. Slaninová, L. Bednárová, L. Monincová, M. Buděšínský and V. Čeřovský, *Amino Acids*, 2012, **43**, 2047–2058.

289 R. Mourtada, H. D. Herce, D. J. Yin, J. A. Moroco, T. E. Wales, J. R. Engen and L. D. Walensky, *Nat. Biotechnol.*, 2019, **37**, 1186–1197.

290 I. Di Bonaventura, S. Baeriswyl, A. Capecchi, B. H. Gan, X. Jin, T. N. Siriwardena, R. He, T. Köhler, A. Pompilio, G. Di Bonaventura, C. Van Delden, S. Javor and J. L. Reymond, *Chem. Commun.*, 2018, **54**, 5130–5133.

291 F. Touti, G. Lautrette, K. D. Johnson, J. C. Delaney, A. Wollacott, H. Tissire, K. Viswanathan, Z. Shriver, S. K. Mong, A. J. Mijalis, O. J. Plante and B. L. Pentelute, *ChemBioChem*, 2018, **19**, 2039–2044.

292 E. I. Vrettos, G. Mező and A. G. Tzakos, *Beilstein J. Org. Chem.*, 2018, **14**, 930–954.

293 U. Hennrich and K. Kopka, *Pharmaceuticals*, 2019, **12**, E114.

294 BT1718 in Patients With Advanced Solid Tumours, https://clinicaltrials.gov/ct2/show/NCT03486730, (accessed 25 February 2020).

295 N. Cook, U. Banerji, T. R. Jeffrey Evans, A. Biondo, T. Germetaki, M. Randhawa, L. Godfrey, S. Leslie, P. Jeffrey, M. Rigby, G. Bennett, S. Blakemore, M. Koehler, A. Niewiarowski, M. Pittman and S. N. Symeonides, The European Society of Medical Oncology 2019 Annual Congress, 2019.

296 BT5528-100 in Patients With Advanced Solid Tumors Associated With EphA2 Expression, https://clinicaltrials.gov/ct2/show/NCT04180371, (accessed 27 February 2020).

297 M. Rigby, G. Bennett, L. Chen, G. Mudd, P. Beswick, H. Harrison, S. Watcham, H. Allen, A. Brown, K. Van Rietschoten, P. Jeffrey, P. U. Park, E. Haines, N. Keen and J. Lahdenranta, AACR-NCI-EORTC International Conference on Molecular Targets and Cancer Therapeutics, 2019.

298 P. M. S. D. Cal, M. J. Matos and G. J. L. Bernardes, *Expert Opin. Ther. Pat.*, 2017, **27**, 179–189.

299 L. Ma, C. Wang, Z. He, B. Cheng, L. Zheng and K. Huang, *Curr. Med. Chem.*, 2017, **24**, 1–24.

300 A. A. David, S. E. Park, K. Parang and R. K. Tiwari, *Curr. Top. Med. Chem.*, 2018, **18**, 1926–1936.

301 H. Chen, C. Liu, D. Chen, K. Madrid, S. Peng, X. Dong, M. Zhang and Y. Gu, *Mol. Pharm.*, 2015, **12**, 2505–2516.

302 N. Ptaszyńska, K. Gucwa, K. Olkiewicz, A. Łęgowska, J. Okońska, J. Ruczyński, A. Gitlin-Domagalska, D. Dębowski, S. Milewski and K. Rolka, *ACS Chem. Biol.*, 2019, **14**, 2233–2242.

303 WO2019018499, 2019.

304 K. Saikia, Y. D. Sravani, V. Ramakrishnan and N. Chaudhary, *Sci. Rep.*, 2017, **7**, 1–9.

305 M. Cossio-Ayala, M. Domínguez-López, E. Mendez-Enriquez, M. del C. Portillo-Téllez and E. García-Hernández, *Peptides*, 2017, **94**, 49–55.

306 P. Papareddy, G. Kasetty, M. Kalle, R. K. V. Bhongir, M. Mörgelin, A. Schmidtchen and M. Malmsten, *J. Antimicrob. Chemother.*, 2016, **71**, 170–180.

307 T. K. Pham, D. H. Kim, B. J. Lee and Y. W. Kim, *Bioorg. Med. Chem. Lett.*, 2013, **23**, 6717–6720.

308 J. M. Park, J. E. Jung and B. J. Lee, *Biochem. Biophys. Res. Commun.*, 1994, **205**, 948–954.

309 H. S. Won, S. J. Kang, W. S. Choi and B. J. Lee, *Mol. Cells*, 2011, **31**, 49–54.

310 X. Zhu, A. Shan, Z. Ma, W. Xu, J. Wang, S. Chou and B. Cheng, *Antimicrob. Agents Chemother.*, 2015, **59**, 3008–3017.

311 K. Chionis, D. Krikorian, A. I. Koukkou, M. Sakarellos-Daitsiotis and E. Panou-Pomonis, *J. Pept. Sci.*, 2016, **22**, 731–736.

312 E. F. Pettersen, T. D. Goddard, C. C. Huang, G. S. Couch, D. M. Greenblatt, E. C. Meng and T. E. Ferrin, *J. Comput. Chem.*, 2004, **13**, 1605–1612.

313 P. W. R. Harris, R. Kowalczyk, S. H. Yang, G. M. Williams and M. A. Brimble, *J. Pept. Sci.*, 2014, **20**, 186–190.

314 H. Jo, N. Meinhardt, Y. Wu, S. Kulkarni, X. Hu, D. Lowe, P. L. Davies, W. F. Degrado and D. C. Greenbaum, *J. Am. Chem. Soc.*, 2012, **134**, 17704–17713.

315 S. J. Walsh, PhD Thesis, University of Cambridge, 2019.

316 EUCAST, *Clin. Microbiol. Infect.*, 2003, **9**, ix–xv.

317 B. W. Holloway, *J. Gen. Microbiol.*, 1955, **13**, 572–581.

318 Y. Morita, Y. Komori, T. Mima, T. Kuroda, T. Mizushima and T. Tsuchiya, *FEMS Microbiol. Lett.*, 2001, **202**, 139–143.

319 L. Zhang, P. Dhillon, H. Yan, S. Farmer and R. E. W. Hancock, *Antimicrob. Agents Chemother.*, 2000, **44**, 3317–3321.

320 J. A. Hindler and R. M. Humphries, *J. Clin. Microbiol.*, 2013, **51**, 1678–1684.

321 J. Klockgether, A. Munder, J. Neugebauer, C. F. Davenport, F. Stanke, K. D. Larbig, S. Heeb, U. Schöck, T. M. Pohl, L. Wiehlmann and B. Tümmler, *J. Bacteriol.*, 2010, **192**, 1113–1121.

322 J. F. Linares, I. Gustafsson, F. Baquero and J. L. Martinez, *Proc. Natl. Acad. Sci.*, 2006, **103**, 19484–19489.

323 H. Chen, R. W. Wubbolts, H. P. Haagsman and E. J. A. Veldhuizen, *Sci. Rep.*, 2018, **8**, 10446.

324 H. S. Won, S. J. Jung, H. E. Kim, M. D. Seo and B. J. Lee, *J. Biol. Chem.*, 2004, **279**, 14784–14791.

325 D. Roccatano, G. Colombo, M. Fioroni and A. E. Mark, *Proc. Natl. Acad. Sci. USA*, 2002, **99**, 12179–12184.

326 H. S. Won, S. J. Kang and B. J. Lee, *Biochim. Biophys. Acta - Biomembr.*, 2009, **1788**, 1620–1629.

327 A. Rehman, W. M. Patrick and I. L. Lamont, *J. Med. Microbiol.*, 2019, **68**, 1–10.

328 M. Rusch, A. Spielmeyer, H. Zorn and G. Hamscher, *Appl. Microbiol. Biotechnol.*, 2019, **103**, 6933–6948.

329 S. T. Nguyen, X. Ding, M. M. Butler, T. F. Tashjian, N. P. Peet and T. L. Bowlin, *Bioorg. Med. Chem. Lett.*, 2011, **21**, 5961–5963.

330 J. A. Jiang, J. J. Zhai, X. H. Yu, X. Teng and Y. F. Ji, *Synthesis*, 2012, **2012**, 207–214.

331 L. D. Patterson and M. J. Miller, *J. Org. Chem.*, 2010, **75**, 1289–1292.

332 N. Grigan, D. Musel, G. A. Veinberg and E. Lukevics, *Synth. Commun.*, 1996, **26**, 1183–1185.

333 J. Azéma, B. Guidetti, J. Dewelle, B. Le Calve, T. Mijatovic, A. Korolyov, J. Vaysse, M. Malet-Martino, R. Martino and R. Kiss, *Bioorg. Med. Chem.*, 2009, **17**, 5396–5407.

334 O. D. Dailey, *J. Org. Chem.*, 1987, **52**, 1984–1989.

335 S. D. Atkin, S. Abid, M. Foster, M. Bose, A. Keller, R. Hollaway, H. S. Sader, D. E. Greenberg, J. D. Finklea, M. Castanheira and R. Jain, *Infect. Drug Resist.*, 2018, **11**, 1499–1510.

336 N. Al Naiemi, B. Duim and A. Bart, *J. Med. Microbiol.*, 2006, **55**, 1607–1608.

337 A. J. Sales, R. Fathi, H. Mobaiyen, F. Rasi Bonab, K. B. Kondlaji and M. Sadeghnezhadi, *Electornic J. Biol.*, 2017, **13**, 253–259.

338 WO 2020025108 A1, 2020.

339 M. Kunishima, C. Kawachi, K. Hioki, K. Terao and S. Tani, *Tetrahedron*, 2001, **57**, 1551–1558.

340 A. Casaschi, R. Grigg and J. M. Sansano, *Tetrahedron*, 2000, **56**, 7553–7560.

341 U. Tehler, J. H. Fagerberg, R. Svensson, M. Larhed, P. Artursson and C. A. S. Bergström, *J. Med. Chem.*, 2013, **56**, 2690–2694.

342 G. Zhao, M. J. Miller, S. Franzblau, B. Wan and U. Möllmann, *Bioorg. Med. Chem. Lett.*, 2006, **16**, 5534–5537.

343 S. Sánchez-Gómez, M. Lamata, J. Leiva, S. E. Blondelle, R. Jerala, J. Andrä, K. Brandenburg, K. Lohner, I. Moriyón and G. Martínez-De-Tejada, *BMC Microbiol.*, 2008, **8**, 196.

344 J. He, C. G. Starr and W. C. Wimley, *Biochim. Biophys. Acta - Biomembr.*, 2015, **1848**, 8–15.

345 J. Varkey and R. Nagaraj, *Antimicrob. Agents Chemother.*, 2005, **49**, 4561–4566.

346 I. Sekirov, S. L. Russell, L. Caetano M. Antunes and B. B. Finlay, *Physiol. Rev.*, 2010, **90**, 859–904.

347 S. Santajit and N. Indrawattana, *Biomed Res. Int.*, 2016, **2016**, 2475067.

348 E. Glukhov, L. L. Burrows and C. M. Deber, *Biopolymers*, 2008, **89**, 360–371.

349 A. Luther, M. Urfer, M. Zahn, M. Müller, S. Y. Wang, M. Mondal, A. Vitale, J. B. Hartmann, T. Sharpe, F. Lo Monte, H. Kocherla, E. Cline, G. Pessi, P. Rath, S. M. Modaresi, P. Chiquet, S. Stiegeler, C. Verbree, T. Remus, M. Schmitt, C. Kolopp, M. A. Westwood, N. Desjonquères, E. Brabet, S. Hell, K. LePoupon, A. Vermeulen, R. Jaisson, V. Rithié, G. Upert, A. Lederer, P. Zbinden, A. Wach, K. Moehle, K. Zerbe, H. H. Locher, F. Bernardini, G. E. Dale, L. Eberl, B. Wollscheid, S. Hiller, J. A. Robinson and D. Obrecht, *Nature*, 2019, **576**, 452–458.

350 T. Mishig-Ochir, D. Gombosuren, A. Jigjid, B. Tuguldur, G. Chuluunbaatar, E. Urnukhsaikhan, C. Pathak and B. J. Lee, *Protein Pept. Lett.*, 2017, **24**, 197–205.

351 J. Y. Kwon, M. K. Kim, L. Mereuta, C. H. Seo, T. Luchian and Y. Park, *AMB Express*, 2019, **9**, 122.

352 M. Ouberai, F. El Garch, A. Bussiere, M. Riou, D. Alsteens, L. Lins, I. Baussanne, Y. F. Dufrêne, R. Brasseur, J. L. Decout and M. P. Mingeot-Leclercq, *Biochim. Biophys. Acta - Biomembr.*, 2011, **1808**, 1716–1727.

353 C. Pitsalidis, A. M. Pappa, M. Porel, C. M. Artim, G. C. Faria, D. D. Duong, C. A. Alabi, S. Daniel, A. Salleo and R. M. Owens, *Adv. Mater.*, 2018, **30**, 1803130.

354 A. A. Romani, M. C. Baroni, S. Taddei, F. Ghidini, P. Sansoni, S. Cavirani and C. S. Cabassi, *J. Pept. Sci.*, 2013, **19**, 554–565.

355 WO 2019145913, 2019.

356 P. Lehouritis, C. Springer and M. Tangney, *J. Control. Release*, 2013, **170**, 120–131.

357 K. A. Pardeshi, T. A. Kumar, G. Ravikumar, M. Shukla, G. Kaul, S. Chopra and H. Chakrapani, *Bioconjug. Chem.*, 2019, **30**, 751–759.

358 E. M. Williams, R. F. Little, A. M. Mowday, M. H. Rich, J. V. E. Chan-Hyams, J. N. Copp, J. B. Smaill, A. V. Patterson and D. F. Ackerley, *Biochem. J*, 2015, **471**, 131–153.

359 J. D. Bargh, A. Isidro-Llobet, J. S. Parker and D. R. Spring, *Chem. Soc. Rev.*, 2019, **48**, 4361–4374.

360 J. D. Bargh, S. J. Walsh, A. Isidro-Llobet, S. Omarjee, J. S. Carroll and D. R. Spring, *Chem. Sci.*, 2020, **11**, 2375–2380.

361 C.-M. Cheng, Y.-L. Lu, K.-H. Chuang, W.-C. Hung, J. Shiea, Y.-C. Su, C.-H. Kao, B.-M. Chen, S. Roffler and T.-L. Cheng, *Cancer Gene Ther.*, 2008, **15**, 393–401.

362 W. J. Liang, K. J. Wilson, H. Xie, J. Knol, S. Suzuki, N. G. Rutherford, P. J. F. Henderson and R. A. Jefferson, *J. Bacteriol.*, 2005, **187**, 2377–2385.

363 S. R. Hanson, M. D. Best and C. H. Wong, *Angew. Chemie - Int. Ed.*, 2004, **43**, 5736–5763.

364 T. Barbeyron, L. Brillet-Guéguen, W. Carré, C. Carrière, C. Caron, M. Czjzek, M. Hoebeke and G. Michel, *PLoS One*, 2016, **11**, e0164846.

365 K. E. Beatty, M. Williams, B. L. Carlson, B. M. Swarts, R. M. Warren, P. D. Van Helden and C. R. Bertozzi, *Proc. Natl. Acad. Sci. USA*, 2013, **110**, 12911–12916.

366 M. B. Miller and B. L. Bassler, *Annu. Rev. Microbiol.*, 2001, **55**, 165–199.

367 G. D. Geske, R. J. Wezeman, A. P. Siegel and H. E. Blackwell, *J. Am. Chem. Soc.*, 2005, **127**, 12762–12763.

368 V. V. Komnatnyy, W. C. Chiang, T. Tolker-Nielsen, M. Givskov and T. E. Nielsen, *Angew. Chemie - Int. Ed.*, 2014, **53**, 439–441.

369 S. Cantel, A. Le Chevalier Isaad, M. Scrima, J. J. Levy, R. D. DiMarchi, P. Rovero, J. A. Halperin, A. M. Ursi, A. M. Papini and M. Chorev, *J. Org. Chem.*, 2008, **73**, 5663–5674.

370 S. Shanmugaraju, A. K. Bar, K. W. Chi and P. S. Mukherjee, *Organometallics*, 2010, **29**, 2971–2980.

371 S. J. Walsh, S. Omarjee, W. R. J. D. Galloway, T. T.-L. Kwan, H. F. Sore, J. S. Parker, M. Hyvönen, J. S. Carroll and D. R. Spring, *Chem. Sci.*, 2019, **10**, 694–700.

372 C. Appiah, K. R. Siefermann, M. Jorewitz, H. Barqawi and W. H. Binder, *RSC Adv.*, 2016, **6**, 6358–6367.

373 M. W. Majewski, R. Tiwari, P. A. Miller, S. Cho, S. G. Franzblau and M. J. Miller, *Bioorg. Med. Chem. Lett.*, 2016, **26**, 2068–2071.

374 European Committee on Antimicrobial Susceptibility Testing, https://eucast.org/, (accessed 26 May 2020).

Appendices

6. Appendices

6.1 Appendix 1 - Selected NMR spectra

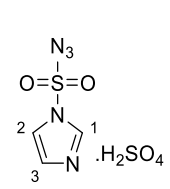

1

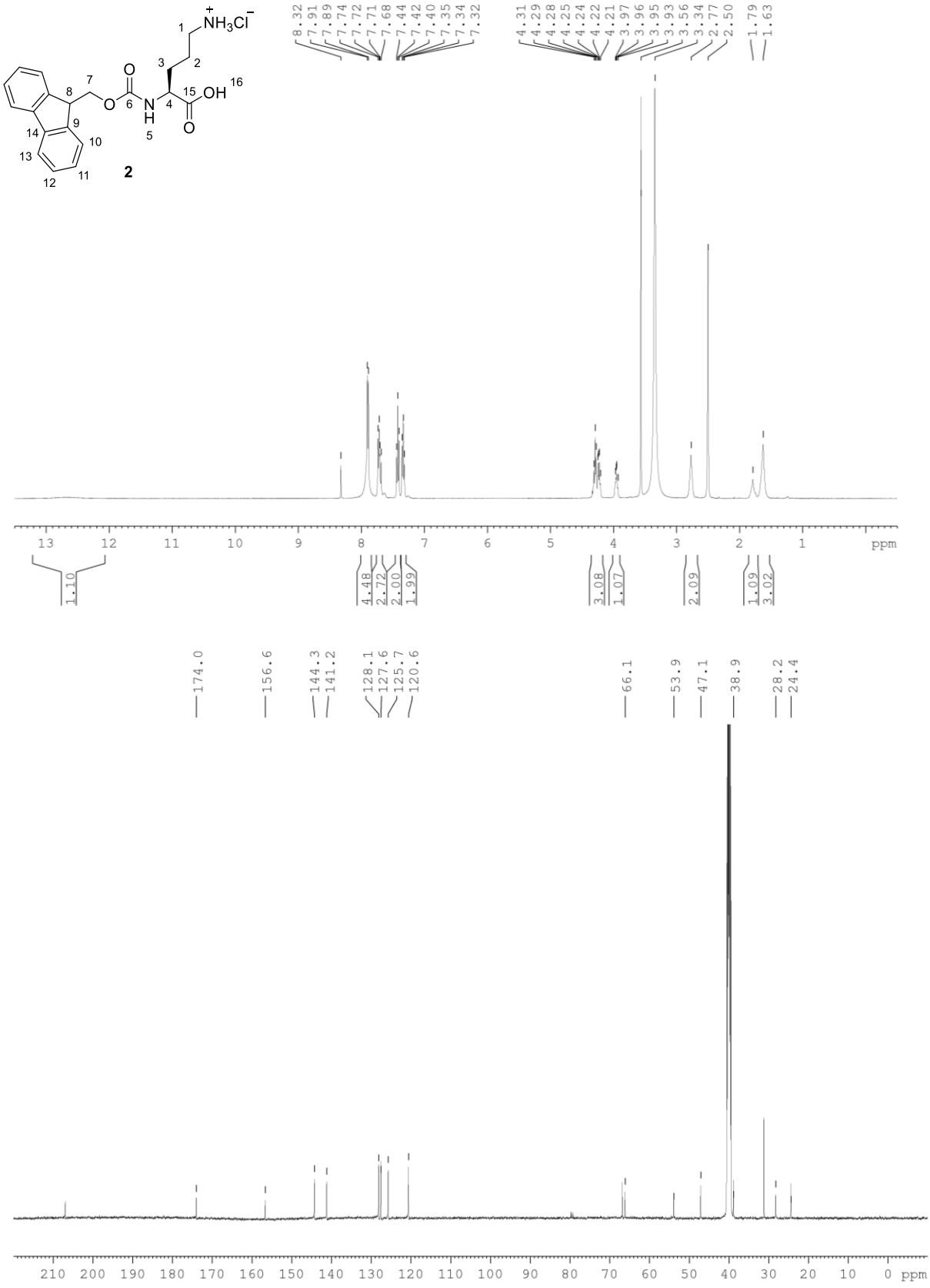
8.32
7.91
7.89
7.74
7.72
7.71
7.68
7.44
7.42
7.40
7.35
7.34
7.32
4.31
4.29
4.28
4.25
4.24
4.22
4.21
3.97
3.96
3.95
3.93
3.56
3.34
2.77
2.50
1.79
1.63
ppm
1.10
4.48
2.72
2.00
1.99
3.08
1.07
2.09
1.09
3.02
174.0
156.6
144.3
141.2
128.1
127.6
125.7
120.6
66.1
53.9
47.1
38.9
28.2
24.4
ppm

2

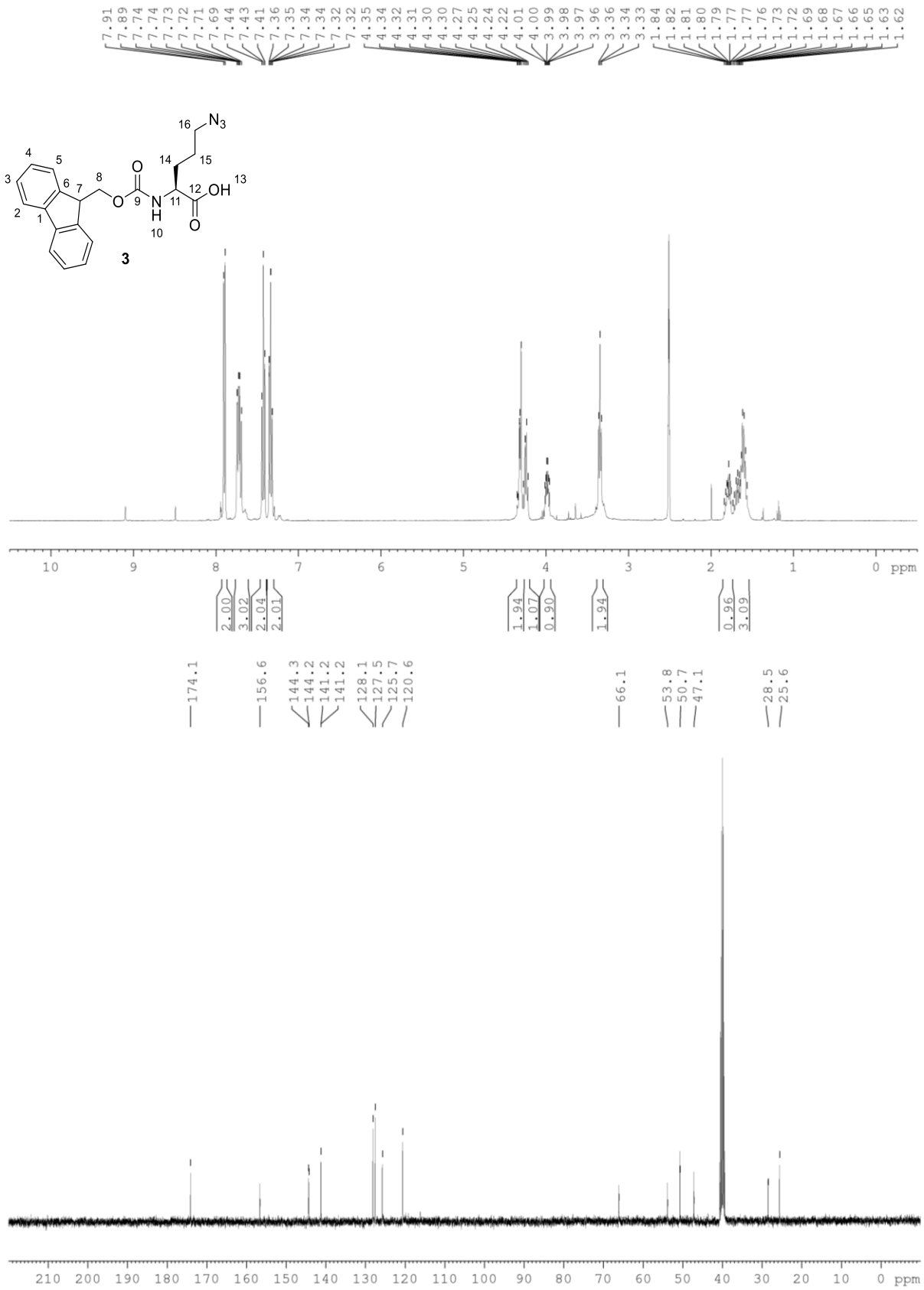
7.91 7.89 7.74 7.74 7.73 7.72 7.71 7.69 7.44 7.43 7.41 7.36 7.35 7.34 7.34 7.32 7.32
4.35 4.34 4.32 4.31 4.30 4.30 4.27 4.25 4.24 4.22 4.01 4.00 3.99 3.98 3.97 3.96 3.36 3.34 3.33
1.84 1.82 1.81 1.80 1.79 1.77 1.77 1.76 1.73 1.72 1.69 1.68 1.67 1.66 1.65 1.63 1.62
16 N3 14 15 4 5 3 6 7 8 O 12 OH 13 2 1 9 N H 11 10 O
3
10 9 8 7 6 5 4 3 2 1 0 ppm
2.00 3.02 2.04 2.01 1.94 1.07 0.90 1.94 0.96 3.09
174.1 156.6 144.3 144.2 141.2 141.2 128.1 127.5 125.7 120.6 66.1 53.8 50.7 47.1 28.5 25.6
210 200 190 180 170 160 150 140 130 120 110 100 90 80 70 60 50 40 30 20 10 0 ppm

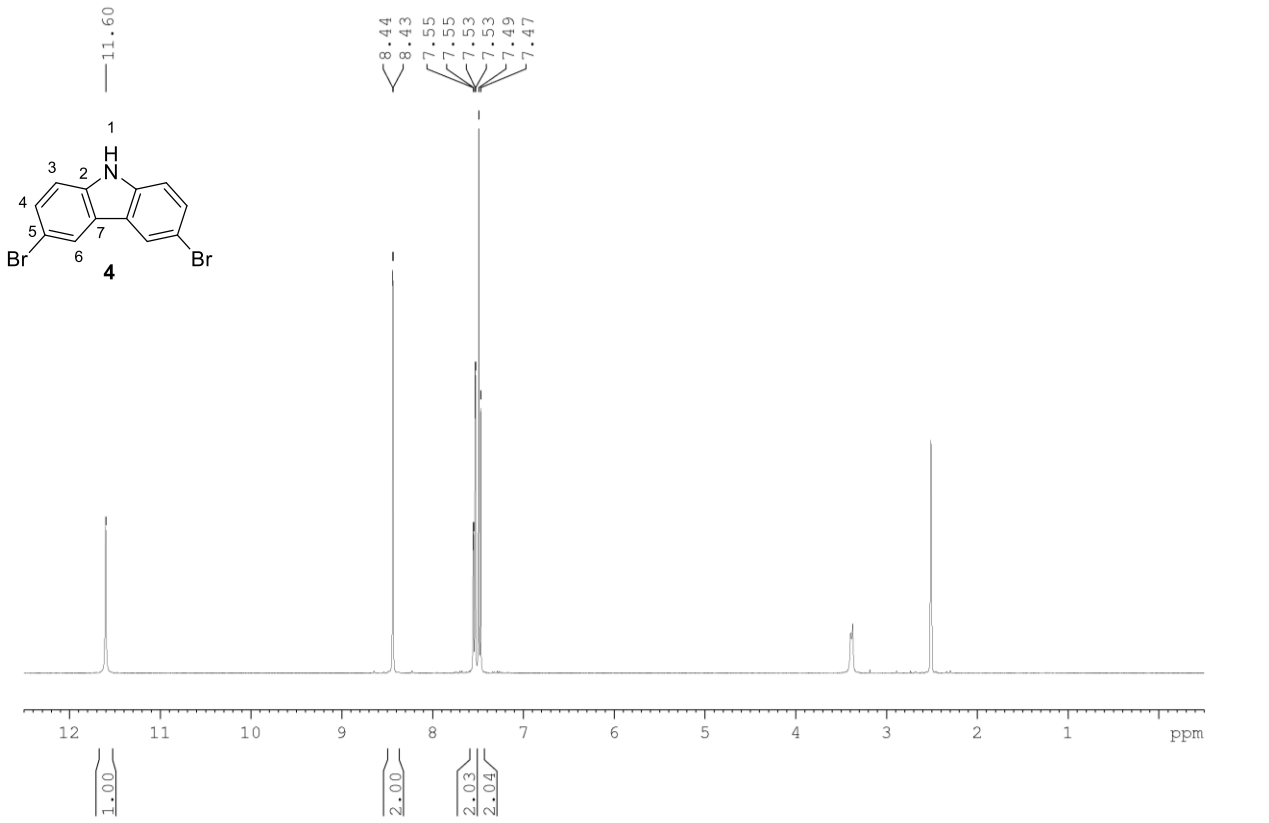
11.60
8.44
8.43
7.55
7.55
7.53
7.53
7.49
7.47
1
2
3
4
5
6
7
H
N
Br
Br
4
12
11
10
9
8
7
6
5
4
3
2
1
ppm
1.00
2.00
2.03
2.04

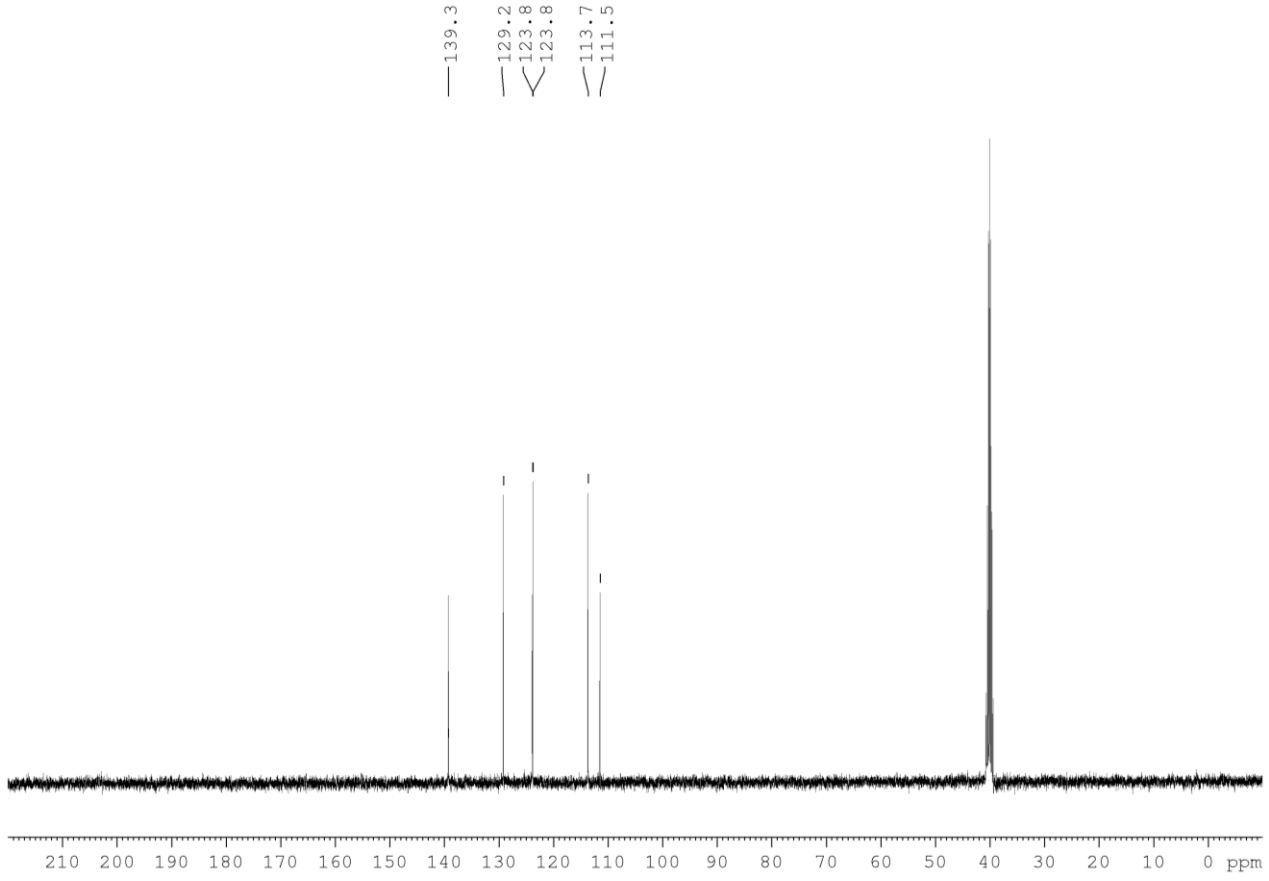
139.3
129.2
123.8
123.8
113.7
111.5
210 200 190 180 170 160 150 140 130 120 110 100 90 80 70 60 50 40 30 20 10 0 ppm

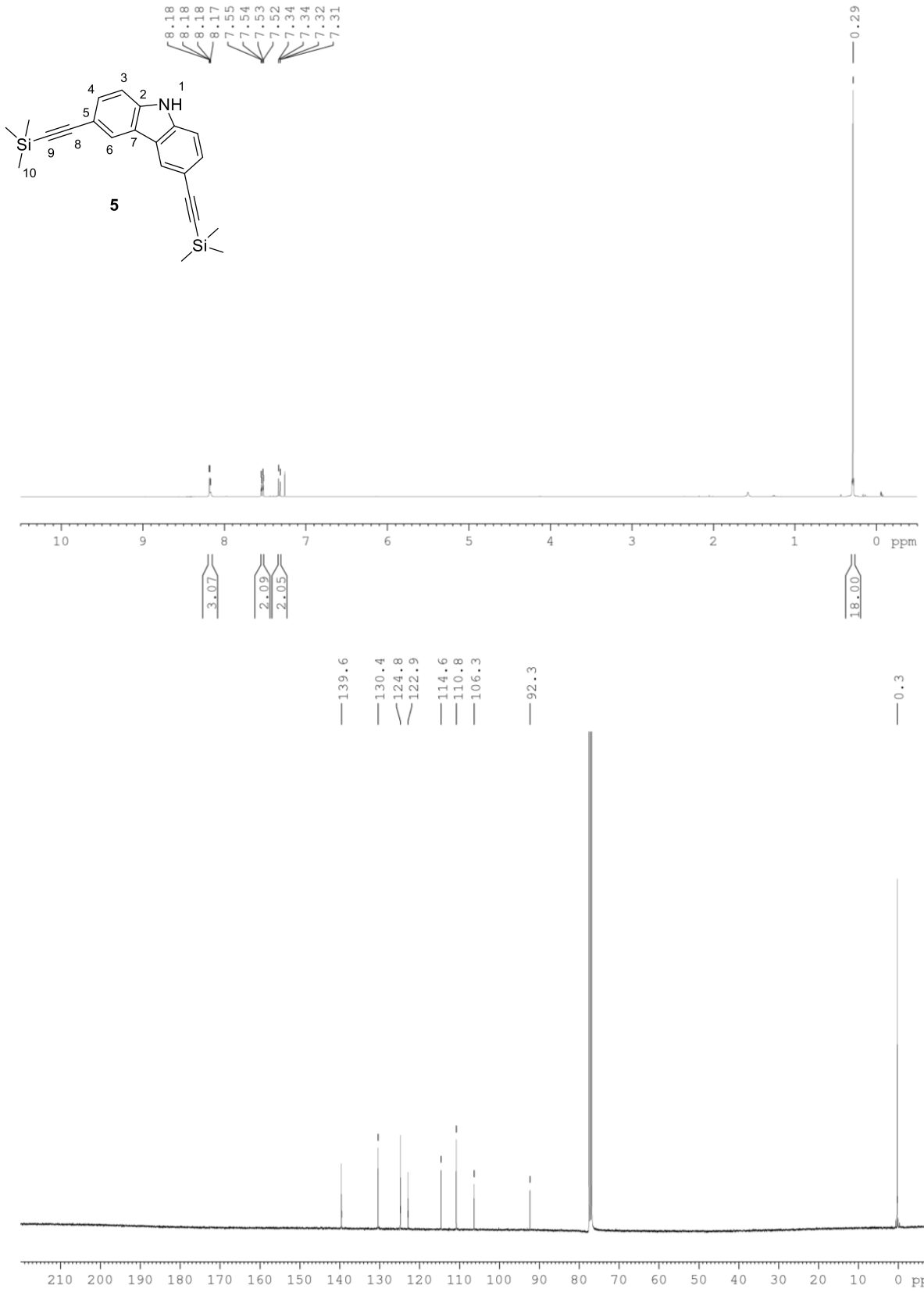
8.18
8.18
8.18
8.17
7.55
7.54
7.53
7.52
7.34
7.34
7.32
7.31
0.29
NH
Si
Si
5
10 9 8 7 6 5 4 3 2 1 0 ppm
3.07
2.09
2.05
18.00
139.6
130.4
124.8
122.9
114.6
110.8
106.3
92.3
0.3
210 200 190 180 170 160 150 140 130 120 110 100 90 80 70 60 50 40 30 20 10 0 ppm

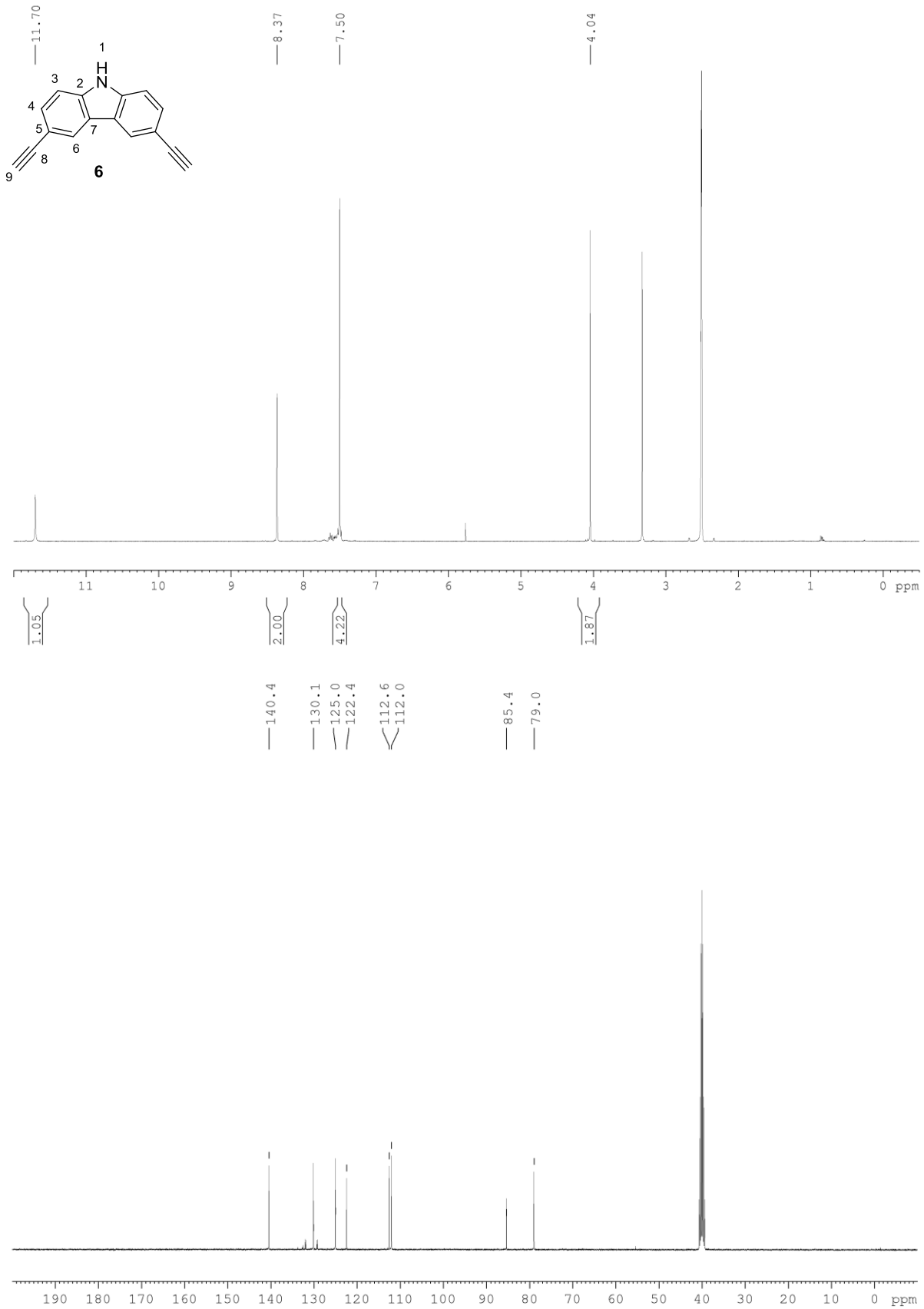
11.70
8.37
7.50
4.04
1
H
N
2
3
4
5
6
7
8
9
6
11
10
9
8
7
6
5
4
3
2
1
0 ppm
1.05
2.00
4.22
1.87
140.4
130.1
125.0
122.4
112.6
112.0
85.4
79.0
190
180
170
160
150
140
130
120
110
100
90
80
70
60
50
40
30
20
10
0 ppm

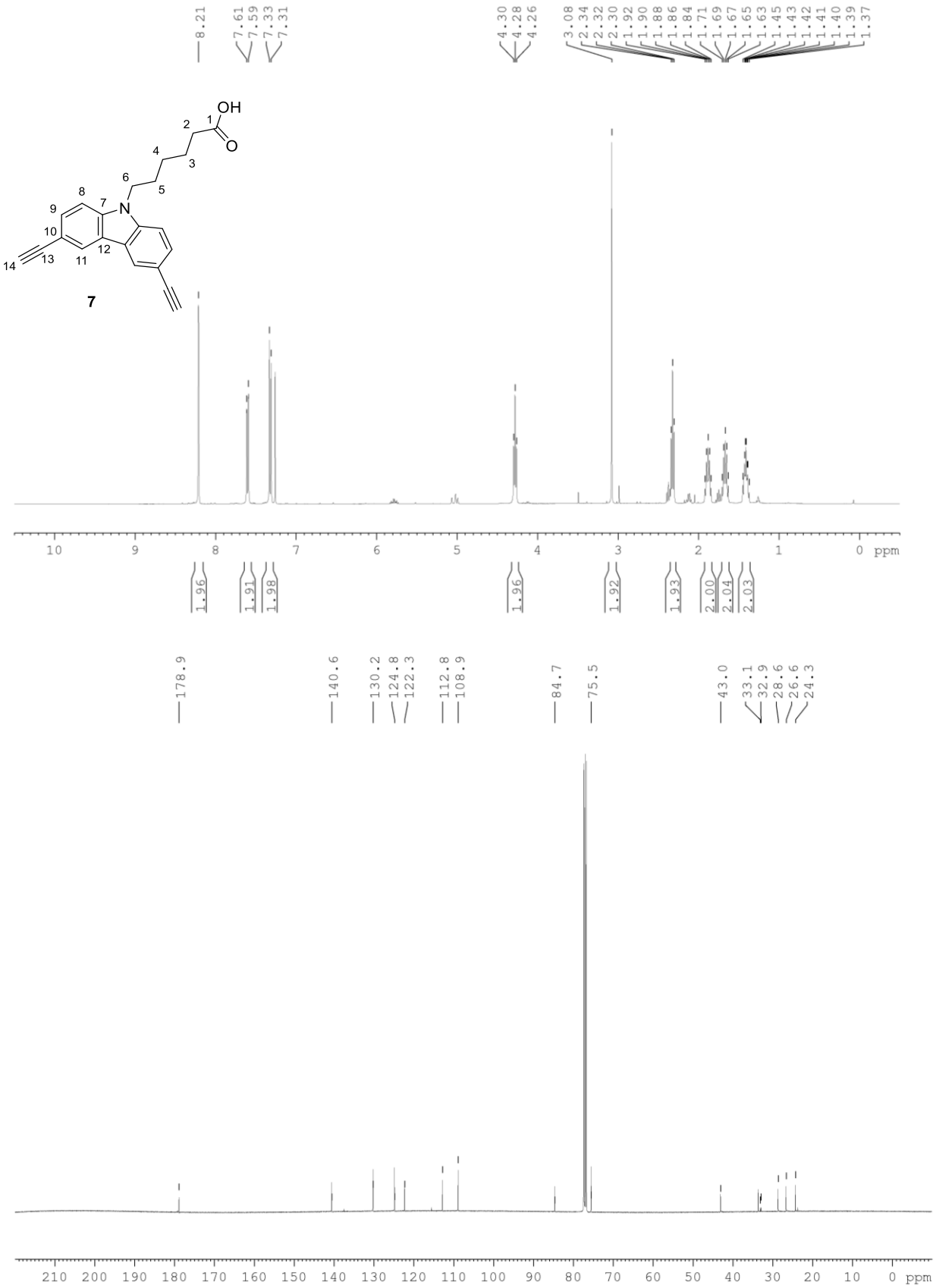
8.21
7.61
7.59
7.33
7.31
4.30
4.28
4.26
3.08
2.34
2.32
2.30
1.92
1.90
1.88
1.86
1.84
1.71
1.69
1.67
1.65
1.63
1.45
1.43
1.42
1.41
1.40
1.39
1.37
OH
O
N
1
2
3
4
5
6
7
8
9
10
11
12
13
14
7
10 9 8 7 6 5 4 3 2 1 0 ppm
1.96
1.91
1.98
1.96
1.92
1.93
2.00
2.04
2.03
178.9
140.6
130.2
124.8
122.3
112.8
108.9
84.7
75.5
43.0
33.1
32.9
28.6
26.6
24.3
210 200 190 180 170 160 150 140 130 120 110 100 90 80 70 60 50 40 30 20 10 0 ppm

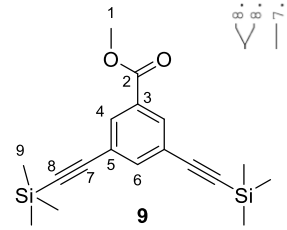
1
O
O
2
3
4
9
8
5
7
6
Si
Si

9

8.04
8.04
7.72
3.91
2.16
0.25
0.24
0.23
10
9
8
7
6
5
4
3
2
1
0 ppm
1.94
0.97
3.00
18.03

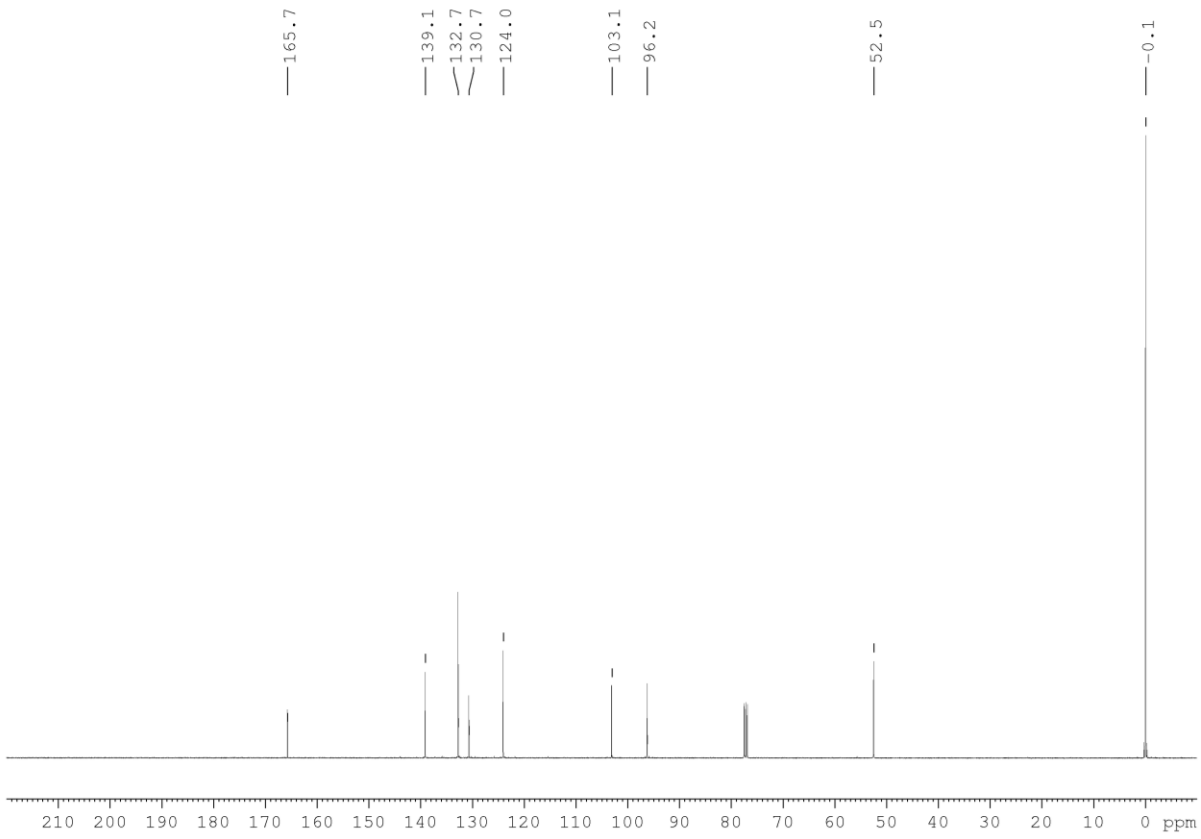
165.7
139.1
132.7
130.7
124.0
103.1
96.2
52.5
0.1
210 200 190 180 170 160 150 140 130 120 110 100 90 80 70 60 50 40 30 20 10 0 ppm

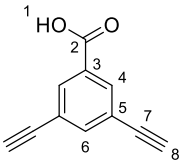
1
HO
O
2
3
4
5
6
7
8

10

7.95
7.94
7.80
7.80
7.80
4.40
3.32
2.51
2.50
2.50
2.50
10
9
8
7
6
5
4
3
2
1
0 ppm
2.00
0.96
1.92
170.8
143.4
131.6
128.9
128.1
87.9
86.7
210
200
190
180
170
160
150
140
130
120
110
100
90
80
70
60
50
40
30
20
10
0 ppm

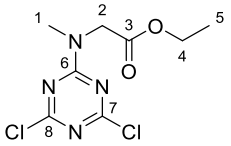
1
2
3
O
5
N
4
6
O
N
N
7
Cl
8
N
Cl

12

4.35
4.25
4.23
4.22
4.20
3.25
1.30
1.28
1.26
11
10
9
8
7
6
5
4
3
2
1
0 ppm
1.96
1.97
2.92
3.00

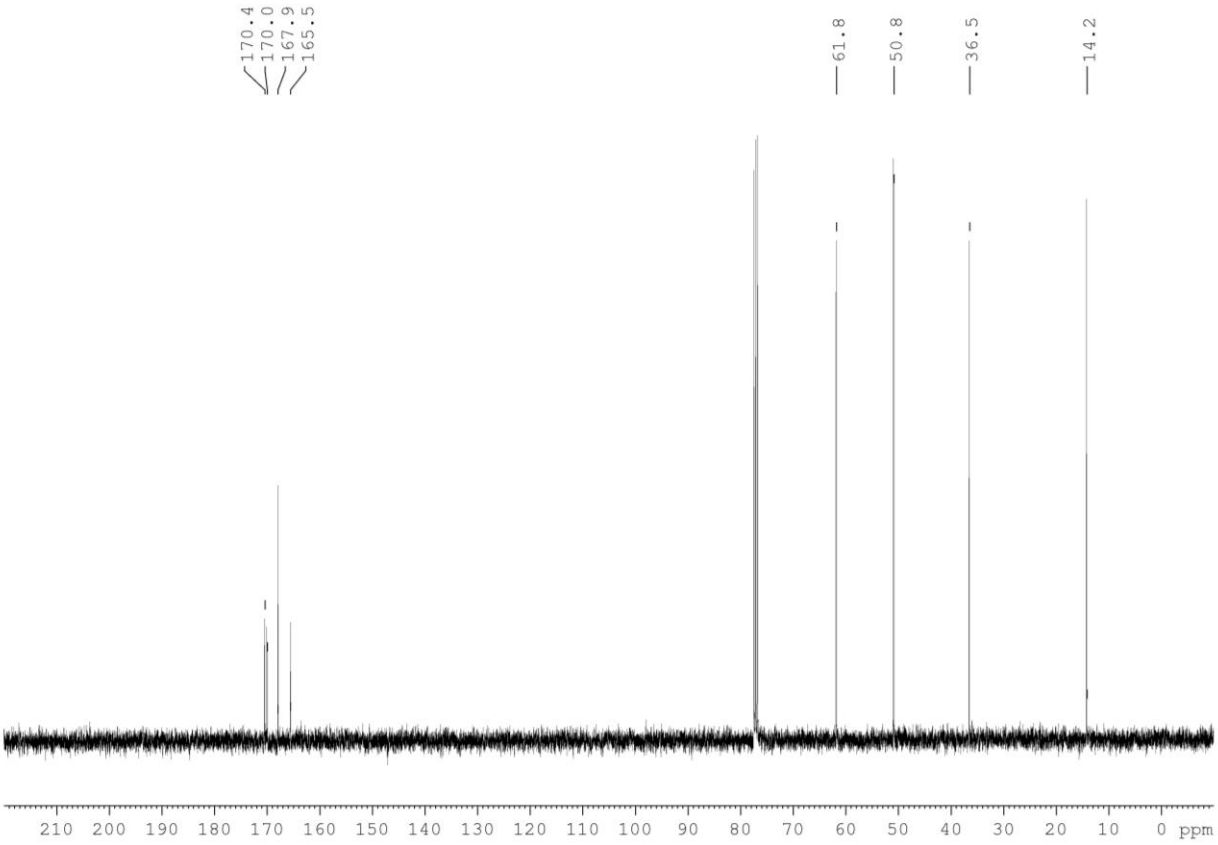
170.4
170.0
167.9
165.5
61.8
50.8
36.5
14.2
210
200
190
180
170
160
150
140
130
120
110
100
90
80
70
60
50
40
30
20
10
0 ppm

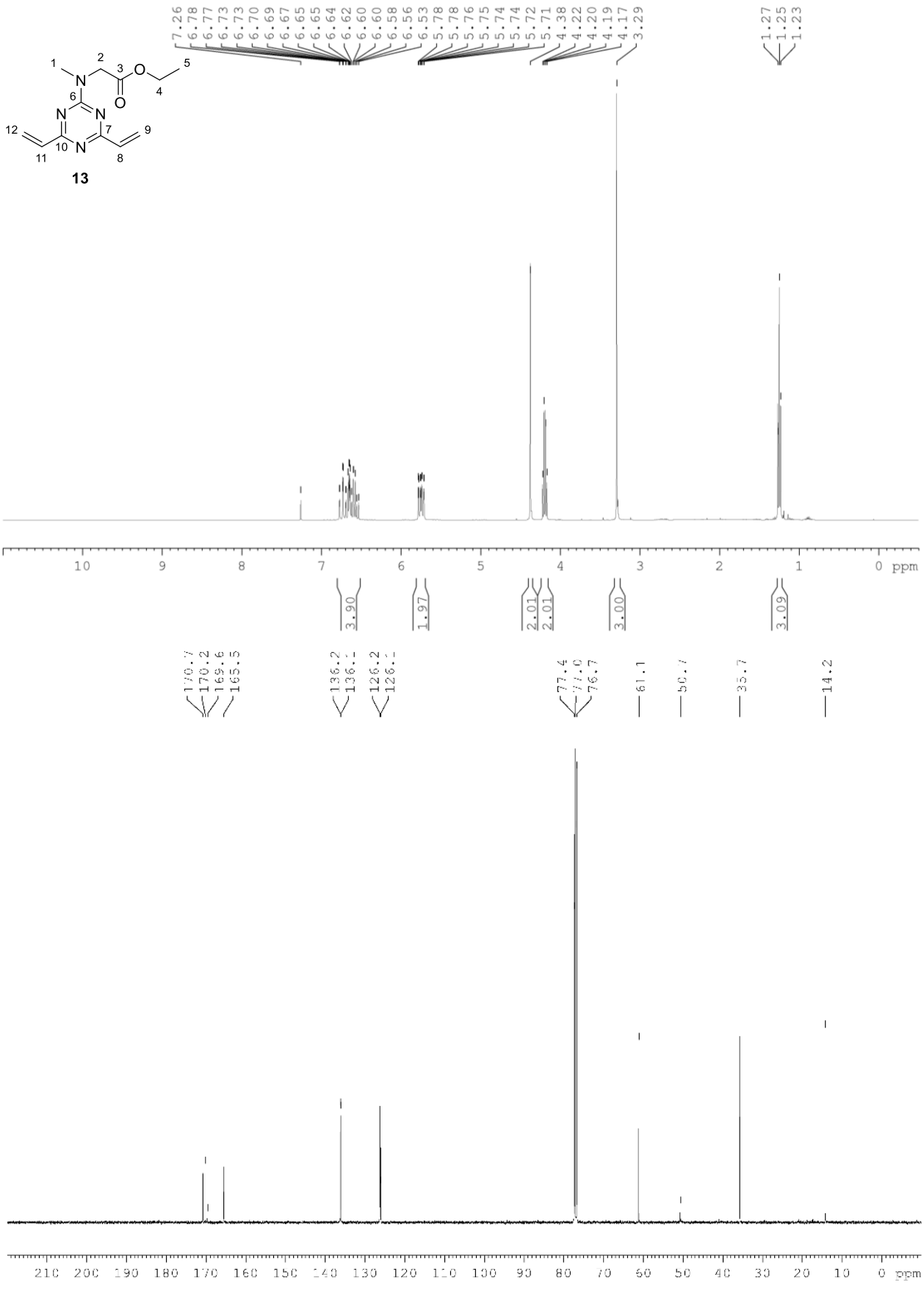
7.26
6.78
6.77
6.73
6.73
6.70
6.69
6.67
6.65
6.64
6.62
6.60
6.60
6.58
6.56
6.53
5.78
5.78
5.76
5.75
5.74
5.74
5.72
5.71
4.38
4.22
4.20
4.19
4.17
3.29
1.27
1.25
1.23
1
2
3
4
5
6
7
8
9
10
11
12
13
10 9 8 7 6 5 4 3 2 1 0 ppm
3.90
1.97
2.01
2.01
3.00
3.09
170.7
170.2
169.6
165.5
136.2
126.2
77.4
77.0
76.7
61.1
35.7
14.2
210 200 190 180 170 160 150 140 130 120 110 100 90 80 70 60 50 40 30 20 10 0 ppm

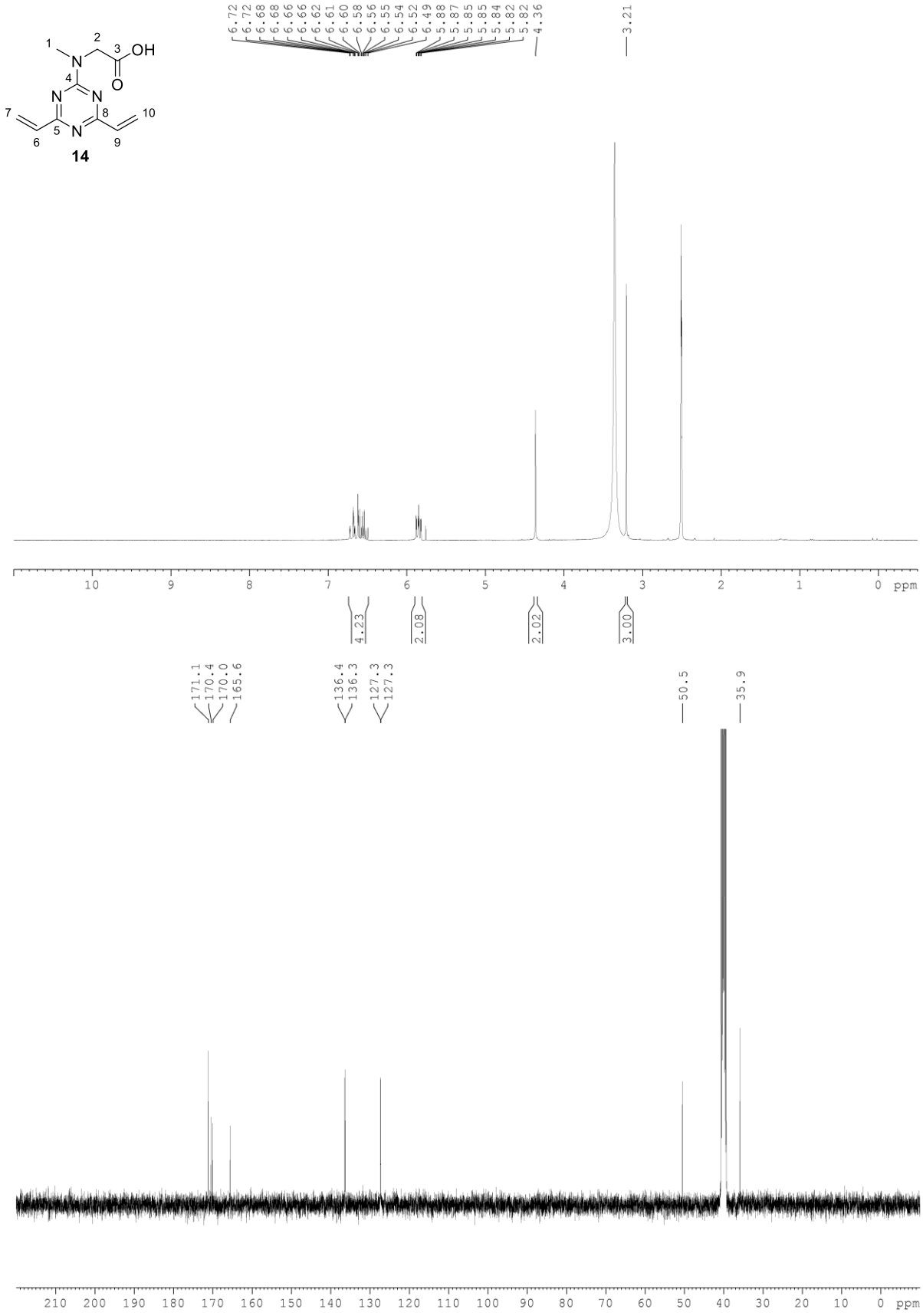
6.72
6.72
6.68
6.68
6.66
6.66
6.62
6.61
6.60
6.58
6.56
6.55
6.54
6.52
6.49
5.88
5.87
5.85
5.85
5.84
5.82
5.82
4.36
3.21
10 9 8 7 6 5 4 3 2 1 0 ppm
4.23
2.08
2.02
3.00
171.1
170.4
170.0
165.6
136.4
136.3
127.3
127.3
50.5
35.9
210 200 190 180 170 160 150 140 130 120 110 100 90 80 70 60 50 40 30 20 10 0 ppm

14

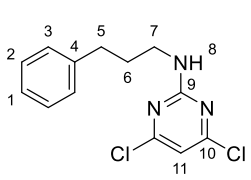
1
2
3
4
5
6
7
NH
8
9
N
N
Cl
10
Cl
11

15

7.34
7.32
7.30
7.28
7.24
7.24
7.23
7.21
6.62
5.45
3.50
3.49
3.47
3.46
2.74
2.72
2.70
2.00
1.98
1.96
1.94
1.92
10
9
8
7
6
5
4
3
2
1
0 ppm
3.00
3.11
0.98
0.96
2.15
2.13
2.21
161.6
141.1
128.5
128.3
126.1
108.9
41.1
33.0
30.8
210
200
190
180
170
160
150
140
130
120
110
100
90
80
70
60
50
40
30
20
10
ppm

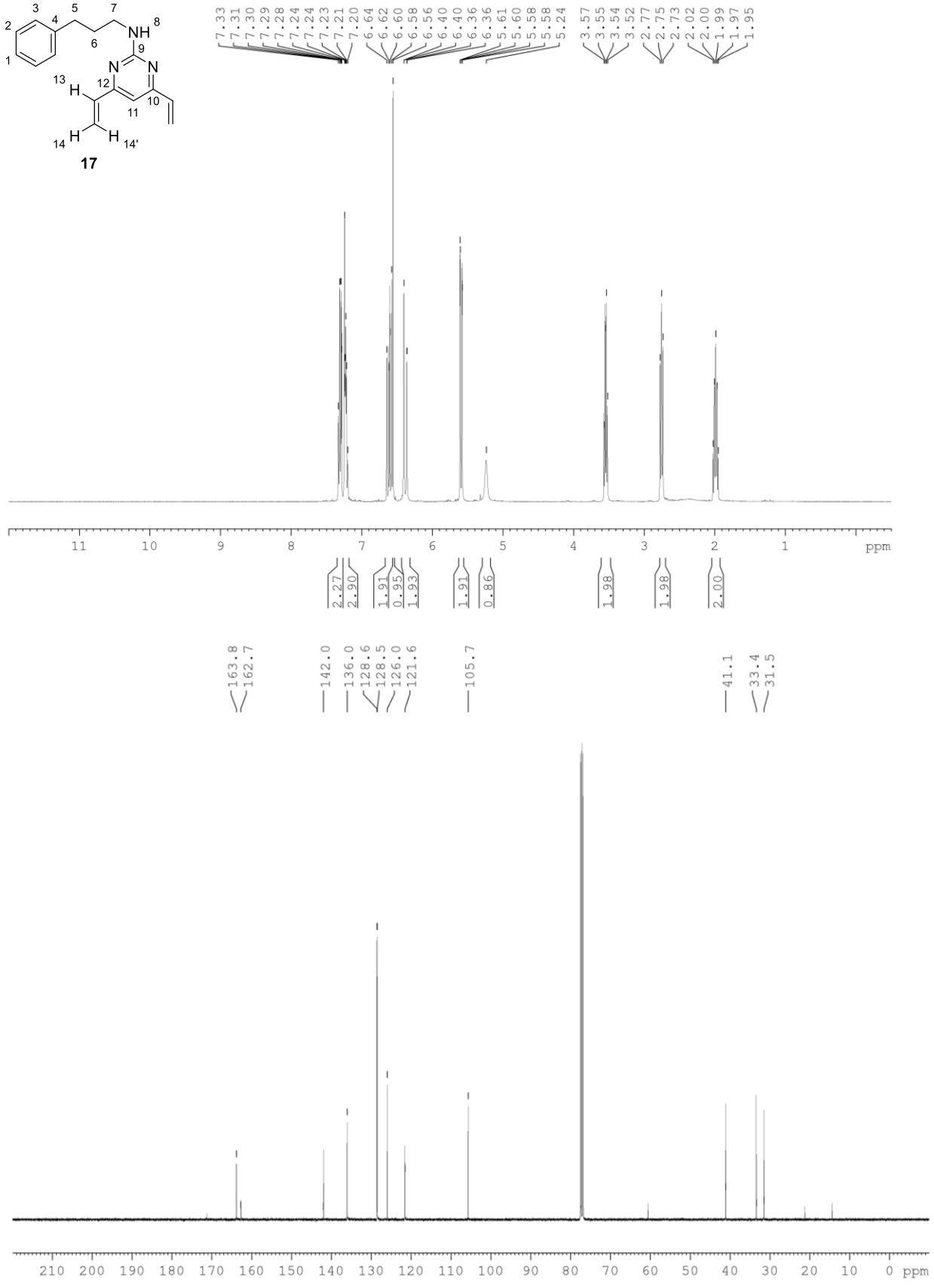
17
7.33
7.31
7.30
7.29
7.28
7.24
7.24
7.23
7.21
7.20
6.64
6.62
6.60
6.58
6.56
6.40
6.40
6.36
6.36
5.61
5.60
5.58
5.58
5.24
3.57
3.55
3.54
3.52
2.77
2.75
2.73
2.02
2.00
1.99
1.97
1.95
ppm
2.27
2.90
1.91
0.95
1.93
1.91
0.86
1.98
1.98
2.00
163.8
162.7
142.0
136.0
128.6
128.5
126.0
121.6
105.7
41.1
33.4
31.5
ppm

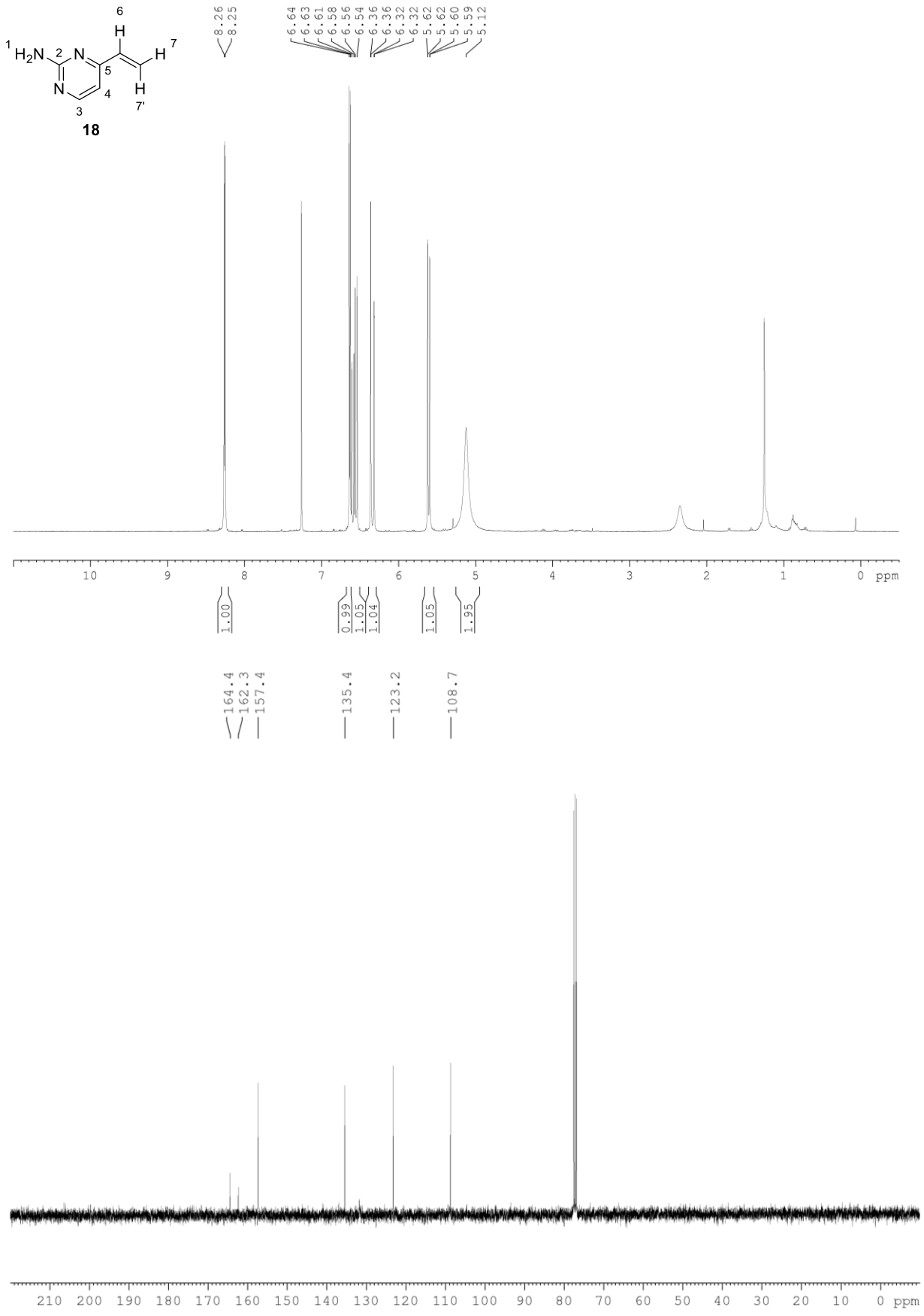
6
H
1
H2N
2
N
H
7
5
N
4
H
3
7'
18
8.26
8.25
6.64
6.63
6.61
6.58
6.56
6.54
6.36
6.36
6.32
6.32
5.62
5.62
5.60
5.59
5.12
10
9
8
7
6
5
4
3
2
1
0 ppm
1.00
0.99
1.05
1.04
1.05
1.95
164.4
162.3
157.4
135.4
123.2
108.7
210 200 190 180 170 160 150 140 130 120 110 100 90 80 70 60 50 40 30 20 10 0 ppm

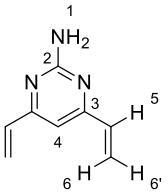
1
NH2
2
N
N
3
H
5
4
6
H
H
6'

24

6.67
6.65
6.62
6.60
6.58
6.38
6.38
6.34
6.33
5.63
5.63
5.61
5.60
5.19
10
9
8
7
6
5
4
3
2
1
0 ppm
1.02
1.96
2.00
2.01
1.76

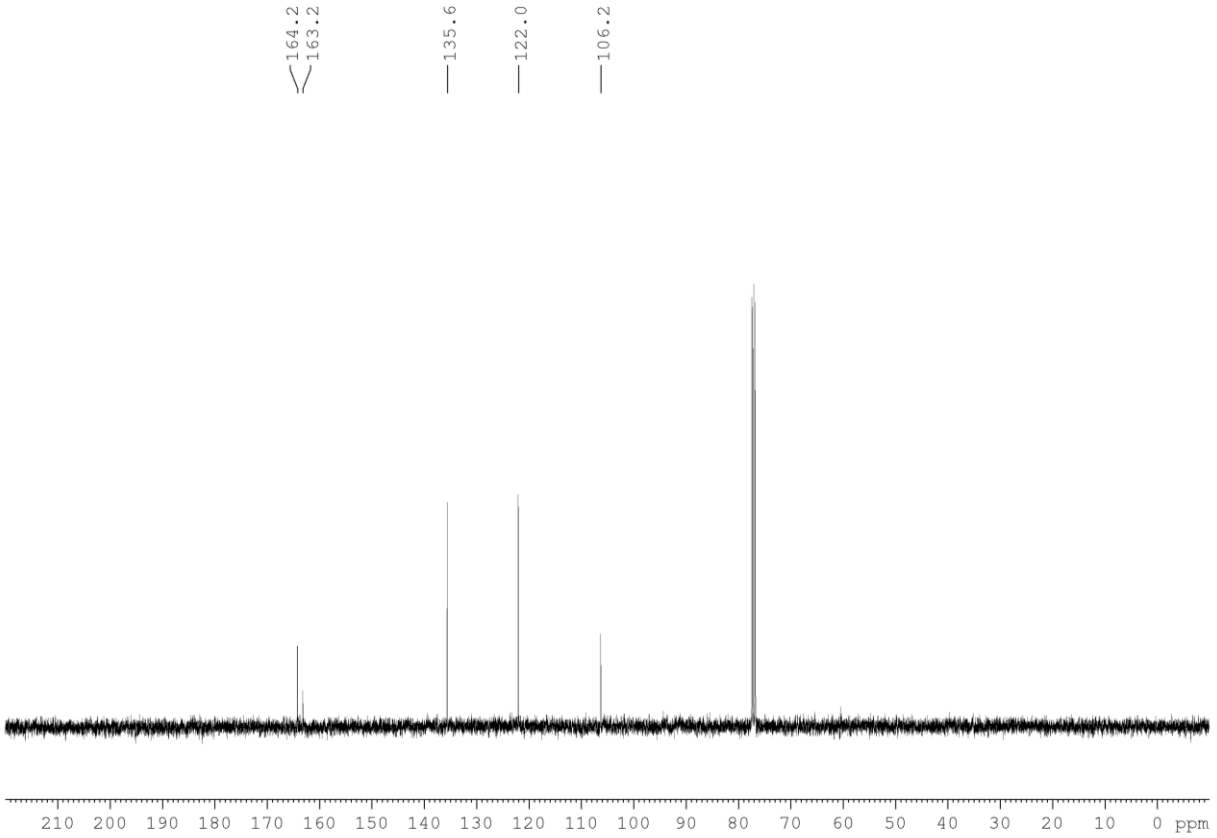
164.2
163.2
135.6
122.0
106.2
210 200 190 180 170 160 150 140 130 120 110 100 90 80 70 60 50 40 30 20 10 0 ppm

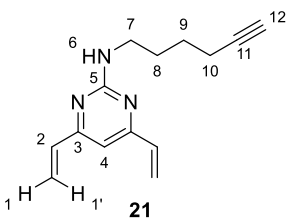
6
HN
5
7
9
12
11
8
10
N
N
2
3
4
1
H
H
1'

21


6.63
6.60
6.59
6.56
6.54
6.39
6.35
5.58
5.56
5.55
5.19
3.54
3.52
3.50
3.49
2.28
2.27
2.26
2.26
2.25
2.24
1.98
1.97
1.96
1.79
1.77
1.76
1.74
1.72
1.68
1.66
1.64
1.63

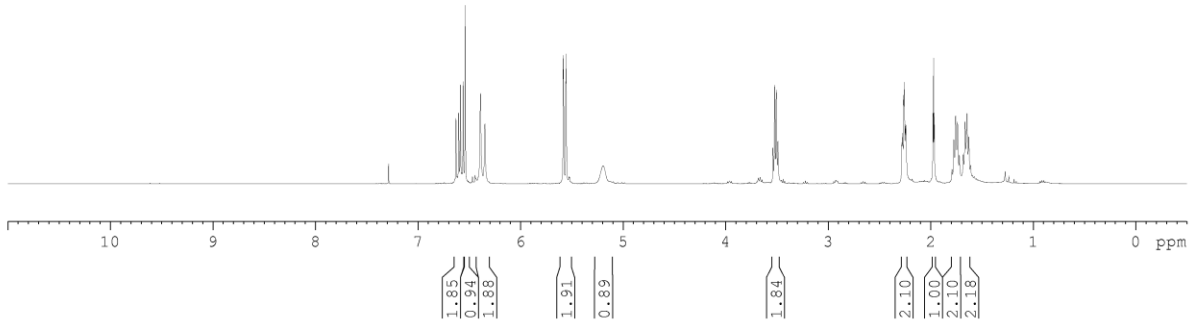
10
9
8
7
6
5
4
3
2
1
0 ppm
1.85
0.94
1.88
1.91
0.89
1.84
2.10
1.00
2.10
2.18

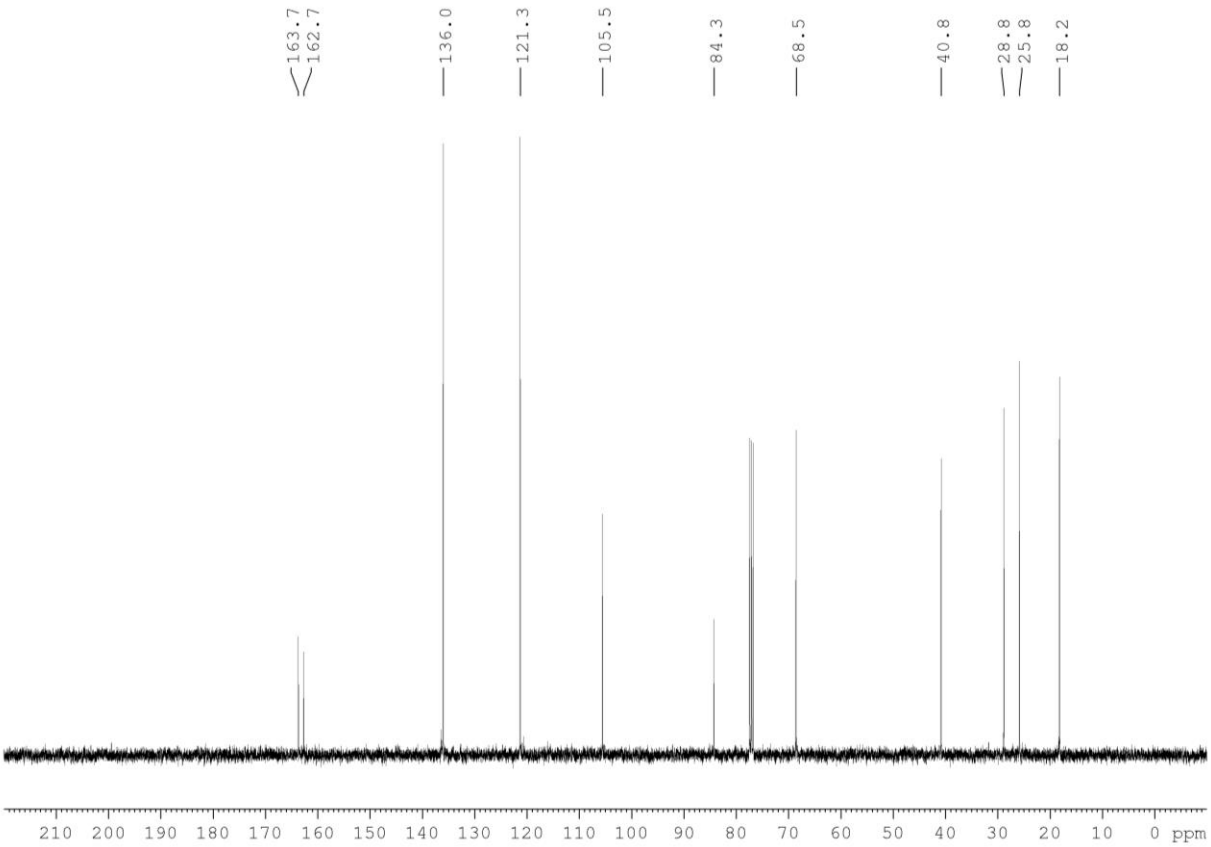
163.7
162.7
136.0
121.3
105.5
84.3
68.5
40.8
28.8
25.8
18.2
210
200
190
180
170
160
150
140
130
120
110
100
90
80
70
60
50
40
30
20
10
0 ppm

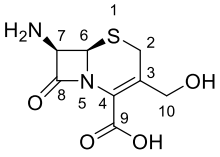
1
H_2N
7
6
S
2
3
OH
O
8
N
5
4
9
10
O
OH

28


4.93
4.92
4.73
4.72
4.21
4.20
3.58
3.54
3.50
3.46

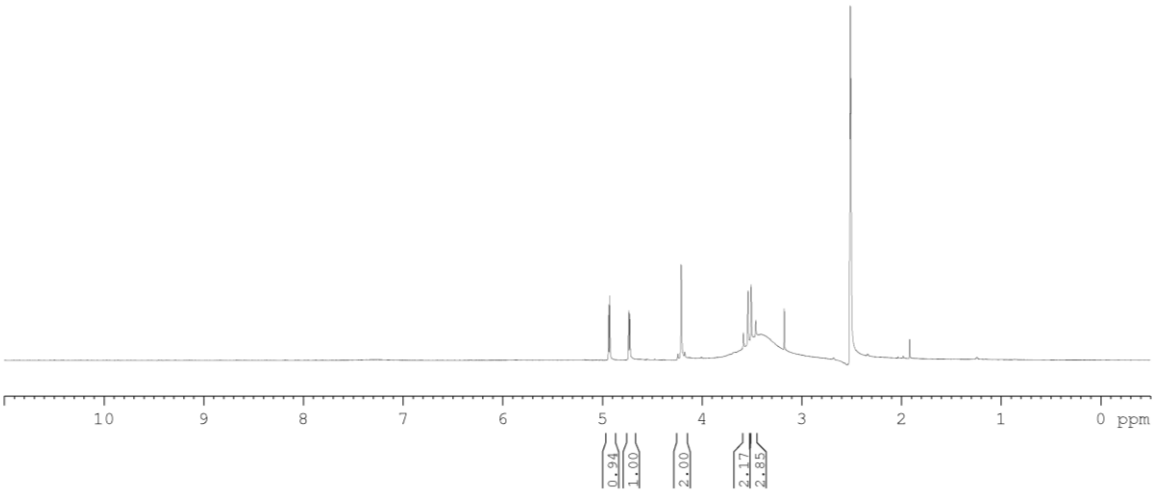
10
9
8
7
6
5
4
3
2
1
0 ppm
0.94
1.00
2.00
2.17
2.85

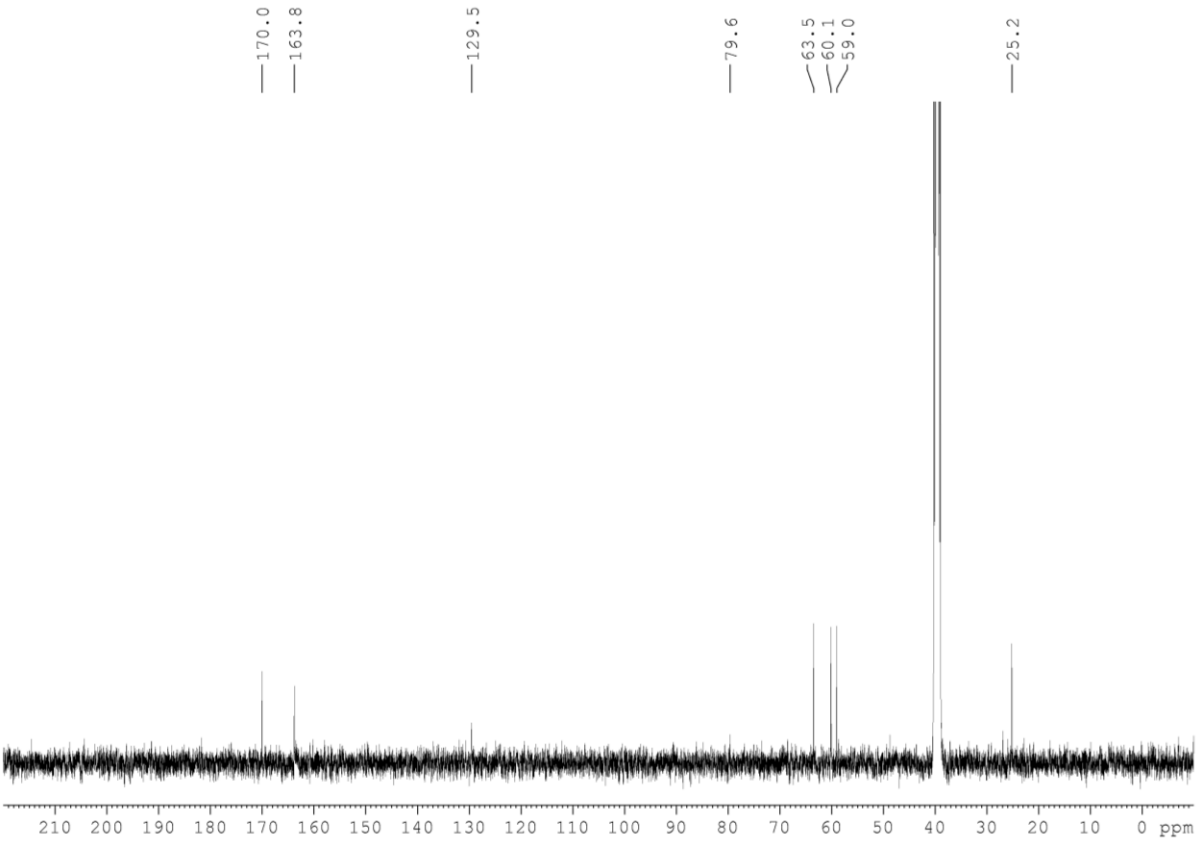
170.0
163.8
129.5
79.6
63.5
60.1
59.0
25.2
210
200
190
180
170
160
150
140
130
120
110
100
90
80
70
60
50
40
30
20
10
0 ppm

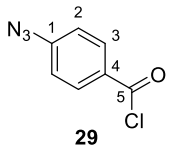
N3
1
2
3
4
5
O
Cl

29


7.97
7.96
7.95
7.95
7.22
7.21
7.20
7.19

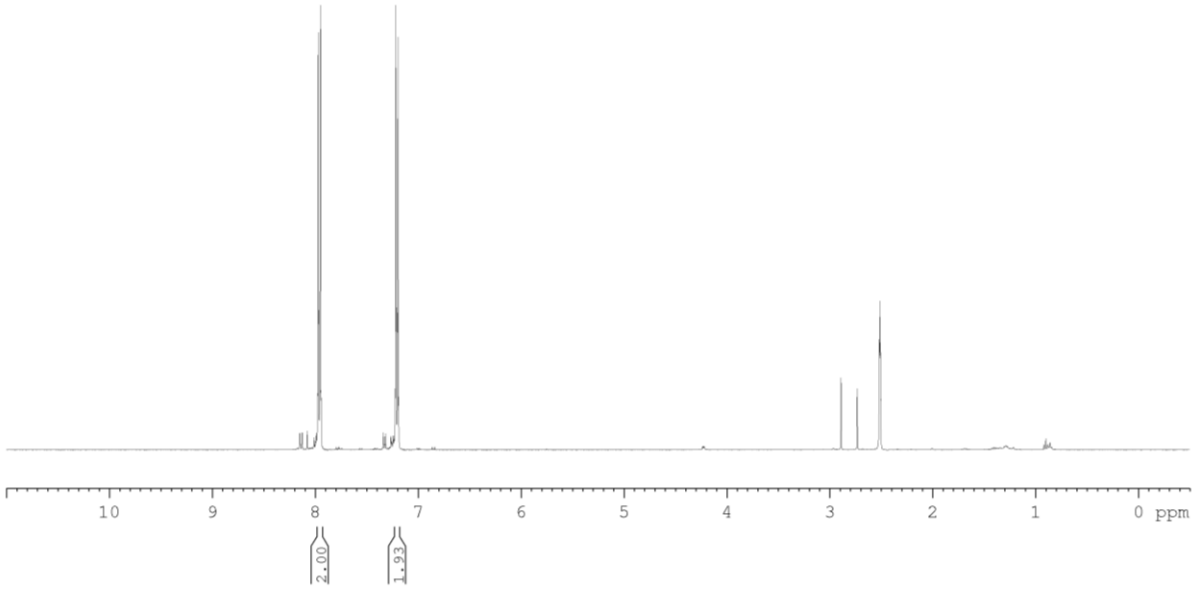
10
9
8
7
6
5
4
3
2
1
0 ppm
2.00
1.93

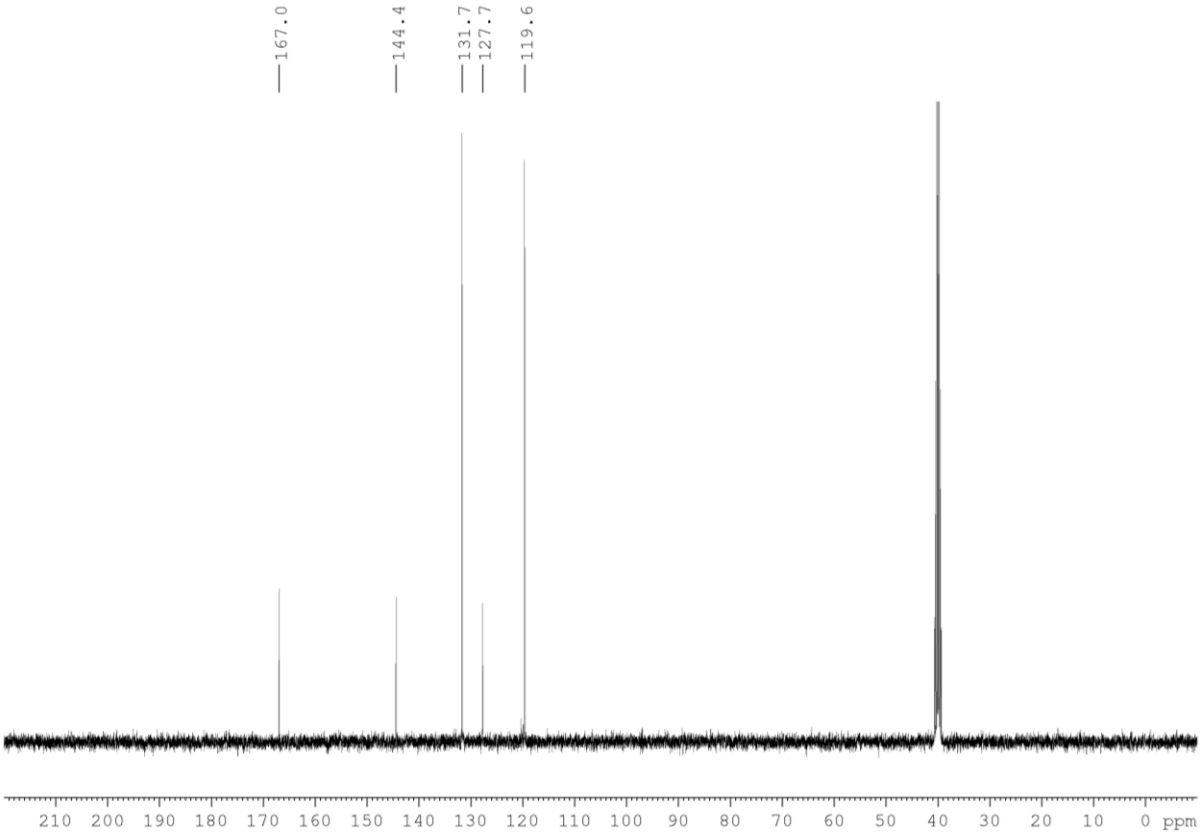
167.0
144.4
131.7
127.7
119.6
210
200
190
180
170
160
150
140
130
120
110
100
90
80
70
60
50
40
30
20
10
0 ppm

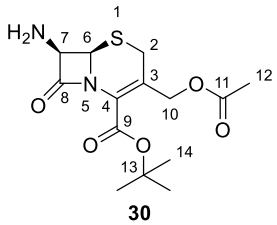

30

4.99
4.98
4.90
4.87
4.80
4.78
4.62
4.59
3.60
3.56
3.45
3.40
3.32
2.02
1.46
10 9 8 7 6 5 4 3 2 1 0 ppm
0.89
0.98
0.92
1.00
1.07
1.00
3.09
8.99
170.3
170.1
160.8
127.1
122.1
82.6
63.8
62.8
59.3
39.6
27.5
25.4
20.7
210 200 190 180 170 160 150 140 130 120 110 100 90 80 70 60 50 40 30 20 10 0 ppm

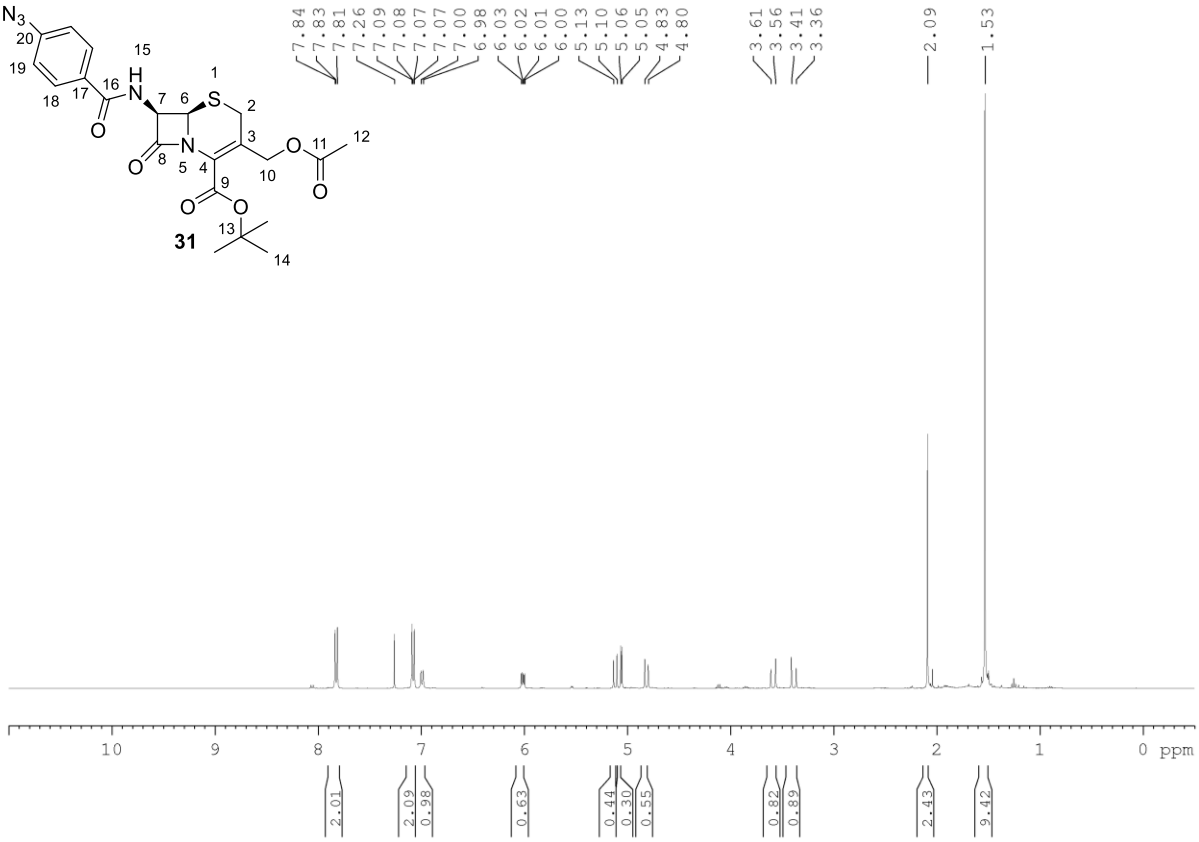
7.84
7.83
7.81
7.26
7.09
7.08
7.07
7.07
7.00
6.98
6.03
6.02
6.01
6.00
5.13
5.10
5.06
5.05
4.83
4.80
3.61
3.56
3.41
3.36
2.09
1.53
10
9
8
7
6
5
4
3
2
1
0 ppm
2.01
2.09
0.98
0.63
0.44
0.30
0.55
0.82
0.89
2.43
9.42

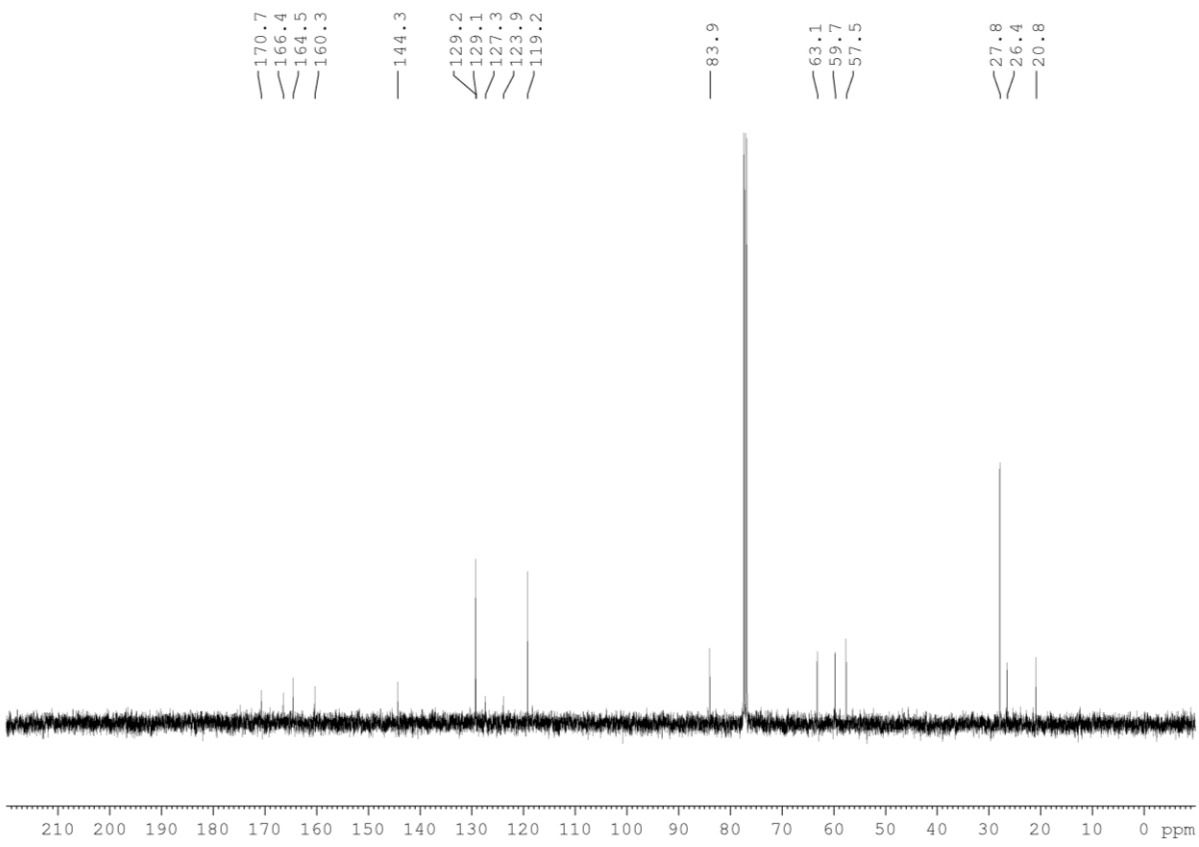
170.7
166.4
164.5
160.3
144.3
129.2
129.1
127.3
123.9
119.2
83.9
63.1
59.7
57.5
27.8
26.4
20.8
210
200
190
180
170
160
150
140
130
120
110
100
90
80
70
60
50
40
30
20
10
0 ppm

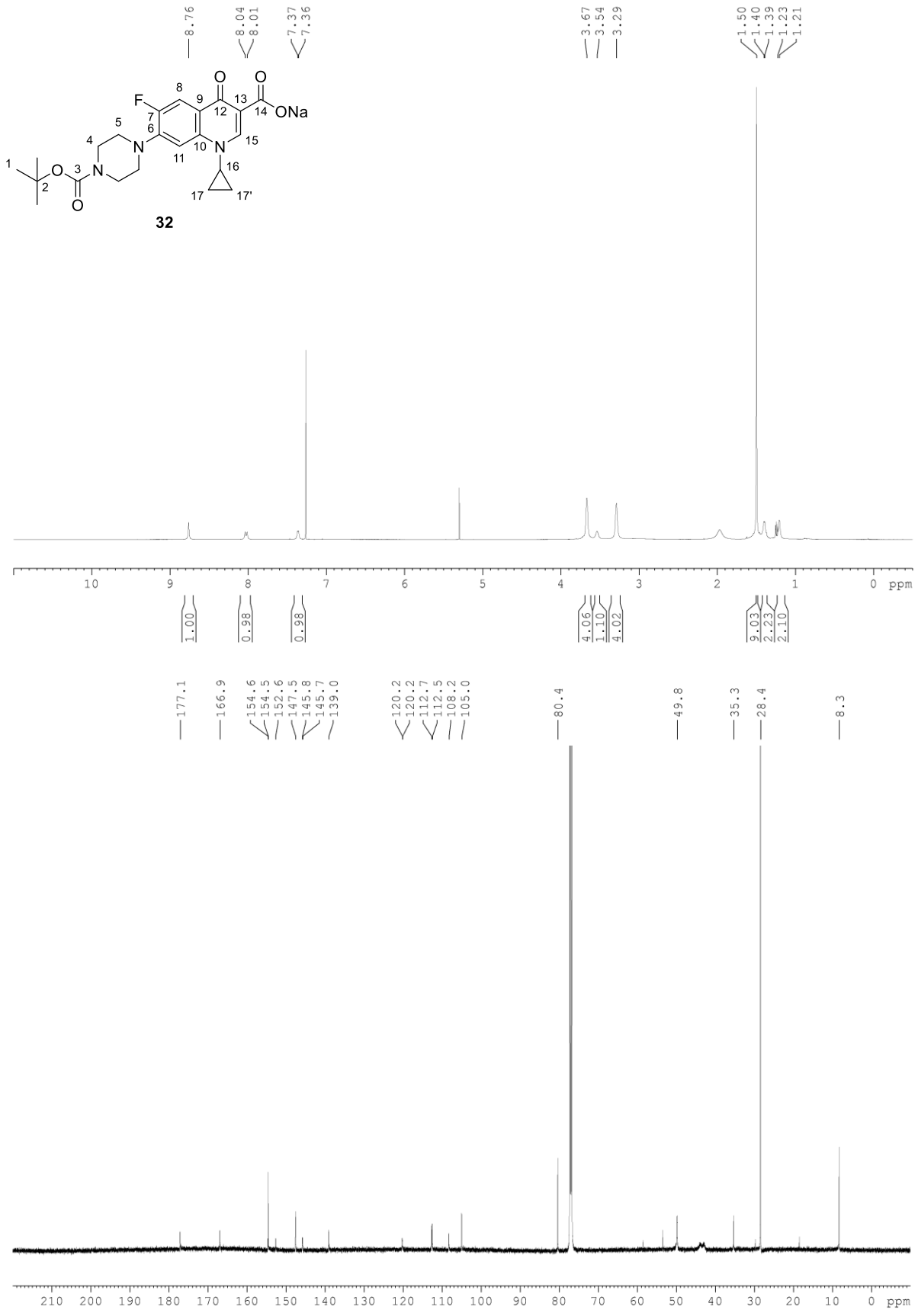
8.76
8.04
8.01
7.37
7.36
3.67
3.54
3.29
1.50
1.40
1.39
1.23
1.21
F
O
O
ONa
N
N
O
O
32
10 9 8 7 6 5 4 3 2 1 0 ppm
1.00
0.98
0.98
4.06
1.10
4.02
9.03
2.23
2.10
177.1
166.9
154.6
154.5
152.6
147.5
145.8
145.7
139.0
120.2
120.2
112.7
112.5
108.2
105.0
80.4
49.8
35.3
28.4
8.3
210 200 190 180 170 160 150 140 130 120 110 100 90 80 70 60 50 40 30 20 10 0 ppm

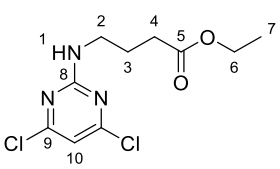
1
HN
2
4
5
O
7
8
3
6
O
N
N
Cl
9
10
Cl

43

6.59
5.87
4.17
4.15
4.13
4.11
3.51
3.50
3.48
3.46
2.41
2.39
2.37
1.97
1.95
1.94
1.92
1.90
1.27
1.25
1.24
10
9
8
7
6
5
4
3
2
1
0 ppm
0.92
0.99
2.00
2.03
2.03
2.01
3.11

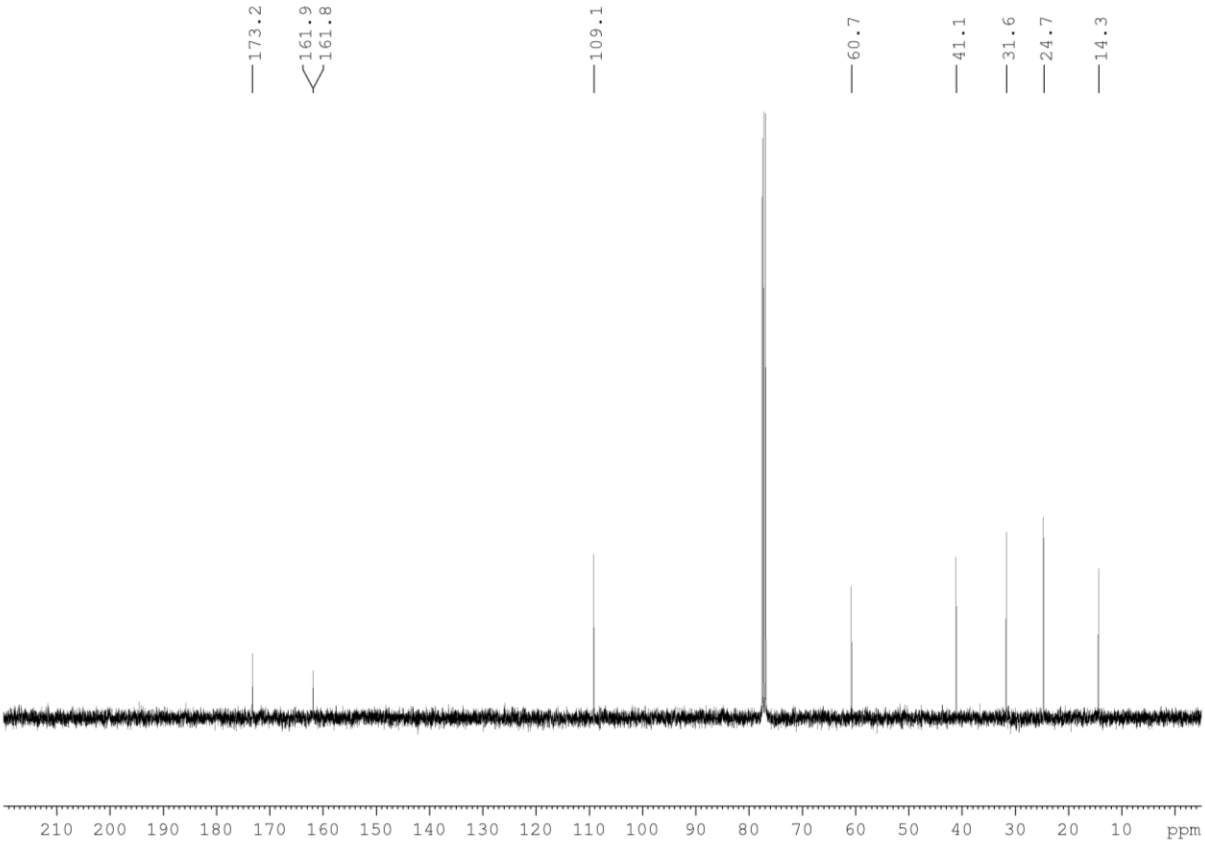
173.2
161.9
161.8
109.1
60.7
41.1
31.6
24.7
14.3
210
200
190
180
170
160
150
140
130
120
110
100
90
80
70
60
50
40
30
20
10
ppm

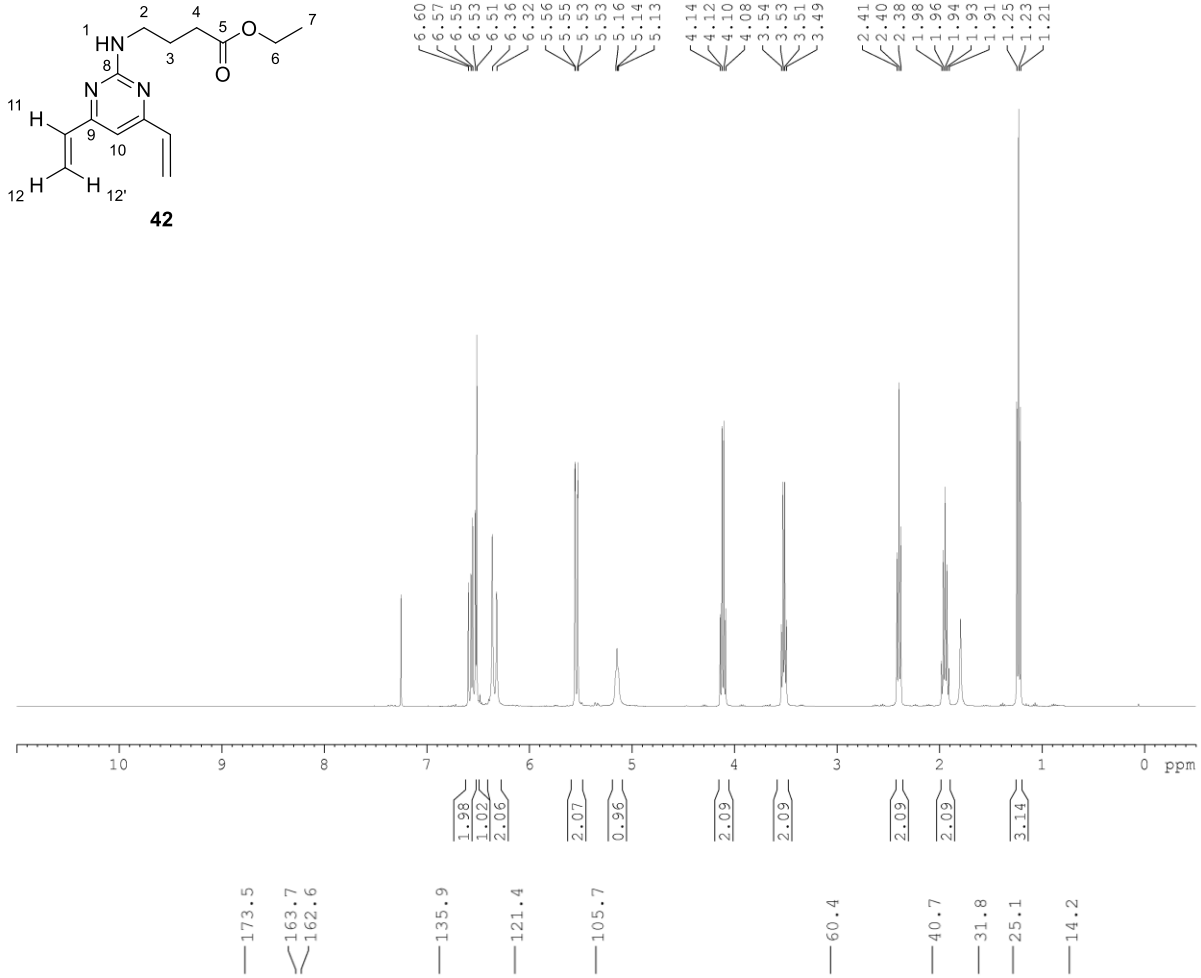
6.60
6.57
6.55
6.53
6.51
6.36
6.32
5.56
5.55
5.53
5.53
5.16
5.14
5.13
4.14
4.12
4.10
4.08
3.54
3.53
3.51
3.49
2.41
2.40
2.38
1.98
1.96
1.94
1.93
1.91
1.25
1.23
1.21
10 9 8 7 6 5 4 3 2 1 0 ppm
1.98
1.02
2.06
2.07
0.96
2.09
2.09
2.09
2.09
3.14
173.5
163.7
162.6
135.9
121.4
105.7
60.4
40.7
31.8
25.1
14.2
210 200 190 180 170 160 150 140 130 120 110 100 90 80 70 60 50 40 30 20 10 0 ppm

42

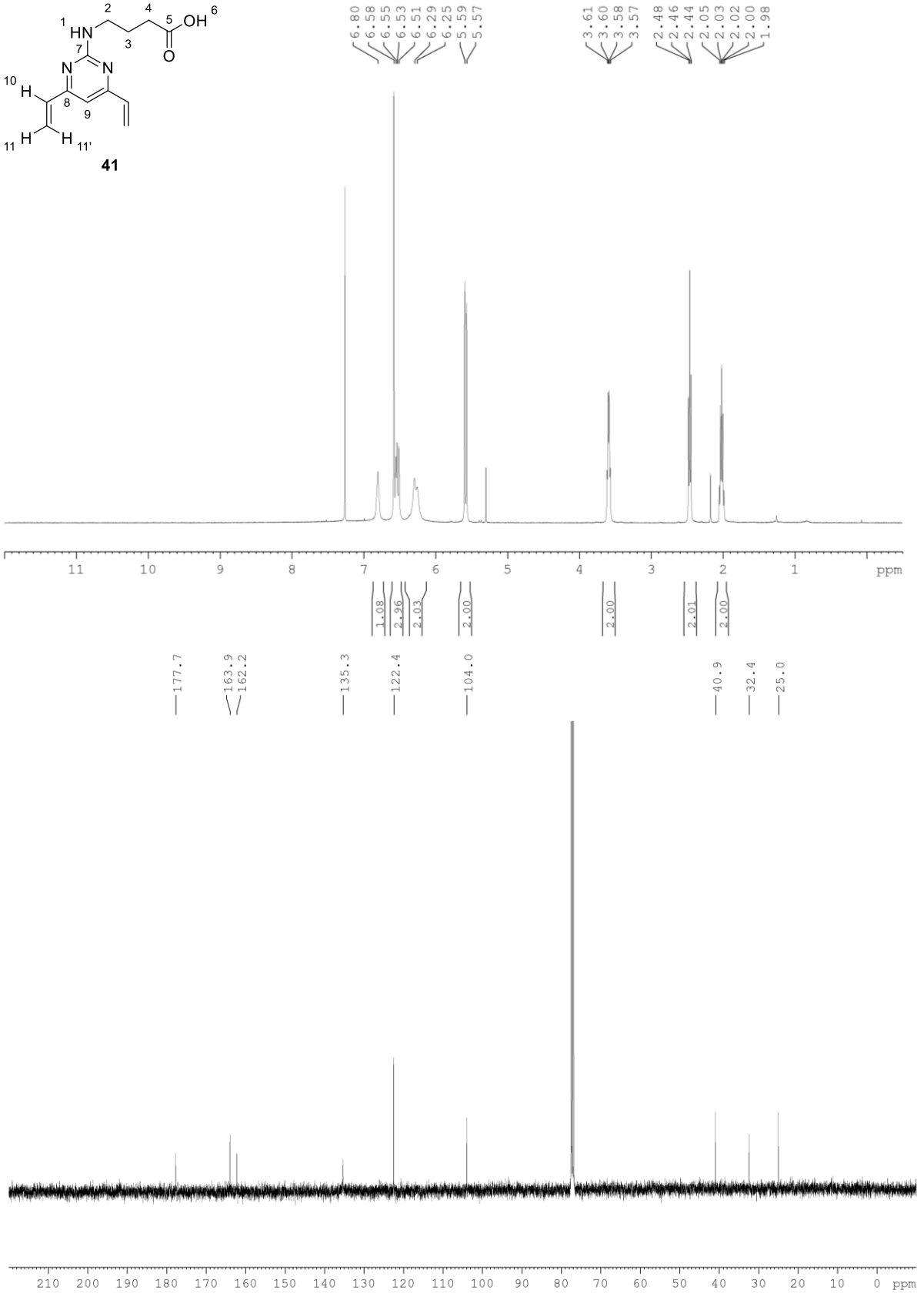
41
6.80
6.58
6.55
6.53
6.51
6.29
6.25
5.59
5.57
3.61
3.60
3.58
3.57
2.48
2.46
2.44
2.05
2.03
2.02
2.00
1.98
ppm
1.08
2.96
2.03
2.00
2.00
2.01
2.00
177.7
163.9
162.2
135.3
122.4
104.0
40.9
32.4
25.0
ppm

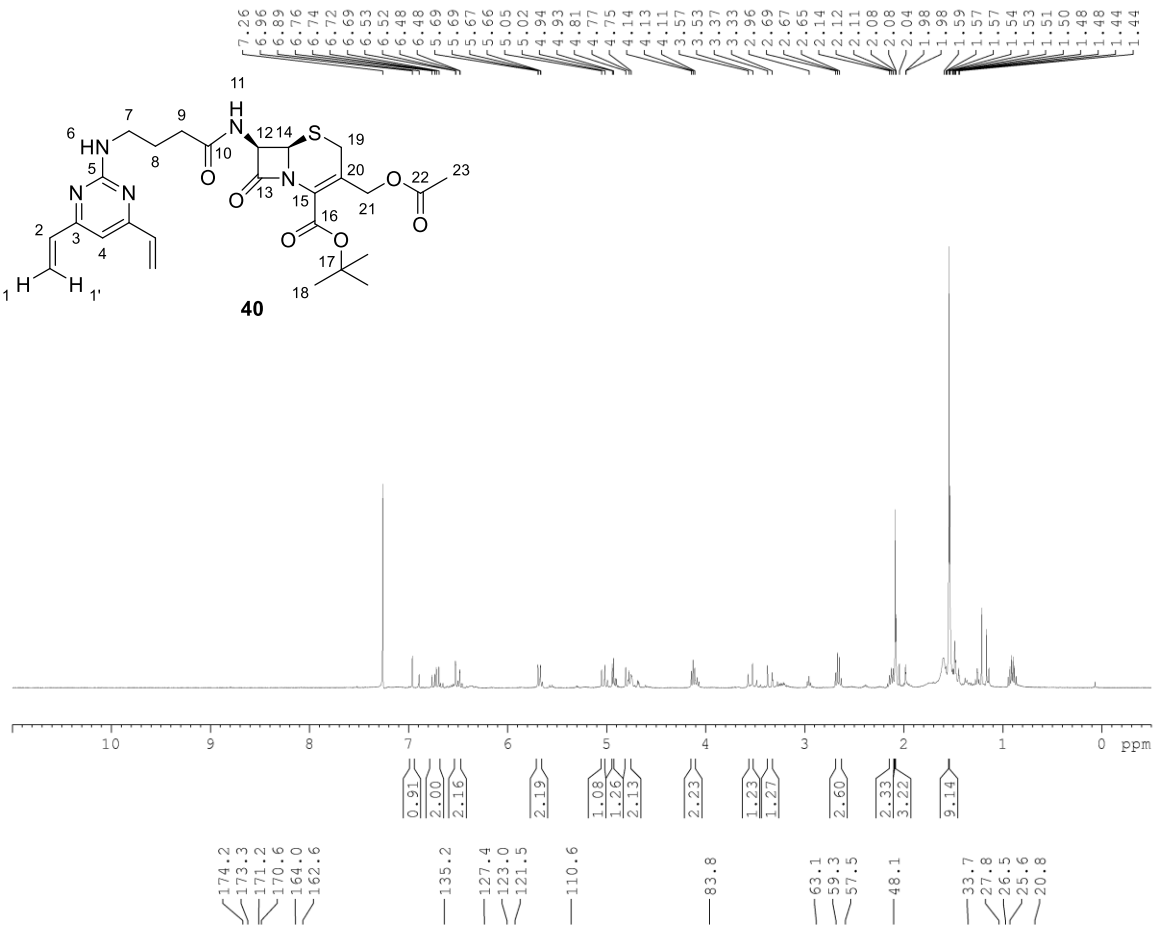
7.26
6.96
6.89
6.76
6.74
6.72
6.69
6.53
6.52
6.48
6.48
5.69
5.69
5.67
5.66
5.05
5.02
4.94
4.93
4.81
4.77
4.75
4.14
4.13
4.11
3.57
3.53
3.37
3.33
2.96
2.69
2.67
2.65
2.14
2.12
2.11
2.08
2.08
2.04
1.98
1.98
1.59
1.57
1.57
1.54
1.53
1.51
1.50
1.48
1.48
1.44
1.44
40
10 9 8 7 6 5 4 3 2 1 0 ppm
0.91 2.00 2.16 2.19 1.08 1.26 2.13 2.23 1.23 1.27 2.60 2.33 3.22 9.14
174.2 173.3 171.2 170.6 164.0 162.6 135.2 127.4 123.0 121.5 110.6 83.8 63.1 59.3 57.5 48.1 33.7 27.8 26.5 25.6 20.8
210 200 190 180 170 160 150 140 130 120 110 100 90 80 70 60 50 40 30 20 10 0 ppm

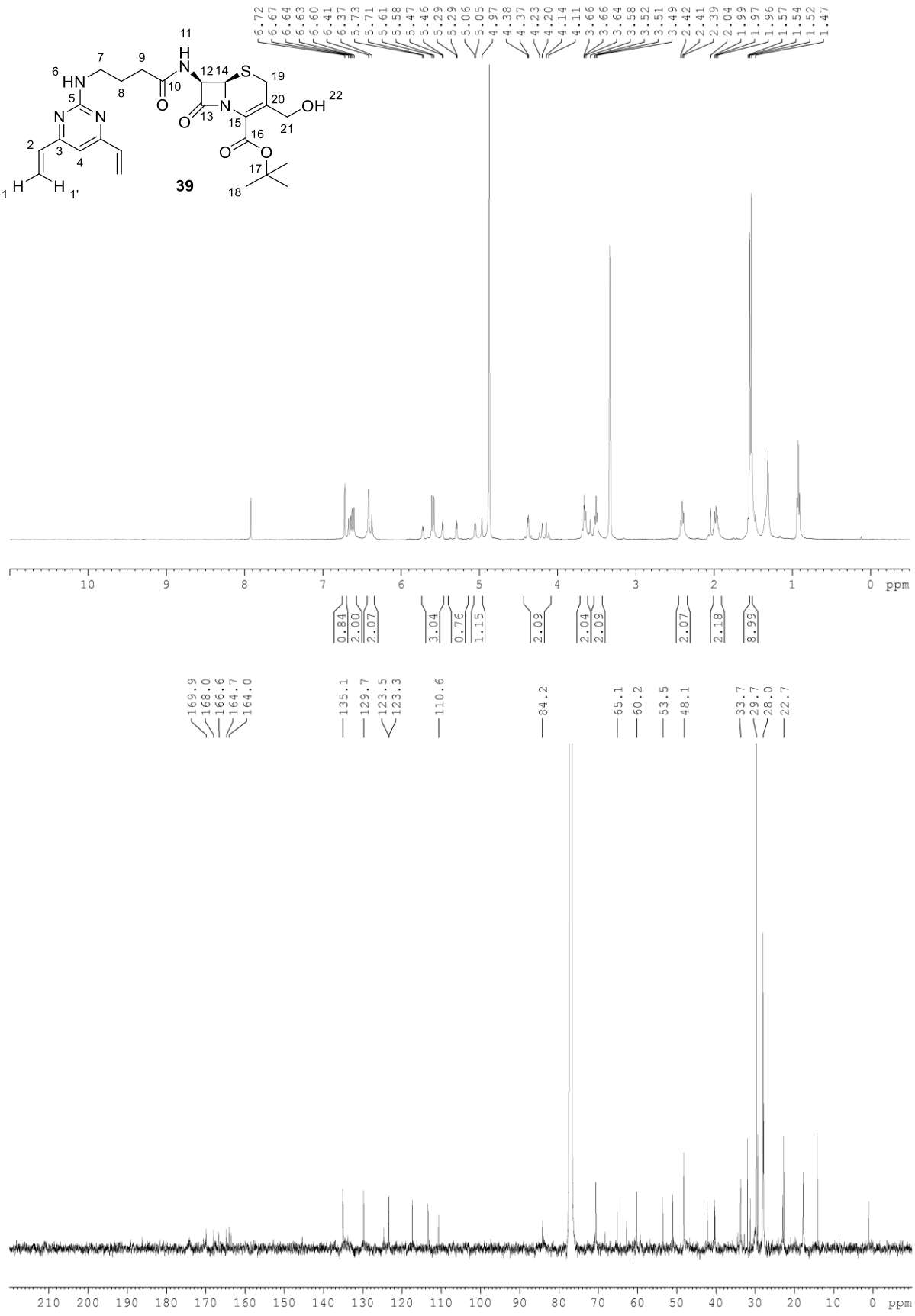
6.72
6.67
6.64
6.63
6.60
6.41
6.37
5.73
5.71
5.61
5.58
5.47
5.46
5.29
5.29
5.06
5.05
4.97
4.38
4.37
4.23
4.20
4.14
4.11
3.66
3.66
3.64
3.58
3.52
3.51
3.49
2.42
2.41
2.39
2.04
1.99
1.97
1.96
1.57
1.54
1.52
1.47
39
10 9 8 7 6 5 4 3 2 1 0 ppm
0.84
2.00
2.07
3.04
0.76
1.15
2.09
2.04
2.09
2.07
2.18
8.99
169.9
168.0
166.6
164.7
164.0
135.1
129.7
123.5
123.3
110.6
84.2
65.1
60.2
53.5
48.1
33.7
29.7
28.0
22.7
210 200 190 180 170 160 150 140 130 120 110 100 90 80 70 60 50 40 30 20 10 0 ppm

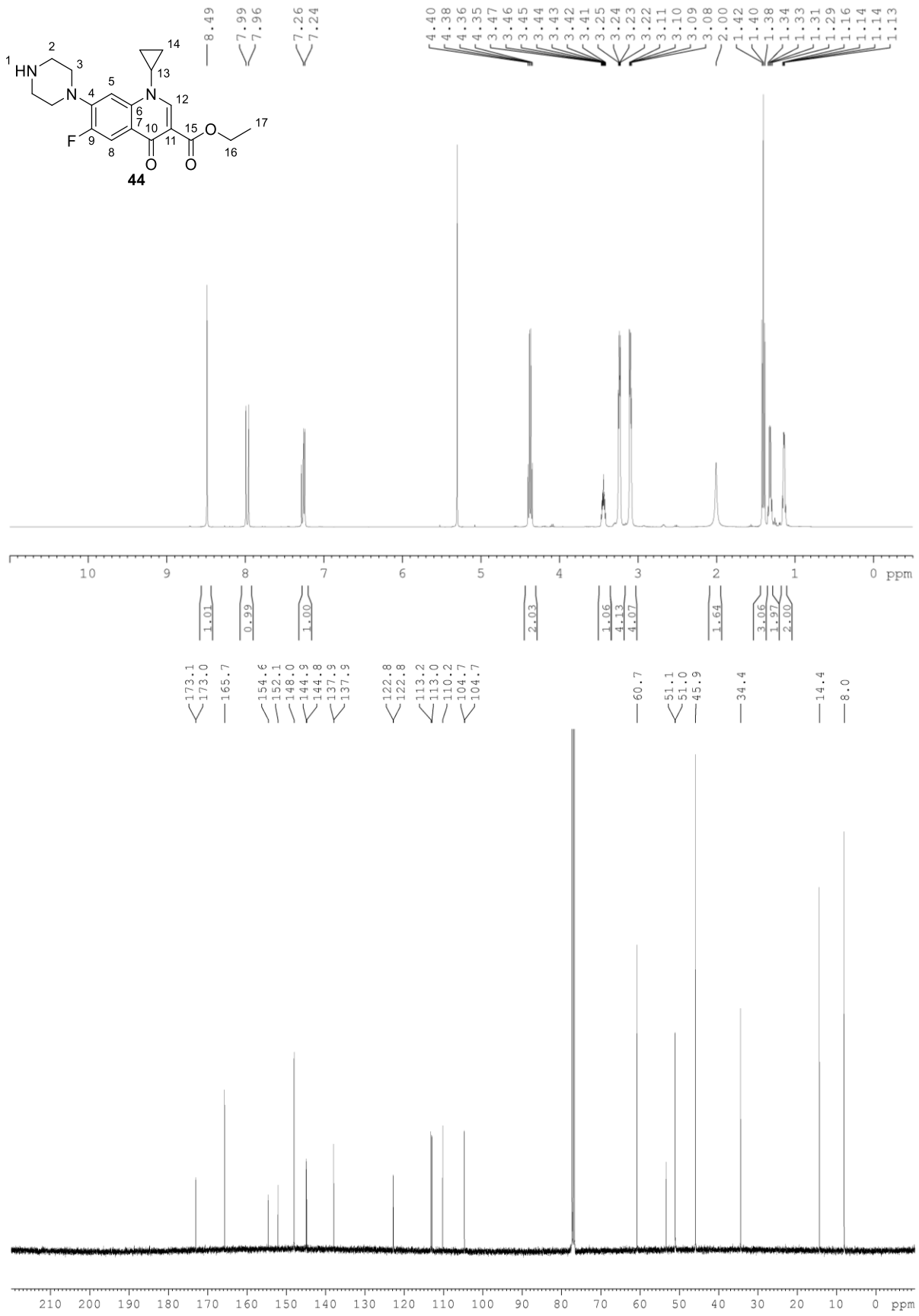
8.49
7.99
7.96
7.26
7.24
4.40
4.38
4.36
4.35
3.47
3.46
3.45
3.44
3.43
3.42
3.41
3.25
3.24
3.23
3.22
3.11
3.10
3.09
3.08
2.00
1.42
1.40
1.38
1.34
1.33
1.31
1.29
1.16
1.14
1.14
1.13
10 9 8 7 6 5 4 3 2 1 0 ppm
1.01
0.99
1.00
2.03
1.06
4.13
4.07
1.64
3.06
1.97
2.00
173.1
173.0
165.7
154.6
152.1
148.0
144.9
144.8
137.9
137.9
122.8
122.8
113.2
113.0
110.2
104.7
104.7
60.7
51.1
51.0
45.9
34.4
14.4
8.0
210 200 190 180 170 160 150 140 130 120 110 100 90 80 70 60 50 40 30 20 10 0 ppm

44

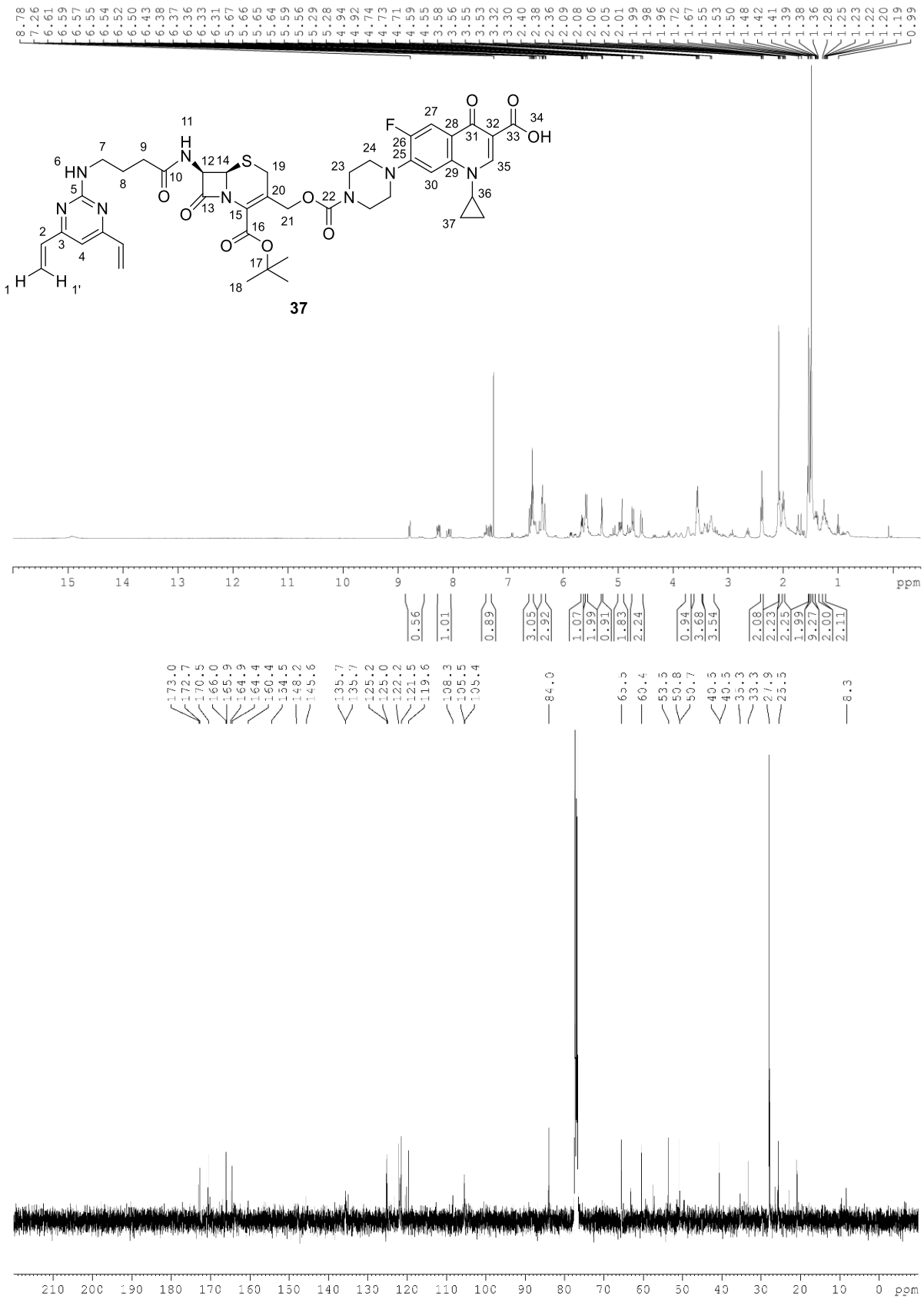

37

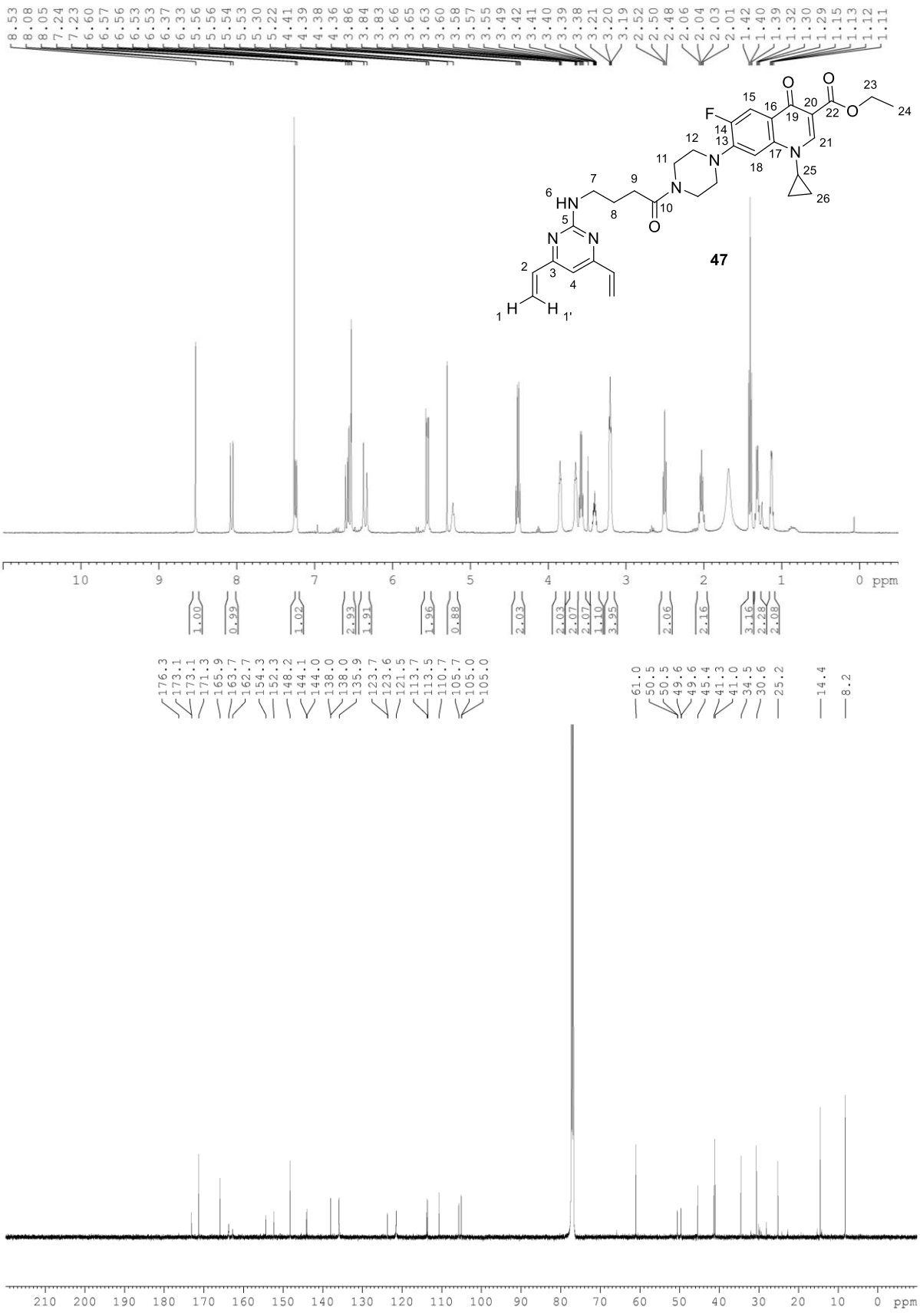
8.53 8.08 8.05 7.24 7.23 6.60 6.57 6.56 6.53 6.53 6.37 6.33 5.56 5.56 5.54 5.53 5.30 5.22 4.41 4.39 4.38 4.36 3.86 3.84 3.83 3.66 3.65 3.63 3.60 3.58 3.57 3.55 3.49 3.42 3.41 3.40 3.39 3.38 3.21 3.20 3.19 2.52 2.50 2.48 2.06 2.04 2.03 2.01 1.42 1.40 1.39 1.32 1.30 1.29 1.15 1.13 1.12 1.11
47
10 9 8 7 6 5 4 3 2 1 0 ppm
1.00 0.99 1.02 2.93 1.91 1.96 0.88 2.03 2.03 2.07 2.07 1.10 3.95 2.06 2.16 3.16 2.28 2.08
176.3 173.1 173.1 171.3 165.9 163.7 162.7 154.3 152.3 148.2 144.1 144.0 138.0 138.0 135.9 123.7 123.6 121.5 113.7 113.5 110.7 105.7 105.0 105.0
61.0 50.5 50.5 49.6 49.6 45.4 41.3 41.0 34.5 30.6 25.2 14.4 8.2
210 200 190 180 170 160 150 140 130 120 110 100 90 80 70 60 50 40 30 20 10 0 ppm

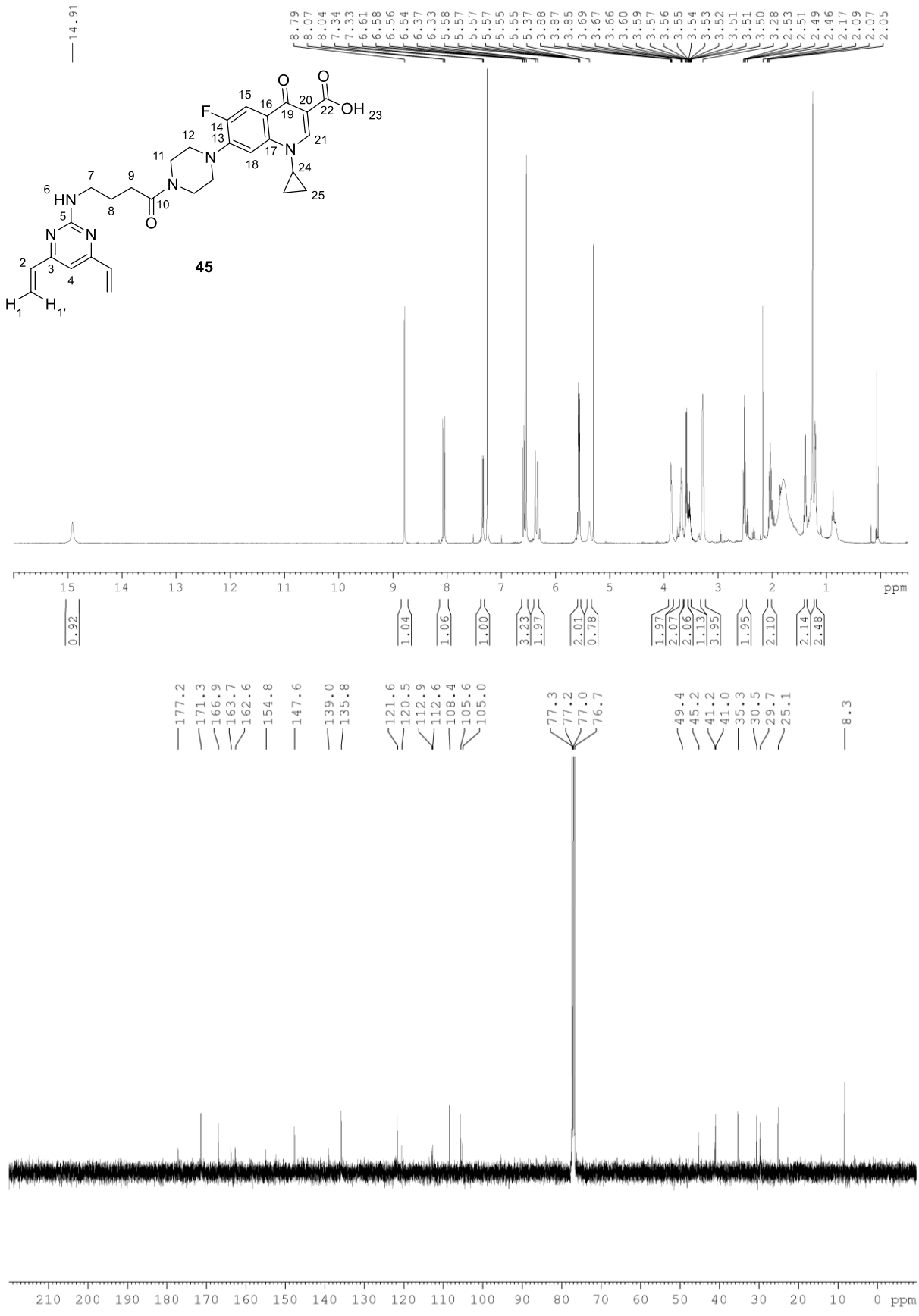
14.91
8.79
8.07
8.04
7.34
7.33
6.61
6.58
6.56
6.54
6.37
6.33
5.58
5.57
5.57
5.57
5.55
5.55
5.37
3.88
3.87
3.85
3.69
3.67
3.66
3.60
3.59
3.57
3.56
3.55
3.54
3.53
3.52
3.51
3.50
3.28
2.53
2.51
2.49
2.46
2.17
2.09
2.07
2.05
45
ppm
0.92
1.04
1.06
1.00
3.23
1.97
2.01
0.78
1.97
2.07
2.06
1.13
3.95
1.95
2.10
2.14
2.48
177.2
171.3
166.9
163.7
162.6
154.8
147.6
139.0
135.8
121.6
120.5
112.9
112.6
108.4
105.6
105.0
77.3
77.2
77.0
76.7
49.4
45.2
41.2
41.0
35.3
30.5
29.7
25.1
8.3
ppm

6.2 Appendix 2 - Selected analytical HPLC traces

Gradients are given as % of MeCN in H_2O with a 0.01% formic acid additive. The spectra shown were recorded at a wavelength of 220 nm. A peak at 2 min corresponds to DMSO which was added to aid the solubility of the peptide.

P1 5-95%

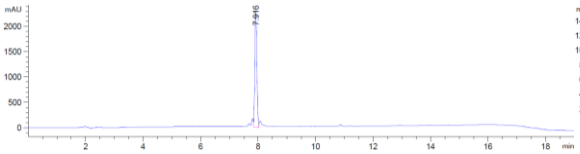

P1 30-80%

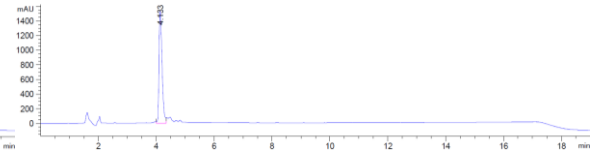

P2 5-95%

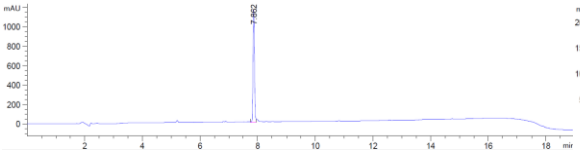

P2 30-80%

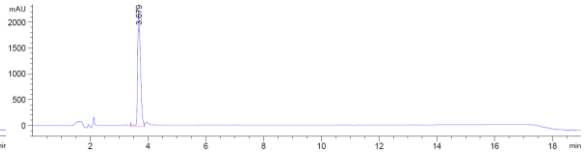

P3 5-95%

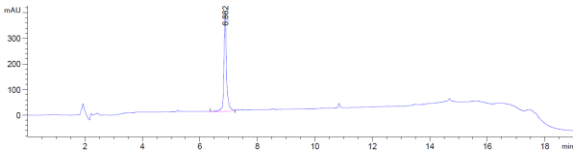

P3 20-70%

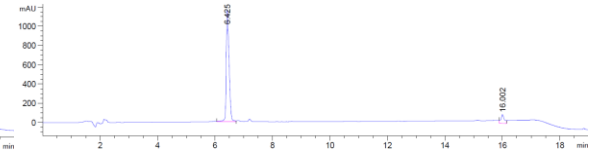

P4 5-95%

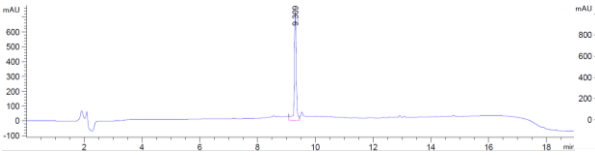

P4 30-80%

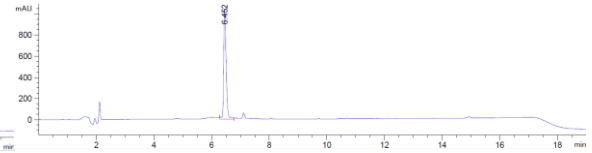

P5 5-95%

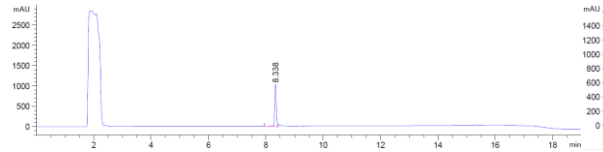

P6 5-95%

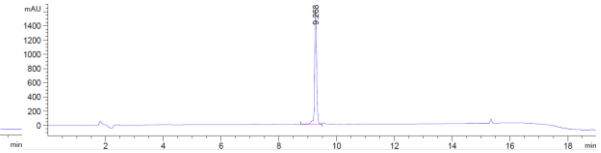

P4-6 5-95%

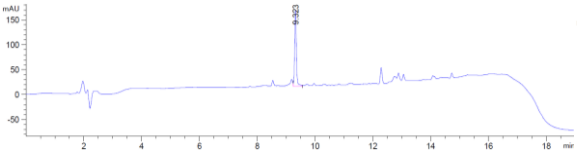

P5-6 5-95%

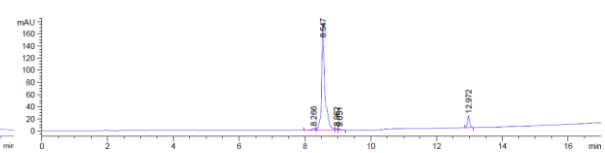

P6-6 5-95%

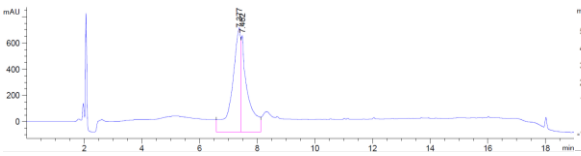

P6-6 10-80%

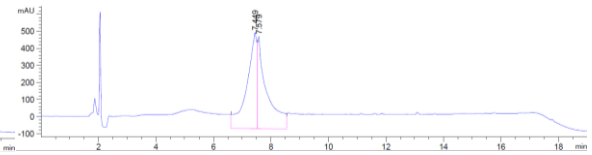

P8 5-95%

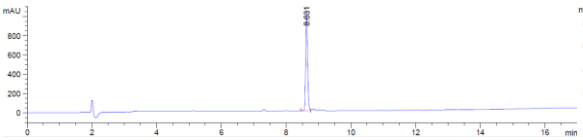

P8 30-95%

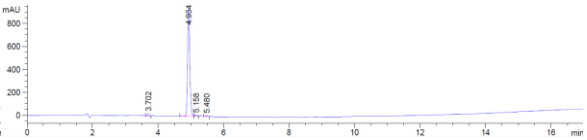

P9 5-95%

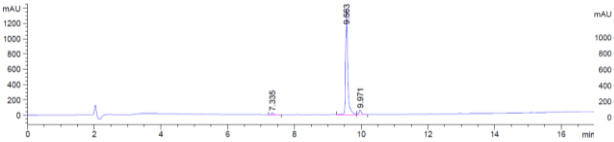

P9 30-95%

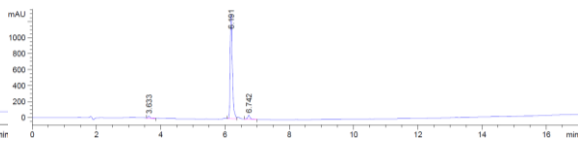

P10 5-95%

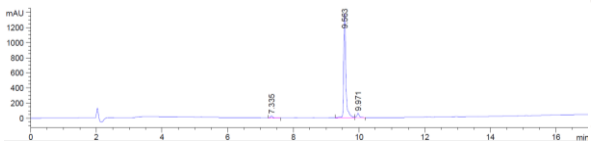

P10 50-95%

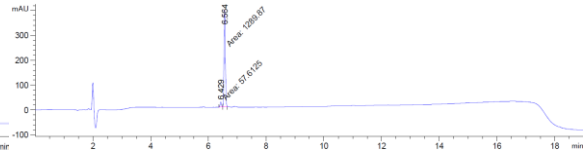

P11 5-95%

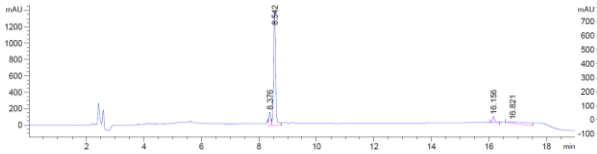

P11 20-80%

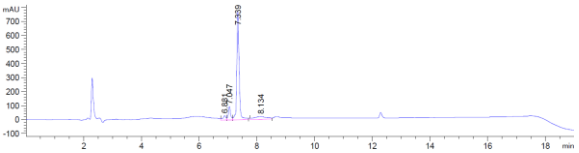

P8-10 5-95%

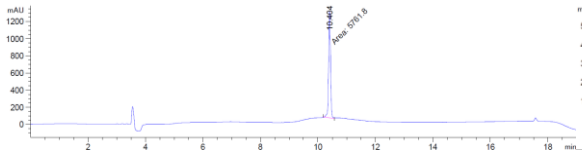

P8-10 30-80%

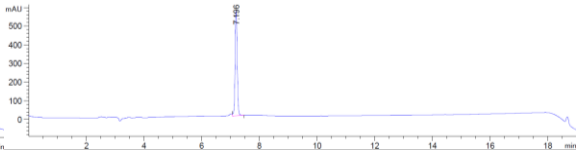

P9-10 5-95%

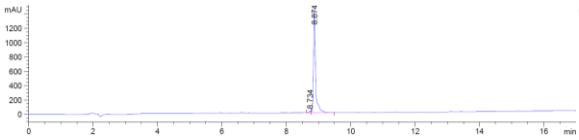

P9-10 20-60%

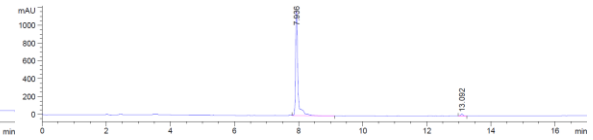

P11-10 5-95%

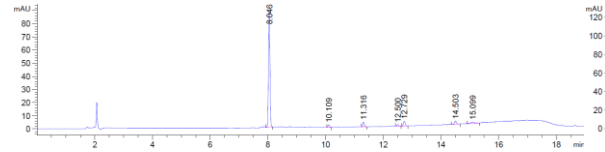

P11-10 10-80%

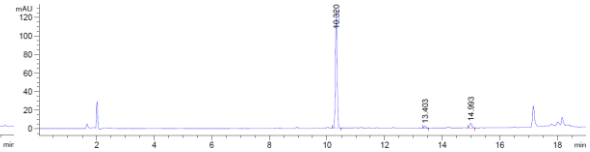

P8-11 5-95%

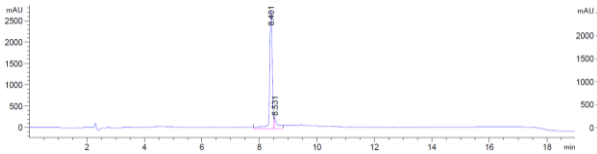

P8-11 30-80%

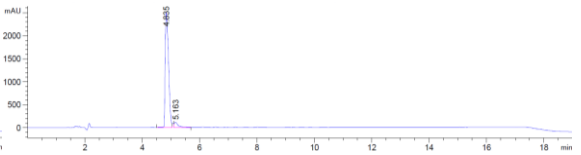

P9-11 5-95%

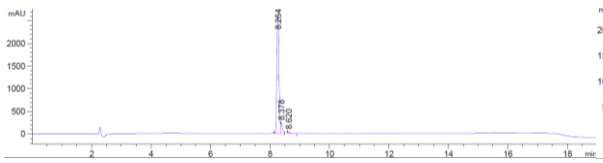

P9-11 30-80%

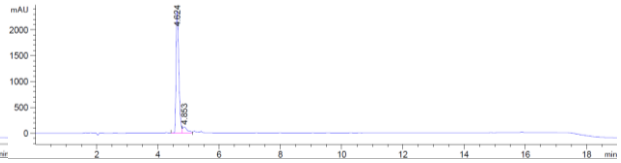

P11-11 5-95%

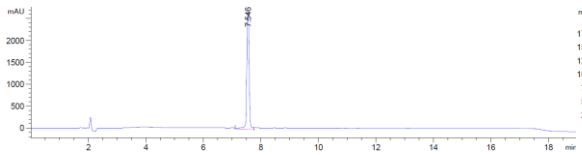

P11-11 20-60%

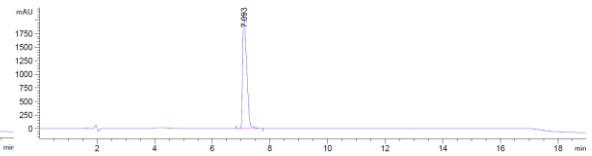

11 5-95%

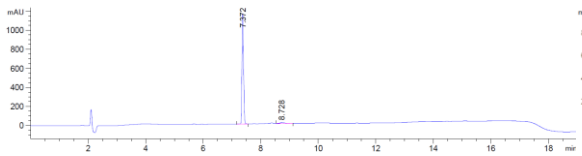

11 5-45%

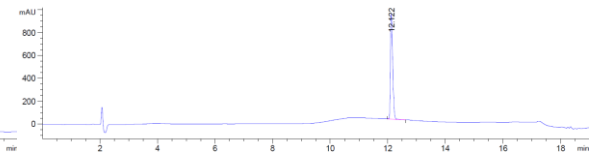

AMP1 5-95%

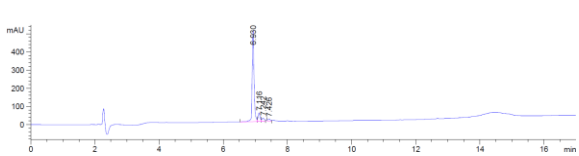

AMP2 5-95%

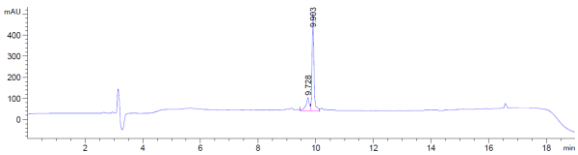

AMP3 5-95%

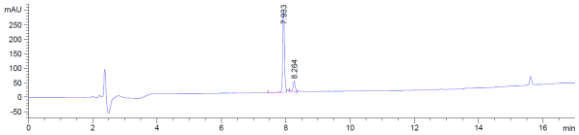

AMP4 5-95%

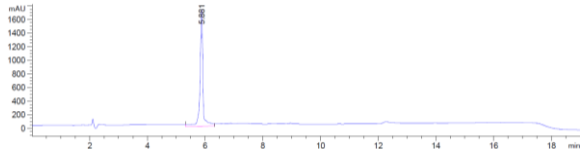

AMP5 5-95%

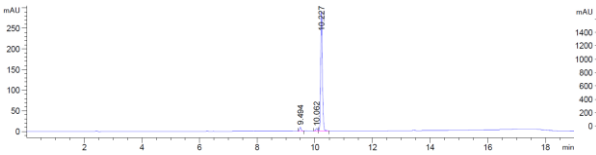

AMP6 5-95%

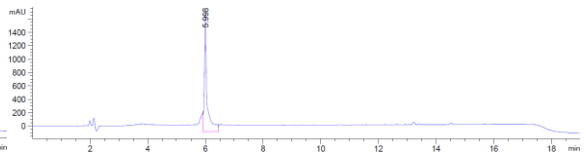

AMP7 5-95%

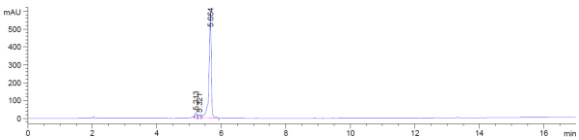

AMP1-17 5-95%

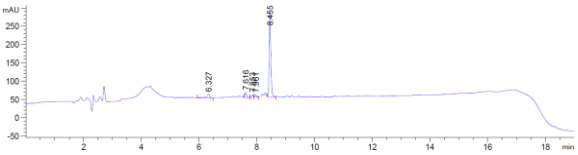

AMP1-17 10-60%

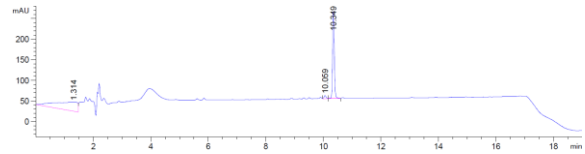

AMP2-17 5-95%

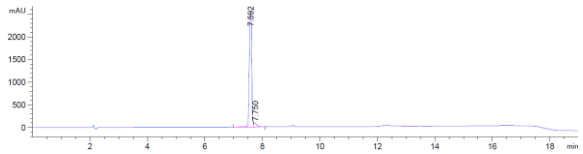

AMP2-17 10-60%

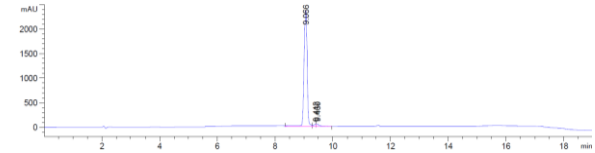

AMP3-17 5-95%

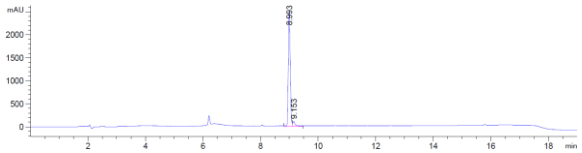

AMP3-17 5-65%

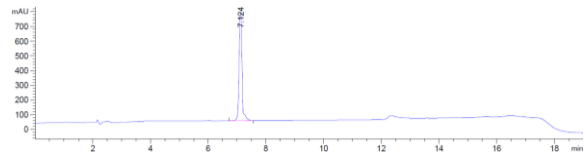

AMP4-17 5-95%

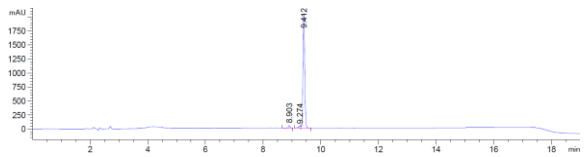

AMP4-17 10-60%

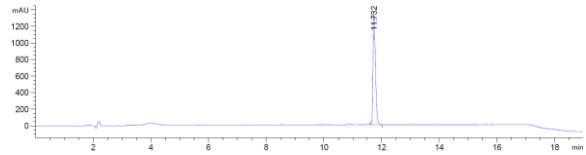

AMP5-17 5-95%

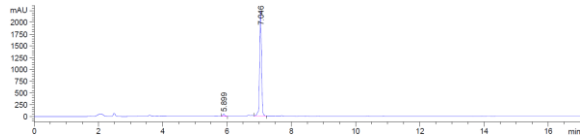

AMP5-17 10-80%

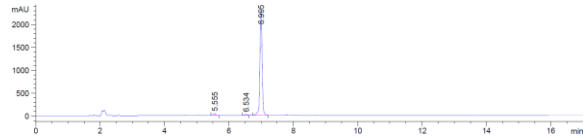

AMP6-17 5-95%

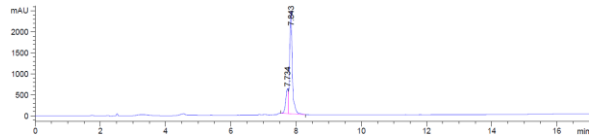

AMP6-17 10-80%

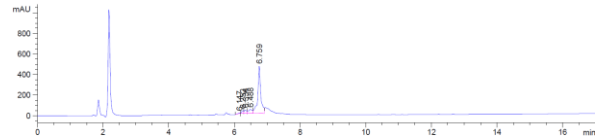

AMP7-17 5-95%

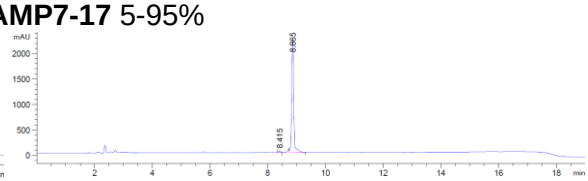

AMP7-17 10-60%

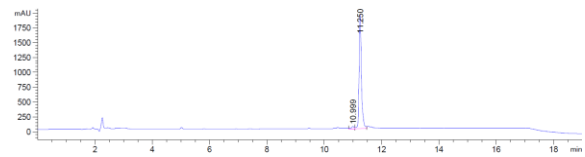

AMP1-18 5-95%

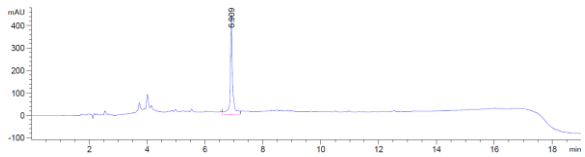

AMP1-18 20-60%

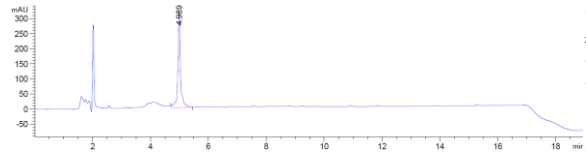

AMP2-18 5-95%

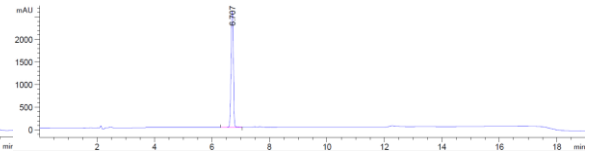

AMP2-18 10-60%

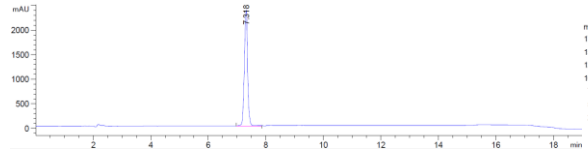

AMP3-18 5-95%

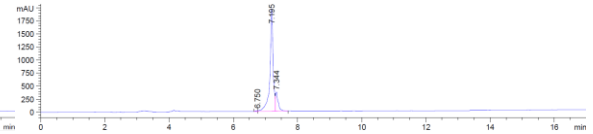

AMP3-18 30-70%

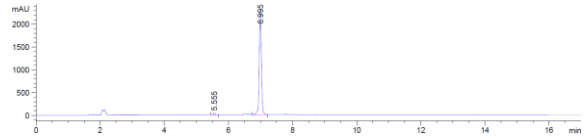

AMP4-18 5-95%

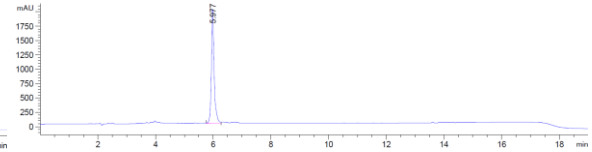

AMP4-18 10-80%

AMP5-18 5-95%

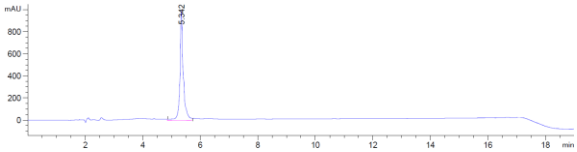

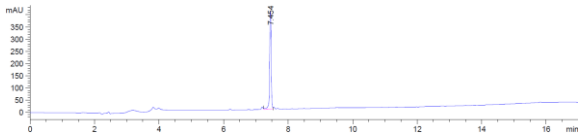

AMP6-18 5-95%

AMP6-18 10-60%

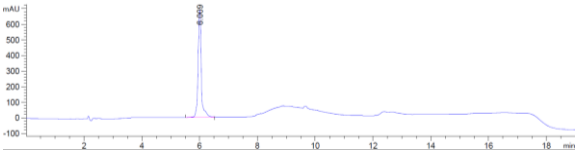

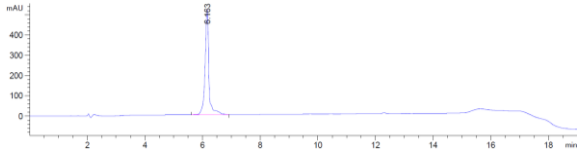

AMP7-18 5-95%

AMP7-18 10-60%

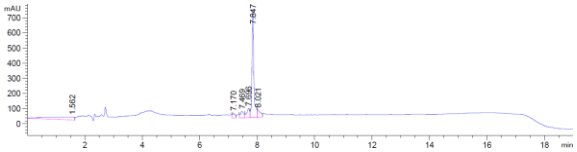

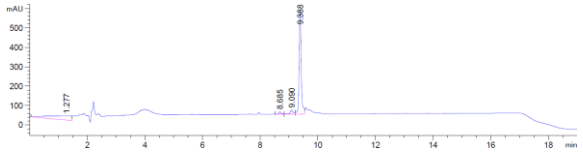

AMP2a 5-95%

AMP2a 5-60%

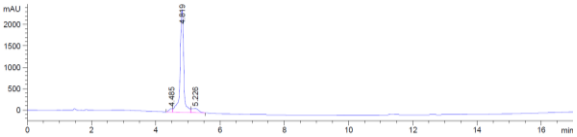

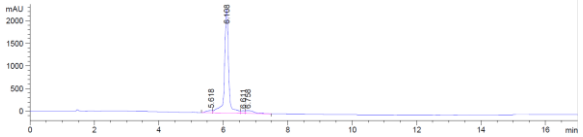

AMP4a 5-95%

AMP4a 5-60%

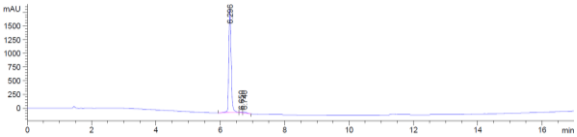

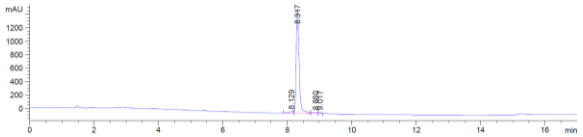

AMP6a 5-95%

AMP6a 5-60%

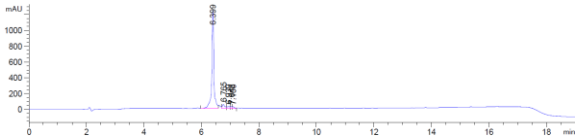

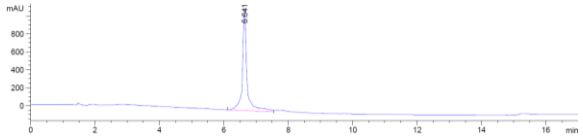

AMP2-45 5-95%

AMP2-45 5-45%

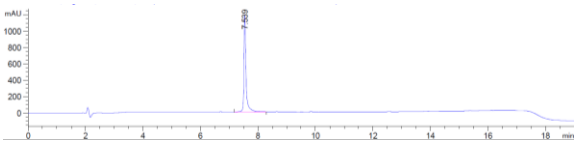

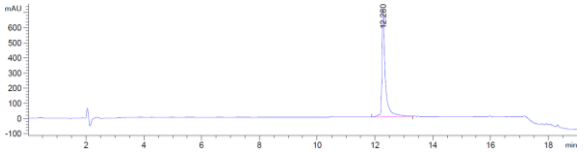

6.3 Appendix 3 - Publication list

Two-Component Stapling of Biologically Active and Conformationally Constrained Peptides: Past, Present, and Future, J. Iegre, J. S. Gaynord, N. S. Robertson, H. F. Sore, M. Hyvönen, D. R. Spring, *Adv. Therap.* **2018**, 1, 1800052.

Stapled peptides as a new technology to investigate protein-protein interactions in human platelets, J. Iegre, N. S. Ahmed, J. S. Gaynord, Y. Wu, K. M. Herlihy, Y. S. Tan, M. E. Lopes-Pires, R. Jha, Y. H. Lau, H. Sore, C. Verma, D. H. O' Donovan, N. Pugh, D. R. Spring, *Chem. Sci.* 2018, **9**, 4638-4643.